PAMAM Dendrimer as Quantized Building Blocks for Biomedical Applications

by

Mallory A. van Dongen-Sohmer

A dissertation submitted in partial fulfillment
of the requirements for the degree of
Doctor of Philosophy
(Chemistry)
in The University of Michigan
2014

Doctoral Committee:

Professor Mark M. Banaszak Holl, Chair
Professor Robert T. Kennedy
Associate Professor Anne J. McNeil
Professor Bradford G. Orr

Dedication

To my husband, Nick, for his never ending support,

And to my parents for helping me get where I am today

Acknowledgements

This work is a result of much wonderful collaboration, of which none would be possible without my advisor, Mark Banaszak Holl. Mark is exceptionally supportive and patient, and at the same time knows exactly how to push his students to do their best work. He has always given me the encouragement I needed when I was ready to give up on a project, and the support when things didn't work out like I expected (which was, of course, almost daily). I am eternally grateful for the research environment, group dynamic, and work/life balance that Mark has created, for it has made my graduate experience truly enjoyable.

I would also like to thank the entire Michigan Nanotechnology Institute for Medicine and Biological Sciences group, past and present. Their expertise has been invaluable throughout my studies. Particularly, I would like to thank Ankur Desai for his contributions to Chapter 2 of this work and for teaching me (almost) all that I know about methods development; Dr. Baohua Huang, for providing the MTX-Azide derivative used in Chapter 5 and assistance with other syntheses throughout my time here; and Dr. Seok Ki Choi for having the answer to pretty much everything. And of course, Prof. Brad Orr, who has been like a second advisor to me and challenged me to approach problems with a different (non-chemist) mindset.

I couldn't have done any of this without the constant support of the Banaszak Holl group members, past and present, whose mixed backgrounds and interests have made every day for the last 4 years into a new learning experience. I would like to specifically thank Dr. Doug Mullen, without whom this project might not have even existed, Dr. Rahul Rattan for the biological studies in Chapter 5, Casey Dougherty for the synthesis of the cyclooctyne ligand used in Chapters 4 and 5 (and for being there through absolutely everything, coffee in hand); Sriram Vaidyanathan for the cartoon figures in Chapter 3; and Justin Silpe for patiently teaching me SPR and listening me to complain about it every step of the way. I also am grateful for all the fruitful discussion over the years,

especially with Dr. Blake Erickson, Dr. Ahleah Rohr Daniel, Dr. Becky Matz, Dr. Flora Fang, and Meagan Cauble. I've also had the pleasure of working with two great undergraduate students over the years, Christina Nieh and Gül Öncü, who should not go unnoticed.

I have also had some wonderful collaborations outside of the University of Michigan. I would like to thank the Low group of Purdue University for providing the folic acid derivative used in Chapter 4. Also, Kumar Sinniah and his group at Calvin College for taking the time to teach me ITC and the related work in Chapter 5.

The access, support, and instruction for all the various instrumentation utilized in this work has been excellent. My thanks go out to Tracy Stevenson for making sure things were always running smoothly, the Chemistry Department NMR Services and Mass Spec services and their corresponding staff, and Brian Shay of the Biomedical Mass Spectrometry Facility.

Of course, no research is free so I want to thank the University and Chemistry Department for their financial support, the Rackham Merit Fellowship, and National Institutes of Health for funds. Also, my thanks go to Dr. Nancy Kerner for giving me an opportunity to fall in love with undergraduate teaching, which has added so much to my own education.

Last but certainly not least are all the people outside of the lab that have supported me all this time. My family (Nick, Mom, Dad, Nicole, Grandma, and Grandpa) for all their love. My Rackham Merit gang (Anna, Se Ryeon, Heidi) who've been there since day one. My non-Chemistry friends for when I needed to just get away. And my hockey team, the Crows, for giving me an outlet for all that free time and leftover energy!

Table of Contents

List of Figures

List of Tables

List of Schemes

List of Appendices

Glossary

βCD…….β-cyclodextrin

Ac ……. acetylated

AFM ……... Atomic Force Microscopy

BSA ……..…… bovine serum albumin

CO ……. cyclooct-1-yn-3-glycolic acid

Con A ……. Concanavalin A

D ……. G5-G5 dimer

Da …….. Dalton

DHFR ……. Dihydrofolate Receptor

DI ……... Deionized water

DMSO ……. dimethylsulfoxide

DNA ……. deoxyribonucleic acid

EDC …… 1-ethyl-3-(3-dimethylaminopropyl)carbodiimide

Equiv …….. equivalents

ESI …….. Electrospray Ionization

FA ……. folic acid

FAR ……. folic acid receptor

FBP …… folate binding protein

FC …….. Flow Channel

FDA …… Food and Drug Administration

g .....……...gram

G …….. generation

GPC ……. Gel Permeation Chromatography

HFBI ……...…… Class II hydrophobin

HPLC …….. High Performance Liquid Chromatography

IR ……. Infrared

ITC ……... Isothermal Titration Calorimetry

L ……. liter

LacNAc ……... N-acetyllactosamine

m …...……. meter

M ……. molar

MALDI-TOF…..... Matrix-Assisted Laser Desorption Ionization Time-of-Flight

MALLS …… Multi Angle Laser Light Scattering

MFCO ……... Click-Easy™ Monofluorinatedcyclooctyne-N-hydroxysuccinimide

min ……...…… minutes

MS ……. Mass Spectrometry

MTX ..... methotrexate

NHS ..... N-hydroxysuccinimide

NMR ..... Nuclear Magnetic Resonance

pAcPhe ..... p-acetylphenylalanine

PAGE ..... polyacrylamide gel electrophoresis

PAMAM ..... poly(amidoamine) dendrimer

PBS ..... phosphate buffered saline

PDI ..... polydispersity index

PEG ..... polyethylene glycol

PEI ..... poly(ethylenimine)

RCA_{120} ..... *Ricinus communis* agglutinin

resp diff ..... response difference

RNA ..... ribonucleic acid

rp ..... reverse phase

RU ..... response units

sec ..... seconds

SEC ..... Size Exclusion Chromatography

SPR ..... Surface Plasmon Resonance

TEM ..... Transmission Electron Microscopy

TFA ..... trifluoroacetic acid

tfRFP ..... tetrameric far-red fluorescent protein

UPLC ..... Ultra-Performance Liquid Chromatography

UV/Vis ..... Ultraviolet/Visible

XTT ..... 2,3-Bis(2-methoxy-4-nitro-5-sulfophenyl)-2*H*-tetrazolium-5-carboxanilide salt

Abstract

Heterogeneity, whether from polydispersity within the polymeric scaffold or due to a broad distribution of covalently conjugated products, is a remaining challenge in theranostics. Chapter 1 of this thesis presents the challenges conjugate heterogeneity introduces to synthesis, characterization, and application of multivalent conjugates. A brief review of recent literature approaches to address sample heterogeneity is also provided. Chapter 2 highlights the heterogeneity of the scaffold of interest, poly(amidoamine) dendrimer. It was found that the mass range of commercial polymer was ~1.4-115 kDa, and that skeletal defects in the dendrimer structure occur at a rate of 8-15%. Methods to isolate dendrimer monomers with decreased polydispersity are introduced. Chapter 3 of this thesis presents the first application of these monomers as soft superatoms for the assembly of new, precise nanostructures. New chromatography strategies to obtain ligand-dendrimer conjugates with precise ratios are introduced, and these conjugates are employed as building blocks for novel megamers. In Chapter 4, dendrimers with precise numbers of ring-strain promoted click ligands are clicked to folic acid-azide derivatives to synthesize dendrimer-folic acid conjugates with narrow ligand-to-dendrimer ratio distributions. These materials are evaluated for binding to a folate binding protein, and the results used to interpret the mechanism of increased binding of these conjugates compared to free folic acid. Mathematical models were developed to differentiate between three proposed mechanisms, and it was determined that the observed increase in avidity is due to nonspecific interactions between the polymer scaffold and protein, which are initiated by a specific interaction between folic acid and the protein. Chapter 5 examines the impact of scaffold size, ligand-to-scaffold linking systems, and conjugate valency on the activity of dendrimer-methotrexate conjugates. The larger mass and diameter of dimer impurities contributed significantly to observed activity of these and previous conjugates. The weaker methotrexate-folate binding protein interaction was not strong enough to key the nonspecific interactions until higher valencies in larger conjugates. The final chapter provides conclusions as to how this

thesis impacts the current field of multivalent conjugates for targeted drug delivery, and gives some insight to where the field must continue to grow.

Chapter 1

Multivalent Polymers for Drug Delivery and Imaging Agents: the challenges of conjugation

This chapter is written as a review article for Biomacromolecules.

The promise of multifunctional polymer scaffolds for therapeutics and diagnostics

Conjugation of polymer scaffolds with multiple copies of targeting ligands, drugs, and dyes has become a popular approach for achieving the aim of "theranostics"; materials useful for both diagnosis and treatment of disease (Figure 1.1).[1-3] Such materials may include enhanced targeting via multivalent binding and optimal impact at the target via delivery of a multidrug payload. In this manner, researchers hope to improve a drug's therapeutic index.[4-7] This critical review examines work to date addressing challenges common to all multivalent polymer-based efforts: heterogeneity introduced by conjugation strategies. First, the source of conjugation heterogeneity will be examined, and some examples will be given of how such heterogeneity is encountered and treated in the literature. We will then discuss why heterogeneity is often overlooked and how it can impact the behavior of multivalent theranostics. Finally, we will review several

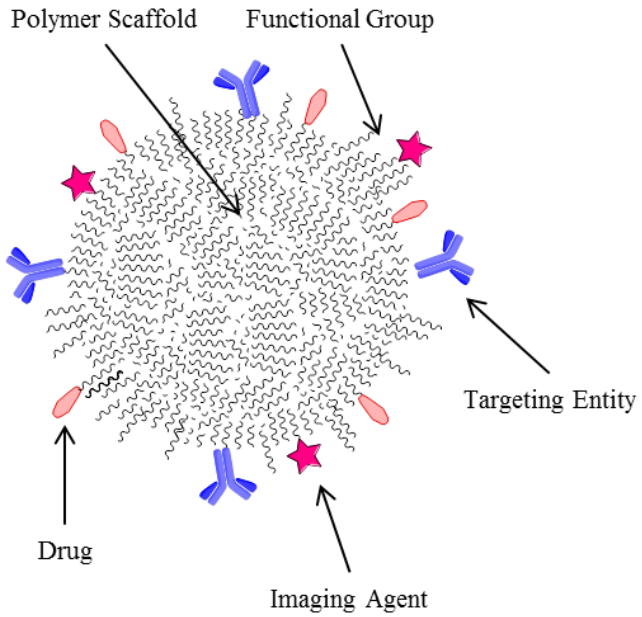

Figure 1.1. Theranostic consisting of targeting agents, drugs, and imaging agents to a polymer scaffold with many functional groups, which may be at the terminal ends of the polymer or spread within the polymer backbone.

interesting approaches from the last ten years to overcome conjugation heterogeneity. Scaffold heterogeneity (i.e. polydispersity index of the polymer) is also an important consideration for developing well defined, clinically relevant polymer therapeutics. Scaffold polydispersity is dependent on both the chemical nature of the polymer (common examples being polyamines and polyethylene glycol) and the backbone structure (linear, branched, dendritic). For this review, scaffold heterogeneity will only be discussed to the extent it directly impacts conjugation heterogeneity.

Approaches to Forming Conjugates on Multivalent Polymers

Attachment of multiple copies of targeting ligands enhances binding of the conjugate to cells and tissues that overexpress a certain receptor.[8, 9] Active targeting can minimize negative side effects in healthy tissues and allow for a higher tolerable dosage of drug. High loading of molecular drugs, such as chemotherapeutics like methotrexate[8] or antibiotics like vancomycin,[10] onto the polymeric scaffold,[11-13] enables multivalent delivery of the drug to the same cell. Commonly, multivalent conjugation of fluorescent dyes is performed, either by design or chance, to allow for *in vitro* and *in vivo* imaging of the polymer conjugate. Two[14-17] or three[18-21] subsequent multivalent modifications are performed on the same scaffold to create a multifunctional, targeted, drug delivery vehicle that can be tracked by fluorescent microscopy. Coupling reactions are often accomplished by one-pot or sequential attachment of the ligands to the scaffold to achieve the desired ligand-to-scaffold ratio. The polymer scaffold must have many sites available for chemical modification of the desired ligands; for example, poly(amidoamine) (PAMAM) dendrimers have (theoretically) 4 to 4000 primary amines depending on generation (G1 – G11), available for peptide coupling.[22, 23] For non-dendritic scaffolds, the number of functionalizable sites varies by formulation, architecture (branched, linear), and molecular weight. For example, consider a generic case where a multivalent scaffold with a large excess of functional sites conjugated to 4 targeting ligands, 5 copies of a drug, and an average of 3 molecular dyes as commonly represented in the literature by an image such as the conjugate illustrated in Figure 1.1. Because each conjugation is a result of a statistical combination between available sites

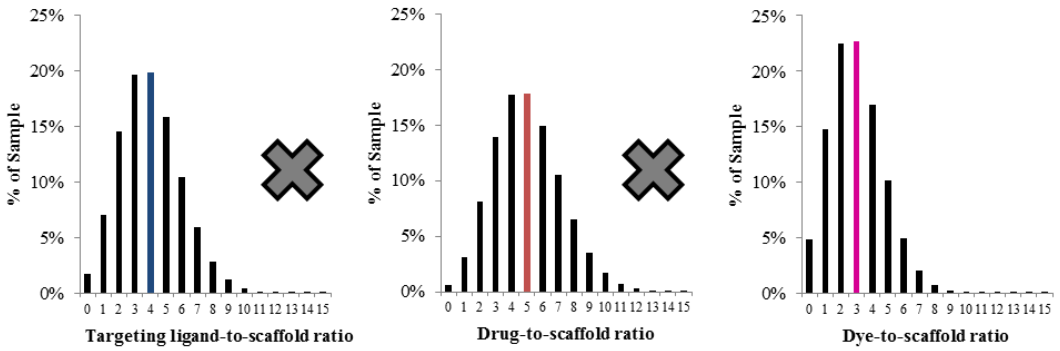

Figure 1.2. Distributions resulting from stochastic conjugations with an average of 4, 5, and 3 have a cumulative, multiplicative effect on sample heterogeneity. With each subsequent serial conjugation, the resulting set of products is the product of the resulting Poisson distributions.

and equivalents of ligand, a Poisson distribution of products is produced (Figure 1.2). In the case of attaching 5 targeting agents to the scaffold, approximately 14 unique species are produced with targeting ligand-to-scaffold ratios ranging from 0 to 13. Although the dendrimer conjugated to 4 targeting agents is the most common species in this theoretical conjugation, it only represents approximately one in five (20%) of the sample. To further complicate matters, heterogeneity due to stochastic conjugation is cumulative. When the targeted vector sample is further reacted with 5 equivalents of a drug, a new distribution is created. Again, approximately 15 drug-to-vector ratios are present in this new sample, with approximately 9 in 50 (18%) particles having exactly 5 copies of the drug attached. However, there are now over 200 unique species present in the sample resulting from the product of the first two Poisson distributions. After adding a third entity (3 equivalents of dye), there are now approximately 2,500 unique species present in the sample. The single entity pictured in Figure 1 illustrates the mean number of each individual distribution (i.e. 4 targeting agents, 5 drugs, 3 dyes), but it represents just 1 out of every 250 (0.8%) particles present. Although it is the "average" material present, this mean may well not be meaningful average in terms of biological behavior for any of the functional behaviors; targeting, therapeutic effects, or imaging characteristics. In addition, for any observed function of this material, whether in cell culture or *in vivo*, a very large challenge is presented to understand which fraction(s) of the 2500 species are providing the desirable activity.

The challenges inherent in these distributions can be further explored by considering some of the quantitative aspects. Two percent of the sample contains no targeting entity; therefore attached drug will be systemically delivered. One out of every 25 (4%) particles has fewer than 2 drugs attached and no longer has the potential for increased activity compared to the free drug. One particle in 20 (5%) has no dye on it and is essentially "invisible" to further analyses. One particle in 20 also has twice the amount of expected dye, and 1 in 100 (1%) particles has three times the average amount of dye, the consequences of which will be discussed later. The preceding analysis has not yet considered the heterogeneity of the sample resulting from the polymeric scaffold, which can vary greatly, or spatial and regioisomers, which can further impact the system. For polymer systems containing substantially restricted motion of the surface groups, spatial isomers can rapidly lead to tens of thousands of functionally different isomers from a targeting, and possibly therapeutic, standpoint for the simple example illustrated in Figure 1. Size heterogeneity can lead to the presence of the > 2500 species present from statistical consideration on materials with remarkably different biodistribution properties. For example, although polymers in the 20-30 kDa range are expected to be excreted through the kidney, oligomers of 60-100 kDa may instead be trafficked to the liver. This full statistical range of materials for each mass range generates further challenges for understanding the origin(s) of both the positive, desired effects as well as origin(s) of the negative side-effects.

Analysis of Conjugation Heterogeneity in the Literature

The above example was a theoretical conjugation; however similar serial conjugations are often encountered in the literature. Explicit analysis to determine even averaged conjugation numbers are often not reported with product averages assumed from initial stoichiometry, further complicating the understanding of the material present. Instead, authors give a visual which "represents" the product, or provide a percent loading of drugs etc. A theranostic synthesized by Baker et al.[8] of G5 PAMAM covalently conjugated to 5 dyes (FITC), 5 targeting ligands (folic acid), and 5 methotrexates showed promising *in vitro* and *in vivo* activity. Close examination of this conjugate reveals that

the three stepwise conjugations result in over 4,000 unique combinations. Only one particle in 200 (0.5% of the sample) has 5 copies of each ligand. Additionally, both folic acid and methotrexate have two carboxylic acids that can react with the amines of the scaffold (one isomer being more active than the other); leading to 14,400 possible combinations of generation 5 PAMAM (M_N~28 kDa, PDI~1.1, with ~110 functional groups) conjugated 5 folic acids and 5 methotrexates. Consequently, less than 1 in 2 million particles (0.00005%) have the average valency of all three ligands conjugated in their most active form. Mullen et al. employed a different approach to generate FITC/folic acid conjugated dendrimer system.[24] First, a generation 5 PAMAM was conjugated to an average of 1.6 alkyne functionalized click chemistry linkers and 3.5 folic acids, generating ~117 combinations. A second sample was conjugated to an average 2.5 azide click ligands and 3.2 FITC dyes, generating ~140 unique combinations. The two samples were then "clicked" together to give a barbell-like dimers with an average of 3.5 folic acids and 3.2 dyes. However, around one in five particles of the alkyne material, and two particles in 25 (~8%) of the azide material contained zero click ligand and was unable to undergo the reaction. Over 80% of both samples contained multiple click ligands, allowing for larger-than-dimer structures to form. Of the material that does form dimers, ~180 combinations of dyes and targeting agents are still possible, of which one in 25 (4%) are still without a dye and 1 in 33 (3%) are untargeted. In another example, Minko et al.[20] reported a comparison of three scaffolding systems: a bifunctional PEG, a G4 PAMAM (M_N~14kDa, PDI~1.1, with ~64 functionalizable groups) conjugate, and a liposome. The systems incorporated a luteinizing hormone-releasing hormone (LHRH) decapeptide as a targeting agent, cyanine Cy5.5 as an imaging agent, and paclitaxel, a chemotherapeutic. Equivalents of each molecule added or a final average number of conjugates was not reported, however a cartoon of the PAMAM conjugate implies that 2 LHRH units, 2 dyes, and 2 drugs were covalently attached. However, this single image depicted in the cartoon is just 1 of ~1,500 (0.07%) species that would exist in a conjugation with these averages, assuming good mixing during the synthetic procedures and a stochastic distribution. Of these many species, 200 (13%) would have no dye attached and 200 would not contain a single targeting moiety. Consequently, 30 particles (2% of the sample) is both untargeted *and* "invisible" by

fluorescent microscopy, so its *in vivo* destination remains a mystery. In the bifunctional PEG system that was also studied, two modified PEGs were mixed together. In this case, only 6 combinations of PEG units are possible (completely unmodified PEG, 3 monofunctionalized PEGs, and 2 bifunctionalized PEG). However, no single PEG unit contains all three entities in this formulation. Holler et al.[25] introduced a particularly complex system involving the serial covalent conjugation of a mouse anti-human TfR mAB (RVS10) as a targeting moiety, AlexaFluor 680, 2 antisense RNA sequences, and PEG to poly(β-L-malic acid) (PLMA) (Mw~50kDa, PDI~1.3, ~435 functionalizable carboxylic acids). In this case, the amount of each entity was reported in terms of percentage of backbone modified. A brief mathematical analysis reveals that, assuming a 50 kDa polymer, each polymer unit contains on average only 1 targeting entity, 11 dyes, 11 copies of each RNA sequence, and around 22 PEGs. The result is around 20,000 unique species (without considering another entity incorporated into the backbone at a high loading to allow endosomal escape). Seven out of every 20 (35%) of these polymers is untargeted. Additionally, there are 600 unique combinations of the two therapeutic sequences present. In this discussion of conjugation heterogeneity, spatial isomers resulting relative placement of each entity along the polymer background was not explicitly considered, and would result in >100,000 species.

Characterizing Sample Heterogeneity

Heterogeneity in polymer conjugation is often overlooked or underestimated due to the difficulty in "seeing" it using traditional characterization tools. Many examples in the literature generate an equivalent to the product schematic in Figure 1 via experimental values that give an "average" value for the entire sample, such as nuclear magnetic resonance or UV/Vis and IR spectroscopies. Although such average values are not incorrect, they do not give any information about the distribution of species present. Non-averaged techniques can also be problematic for characterizing sample distributions due to conjugation because of the presence of mass and structural distributions of the scaffold. Dendrimers are often touted as having some of the lowest polydispersity indices (PDIs) for a polyvalent scaffold with values reported well less than 1.1. However,

G5 PAMAM dendrimers (considered to be highly homogeneous compared to linear or branched polymers) have been shown to have branching defects leading to mass ranges of ~8,000 Daltons (even after oligomer and trailing defects are removed),[26] compared to the molecular weights of the molecular drugs or dyes which are generally under 1000 Daltons. Therefore, the distribution of molecular weights generated by multivalent attachment of such ligands is generally narrower than the mass distribution of the polymer scaffold itself (even for a highly monodisperse polymer like a dendrimer). Mass spectrometry or size exclusion chromatography are generally incapable of distinguishing the unique species.[27, 28] Chromatographic techniques, such as high performance liquid chromatography (HPLC), have recently been shown to have the potential to be used to visual conjugate distributions of hydrophobic ligands on hydrophilic dendrimers (Figure 1.3).[27-31] This visualization allows for analyses of the mean and median of conjugation, as well as the full distribution of ligands/dendrimer present within a sample. In order to enable such an analysis, the chromatographic methods employed must be tailored to resolve the entities (i.e. stationary phase selection, mobile phase gradient development). Such processes can be time consuming and are not applicable to all scaffold and ligand systems. However, at present, these approaches offer a powerful window into the details of conjugate heterogeneity for some classes of bioconjugates.

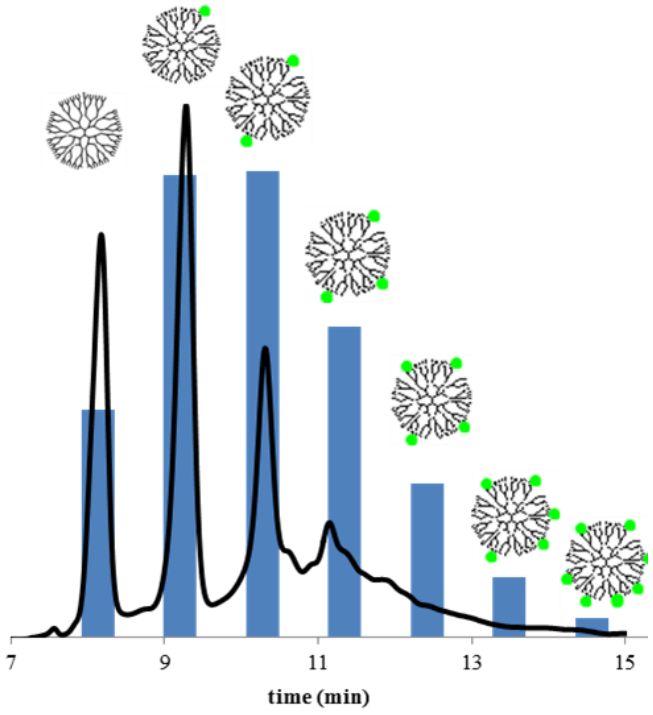

Figure 1.3. HPLC chromatogram of an average conjugate overlaid with the predicted distribution for an average of 2 ligands-per-particle.

The previous scenario assumed perfectly random statistics, which is not necessarily the case for real samples where properties such as mass transport, solubility, and cooperativity in binding

may be encountered. Non-ideal conjugations can lead to drastically different samples that "appear" the same by various characterization techniques (Figure 1.4). Mullen et al.[28, 32] examined a scenario where non-optimal reaction conditions created a less reactive subpopulation within the parent scaffold. In the optimized case (Figure 1.4a), a Poisson distribution of ligand-to-scaffold ratios is observed, with around 4% of the material having no ligands, and around 7% being monofunctional. However, the non-ideal distribution generated by the non-ideal conjugation has 4 times as much unfucntionalized material, and 10% monofunctionalized material. These two vastly different samples would appear the same by NMR spectroscopy, but likely have immensely different biological profiles.

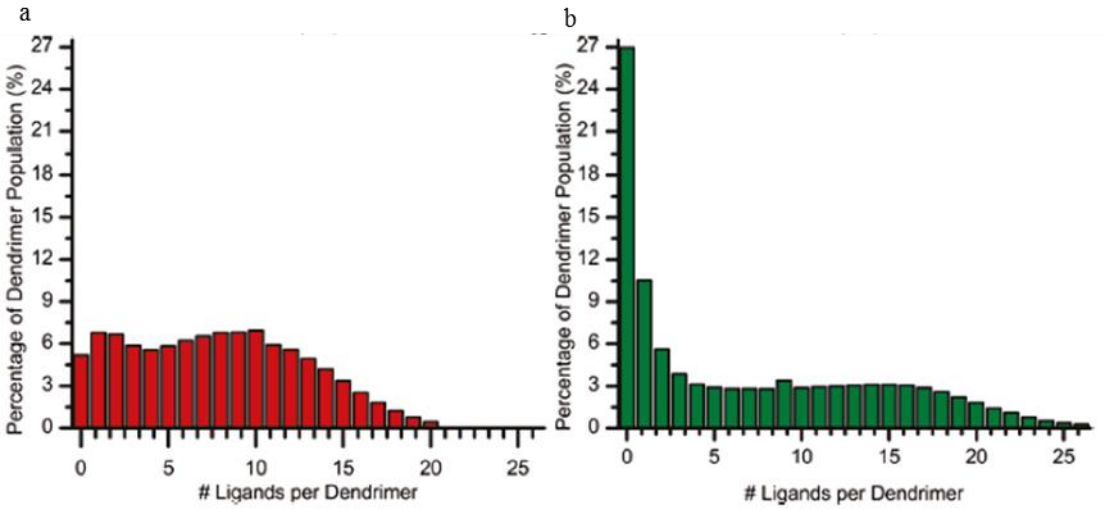

Figure 1.4. The distributions of samples from two actual conjugations with an average of 6.8 ligands-per-dendrimer scaffold generated by (a) conditions where mass transport was effective and (b) conditions in which ineffective mass transport hindered the reaction. Adapted from Mullen et al., *Accounts of Chemical Research*, 2012.

Impact of Conjugation Heterogeneity on Multivalent Behavior

The modes of multivalent binding have been thoroughly reviewed elsewhere.[33, 34] Briefly, three mechanisms are generally described to explain the favorable influence of multivalency on binding kinetics (Figure 1.5). The first mechanism is effective concentration. Attaching multiple copies of a ligand to a single scaffold in essence "prepays" the entropic penalty of achieving high local concentrations. This local increase

in concentration is higher than the equivalent solution concentration containing the same amount of free ligand, as the scaffold immobilizes the ligand in a defined volume (Figure 1.5a). Statistical rebinding describes the increased chance of a reattachment of the ligand/target interaction upon dissociation of the initial event, due to the high local ligand concentration (Figure 1.5b). The localization of additional ligands increases the chances that, upon dissociation of the initial reaction, the same conjugate will rebind to the protein. Both of these concentration-dependent mechanisms become important when considering sample populations like those in Figure 1.4. There is a significantly larger population of particles in the non-ideal (Figure 1.4b) sample with ligand-to-scaffold ratios over 15 (~20%) as compared to the ideal case (Figure 4a, ~7%). This population would have a much greater effective concentration than the average sample, which has less than half as many ligands attached. This high population will likely decrease the time needed to form a single binding event with a target, such as protein on a surface. On the other hand, the non-ideal sample also has significantly more unfunctionalized and monofunctional material, which will have distinctly different binding behavior as the effective concentration is much lower, and re-binding events are less favored. The third mechanism, the chelate effect, describes the ability of a multivalent conjugate to undergo multiple binding interactions, which can increase avidity more than the sum just the sum of the independent interactions. This

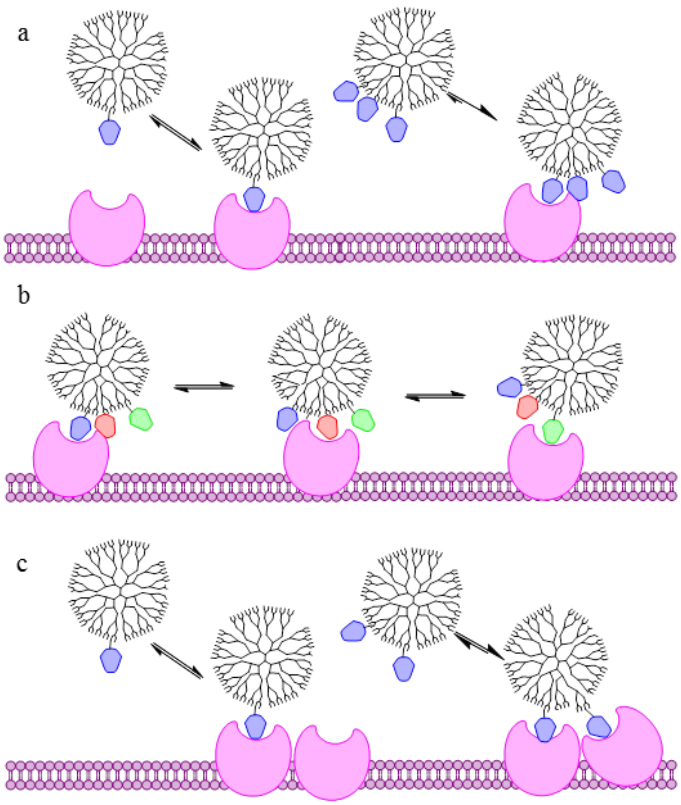

Figure 1.5. Multivalent mechanisms (a) Effective concentration increases chances of binding. (b) Statistical rebinding is higher for multivalent conjugates if the original interaction dissociates. (c) The chelate effect allows for multiple interactions through one conjugate

mechanism, which is likely the first that comes to mind when discussing multivalency, can be achieved by 98% of the blue population in Figure 4, but only 80% of the red population. These mechanisms work together, and large differences in behavior as a function of sample distributions can be expected.

Measuring Multivalent Behavior

Multivalent conjugates are oft touted as having favorable kinetic, thermodynamic, and biological activity compared to their monovalent and/or small molecule counterparts. This behavior is typically demonstrated by *ex vivo* and *in vitro* methodologies that show an increase in a desired behavior (i.e. binding, inhibition, toxicity) for the conjugate species. Problematically, like many characterization techniques, these methods are often "average" techniques that are incapable of measuring separate contributions from different species within a sample distribution. Surface plasmon resonance (SPR) spectroscopy is employed to measuring the association and dissociation rates of multivalent ligand-conjugates being flowed over a surface functionalized with that ligand's receptor.[35, 36] Although each unique binding or dissociation event is measured by this sensitive technique, the signal observed is the summation of all simultaneous events. Therefore, it is impossible to extract the contribution of each individual species to the overall kinetic measurement. A detailed example is provided in the next section. Thermodynamic information about multivalent interactions can be measured by Isothermal Titration Calorimetry (ITC), which measures the enthalpy and stoichiometry of binding in solution.[37] Like in SPR, however, the values obtained are averaged across the entire solution. Neither of these techniques can discriminate differences in binding affinities, for example, between a bivalent and trivalent interaction occurring from separate species within a sample. Instead, the observed measurement is a weighted average of all species within the sample. Assays of biological activity, for example to measure cellular uptake,[38-40] activity inhibition,[41-44] or cytotoxicity[8] of a conjugate are commonly employed to demonstrate clinical advantages of multivalent conjugates. However, such techniques are incapable of identifying the active components within a heterogeneous sample. In addition, for in vivo assays, large differences in particle hydrophobicity caused by different total numbers of particles per

particle has the potential to substantially change bio-localization properties. Thus, changes in activity can be further complicated by differential localization. It is not unfeasible, for example, to imagine that the high average subpopulation in Figure 1.4 could be responsible for the majority of cytotoxicity, even though it only composes half of the sample. The presence of an inactive population would consequently lead to an underestimation of biological activities of active species because of an overestimation of concentration.

Challenges in Interpretation of Models

The presence of a range of ligand-to-scaffold ratios complicates evaluation of physical models of multivalent activity. Without a solid understanding of the distribution of conjugates present within a sample, it becomes impossible to assign the active components in the mixture. What minimum valency is needed to accomplish a multivalent interaction on a surface? Is there a kinetic advantage to achieving higher valencies? At what valency do thermodynamic effects (i.e. reduced solubility, steric crowding) negatively impact binding? How can activity differences be explained for samples that appear the same by other techniques such as NMR? Mechanistic understanding of multivalent behavior would allow for designing new conjugates with optimized behavior, but to date has remained an elusive challenge. Let us consider a specific example from the literature. In 2007, Banaszak Holl et al. examined the binding of a series of stochastic G5 PAMAM conjugates to folic acid via

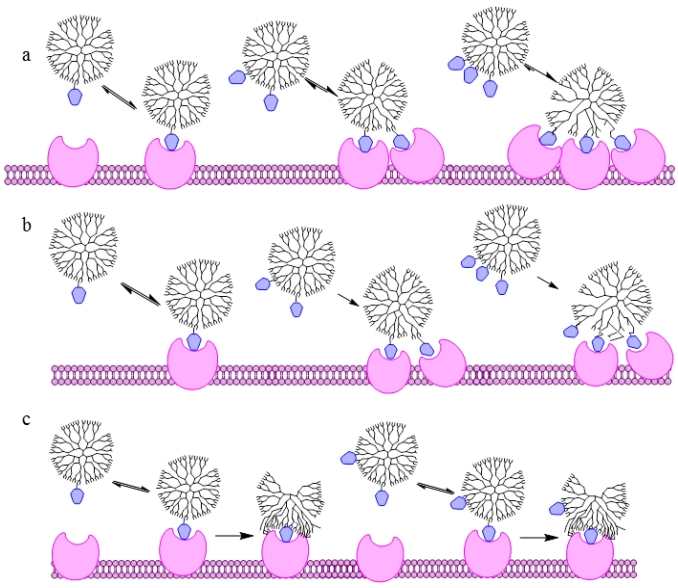

Figure 1.6. Three proposed mechanisms proposed to explain G5-FA binding behavior. (a) Avidity increases with valency. (b) Two populations experience two different binding mechanisms. (c) Folic acid keys a stronger, nonspecific interaction between the conjugate and protein.

SPR.[36] A decrease in dissociation constant was observed as the average valency of the conjugate was increased from 2.6 to 13.7. The authors proposed a mechanism to explain this trend in which dissociation slows with each additional conjugated folic acid because a new ligand-protein interaction is formed (Figure 1.6a). However, upon further consideration of the distributions of folic acid-to-dendrimer ratios present in such samples, the authors proposed a different mechanism.[45] This model establishes two binding populations for each sample; monovalent conjugates that are only capable of weak, reversible interactions, and multivalent conjugates with two or more folic acids which all experience a strong, irreversible binding (Figure 1.6b). This model attributes differences in dissociation between samples not to separate mechanisms, but to the decrease in zero and monovalent material as the overall average increases (Figure 1.7). A third model was proposed by Licata and Tkachenko in 2008.[46] This model attributes the increased interaction of the conjugate to be due to nonspecific interaction between the protein and dendritic scaffold. This interaction must initially be keyed by the specific interaction of folic acid and folate binding protein (Figure 1.6c). The presence of 8 or more species with folic acid valency ranging from 0 to 20 in the original samples make distinguishing which mechanism is responsible for the observed behavior impossible. For example, imagine the two distributions with an average of 6 were in Figure 4 represent two conjugations of G5 PAMAM to folic acid that were tested in a similar study. The original mechanism would likely show an overall stronger binding for the non-ideal case, because it contains significant materials with 15 or more folic acids that would experience much stronger binding than anything in the ideal sample. However, the non-ideal

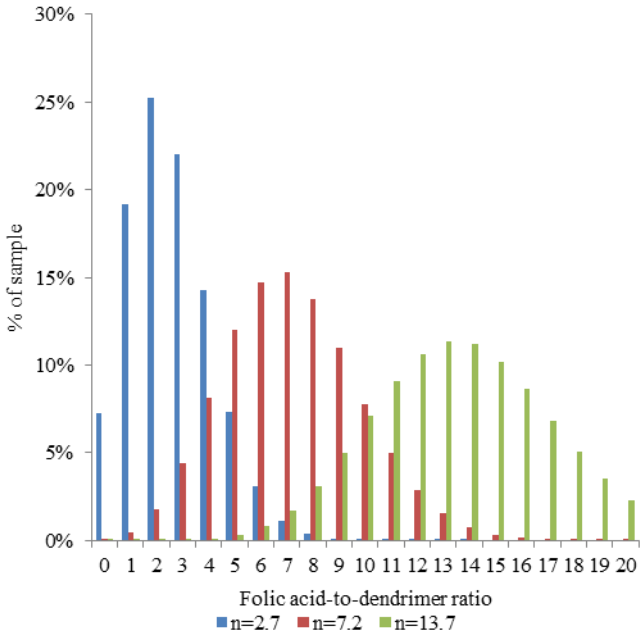

Figure 1.7. Ideal distributions for three G5-FA conjugates.

conjugation has ~14 in 100 particles (14%) monovalent material compared to just 1 in 100 (1%) in the ideal conjugation; therefore the second model would predict weaker overall binding for the non-ideal case. The third mechanism would likely not distinguish between the two samples beyond a ~5% decrease in signal, because binding strength has no increase with valency.

These problems translate to more complicated biological experiments, the effects of which are difficult to measure. Earlier, problems due to multiple conjugations were introduced, such as the presence of non-targeted particles, "invisible" particles without dye, or monovalent drugs without improved activity profiles. The preceding example, however, hints that heterogeneity can cause complications due to single distributions, as well. The possible effects of ligand-to-scaffold distributions will be closely examined the next section.

Impacts of Conjugate Heterogeneity in Biological Applications

Targeting and Specificity. In 2011, a simulation study by Martinez-Veracoechea and Frenkel on targeting specificity determined the relationship of ligand valency and binding strength to conjugate specificity to a biological target with high or low expression of a receptor.[47] The authors concluded that monovalent conjugates had no specificity regardless of receptor density; absorption varies linearly with receptor density. Multivalent conjugates, by contrast, exhibit super-selective behavior (i.e. absorption increases much faster than linearly with receptor density). Therefore, low concentrations of multivalent conjugates can specifically target cell surfaces that are overexpressing a receptor protein, without affecting low expressing, healthy cells. However, stochastic multivalent conjugates with average ligand-to-scaffold ratios of ~5 or less have significant populations of unfucntionalized or monovalent conjugates. The monovalent species will bind to healthy or unhealthy cells equally, and may still be up taken via a receptor mediated pathway. There is also the possibility that valency may influence the localization of a conjugate within a patient's body, tissue, or cells. Figure 1.8 presents a scenario where unfucntionalized materials bind non-selectively to a cell membrane (a possible case for positively charged polymer scaffolds), whereas functionalized particles

can bind to a surface receptor and be up taken via receptor mediated endocytosis.[48] In this hypothetical case, monovalent species cannot cause receptor clustering and endocytosis does not occur. By contrast, conjugates with 2 or more ligands are up taken, and may escape into the cytosol. However, over functionalized conjugates (with 5 or more ligands) are too hydrophobic to escape and are trapped within lysosomes and do not deliver their payload. In this case, all therapeutic activity measured would be from the subset of particles with 2-4 ligands-per-scaffold, while the remainder of the sample (at least 40% of the total) does not reach the intended target. The identification of such "active" populations for real samples, however, is impossible with stochastically synthesized conjugates.

Therapeutic Effects. Beyond localization effects, the biological behavior of conjugates has been shown to vary as an effect of valency. The simplest mode of therapeutic enhancement is the delivery of a higher drug payload to a single cell than the monovalent equivalent. The amount of drug delivered, of course, varies directly with conjugate valency and therefore a conjugate with a distribution of drug-to-scaffold ratios will exhibit a distribution of effective enhancement, with the measured enhancement being the

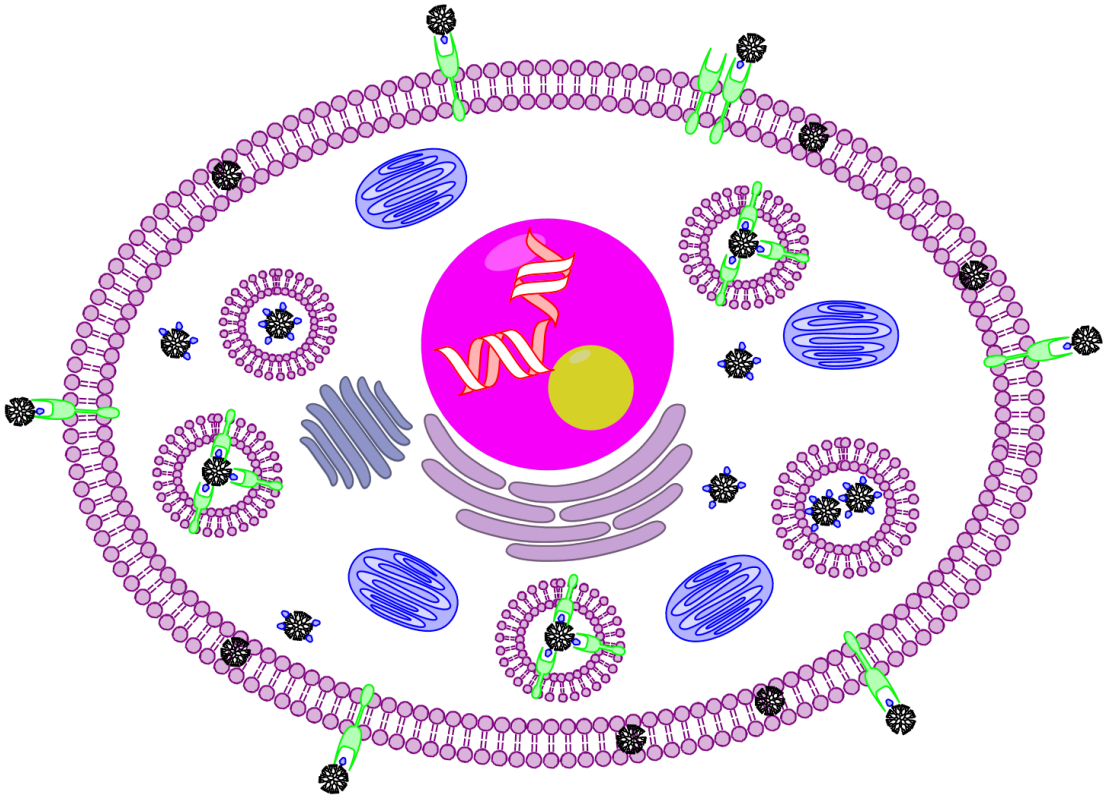

Figure 1.8. Conjugate valency may affect the biodistribution of the scaffold inside a cell or tissue.

average valency. However, a study by DeSimone et al.[49] observed a new behavior at high valency that was not observed at all in low valency conjugates or the monovalent ligand. The authors demonstrated that non-toxic transferrin and transferrin antibodies, which are employed as ligands to target various cancers for drug delivery, when multivalently conjugated to a PRINT nanoparticle, exhibit selective toxicity to a Ramos lymphoma cell, while remaining non-toxic to solid tumor cells and healthy kidney cells. The exhibition of novel behaviors at high valencies can create subpopulations within a sample with entirely unique properties. In our non-ideal conjugation in Figure 1.4, for example, the high average population may have desired cytotoxicity while the remaining 50% of the sample would be inactive.

Imaging Agents. Organic dyes are used as fluorescent probes in order to image biological processes, however, organic dyes are prone to photobleaching and self-quenching. The effects of the dye can change once conjugated to a polymer which can make polymer-dye conjugates useful for biological imaging. Poly(amidoamine) (PAMAM) dendrimers conjugates have shown promise as MRI contract agents, since they are large enough to prevent extravasation which is necessary for an effective imaging agent in biological tissue.[50] In 2013, Schroeder et al. determined the enhancement of organic fluorophore optical properties once conjugated to a G5 PAMAM or a G6 PAMAM dendrimer in order to create a new set of materials for biological imaging with enhanced stability and increased accuracy in single molecule imaging. Cy3 and Cy5 dyes were both used in order to determine if their organic properties could be optimized.[51] The fluorescent dendrimer nanoprobes (FDN) they synthesized showed that the stochastic materials they synthesized with average of 8 and 14 Cy5 dyes[2]. Dendrimers with an average of 8 Cy5 dyes show slower photobleaching compared to the small molecule dye alone in solution with a 6 to 10 times increase in lifetime. The dendrimers with an average of 14 Cy5 dyes showed a 17 times increase in lifetime values. Schroeder et al. used these materials in single molecule fluorescence microscopy in order to determine localization of these materials in a cell. Sets of materials such as these are extremely useful biologically since the dendrimer allows for enhanced photostability and increased fluorescence intensity (brightness) which allows for more accurate imaging of where materials go in a biological environment that contain DNA, RNA, or proteins. Multivalent polymers such

as dendrimers are shown that they can be useful imaging agents due to their ability to change a small molecule dyes' photophysical properties to increase stability and also their ability to conjugate multiple dyes per polymer.

Synthetic Approaches to Overcoming Heterogeneity Problems in Multivalent Conjugates

As indicated above, heterogeneous product can complicate the synthesis, evaluation, and clinical application of these multivalent conjugates. Many synthetic approaches to overcome this problem have been employed (Figure 1.9). Methods that have employed include using high densities of ligands to avoid under-modified populations with limited activity, techniques that create clusters of ligands to optimize local concentration effects, and the synthesis of precise conjugates, using biologically inspired scaffolds and both bottom up and top down synthetic approaches, in which all species in the sample have the same ligand-to-scaffold ratio. In this section, we will provide a brief review of some successful applications of controlled multivalent conjugates over the last 10 years.

High Density Conjugates. At high percentages of modification, and assuming ideal or close to ideal conjugations (to avoid non-ideal popluations like the example in Figure 1.4), the amount of unmodified and low average conjugates becomes insignificant, allowing for benefits of effective concentration based multivalent behavior. The average distances between conjugated ligands on a

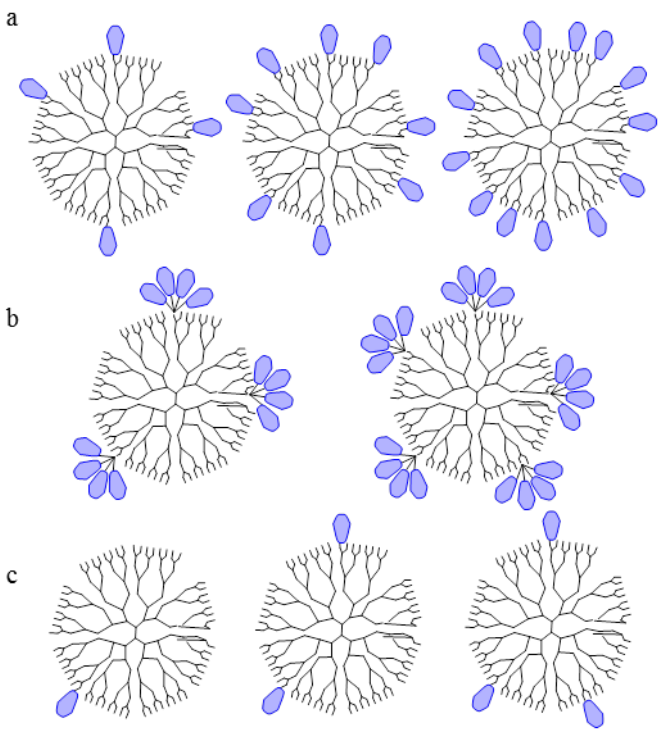

Figure 1.9. Synthetic approaches to control multivalency include (a) ligand density variation, (b) ligand clustering, and (c) synthesis of precise ligand-to-scaffold structures.

scaffold also decreases, and at some point it can be assumed that the ability to have chelate effect type multivalent interaction is limited by the scaffold size and not the relative location of the ligands.

One approach is the complete (100%) modification of a multivalent scaffold, which creates a conjugate where the heterogeneity is limited by the scaffold polydispersity. The most notable examples of such modification are glycodendrimers.[52-54] This class of materials is one of many that exhibit the "cluster glycoside effect", which is broadly used to describe the enhanced binding and activity of multivalent carbohydrates compared to the monovalent equivalent to proteins involved in a variety of biological events.[55] The surface groups of the dendrimer are modified with a saccharide via coupling or click chemistry, using an excess of the saccharide to ensure full conversion. In this way, absolute valency can be controlled by generation number, as the number of end groups scales with generation.[22] For example, in recent work by Jayarman et al.,[56] generation 2, 3, 4, and 5 glycodendrimers were prepared with an expected 4, 8, 16, and 32 mannos-6-phosphate valency, respectively. These structures were confirmed by NMR spectroscopy; however, mass spectrometry and elemental analysis failed due to the nature of the structures. The larger dendrimers had less-than-expected valencies (15 and 28, respectively). This example demonstrates the limit of such approaches in obtaining homogenous structures. Without further structural characterization, it is difficult to determine if the coupling reactions failed to go to completion, leaving unreacted carboxylic acids on the dendrimer, due to steric crowding. It is more likely, however, that this observation is actually a reflection of heterogeneity in the scaffold (PAMAM dendrimer), which is known to contain skeletal defects which reduce the average number of reactive groups and create a distribution of possible products including variation in terminal arm number.[26, 57] Another recent example of glycodendrimers by Riguera et al.[42] highlights the inherent coupling of size and valency by this technique. Generation 1-3 dendrimers with 3, 9, or 27 surface conjugated mannose units were prepared and evaluated by SPR for the ability to bind to high and low density Concanavalin A (Con A) surfaces. In this work, two separate binding mechanisms were observed: a low affinity binding for all generations on the low density protein surface, and a high affinity binding for the largest dendrimer on the high density surface. The authors point out that the

distance between proteins on the low density surface is greater than the diameter of any of the dendrimers, and the only monovalent effects possible are based on effective concentration and rebinding. However, the distance between the proteins on the high density surface allows for the generation 3 structure to experience the chelate effect. However, this work cannot determine what multivalent effects a larger but lower valency dendrimer would experience, and whether there is any additional benefit to fully functionalizing the dendrimer surface.

Other scaffolds have been 100% functionalized to achieve the glycoside cluster effect. Work by Jimenez Blanco et al.[43] exploited the architecture of β-cyclodextrin (βCD) to create multivalent precise, multifunctional mannose and lactose clusters with orientation specificity. A convergent synthesis of bifunctional dendrons followed by attachment to the βCD scaffold allows for precise control of both ligands and orients all the ligands in the same direction to maximize effective concentration effects. The resulting structures are monodisperse; however, unlike dendritic approaches this scaffold does not lend itself to easily increased valency or extending the reachable surface area of the conjugate. Renaudet et al.[44] employed a dendrimer-like multivalent display mannose. Their findings confirmed that display of 16 carbohydrates showed more multivalent interactions than a corresponding tetravalent unit. However, this work also used two linking systems to combine the four tetraclusters, and showed a significant enhancement of multivalent interaction with ConA with a more flexible linker. This observation hints at the importance of scaffold architecture in multivalent binding, a topic which will not be further explored here.

Other ligands beyond glycosides have been used to 100% functionalize multivalent scaffolds. In 2008, Mier et al. showed that a PAMAM dendrimer derivative can be functionalized with a variety of different averages of organic dyes in order to show a change in fluorescence intensity; they determined a dendrimer 100% functionalized with dansyl chlorides showed the highest fluorescence intensity. This conclusion is dye dependent as they also show a decrease in fluorescence when stochastically functionalizing a dendrimer with multiple coumarins, rhodamines, and fluoresceins.[58] Dendrons were also used as scaffolds for multivalent peptides by Welsh and Smith.[59]

First and second generation dendrons conjugated to precisely 3 and 9 Arg-Gly-Asp peptides were prepared and evaluated for integrin binding affinity as a potential cancer targeting agent. Although the trivalent dendron showed enhanced affinity compared to the equivalent monovalent peptide, the higher valency generation 2 dendron had lower affinity for the integrin. The authors speculate that this trend is due to steric crowding of the ligands, interfering with the interaction between the peptide and target. This study emphasizes the importance of identifying the ideal valency for complex biological systems.

As indicated by the peptide-dendron example, the higher-valency-is-better approach is not always optimal for multivalent activity. Complete modification of the scaffold is not always ideal, as well. Not all ligands can be solvated at such high valencies, and non-toxic ligands may become toxic at high valencies as discussed earlier[49], which may not always be a desirable trait. Therefore, the distribution problem has been addressed by Choi et al. by systematically increasing the ligand density to reach desired activity levels. This approach allows for the comparison of the multivalent behavior at low average and high average valencies. In addition to the PAMAM-folic acid sample detailed in an earlier section, generation 5 PAMAM conjugates to methotrexate, a chemotherapeutic, and vancomycin, an antibiotic, have been studied. In a recent study by Choi et al.[38], two conjugates with average methotrexate valencies of 5 and 10 were prepared and evaluated by SPR for binding to a folate binding protein, and tested for uptake into FAR+ KB cells. The higher averaged conjugate was found to have both stronger binding to protein surfaces of various densities, and higher uptake into the FAR+ cells. Interestingly, the high (n=10) average sample exhibited multivalent binding on an intermediately dense surface, as indicated by incomplete dissociation of the conjugate on the SPR timescale, whereas the low (n=5) conjugate did not. This lack of activity cannot be explained simply by considering the ~4% of the n = 5 sample that is unfunctionalized or monovalent (Figure 1.10a). Therefore, it must be assumed that the portion of the population that is active at this protein density is not present at significant concentrations in the n=5 samples but is in the n = 10, which likely places it somewhere at valency of ~7 or higher. Further studies would need to be undertaken to identify the exact ligand-to-scaffold ratio of the active entities in the sample. In a vancomycin conjugate SPR study, several ligand-

to-scaffold ratios ranging from 1.2 to 8.3 (Figure 1.10b) were tested for the ability to bind to two surfaces, one which mimicked vancomycin susceptible bacteria and a second which mimicked vancomycin resistant bacteria.[10] While free vancomycin did not significantly bind to the "resistant" surface, all of the multivalent conjugates did. Interestingly, the strength of binding was not influenced by valency, even when the average valency was increased from 1.2 to 8.3, a reduction of the monovalent population from around 180 particles of 500 (36%) to less than 1 in 500 (0.2%). This observation suggests that either the monovalent species is not participating at all in the binding and therefore is not observed, or that the mechanism of binding depends more on the attachment of the ligand to the scaffold than the valency (similar to the proposed mechanism for PAMAM-folic acid in Figure 6 c). A purely monovalent conjugate without the presence of a distribution of would be necessary to distinguish between these mechanisms. As demonstrated by these examples, employing high ligand density samples is an approach that can be successful in creating conjugates with desired properties, but it does not generally lead to mechanistic insight of the systems being studied.

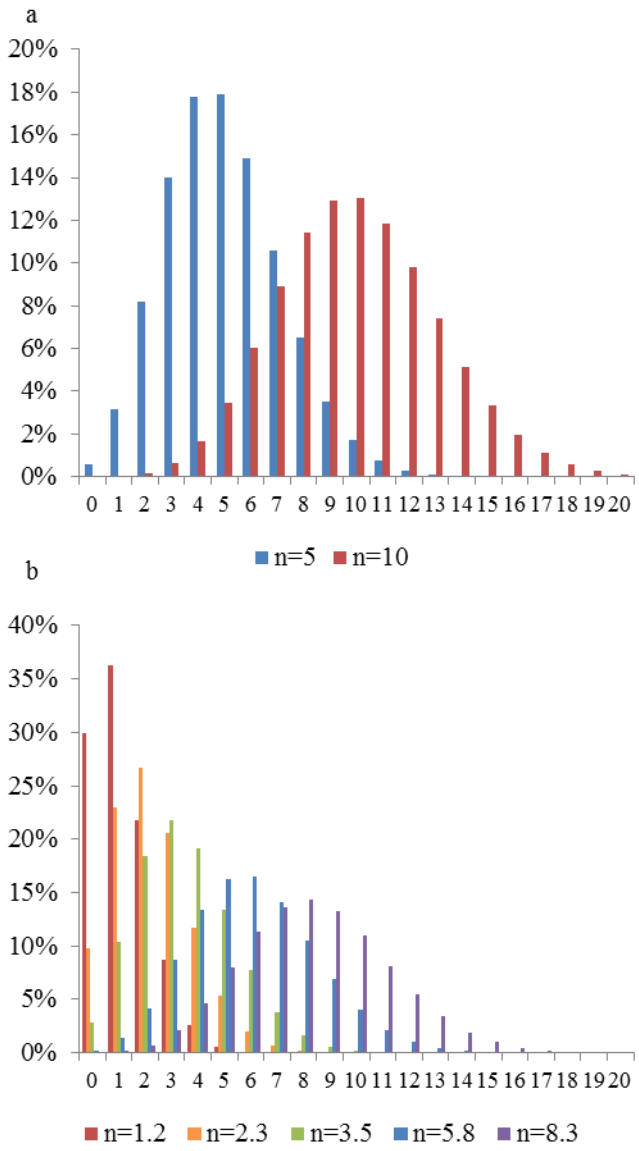

Figure 1.10. Distributions present in multivalent conjugates of PAMAM to (a) 5 or 10 methotrexates and (b) various amounts of vancomycin.

Ligand Clustering. High ligand densities are in part successful because they maximize local concentration and statistical rebinding mechanisms of multivalency. However, as alluded to in the preceding section, 100% modification is not possible for many ligand/scaffold systems due to challenges with solubility and steric crowding. However, lowering the density increases the separation of ligands on the surface, which reduces the effective concentration. This approach can be particularly problematic if the scaffold architecture is not flexible enough to allow localization of ligands. An approach to increase local ligand concentrations without fully functionalizing a surface is to create patches or clusters of the ligand on the scaffold (Figure 1.9b). In a recent study by Gilles et al.,[60] polymer vesicles were functionalized with dendritic clusters of ~7 mannose units. The surface density of these clusters was also varied by controlling the amount of azido-functionalized polymer in the vesicle scaffold to give statistical distributions. As a control, the same vesicles were functionalized with a monomeric azido-modified mannose to create multivalent mannose structures which did not have the localization effects of the clusters. The vesicles were evaluated by a hemagglutination assay, which measured the ability of the vesicles to inhibit red blood cell clustering by selectively binding the ConA. When compared to free mannose, the multivalent but non-clustered vesicle had a proximately 4 times the activity as free mannose relative to the amount of mannose present, likely due to a chelate type interaction. However, the activity of the equivalent cluster functionalized vesicle was over 40 times that of the monomer on a mannose-to-mannose basis. This example highlights the importance of controlling the distribution of ligands on a scaffold system for such systems. Pine and coworkers have recently published methods to synthesize polymeric scaffolds with localized, directional binding patches.[61] In this work, colloidal particles were prepared from nanoclusters with 1-7 amidine patches in symmetric orientations. The original work utilized these selectively active sites to assemble larger nanostructures; however the translation of these sites to directional multivalent binding scaffolds is clear. Complete functionalization of these sites with multivalent ligands would create areas of high local concentration, and multiple patch sites allow for well-defined, chelate type crosslinking. Other scaffolds, such as PAMAM dendrimers, are more flexible then the cross-linked vesicle, which allows the ligands to be localized even if they are bound on different polymer

branches.[62] However, creating bifunctional conjugates (e.g. with a drug and a targeting ligand) still creates a more heterogeneous population. In 2012, Baker et al.[63] synthesized triazine-based clusters of a single folic acid (targeting ligand) and a single methotrexate (drug ligand) with an azide click chemistry group. These clusters were then clicked to a previously synthesized, stochastic distribution of dendrimer-alkyne click ligand conjugate. In the resulting product, which still contained a distribution of ligand-to-scaffold ratios, each unique species contained exactly the same number of drugs and target ligands. There is a reduction in unique species from ~170 in the equivalent, double conjugation approach (Figure 1.11a) to ~13 by employing only one conjugation (Figure 1.11b). Importantly, the single distribution conjugate exhibited higher growth inhibition for KB cells than a double-conjugation sample that actually had a higher methotrexate valency. This observation is possibly due to the elimination of untargeted treatment populations and drugless targeted species from the sample. In this case, presence of a larger distribution of samples actually counteracts the benefits of multivalency. This example emphasizes the importance of considering the activity impacts of complicated, sequential synthesis

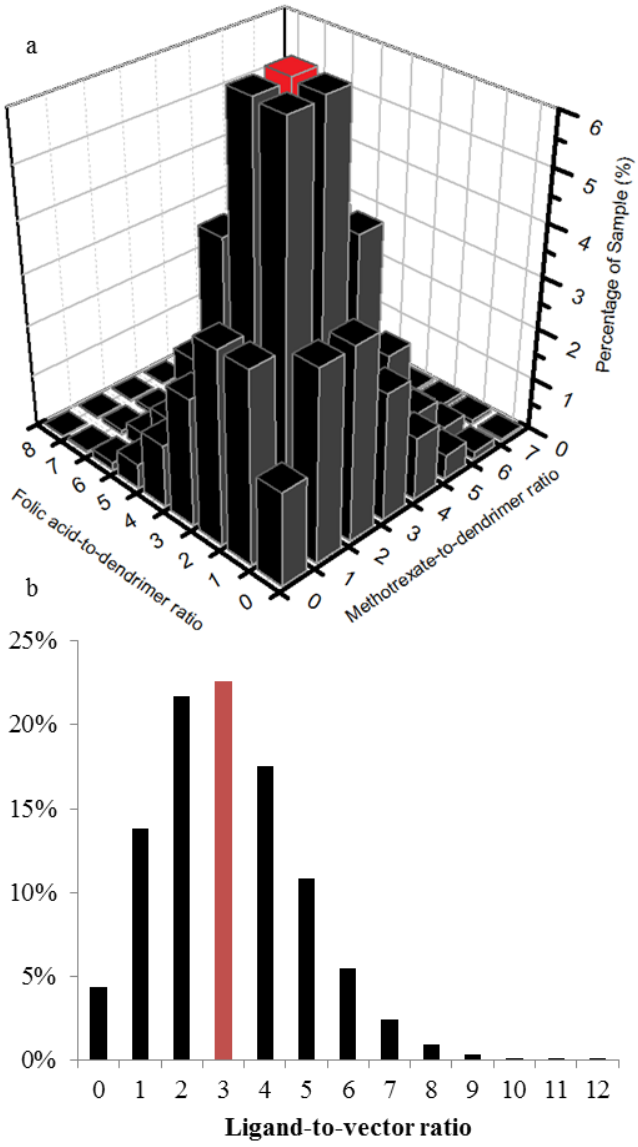

Figure 1.11. Product species present in (a) a double conjugation of methotrexate and folic acid and (b) the single conjugation of the bivalent cluster.

of multifunctional systems.

Precise Ligand/Polymer Ratio Conjugates. Although high density surfaces and ligand clustering improve conjugate behavior, mechanistic assignment of activity and identification of populations with optimal behavior are best done with homogenous samples. The presence of a heterogeneous mixture of products in these approaches (except for 100% functionalization approaches) may also present complications in scale-up, prevent clinical application, or fail to meet FDA requirements for approval. Therefore, several strategies have been employed to synthesize precise, multivalent conjugates in which all species have the same exact ligand-to-scaffold ratio. These approaches can be broadly categorized as biologically inspired approaches, bottom-up approaches, and top-down approaches.

Several groups have taken advantage of the homogeneity of biological nanoparticles as precise scaffolds. Proteins are of great interest as multivalent scaffolds because of their nanoscale sizes allowing them to span large areas for chelate effect binding, well defined structure which allows for precise functionalization, and the possible therapeutic potential of the protein itself. One such application by Zhang and coworkers[64] employed a tetrameric far-red fluorescent protein (tfRFP) as both an imaging agent and a scaffold conjugated multivalently to cancer targeting peptides. The N and C termini of each unit in the tfRFP were conjugated to a copy of the targeting peptide to create conjugates consisting of exactly 8 targeting peptides per tfRFP. By comparison, random conjugation of an average of one fluorescent probe and 8 peptides to a PAMAM dendrimer would result in over 300 unique combinations, of which over 30% would not contain an imaging agent. Conjugation of the peptides to the tfRFP significantly increased the uptake of the probe, although it was shown to decrease the fluorescent intensity of the tfFRP. The location and number of functionalizable sites limits the placement of multivalent ligands on proteins, however, which may not allow for optimal effective concentration enhancements. Ikkala et al.[65] addressed this challenge by utilizing dendrons of varying generations to create DNA binding patches of varying valency on two different protein scaffolds, bovine serum albumin (BSA) and a genetically engineered Class II hydrophobin (HFBI). This work takes advantage of a single cysteine residue available on

each protein for thiol reactions to the dendrons. Employing dendrons with 3 or 9 surface primary amines allows for precise valency control of the resulting conjugate. Although there was only a 50% yield for the BSA scaffold (due to oxidation of the cysteine), the purified products contained a single dendron per protein. The DNA binding of the conjugates were then evaluated by an ethidium bromide displacement assay. The unmodified proteins did not bind the DNA, whereas the conjugates bound the DNA to varying degrees. The smaller HFBI conjugates had relatively higher affinity compared to the larger BSA conjugates, which the authors attributed to the differences dendron-to-protein size (which could translate to a percent functionalization effect). As expected, the higher valency of the larger dendron also promoted DNA binding.

The precise interactions of nucleic and amino acids have also been utilized to craft homogenous multivalent structures. Antibodies can be employed to target cancer cells presenting tumor-associated antigens. Schultz et al.[66] genetically engineered an anti-Her2 antibody to site-specifically incorporate two unnatural amino acids, p-acetylphenylalanine (pAcPhe). The pAcPhe can be orthogonally modified to form an oxime bond with an alkoxy-amine derivatized drug. In their recent work, Schultz and coworkers created antibody conjugates containing exactly two copies of a tubulin inhibitor, ausirtatin. Comparatively, randomly coupling a drug to natural amino acids can lead to up to ~1,000,000 unique species. The precise conjugates showed improved selectivity for the drug, due to the targeting ability of the antibody, although there did not appear to be a multivalent effect for having multiple drug copies. Importantly, the precise conjugate showed favorable pharmacokinetics, selectivity, and stability compared to similar work with traditionally (non-site specific) antibody conjugates. Seitz and coworkers[67] recently performed a thorough proof of concept study proving the usefulness of DNA as a template for creating precise multivalent architectures. In this work, base pairing between DNA and synthetic peptide nucleic acids modified with N-acetyllactosamine (LacNAc) was employed to tailor scaffolds with precisely defined valency, precisely defined spacing, and varied flexibility. The binding of LacNAc to *Ricinus communis* agglutinin (RCA_{120}) is known, with two binding sites that are ~130 angstroms apart across the concave surface of the protein. As such, valency effects were studies by synthesizing complexes with 1-4 LacNAc. The strongest absolute binding, as

measured by K_D, was observed for the tetravalent construct, although this sample did not have the highest relative potency per LacNAc, indicating that this enhancement was due to increased effective concentration/statistical rebinding. Two different spacers were used to vary the length between LacNAc units in divalent complexes. As expected, the spacer that more closely matched the separation of the active sites showed approximately twice the binding activity as the complex where the distance between the LacNAc units were too close. Finally, flexibility was evaluated be synthesizing divalent structures that were completely double stranded and partially single stranded between the LacNAc units. The less flexible complex had slightly higher binding, which may indicate unfavorable thermodynamic penalties to obtain binding conformation in the flexible complex. Biologically inspired approaches provide excellent control of scaffold heterogeneity, ligand valency and placement. However, implementation *in vivo* is often limited by immunogenicity. Therefore, non-biological but precise conjugates which may be masked from immune systems are still actively pursued.

Fully synthetic, bottom-up approaches to creating precise multivalent architectures allows for molecular control of stoichiometry and geometry optimized for a specific target. One such example is the sub-monomer unit assembly of peptoids to form oligomers with monomer chemical functionality in the desired positions. Kirshenbaum and coworkers[68] demonstrated this technique by synthesizing peptoids with precisely 1-6 azide entities in the monomer side chains. From these multivalent constructs, multivalent displays of estradiol were prepared from alkyne modified steroids. The multivalent constructs were evaluated by a radiometric competitive binding assay. The monovalent peptoid showed ~6,500 weaker affinity than the free estradiol, perhaps due to entropic penalties due to immobilization on the scaffold, however the bivalent conjugate recovered to ~100 fold weaker affinity. This observation could possibly be attributed to chelate type binding as estrogen receptors can exist as dimers. Minor improvements for the tri and hexavalent conjugates can likely be attributed to effective concentration effects. The solid phase peptoid synthesis allows for tailoring of space between the active monomers, so that the biological structures of interest may be matched. Vidal et al.[69] employed peptoid and porphyrins as small scaffolds to match lectin symmetry. Two lectins with different symmetries were studied. A flexible, linear tetravalent glycol-

peptoid conjugates and cyclic peptoids of the same valency were first compared. The linear peptoid did not exhibit any inhibition behavior in a hemagglutination inhibition assay, while the cyclic cluster selectively inhibited coagulation with one erythrocyte (*Pseudomonas aeruginosa*) but not the other (*Erythrina cristagalli*) tested. However, there was very little measurable effect of multivalency over the monovalent ligand (~4 times the potency). By way of contrast, a square planar tetravalent porphyrin selectively inhibited the *Erythrina cristagalli* with over 150 times the relative potency of the monovalent glycoside. Increasing the valency to 6 had no additional favorable effect, and changing the symmetry to orient all 4 glycosides in one direction or placing 2 in an opposite direction both negatively impacted the behavior of the conjugate. This study demonstrates the importance of precise control of ligand orientation for minimizing thermodynamic costs in achieving ligand-target interactions, especially with inflexible scaffolds.

One approach to achieve precise nano-size dendrimer conjugates is to use convergent synthesis of dendrons with small molecule precision to form nanoscaled conjugates with well-defined functionality. In 2010, Weck et al. developed a method to construct generation 2 poly(amide) based dendrons and dendrimer materials using copper catalyzed and copper free click chemistry developed by Sharpless and Bertozzi. These materials had the multi-functionality of amine, azide, and alkynes.[70] These materials made a large step in creating monodisperse polymers since the dendrimers synthesized had 100% completion reactions for each generation as determined by various characterization techniques which is a major challenge in creating many dendrimer materials, including the PAMAM dendrimer.[70] In 2011, Weck et al. used these well-defined dendrimer materials to click on near infrared cyanine dyes in order to create monodisperse polymer imaging agents that have the ability to be used in biological experiments due to their non-cytotoxic nature.[71]

Convergent approaches are difficult to extend to higher generation dendrimers. Recent work by Banaszak Holl et al.[27-30] utilized high performance liquid chromatography to isolate generation 5 PAMAM dendrimers with precise ligand-to-scaffold ratios. Stochastic average mixtures of products are prepared by mixing multiple equivalents of

the ligand drop wise into a solution of the dendrimer scaffold. By employing hydrophobic ligands, favorable interaction with a reverse phase, hydrophobic stationary phase column is exploited so that column retention is determined by the precise ligand-to-dendrimer ratio (Figure 1.3). Scaling these methods to the semi-preparative scale allows for generation of up to 30 milligrams of product with a single, precise ligand-to-dendrimer ratio. Extending this approach from click ligands to biologically interesting molecules will provide a route to precise drug/targets/dye-to-dendrimer ratio materials.

Future Directions

In the pursuit of more active multivalent polymer conjugates, there are many directions that must be pursued. First, it is important to acknowledge the heterogeneity present in a ligand-scaffold conjugate and the impacts of this heterogeneity on the desired application. Then, the best way to minimize or eliminate the impacts of sample heterogeneity can be determined. Systematic variation of ligand density has proven to be a facile route to improved conjugate activity. Continued studies such as those by Choi et al. lead to samples that, while still heterogeneous, limit the population of inactive species. Such high average samples, when not plagued with undesired properties such as insolubility or nonspecific cytotoxicity, may be the easiest and/or fastest method to bring a conjugate to clinical scales. Achieving precise ratio ligand/polymer control of these widely employed multivalent conjugates, such as the work by Banaszak Holl et al., must also continue as the best way to distinguish mechanisms of activity and identification of active components within a sample, although this approach may not be scalable. For other applications, a more structured approach to maximize specific multivalent effects is best for achieving the desired interaction. If target chelation is not a desired outcome (for example, in the PAMAM-folic acid case when even 1 ligand is sufficient to achieve the desired behavior), it is best to pursuit conjugate techniques such as ligand clustering to maximize local concentration effects. Employing flexible scaffolds might also minimize the need for precise control over ligand spatial distributions. If the exact geometry is known, effort might be best spent in optimization of the scaffold choice for precise control ligand placement to minimize entropic penalties of bringing multiple ligands into

the desired geometry. It is easy to neglect the contribution of effective concentration effects in favor of achieving architectures that exhibit chelate binding in such systems; however the works highlighted here indicate that that these effects are far from negligible. Although much work revolving around clustering has been with glycoclusters, it is not unreasonable to believe such effects may translate to other ligands of biological interest. An interesting area to pursue would be to combine a precisely tailored geometry, such as seen with the square planar complexes of Vidal et al.,[69] with pre-clustered ligands on a dendron to high local concentrations and precise localization of cluster geometry. Recent work by Baker et al. have shown the promise of heterobifunctional ligand clustering on random, flexible architectures.[63] As such, applying ligand clustering via click reaction to either distributed or precise conjugates on flexible scaffolds like PAMAM may provide new optimization of multivalent behavior.

In summary, multivalent, multifunctional polymeric conjugates are highly attractive for the targeted delivery of drugs and imaging agents. However, common approaches to the synthesis of conjugates involve many steps and can lead to complex mixtures of products. The presence of these product distributions, while intellectually obvious, is hard to visualize by most chemical and biological techniques employed to evaluate the samples. As such, progress toward understanding the impact of such heterogeneous distributions on the activity of the conjugates is slow. However, recent work in systematically modifying the distributions of ligands present and crafting of precise multivalent architectures has allowed for better elucidation of multivalent behavior.

References

1. Pasut, G. and F.M. Veronese, *Polymer–drug conjugation, recent achievements and general strategies.* Progress in Polymer Science, 2007. **32**(8–9): p. 933-961.
2. Duncan, R. and R. Gaspar, *Nanomedicine(s) under the Microscope.* Molecular Pharmaceutics, 2011. **8**(6): p. 2101-2141.
3. Duncan, R. and S.C.W. Richardson, *Endocytosis and Intracellular Trafficking as Gateways for Nanomedicine Delivery: Opportunities and Challenges.* Molecular Pharmaceutics, 2012. **9**(9): p. 2380-2402.
4. Boas, U. and P.M.H. Heegaard, *Dendrimers in drug research.* Chemical Society Reviews, 2004. **33**(1): p. 43-63.

5. Temming, K., et al., *RGD-based strategies for selective delivery of therapeutics and imaging agents to the tumour vasculature.* Drug Resistance Updates, 2005. **8**(6): p. 381-402.
6. Haag, R. and F. Kratz, *Polymer Therapeutics: Concepts and Applications.* Angewandte Chemie International Edition, 2006. **45**(8): p. 1198-1215.
7. van der Meel, R., et al., *Ligand-targeted particulate nanomedicines undergoing clinical evaluation: Current status.* Advanced Drug Delivery Reviews, 2013. **65**(10): p. 1284-1298.
8. Kukowska-Latallo, J.F., et al., *Nanoparticle Targeting of Anticancer Drug Improves Therapeutic Response in Animal Model of Human Epithelial Cancer.* Cancer Research, 2005. **65**(12): p. 5317-5324.
9. Kamen, B.A. and A. Capdevila, *Receptor-mediated folate accumulation is regulated by the cellular folate content.* Proceedings of the National Academy of Sciences, 1986. **83**(16): p. 5983-5987.
10. Choi, S.K., et al., *Dendrimer-Based Multivalent Vancomycin Nanoplatform for Targeting the Drug-Resistant Bacterial Surface.* ACS Nano, 2012. **7**(1): p. 214-228.
11. Janib, S.M., A.S. Moses, and J.A. MacKay, *Imaging and drug delivery using theranostic nanoparticles.* Advanced Drug Delivery Reviews, 2010. **62**(11): p. 1052-1063.
12. Xie, J., S. Lee, and X. Chen, *Nanoparticle-based theranostic agents.* Advanced Drug Delivery Reviews, 2010. **62**(11): p. 1064-1079.
13. Kelkar, S.S. and T.M. Reineke, *Theranostics: Combining Imaging and Therapy.* Bioconjugate Chemistry, 2011. **22**(10): p. 1879-1903.
14. Le Droumaguet, B., et al., *Versatile and Efficient Targeting Using a Single Nanoparticulate Platform: Application to Cancer and Alzheimer's Disease.* ACS Nano, 2012. **6**(7): p. 5866-5879.
15. Shamay, Y., et al., *Light induced drug delivery into cancer cells.* Biomaterials, 2011. **32**(5): p. 1377-1386.
16. Tansey, W., et al., *Synthesis and characterization of branched poly(l-glutamic acid) as a biodegradable drug carrier.* Journal of Controlled Release, 2004. **94**(1): p. 39-51.
17. Wang, J., et al., *Folate-Decorated Hybrid Polymeric Nanoparticles for Chemically and Physically Combined Paclitaxel Loading and Targeted Delivery.* Biomacromolecules, 2010. **12**(1): p. 228-234.
18. Sharma, A., et al., *Design and Evaluation of Multifunctional Nanocarriers for Selective Delivery of Coenzyme Q10 to Mitochondria.* Biomacromolecules, 2011. **13**(1): p. 239-252.
19. Chandna, P., et al., *Targeted Proapoptotic Anticancer Drug Delivery System.* Molecular Pharmaceutics, 2007. **4**(5): p. 668-678.
20. Saad, M., et al., *Receptor targeted polymers, dendrimers, liposomes: Which nanocarrier is the most efficient for tumor-specific treatment and imaging?* Journal of Controlled Release, 2008. **130**(2): p. 107-114.
21. Santra, S., C. Kaittanis, and J.M. Perez, *Cytochrome c Encapsulating Theranostic Nanoparticles: A Novel Bifunctional System for Targeted Delivery of Therapeutic Membrane-Impermeable Proteins to Tumors and Imaging of Cancer Therapy.* Molecular Pharmaceutics, 2010. **7**(4): p. 1209-1222.
22. Tomalia, D.A., J.B. Christensen, and U. Boas, *The Dendritic State*, in *Dendrimers, Dendrons and Dendritic Polymers: Discovery, Applications, the Future*

2012, Cambridge University Press

NY. p. 30.
23. Christensen, J.B. and D.A. Tomalia, *Designing Dendrimers*, in *Dendrimers as Quantized Nano-modules in the Nanotechnology Field*, S. Campagna, P. Ceroni, and F. Puntoriero, Editors. 2012, J. Wiley & Sons: Hoboken. p. 1-33.
24. Mullen, D.G., et al., *Design, Synthesis, and Biological Functionality of a Dendrimer-Based Modular Drug Delivery Platform.* Bioconjugate Chem., 2011. **22**: p. 679-689.
25. Ljubimova, J.Y., et al., *Nanoconjugate based on polymalic acid for tumor targeting.* Chemico-Biological Interactions, 2008. **171**(2): p. 195-203.
26. van Dongen, M.A., et al., *Quantitative analysis of generation and branch defects in G5 poly(amidoamine) dendrimer.* Polymer, 2013. **54**: p. 4126-4133.
27. Mullen, D.G., et al., *A Quantitative Assessment of Nanoparticle-Ligand Distributions: Implications for Targeted Drug and Imaging Delivery in Dendrimer Conjugates.* ACS Nano, 2010. **4**: p. 657-670.
28. Mullen, D.G. and M.M. Banaszak Holl, *Heterogeneous Ligand–Nanoparticle Distributions: A Major Obstacle to Scientific Understanding and Commercial Translation.* Accounts of Chemical Research, 2011. **44**(11): p. 1135-1145.
29. Mullen, D.G., et al., *Isolation and Characterization of Dendrimers with Precise Numbers of Functional Groups.* Chemistry – A European Journal, 2010. **16**(35): p. 10675-10678.
30. van Dongen, M., S.m.u.e. Vaidyanathan, and M.M. Banaszak Holl, *PAMAM Dendrimers as Quantized Building Blocks for Novel Nanostructures.* Soft Matter, 2013.
31. Mullen, D.G., et al., *The Implications of Stochastic Synthesis for the Conjugation of Functional Groups to Nanoparticles.* Bioconjugate Chemistry, 2008. **19**(9): p. 1748-1752.
32. Mullen, D.G., et al., *Effect of Mass Transport in the Synthesis of Partially Acetylated Dendrimer: Implications for Functional Ligand−Nanoparticle Distributions.* Macromolecules, 2010. **43**(16): p. 6577-6587.
33. Krishnamurthy, V.M., L.A. Estroff, and G.M. Whitesides, *Multivalency in Ligand Design*, in *Fragment-based Approaches in Drug Discovery*. 2006, Wiley-VCH Verlag GmbH & Co. KGaA. p. 11-53.
34. Chittasupho, C., *Multivalent ligand: design principle for targeted therapeutic delivery approach.* Therapeutic Delivery, 2012. **3**(10): p. 1171-1187.
35. Mann, D.A., et al., *Probing Low Affinity and Multivalent Interactions with Surface Plasmon Resonance: Ligands for Concanavalin A.* Journal of the American Chemical Society, 1998. **120**(41): p. 10575-10582.
36. Hong, S., et al., *The Binding Avidity of a Nanoparticle-Based Multivalent Targeted Drug Delivery Platform.* Chemistry & Biology, 2007. **14**(1): p. 107-115.
37. Dam, T.K. and C.F. Brewer, *Thermodynamic Studies of Lectin−Carbohydrate Interactions by Isothermal Titration Calorimetry.* Chemical Reviews, 2002. **102**(2): p. 387-430.
38. Silpe, J.E., et al., *Avidity Modulation of Folate-Targeted Multivalent Dendrimers for Evaluating Biophysical Models of Cancer Targeting Nanoparticles.* ACS Chemical Biology, 2013. **8**: p. 2063-2071.
39. Nakagawa, O., et al., *Targeted Intracellular Delivery of Antisense Oligonucleotides via Conjugation with Small-Molecule Ligands.* Journal of the American Chemical Society, 2010. **132**(26): p. 8848-8849.
40. Zhou, Q.-H., et al., *Cyclic RGD-targeting of reversibly stabilized DNA nanoparticles enhances cell uptake and transfection in vitro.* Journal of Drug Targeting, 2009. **17**(5): p. 364-373.
41. Reuter, J.D., et al., *Inhibition of Viral Adhesion and Infection by Sialic-Acid-Conjugated Dendritic Polymers.* Bioconjugate Chemistry, 1999. **10**(2): p. 271-278.

42. Munoz, E.M., et al., *Probing the Relevance of Lectin Clustering for the Reliable Evaluation of Multivalent Carbohydrate Recognition.* Journal of the American Chemical Society, 2009. **131**(49): p. 17765-17767.
43. Gómez-García, M., et al., *Probing Carbohydrate-Lectin Recognition in Heterogeneous Environments with Monodisperse Cyclodextrin-Based Glycoclusters.* The Journal of Organic Chemistry, 2011. **77**(3): p. 1273-1288.
44. Bossu, I., et al., *Dendri-RAFTs: a second generation of cyclopeptide-based glycoclusters.* Organic & Biomolecular Chemistry, 2011. **9**(6): p. 1948-1959.
45. Waddell, J.N., et al., *Origin of broad polydispersion in functionalized dendrimers and its effects on cancer-cell binding affinity.* Physical Review E, 2010. **82**: p. 036108.
46. Licata, N.A. and A.V. Tkachenko, *Kinetic Limitations of Cooperativity-Based Drug Delivery Systems.* Physical Review Letters, 2008. **100**: p. 158102.
47. Martinez-Veracoechea, F.J. and D. Frenkel, *Designing super selectivity in multivalent nano-particle binding.* Proceedings of the National Academy of Sciences, 2011. **108**(27): p. 10963-10968.
48. Leucuta, S.E., *Subcellular drug targeting, pharmacokinetics and bioavailability.* Journal of Drug Targeting. **0**(0): p. 1-21.
49. Wang, J., et al., *The Complex Role of Multivalency in Nanoparticles Targeting the Transferrin Receptor for Cancer Therapies.* Journal of the American Chemical Society, 2010. **132**(32): p. 11306-11313.
50. Menjoge, A.R., R.M. Kannan, and D.A. Tomalia, *Dendrimer-based drug and imaging conjugates: design considerations for nanomedical applications.* Drug Discovery Today, 2010. **15**(5–6): p. 171-185.
51. Kim, Y., et al., *Dendrimer Probes for Enhanced Photostability and Localization in Fluorescence Imaging.* Biophysical Journal, 2013. **104**(7): p. 1566-1575.
52. Zanini, D., W.K.C. Park, and R. Roy, *Synthesis of novel dendritic glycosides.* Tetrahedron Letters, 1995. **36**(41): p. 7383-7386.
53. Ashton, P.R., et al., *Synthesis of Glycodendrimers by Modification of Poly(propylene imine) Dendrimers.* Chemistry – A European Journal, 1997. **3**(6): p. 974-984.
54. André, S., et al., *Wedgelike Glycodendrimers as Inhibitors of Binding of Mammalian Galectins to Glycoproteins, Lactose Maxiclusters, and Cell Surface Glycoconjugates.* ChemBioChem, 2001. **2**(11): p. 822-830.
55. Lundquist, J.J. and E.J. Toone, *The Cluster Glycoside Effect.* Chemical Reviews, 2002. **102**(2): p. 555-578.
56. Srinivas, O., et al., *Synthesis and biological evaluation of mannose-6-phosphate-coated multivalent dendritic cluster glycosides.* Organic & Biomolecular Chemistry, 2005. **3**(23): p. 4252-4257.
57. Shi, X., et al., *Generational, skeletal and substitutional diversities in generation one poly(amidoamine) dendrimers.* Polymer, 2005. **46**(9): p. 3022-3034.
58. Wängler, C., et al., *PAMAM Structure-Based Multifunctional Fluorescent Conjugates for Improved Fluorescent Labelling of Biomacromolecules.* Chemistry – A European Journal, 2008. **14**(27): p. 8116-8130.
59. Welsh, D.J. and D.K. Smith, *Comparing dendritic and self-assembly strategies to multivalency-RGD peptide-integrin interactions.* Organic & Biomolecular Chemistry, 2011. **9**(13): p. 4795-4801.
60. Martin, A.L., B. Li, and E.R. Gillies, *Surface Functionalization of Nanomaterials with Dendritic Groups: Toward Enhanced Binding to Biological Targets.* Journal of the American Chemical Society, 2008. **131**(2): p. 734-741.

61. Yufeng, W., et al., *Colloids with valence and specific directional bonding.* Nature, 2012. **491**(7422): p. 51-55.
62. Mecke, A., et al., *Deformability of poly(amidoamine) dendrimers.* The European Physical Journal E, 2004. **14**(1): p. 7-16.
63. Zong, H., et al., *Bifunctional PAMAM Dendrimer Conjugates of Folic Acid and Methotrexate with Defined Ratio.* Biomacromolecules, 2012. **13**(4): p. 982-991.
64. Luo, H., et al., *Tetrameric far-red fluorescent protein as a scaffold to assemble an octavalent peptide nanoprobe for enhanced tumor targeting and intracellular uptake in vivo.* The FASEB Journal, 2011. **25**(6): p. 1865-1873.
65. Kostiainen, M.A., et al., *Precisely Defined Protein–Polymer Conjugates: Construction of Synthetic DNA Binding Domains on Proteins by Using Multivalent Dendrons.* ACS Nano, 2007. **1**(2): p. 103-113.
66. Axup, J.Y., et al., *Synthesis of site-specific antibody-drug conjugates using unnatural amino acids.* Proceedings of the National Academy of Sciences, 2012. **109**(40): p. 16101-16106.
67. Scheibe, C., et al., *Carbohydrate–PNA and Aptamer–PNA Conjugates for the Spatial Screening of Lectins and Lectin Assemblies.* ChemBioChem, 2013. **14**(2): p. 236-250.
68. Holub, J.M., M.J. Garabedian, and K. Kirshenbaum, *Peptoids on Steroids: Precise Multivalent Estradiol–Peptidomimetic Conjugates Generated via Azide–Alkyne [3+2] Cycloaddition Reactions.* QSAR & Combinatorial Science, 2007. **26**(11-12): p. 1175-1180.
69. Cecioni, S., et al., *Selectivity among Two Lectins: Probing the Effect of Topology, Multivalency and Flexibility of "Clicked" Multivalent Glycoclusters.* Chemistry – A European Journal, 2011. **17**(7): p. 2146-2159.
70. Ornelas, C., J. Broichhagen, and M. Weck, *Strain-Promoted Alkyne Azide Cycloaddition for the Functionalization of Poly(amide)-Based Dendrons and Dendrimers.* Journal of the American Chemical Society, 2010. **132**(11): p. 3923-3931.
71. Ornelas, C., et al., *Combining Aminocyanine Dyes with Polyamide Dendrons: A Promising Strategy for Imaging in the Near-Infrared Region.* Chemistry – A European Journal, 2011. **17**(13): p. 3619-3629.

Chapter 2

Structural Defects in G5 PAMAM Dendrimer

This chapter was previously published as "Quantitative analysis of generation and branch defects in G5 poly(amidoamine) dendrimer" Polymer *(2013), 54, 4126. The corresponding supporting information can be found in Appendix A.*

Introduction.

Poly(amidoamine) (PAMAM) dendrimers are a class of polymers characterized by dendritic structure and low polydispersity. [1-3] Additionally, water solubility, low cytotoxicity when acetyl capped, and readily conjugated surface groups have contributed to make PAMAM dendrimers particularly interesting for biological applications.[4] Generation 5 (G5) PAMAM dendrimer has been of specific interest because it is able to move through biological tissue, due to its 5 nm diameter. This allows the dendrimer to cross cell membranes thereby increasing blood circulation times of conjugated or entrapped drugs (for example, from 2 to 6 hours)[5] and avoiding rapid clearance by liver and spleen.[6, 7] On the other hand, the G5 material is also large enough to conjugate up to at least 14 hydrophobic drugs, targeting molecules, and/or dyes while retaining water solubility.[8] Consequently, G5 PAMAM has been extensively studied[8, 9] as a platform for multivalent conjugates[10-12] combining specific cell targeting,[13-15] drug delivery,[16-19] RNA,[20] and gene delivery,[21-23] and/or imaging agents,[24-29] with over 900 publications to date.

Although PAMAM dendrimers can have polydispersity indices as low as 1.01, they are known to have generational defects (trailing generations and oligomers) and branching defects (missing arms and intramolecular loops).[30, 31] Generational defects lead to substantial portions of the sample population with significantly lower and higher molecular weights and diameters. For example, a G5 sample containing trailing

generations and oligomers could in principle contain particles with molecular weights ranging from about 1400 Da (G1) to 114,000 Da (G5 tetramer), leading to significantly different biodistributions of differently sized materials.[7] Additionally, host-guest behavior depends on internal void volume of the dendrimer, which is greatly reduced for the lower generations present as trailing defects in a sample.[6]

The structure of PAMAMs has been explored by a variety of experimental and theoretical methods. Theoretical studies using atomistic,[32-37] coarse grain,[34, 38] and explicit solvent molecular dynamics,[33, 36] have been carried out to address the size, shape, and interior volumes of dendrimers in response to different pH and solvent environments. These measurements have been compared to experimental methods such as small angle neutron scattering[39-41] and X-ray diffraction[39] with generally good agreement. Mass characterization techniques, such as electrospray ionization mass spectrometry (ESI-MS),[31] matrix assisted laser desorption ionization time-of-flight mass spectrometry (MALDI-TOF-MS),[30] centrifugation,[8, 9] and size exclusion chromatography,[8, 9] have detected the presence of defects in the dendrimers. Capillary electrophoreses exclusion chromatography[42] has been frequently used to explore sample uniformity.[43, 44] For example, Lopp et al. employed capillary zone electrophoresis to characterize homogeneity for G0 to G4 PAMAM.[45] They observed differences in electrophoretic mobilities leading to fast migrating trailing generations, and slowly migrating impurities that were attributed to lower charges due to missing or looped arms, and high weight oligomers; however, this technique cannot explicitly distinguish between these structures, and no further complementary characterization was performed. Lee et al. used field flow fractionation to do size dependent separation of G4-G9 at various pH conditions.[42] They observed the presence of high (dimers) and low (trailing and skeletal defects) molecular weights via changes in sample mobility, in all generations and conditions, but did not employ further techniques to study the materials. Baker et al. utilized ion-pair reverse phase High Performance Liquid Chromatography (RP-HPLC) to analyze G1-G9.[46, 47] This work hypothesized that RP-HPLC can separate dendrimer as a function of density of paired primary amine/trifluoroacetate surface groups. Defects leading to missing end groups changed retention, readily apparent for lower generations, and dimeric species having more surface groups were retained longer. The authors

speculated that this work could be scalable to preparative work for the isolation of large amounts of relatively pure materials.

Recent work has demonstrated the ability to isolate dendrimers with precise numbers of click-functional ligands from a stochastically synthesized distribution utilizing RP-HPLC.[48, 49] Presently, however, the purity of these isolated materials is limited by the presence of high weight oligomers that co-elute with the monomer conjugates. These materials contain fewer than ideal numbers of ligands but contribute significantly to the sample mass due to their high molecular weights. Low weight, trailing impurities are often eliminated by size exclusion techniques,[48] but removal of dimer and larger structures has to date not been on a preparative scale. Isolation of generationally pure dendrimer monomer materials will allow for preparation of conjugates with a narrow size distribution and precise numbers of functional ligand with enhanced purity and yield.

Here we report the isolation and characterization of major generational defects in the commercial samples of G5 PAMAM dendrimer typically employed for scientific studies and applied uses of these materials. We employed semi-preparative scale RP-HPLC on a representative sample of commercial G5 PAMAM to isolate major generational components in quantities of hundreds of milligrams. Isolated components were characterized by mass spectrometry, size exclusion chromatography (SEC), and ^{1}H NMR spectroscopy. The NMR spectra were found to be highly pH sensitive, so these experiments were performed at a series of pH values using a pH 3, 5, 7, and 9 buffers for as-received samples, and pH 9 buffer for fractionated samples. The rp-HPLC separation procedure described herein has proven robust and been used to obtain gram quantities of generationally purified PAMAM dendrimer that is suitable for synthesizing conjugates with precisely defined numbers of ligands per polymer particle.

Experimental Section.

Biomedical grade G5 PAMAM dendrimer was purchased from Dendritech Inc. and used as received. All other chemicals were purchased from Sigma Aldrich, Fisher Scientific,

or VWR and used as received. Size exclusion chromatography and potentiometric titration were carried out as previously reported.[48]

*Isolation of Generational Components of G5 PAMAM dendrimer***.** Isolation of dendrimer components was achieved using a Agilent Zorbax 300SB-C18 Prep Column (21.2 x 150 mm, 5 µm particles) with a Waters 600 Controller, Waters 2707 Autosampler, and Waters 2998 Photodiode Array running Empower 2 Software, additionally equipped with a Waters Fraction Collector III. The weak solvent (Solvent A) was HPLC Grade Water with 0.1% TFA, and the strong solvent (Solvent B) was HPLC Grade Acetonitrile with 0.1% TFA. The gradient employed was as follows: Flow rate of 12 mL per minute, 2.1 minute isocratic load step at 95% A and 5% B, 4.9 minute gradient curve 6 to 80% A and 20% B, 6.5 minute gradient curve 6 to 74% A and 26 % B, followed by a 3.5 minute wash of 1% A and 99% B before returning to starting conditions. Eighty, two second fractions were collected starting at 9 min into the procedure. Multiple, consecutive, 0.2 µm syringe filtered, 710 µL injections at a concentration of 18 mg/mL dialyzed G5 dendrimer dissolved in solvent A were performed with a 5 minute equilibration step in between. Chromatograms detected at 210 nm and fractions were then analyzed using Origin Pro 8.1 software, which was used to select fractions to combine for each sample. A small sample was taken from the combined fractions and analyzed using a Waters Acquity Ultra Performance LC with a scaled gradient method calculated using the Water's Analytical to Prep Gradient Calculator on an Agilent 2.1 x 100 mm column with all included chromatograms detected at 210 nm. The combined fractions were exposed to a nitrogen stream to remove acetonitrile and lyophilized. Dried samples were then re-dissolved in PBS buffer pH 7.4 and purified using GE Healthcare PD-10 Columns using the manufacturer's gravimetric protocols using DI water as the buffer, and lyophilized prior to subsequent analyses.

*Mass Spectrometry***.** Matrix-assisted Laser-Desorption Time-of-Flight Mass Spectrometry (MALDI-TOF-MS) was performed using a Micromass TofSpec-2E running MassLynx Version 4.0 software. Dendrimer samples were prepared by dissolving in DI water at concentration 10 mg/mL, then serial diluting with methanol 1:1, then 1:4. The samples were then mixed 1:1 with the matrix dihydroxybenzoic acid (concentration of 10 mg/mL

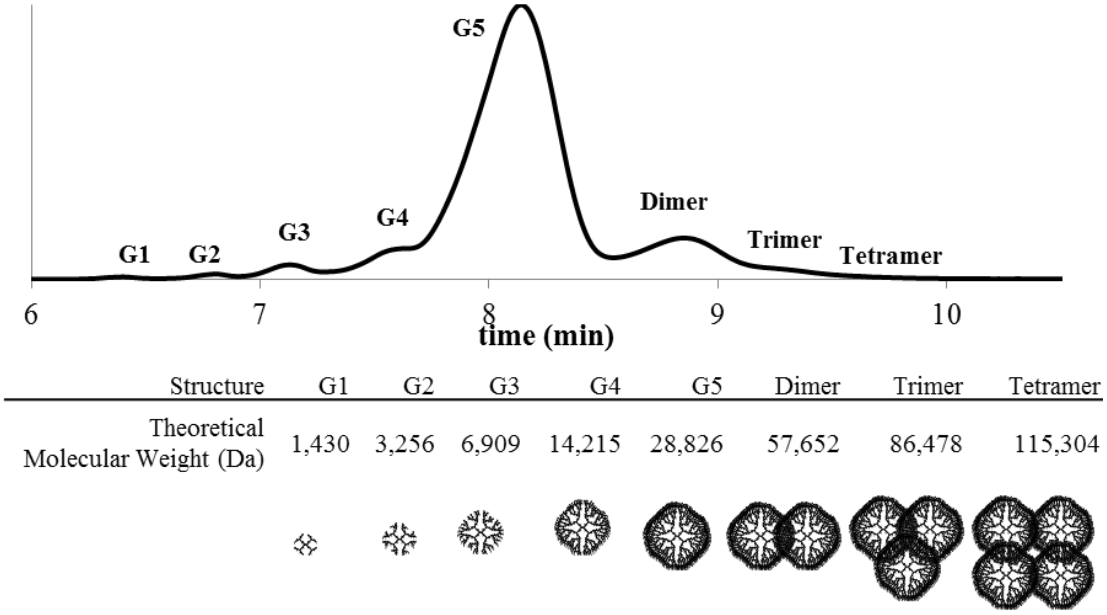

Figure 2.1. UPLC chromatogram at 210 nm of as received G5 dendrimer indicates the presence of trailing generation impurities as well as oligomerized defects.

in 1:1 water/acetonitrile) and spotted on to a MALDI plate. Samples were calibrated using bovine serum albumin with a matrix of sinapic acid. At least 150 laser shots were compiled for each spectrum. The spectra were smoothed using the MassLynx Software settings of Smooth window (channels) equals 12, and Number of smooths equals 12. No baseline subtraction or peak centering was performed.

NMR spectroscopy. NMR experiments were performed on Varian VNMRS 500 and Varian MR400 instruments. ^{1}H-NMR spectra were obtained used 10 second pre-acquisition delays and a total of 64 scans. All sample solutions were set to a dendrimer concentration of 5 mg/mL. Buffered NMR solutions were prepared using deuterium oxide, deuterium chloride, sodium deuteroxide, potassium hydrogen phthalate (pH 3 and 5), potassium dihydrogen phosphate (pH 7), and disodium hydrogen phosphate (pH 9). Internal standard NMRs were taken by spiking 1,4-dioxane, chosen for its miscibility with water, non-interfering shifts, and pH independence, into deuterium oxide or buffered solution at a concentration of 36.1 µM.

R**esults and Discussion**.

Biomedical grade G5 PAMAM dendrimer contains substantial amounts of trailing and oligomer (dimer, trimer, etc.) type defects as visualized by UPLC in Figure 2.1, the relative amounts of which have previously been reported to vary from batch to batch or source to source.[48] Previous reports[46, 47] indicate that RP-HPLC of amine-terminated PAMAM dendrimers operates via ion-pairing of terminal amines with trifluoroacetate. By this principle, retention on the column has a positive correlation with number of primary amine-terminated arms on the dendrimer species. The largest peak, eluting at 8.5 minutes, has been identified as the full molecular weight distribution of G5 species and contains, even in a sample such as this with a PDI of 1.090, only about 64% of the sample, as determined by peak fitting. The smaller peaks eluting prior to the G5 peak indicate the presence of all possible trailing generations, comprising about 14% of the sample by weight (see supporting information for determination of extinction coefficients for all species). Two broad peaks that exhibit higher retention on the reverse-phase column are identified as the G5 dimer and trimer making up 14% and 8% of the sample by weight, respectively, with trace amounts of tetramer also present. Analysis of the extinction coefficients in mg/mL of each species at 210 nm (see supporting information) indicated a decrease as a function of degree of oligomerization leading to a systematic underestimation of the mass fraction of these species if a constant extinction coefficient is assumed. The high percentage of oligomeric defects for G5 leads us to conclude that there are likely species such as G4-G4 dimers and G3-G3-G3 trimers coeluting with the G5 dendrimers, as these structures would have similar molecular weights and primary amine-terminated arms, and cannot be separated by the principles of ion-paired RP-HPLC. By these estimates, a commercial sample contains approximately 30% more particles than calculated using the ideal molecular weight, with only about 50% of the total number of particles being G5 sized.

Semi-preparative HPLC (Figure 2.2) was used to collect eluting dendrimer components in 3 second fractions (vertical white bars). The major species were identified and combined (wide colored bars T, I-IV). The combined fractions represent remaining trailing generation (red bar, T), the full range of G5 branching defects (green bar, I), G5-G5 dimer (purple bar, II), trimer (blue bar III), and tetramer (orange bar, IV). Single, 3 second fractions were also collected as indicated by the gray scale vertical bars (i-iv). Figure 2.3 a shows subsequent re-injection of the combined fractions, T-V, as eluted onto an equivalent UPLC system, while Figure 2.4 a shows re-injection of single fractions, i-iv. The single fractions taken from throughout the G5 peak do not re-center upon injection, indicating that different types and degrees of structural defects contribute to the breadth of the G5 peak and that the peak width is primarily controlled by polymer defects, as isolation and reinjection of 3 second fractions i-iv result in diffusional peak widths of about 75% of the peak-width-at-half-height of the as-received peak, and

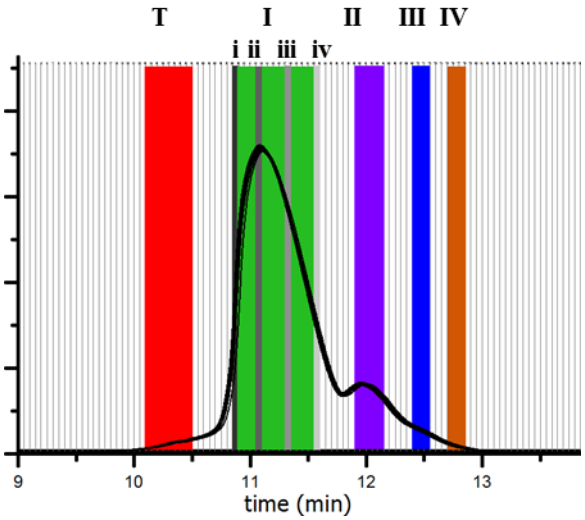

Figure 2.2. Fractions (white bars) collected from semi-preparative HPLC (210 nm) of dialysis purified G5 and combined into generational (colored bars, T,I-V) and single fraction (gray scale bars, i-iv) sets.

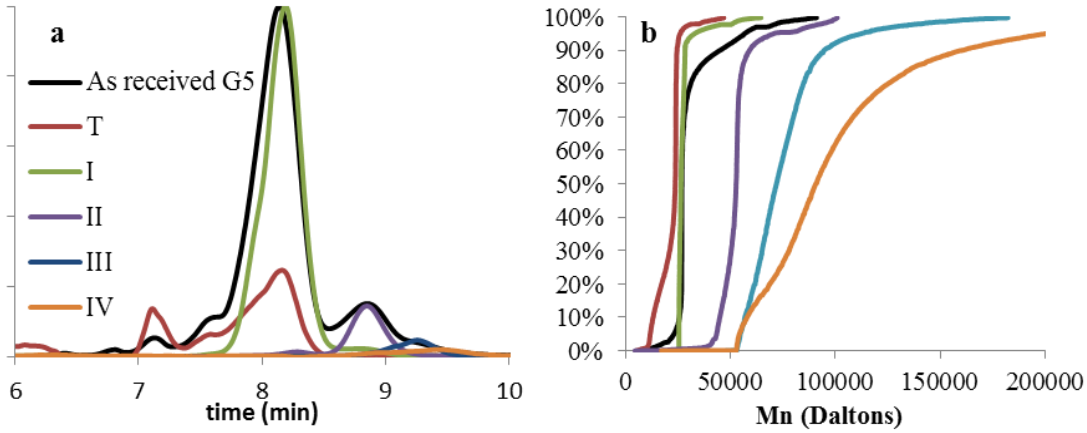

Figure 2.3. Characterization of fractions T,I-IV. (a) UPLC chromatograms at 210 nm of generational fractions T,I-IV. (b) Cumulative data plot of contributing molecular weights from GPC analysis of fractions T,I-IV.

do not re-center. Structures with more branch defects, or defects that occurred earlier in the synthetic process, will contain significantly fewer surface amines and have shorter retention time. The G5 dimer, trimer, and tetramer fractions also do not re-center to the main peak, indicating a significant difference in surface amine presence. The isolated trailing generation is still contaminated with a significant portion of G5, and a small amount of G5 peak can be seen in the dimer fraction, which was confirmed in further experiments.

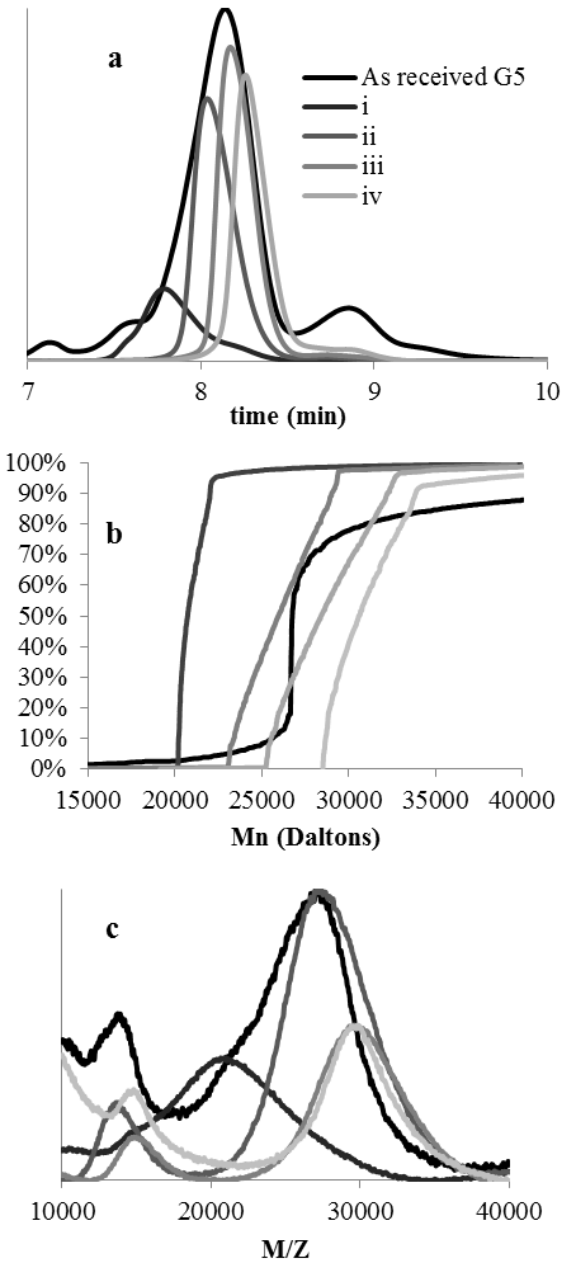

Figure 2.4. Characterization of fractions i-iv. (a) UPLC chromatograms at 210 nm of fractions i-iv do not re-center about the main G5 peak. (b) Cumulative data plot of GPC molar masses for fractions i-iv. (c) MALDI-TOF-MS spectra of fractions i-iv.

After desalting, the trailing generation, branch defective G5, dimer, trimer, and tetramer fractions obtained by RP-HPLC were analyzed by size-exclusion chromatography and compared to as-received G5 PAMAM. The ideal molecular weight of G5 PAMAM is 28,826. The as-received mixture of material has a M_n very similar to this value, but the PDI of 1.090 is consistent with the observation that this M_n is a contribution of G5, low weight (trailing), and high weight (oligomer) impurities. Fractions T,1-III all showed reduced PDIs (Table A1), indicating improved sample homogeneity. Fraction II (dimer) has a M_n which is slightly less than twice that of an ideal G5 dendrimer, and fraction III (trimer) just under three times the M_n of fraction I, in

good agreement with the identification of these structures. Fraction IV shows the largest weight and PDI, and is most likely comprised of a mixture of trimer, tetramer, and higher oligomers. Figure 2.3 b is a cumulative data plot that visualizes the percent contribution of M_n to each fraction. The near vertical line in the cumulative molar mass plot for fraction I is indicative of very homogeneous material. Fraction II has a very similar shape, but is shifted to roughly twice the molecular weight. By fraction III, the average M_n has roughly tripled and the cumulative curve is much shallower. This is consistent with increased polydispersity due to the formation of trimer from G5 monomers with different degrees of branching defects, leading to a larger range of contributing materials. About 20% of fraction IV falls into the trimer range, while about 50% falls into a range approximately 4 times the mass of a G5 monomer, and species with even higher molecular weights are detected.

Molecular weights were also measured by MALDI-TOF-MS for the five generational fraction sets (Table A1) and were in good agreement with GPC data. The higher-than-ideal weights observed is most likely attributed to presence of various salts, as the peaks are all slightly shifted to high weights when compared to the as received material prior to trifluoroacetate and phosphate buffer exposure. The presence of phosphate and TFA salts can be observed via NMR (Figure A1). Removal of these two salts to less than one equivalent per dendrimer can be achieved using less than 20 mg of dendrimer loaded per PD-10 column; however they are most likely exchanged for chlorides and other salts that cannot be probed by NMR. The commercial material had MALDI peaks at 13kDa, 26kDa, 52kDa, 79kDa, and 105kDa, corresponding to those observed in each individual fraction's (T, I-IV) spectra. Fraction T has a distinct peak at 7kDa, either a strong $[M]^{2+}$ signal or G3 sized particles, not seen in the other spectra, which are dominated by matrix signal at that M/Z ratio. The spectra for the fraction I contains peaks that correspond to $[M]^{+}$, $[M]^{2+}$, and $[M\text{-}M]^{+}$ peaks (Figure 2.5). Fraction II, dimer, has a peak that could correspond to either G5 or a doubly ionized dimer, however fraction III, trimer, has a peak at the dimer weight which cannot be explained by ionization alone. Fraction IV, tetramer, has a peak at an M/Z ratio around 110,000 which is not present in the dimer or monomer samples, although this peak is not the most intense peak in the sample. This could be caused by the ionization process favoring much smaller species. Figure 2.4 b-c

shows a distinct increase in molecular weight as a function of HPLC retention for the fractions i-iv, further confirming that the width of the main G5 peak in the HPLC chromatograms is caused by the molecular weight distribution due to branching defects, with the least defected material containing the highest number of primary amine/trifluoroacetate pairs, and being most retained on the hydrophobic column. The presence of a peak in all samples corresponding to the monomer mass arises from multiple ionization of single particles (e.g. double charged dimer $[M\text{-}M]^{2+}$ has the same M/Z as singly charged monomer$[M]^{+}$). PAMAM dendrimers roughly double in molecular weight and number of atoms when they dimerize, making quantitative comparisons of the number of hydrogens contributing to each NMR shift challenging. It was observed that acidic pH caused by HPLC conditions caused upfield shifts of proton peaks, peak broadening, and loss of fine structure in ^{1}H-NMR due to swelling and solvent penetration when primary amines are protonated (Figure A2). To account for this, subsequent spectra were obtained using buffered solvents. To analyze the relative number of each type of hydrogen in the purified fractions, an internal standard (1,4-dioxane) was used (see supporting Figure A3). Trailing generations (T), G5 monomer (I), dimer (II), trimer (III), and tetramer (IV) fractions have similar spectra at the identical mass

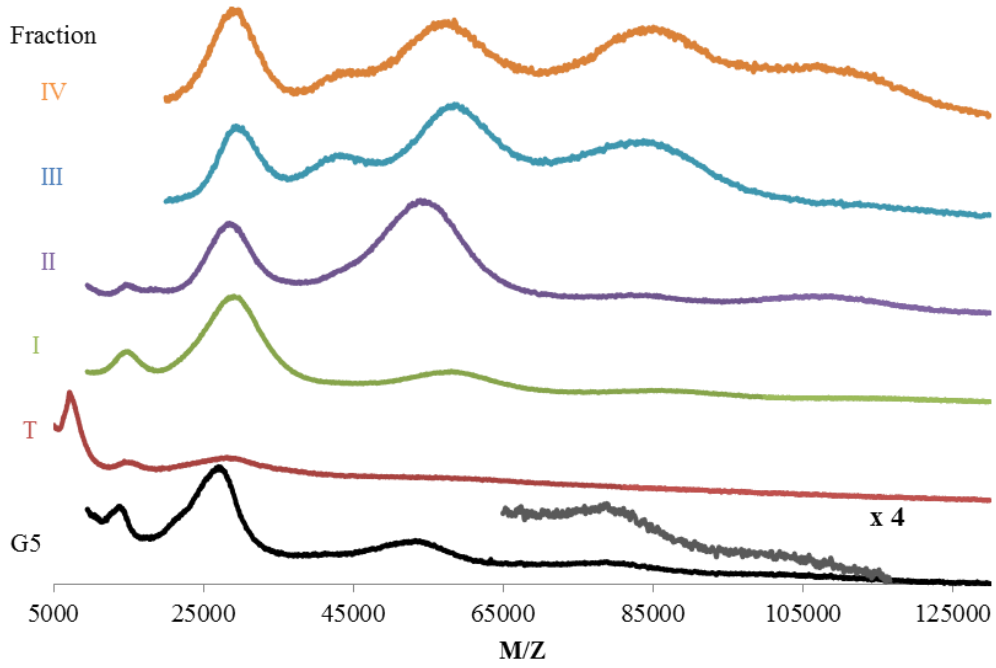

Figure 2.5. MALDI-TOF-MS spectra of fractions T, I-IV.

concentration and similar pH. However, the absolute values of all observed peaks changed for each fraction. On average, fraction T peaks integrated to 59% of fraction I, while II and III integrated to 177% and 215% of the values of fraction I respectively (absolute integration values, see Table A2). These substantial changes in integration values will impact the calculation of dendrimer-conjugate ratios by NMR if not accounted for in the analysis. Solubility of the trimer and tetramer fractions was normal for low pH (highly charged), slightly reduced for neutral pH (charged), and significantly reduced for more basic conditions (no charge). Broadening seen in the NMR spectra could be related to decreased solubility of the samples. All spectra lost some fine structure compared to the as received material, which was never exposed to TFA or buffer.

The structural variation of dimer has been further quantified by potentiometric titration. A molecularly perfect G5 PAMAM has 128 primary amines, but titration of the as-received batch used in this paper revealed on average 112 due to a combination of branch and generational defects. Fraction I, RP-HPLC-purified monomer, was titrated to have 93 primary amines per dendrimer (see supporting information). This indicates the presence a substantially larger amount of defects in G5 dendrimer than commonly believed to be present based on analyses of mixtures such as that indicated in Figure 2.1 (~110) or as compared to the theoretical perfect molecular structure (128). The number of primary amines detected on the RP-HPLC purified material decreases due to the removal of high amine-containing dimer, trimer, and tetramer defects, which comprised 22% of the as-received sample, and is 35 surface groups less than ideal due to branch defects. Likely many combinations contribute to the measured average; for example one CAP2 defect (*vide infra*) at G2, or two end caps at G3, or three at G4, would all give an average of 112 amines per dendrimer. If a new branch defect is formed at every step from G2 to G5, the final product would have 98 primary amines. The measured value of 93 amines per dendrimer would be obtained if 2.2 capping events occurred during the formation of G2, 4.4 at the formation of G3, 8.6 at G4, or 17.5 at G5. The purple dimer fraction (II) was titrated to have 180 primary amines per dendrimer, about 6 primary amines short of an exact dimer of the defected G5; however, this number is in good agreement with the scenario of dimerizing two G3 dendrimers with the average of 4.4 cap defects (resulting

in 178 primary amines) or dimerizing the G4 with an average of 8.6 branch defects (182 amines). This data suggests that dimerization events commonly occur at later synthetic steps.

It has been speculated in the literature that the width of dendrimer peaks from flow-based separations is due to molecular weight distributions caused by structural defects,[17, 23] however to date no molecular weight measurements have been coupled to these techniques. Single, three second fractions were isolated from across the monomer and dimer HPLC peaks (Figure 2.4a) and studied by MALDI-TOF-MS (Figure 2.4c). MALDI-TOF-MS of these fractions indicate a trend of increasing molecular weight with increasing retention time on the hydrophobic C18 column. As all known branching defects lead to both decreases in molecular weight and total number of primary amines, it can be inferred from this data that dendrimer eluting early in the chromatogram contains the most defects, and that a theoretically perfect G5 containing 128 primary amines would elute later, on the far right side of the G5 peak.

Using the GPC and titration data from the G5 monomer sample, we have generated simple computational models for two specific defects types that represent limiting cases for arm growth defects.[14] The CAP2 model uses an endcapping event that blocks two primary amines and does not allow further reaction. To fit the titration data of 93 primary amines an error rate of 7.6% was used. This means that at each point of growth in each step there is a 7.6% chance of a CAP2 defect. Similarly, a MA2 defect refers to a single primary amine not branching to the next full generation. This leads to an arm that is a generation behind the current, but unlike the CAP2 model still able to undergo further reaction. To fit the titration data, an error rate of 15% was used to reproduce the average number of primary amines of 93. Histograms of the simulation results of the primary amine number are shown in Figures 2.6 and 2.7, overlaid with the UPLC of fraction I. The x-axis of the simulation and RP-HPLC data were aligned by comparing the experimental molecular weights obtained from fractions i and iv (the leading and trailing edges of fraction I) to the molecular weights predicted by the defect schematics, approximate 21kDa and 28kDa.

Both types of defect models indicate that perfect G5 with 128 primary amines represents less than 0.006% of the total population. The histograms of primary amines of dendrimers generated by these models can be overlaid onto the UPLC chromatogram of G5 monomer fraction I with relatively good agreement; however when considering the predicted masses of the CAP2 and MA2 leading edge and trailing edge structures, the MA2 limiting case model compares better to the experimental data. Despite the apparent good agreement of the MA2 model, a mixture of defects, including the CAP2 model that has been confirmed experimentally for G1 and G2 material, is expected to be present.[13]

Schematic CAP2 structures are portrayed in Figure 2.6, which demonstrates the fundamental changes in overall shape and internal space in even the most common species as compared to the perfect G5. The schematic MA2 type defects, illustrated in Figure 2.7, occur almost exclusively on unique branches and not on the same branch twice, leading to structures containing both G4 and G5 shells. Some of the more defected structures have defects occurring twice on the same arm, leading to the presence of G3 shells, which are much closer to the dendrimer core. Figure 2.7 indicates that the more

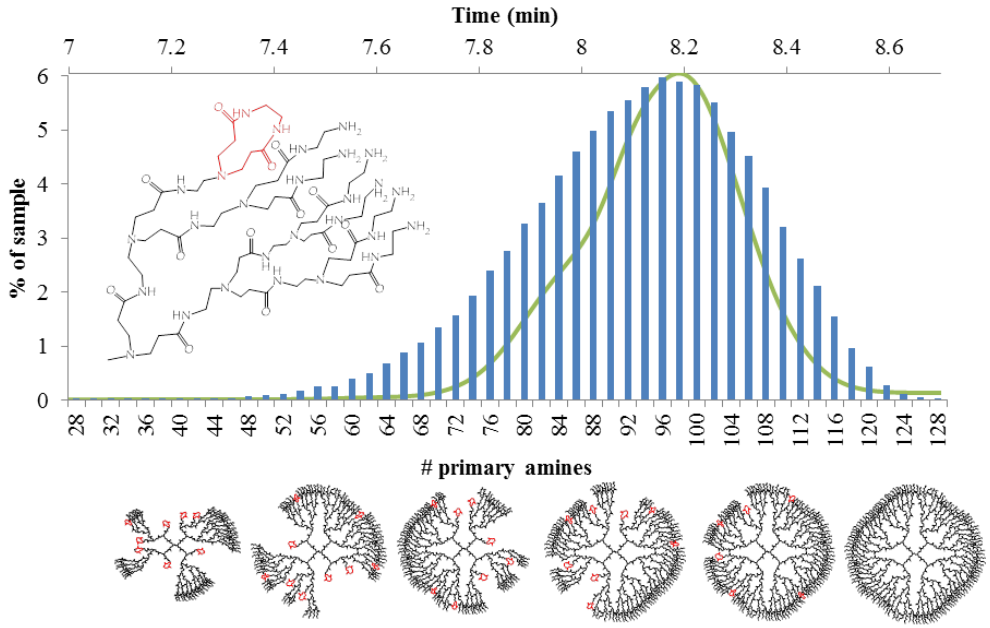

Figure 2.6. CAP2 model histogram (blue bars) overlayed with fraction I UPLC chromatogram at 210 nm. Below, from left to right, the most common structures resulting for various numbers of primary amines and their corresponding molecular weights.

defected structures have roughly equivalent contributions of G4 and G5 like size and surface groups if only MA2 defects are considered. By assuming that dendrimer mass directly correlates with the number of primary amines present, which is generally supported by our UPLC, GPC, and titration data, the PDI of the samples generated by both the CAP2 and MA2 models is calculated to be 1.01, which is in good agreement with the fraction I value of 1.019.

This agreement between this model and experimental data concludes that the observed polydispersity in generationally pure G5 PAMAM can be explained by experimental defect rates of 7-15%. By these estimations, approximately one in four G5 dendrimers have less than 85 primary amines, while three in four particles has less than 100. The entire molecular weight distribution of commercially available G5 dendrimer consists of combinations of these two defect types, as well as defects other known defects such as a

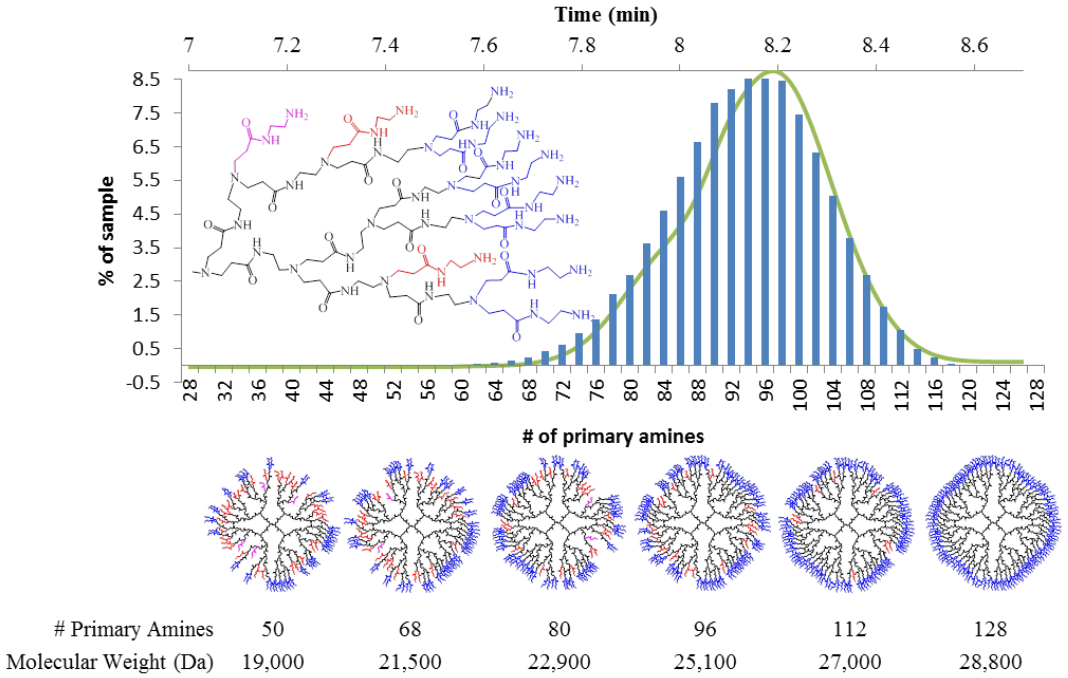

Figure 2.7. MA2 model histogram (blue bars) overlayed with fraction I UPLC chromatogram at 210 nm. Below, from left to right, the most common structures for various numbers of primary amines and their molecular weights. Core groups are black, shell groups colored. Blue she indicate G5 level amines, red have one defect (G4 shell), and purple have 2 defects on the same branch (G3).

half reacted primary amine leading to one missing primary amine as opposed to two, and the trailing and oligomer generational defects. HPLC provides a powerful tool to both observe and isolate these defect structures to allow for analyses of structure, chemical behavior, and eventually biological behavior.

Previous work from the group[50, 51] has demonstrated the ability to employ rp-HPLC to obtain G5 PAMAM samples conjugated to precise numbers of functional ligands from stochastic distributions. However, as Figure 2.8a demonstrates, dimeric and trimeric contaminants in as-received dendrimer co-elute with the G5 monomer that is bound to one ligand. Similarly, G5 dimer with one ligand co-elutes with the monomer conjugated to two ligands, e*tc*. The resulting nominally "monomer" products will thus contain substantial amount of dimer impurities that also contain n-1 of the desired n number of ligands per polymer particle. The work presented here done on a preparative scale can be used to obtain gram quantities of generationally pure starting material. This allows for synthesis of dimer-free conjugates and subsequently, generationally pure G5 samples with precise numbers of functional ligands. Removal of trailing and generational impurities from conjugated materials also enhances the effective resolution of the rp-HPLC separation (Figure 2.8b). This results in samples with improved ligand number homogeneity, higher purity, and increases overall sample recovery.

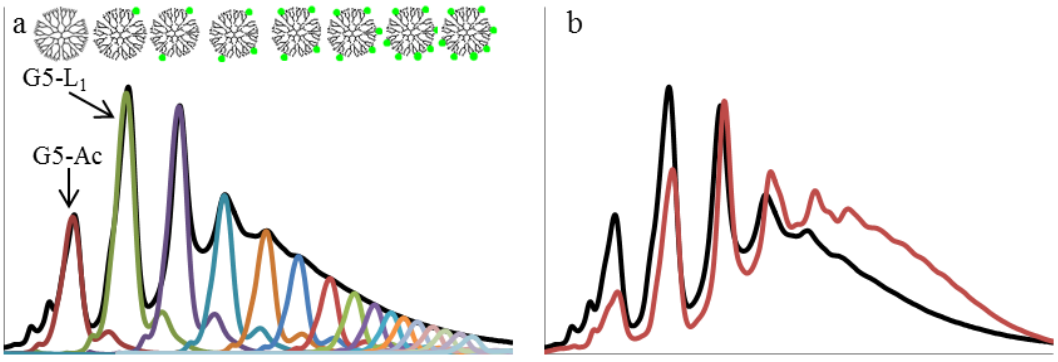

Figure 2.8: UPLC at 210 nm. (a) as-received acetylated G5 PAMAM (G5-Ac, red trace) contains high weight impurities with no ligand that co-elute with G5 monomers containing one ligand (G5-L_1, green trace) in a conjugated sample (black trace). (b) Conjugation to an HPLC purified G5 monomer sample (red trace) has narrowed peak width and improved peak resolution compared to the as-received conjugation (black trace).

Conclusions

The narrow size range, aqueous solubility, and functionalizable surface of G5 PAMAM dendrimer give it great promise for future biomedical applications. However, structural imperfections create sub-populations within the sample that have different chemical and biological characteristics. A significant portion of commercial material contains species with up to threefold higher molecular weights, reduced solubility, and different chemical behavior. This will impact the drug loading capacity, accuracy of loading measurements, and likely the biodistribution of dendrimer based drug delivery systems. The G5 sized dendrimers present in the as-received material also contained an average of 93 primary amines, approximately 23% defected, compared to previous estimates of 110, 14% defected, indicating that branching type defects are twice as prevalent as previously proposed. We have successfully employed rp-HPLC to not only produce higher purity G5 dendrimer, but to isolate dimer and trimer samples for study. These samples have been thoroughly characterized by molecular weight and NMR techniques. These new purification protocols are of central importance for obtaining materials that can be used to generate polymer with precisely defined numbers of ligands. This methodology can be used to isolate gram-scale quantities of generationally purified, well characterized G5 PAMAM dendrimer, and potentially can be extended to include other generations of PAMAM.

References

1. Pettit, M.W., et al., *Poly(amidoamine) polymers: soluble linear amphiphilic drug-delivery systems for genes, proteins and oligonucleotides.* Therapeutic Delivery, 2011. **2**(7): p. 907-917.
2. Tomalia, D.A., *Dendrimers as multi-purpose nanodevices for oncology drug delivery and diagnostic imaging.* Nanomedicine : nanotechnology, biology, and medicine, 2006. **2**(4): p. 309.
3. Svenson, S., *Dendrimers as versatile platform in drug delivery applications.* Eur. J. Pharm. Biopharm., 2009. **71**(3): p. 445-462.
4. Nanjwade, B.K., et al., *Dendrimers: Emerging polymers for drug-delivery systems.* European Journal of Pharmaceutical Sciences, 2009. **38**(3): p. 185-196.
5. Gingras, M. and M. Roy, *Degradable Dendrimers for Drug Delivery*, in *Dendrimer-Based Drug Delivery Systems*. 2012, John Wiley & Sons, Inc. p. 239-305.

6. Esfand, R. and D.A. Tomalia, *Poly(amidoamine) (PAMAM) dendrimers: from biomimicry to drug delivery and biomedical applications.* Drug Discovery Today, 2001. **6**(8): p. 427-436.
7. Yang, H. and W.J. Kao, *Dendrimers for pharmaceutical and biomedical applications.* Journal of Biomaterials Science, Polymer Edition, 2006. **17**(1-2): p. 3-19.
8. Huang, B., et al., *The facile synthesis of multifunctional PAMAM dendrimer conjugates through copper-free click chemistry*. Bioorganic & Medicinal Chemistry Letters, 2012. **22**(9): p. 3152-3156.
9. Nourse, A., D.B. Millar, and A.P. Minton, *Physicochemical characterization of generation 5 polyamidoamine dendrimers.* Biopolymers, 2000. **53**(4): p. 316-328.
10. Majoros, I.J., et al., *PAMAM Dendrimer-Based Multifunctional Conjugate for Cancer Therapy: Synthesis, Characterization, and Functionality.* Biomacromolecules, 2006. **7**(2): p. 572-579.
11. Shi, X., et al., *Multifunctional Dendrimer-Modified Multiwalled Carbon Nanotubes: Synthesis, Characterization, and In Vitro Cancer Cell Targeting and Imaging.* Biomacromolecules, 2009. **10**(7): p. 1744-1750.
12. Wolfenden, M.L. and M.J. Cloninger, *Mannose/Glucose-Functionalized Dendrimers To Investigate the Predictable Tunability of Multivalent Interactions.* Journal of the American Chemical Society, 2005. **127**(35): p. 12168-12169.
13. Shukla, R., et al., *HER2 Specific Tumor Targeting with Dendrimer Conjugated Anti-HER2 mAb.* Bioconjugate Chemistry, 2006. **17**(5): p. 1109-1115.
14. Shukla, R., et al., *Tumor angiogenic vasculature targeting with PAMAM dendrimer–RGD conjugates.* Chemical Communications, 2005(46): p. 5739.
15. Hong, S., et al., *The Binding Avidity of a Nanoparticle-Based Multivalent Targeted Drug Delivery Platform.* Chemistry & Biology, 2007. **14**(1): p. 107-115.
16. Kim, Y., A.M. Klutz, and K.A. Jacobson, *Systematic Investigation of Polyamidoamine Dendrimers Surface-Modified with Poly(ethylene glycol) for Drug Delivery Applications: Synthesis, Characterization, and Evaluation of Cytotoxicity.* Bioconjugate Chemistry, 2008. **19**(8): p. 1660-1672.
17. Majoros, I.J., et al., *Poly(amidoamine) Dendrimer-Based Multifunctional Engineered Nanodevice for Cancer Therapy*. Journal of Medicinal Chemistry, 2005. **48**(19): p. 5892-5899.
18. Wang, Y., et al., *Targeted delivery of doxorubicin into cancer cells using a folic acid–dendrimer conjugate.* Polymer Chemistry, 2011. **2**(8): p. 1754.
19. Wang, Y., et al., *Encapsulation of 2-methoxyestradiol within multifunctional poly(amidoamine) dendrimers for targeted cancer therapy.* Biomaterials, 2011. **32**(12): p. 3322-3329.
20. Kang, H., et al., *Tat-Conjugated PAMAM Dendrimers as Delivery Agents for Antisense and siRNA Oligonucleotides.* Pharmaceutical Research, 2005. **22**(12): p. 2099-2106.
21. Fant, K., et al., *DNA Condensation by PAMAM Dendrimers: Self-Assembly Characteristics and Effect on Transcription†.* Biochemistry, 2008. **47**(6): p. 1732-1740.
22. Navarro, G. and C. Tros de Ilarduya, *Activated and non-activated PAMAM dendrimers for gene delivery in vitro and in vivo.* Nanomedicine: Nanotechnology, Biology and Medicine, 2009. **5**(3): p. 287-297.
23. Tang, Y., et al., *Effecient in Vitro siRNA Delivery and Intramuscular Gene Silencing using PEG-Modified PAMAM Dendrimers.* Molecular Pharmaceutics, 2012. **9**: p. 1812-1821.
24. Myc, A., et al., *Dendrimer-Based Targeted Delivery of an Apoptotic Sensor in Cancer Cells.* Biomacromolecules, 2006. **8**(1): p. 13-18.

25. Ali, M.M., et al., *Synthesis and Relaxometric Studies of a Dendrimer-Based pH-Responsive MRI Contrast Agent.* Chemistry - A European Journal, 2008. **14**(24): p. 7250-7258.
26. Yang, W., et al., *Targeting cancer cells with biotin–dendrimer conjugates.* European Journal of Medicinal Chemistry, 2009. **44**(2): p. 862-868.
27. Wang, H., et al., *Computed tomography imaging of cancer cells using acetylated dendrimer-entrapped gold nanoparticles.* Biomaterials, 2011. **32**(11): p. 2979-2988.
28. Peng, C., et al., *PEGylated dendrimer-entrapped gold nanoparticles for in vivo blood pool and tumor imaging by computed tomography*. Biomaterials, 2012. **33**(4): p. 1107-1119.
29. Wang, H., et al., *Folic acid-modified dendrimer-entrapped gold nanoparticles as nanoprobes for targeted CT imaging of human lung adencarcinoma.* Biomaterials, 2013. **34**(2): p. 470-480.
30. Peterson, J., et al., *Structural deviations in poly(amidoamine) dendrimers: a MALDI-TOF MS analysis.* European Polymer Journal, 2003. **39**(1): p. 33-42.
31. Tolić, L.P., et al., *Electrospray ionization Fourier transform ion cyclotron resonance mass spectrometric characterization of high molecular mass Starburst™ dendrimers.* International Journal of Mass Spectrometry and Ion Processes, 1997. **165–166**(0): p. 405-418.
32. Opitz, A.W. and N.J. Wagner, *Structural investigations of poly(amido amine) dendrimers in methanol using molecular dynamics.* Journal of Polymer Science Part B: Polymer Physics, 2006. **44**(21): p. 3062-3077.
33. Liu, Y., et al., *PAMAM Dendrimers Undergo pH Responsive Conformational Changes without Swelling.* Journal of the American Chemical Society, 2009. **131**(8): p. 2798-2799.
34. Maiti, P.K. and W.A. Goddard, *Solvent Quality Changes the Structure of G8 PAMAM Dendrimer, a Disagreement with*

Some Experimental Interpretations. J. Phys. Chem. B, 2006. **110**: p. 25628-25632.
35. Maiti, P.K., et al., *Structure of PAMAM Dendrimers: Generations 1 through 11.* Macromolecules, 2004. **37**(16): p. 6236-6254.
36. Maiti, P.K., et al., *Effect of Solvent and pH on the Structure of PAMAM Dendrimers.* Macromolecules, 2005. **38**(3): p. 979-991.
37. Maiti, P.K. and R. Messina, *Counterion Distribution and ζ-Potential in PAMAM Dendrimer.* Macromolecules, 2008. **41**(13): p. 5002-5006.
38. Maiti, P.K., et al., *Structure of polyamidoamide dendrimers up to limiting generations: A mesoscale description.* The Journal of Chemical Physics, 2009. **130**(14): p. 144902.
39. Nisato, G., R. Ivkov, and E.J. Amis, *Structure of Charged Dendrimer Solutions As Seen by Small-Angle Neutron Scattering.* Macromolecules, 1999. **32**(18): p. 5895-5900.
40. Liu, Y., et al., *Electrostatic Swelling and Conformational Variation Observed in High-Generation Polyelectrolyte Dendrimers.* The Journal of Physical Chemistry Letters, 2010. **1**(13): p. 2020-2024.
41. Chen, W.-R., et al., *Small Angle Neutron Scattering Studies of the Counterion Effects on the Molecular Conformation and Structure of Charged G4 PAMAM Dendrimers in Aqueous Solutions.* Macromolecules, 2007. **40**(16): p. 5887-5898.
42. Lee, S., et al., *Study on elution behavior of poly(amidoamine) dendrimers and their interaction with bovine serum albumin in asymmetrical flow field-flow fractionation.* Analytical and Bioanalytical Chemistry, 2009. **396**(4): p. 1581-1588.
43. Shi, X., et al., *Capillary electrophoresis of polycationic poly(amidoamine) dendrimers.* ELECTROPHORESIS, 2005. **26**(15): p. 2949-2959.
44. Brothers Ii, H.M., L.T. Piehler, and D.A. Tomalia, *Slab-gel and capillary electrophoretic characterization of polyamidoamine dendrimers.* Journal of Chromatography A, 1998. **814**(1–2): p. 233-246.

45. Ebber, A., et al., *Application of capillary zone electrophoresis to the separation and characterization of poly(amidoamine) dendrimers with an ethylenediamine core*. Journal of Chromatography A, 2002. **949**(1–2): p. 351-358.
46. Islam, M.T., et al., *HPLC Separation of Different Generations of Poly(amidoamine) Dendrimers Modified with Various Terminal Groups.* Analytical Chemistry, 2005. **77**(7): p. 2063-2070.
47. Shi, X., et al., *HPLC analysis of functionalized poly(amidoamine) dendrimers and the interaction between a folate-dendrimer conjugate and folate binding protein.* Analyst, 2006. **131**(7): p. 842-848.
48. Mullen, D.G., et al., *Best Practices for Purification and Characterization of PAMAM Dendrimer.* Macromolecules, 2012. **45**(12): p. 5316-5320.
49. Waddell, J.N., et al., *Origin of broad polydispersion in functionalized dendrimers and its effects on cancer-cell binding affinity.* Physical Review E, 2010. **82**: p. 036108.
50. Mullen, D.G. and M.M. Banaszak Holl, *Heterogeneous Ligand–Nanoparticle Distributions: A Major Obstacle to Scientific Understanding and Commercial Translation.* Accounts of Chemical Research, 2011. **44**(11): p. 1135-1145.
51. Mullen, D.G., et al., *Isolation and Characterization of Dendrimers with Precise Numbers of Functional Groups.* Chemistry – A European Journal, 2010. **16**(35): p. 10675-10678.

Chapter 3

PAMAM Dendrimers for Quantized Megamers

This chapter was previously published as "PAMAM dendrimers as quantized building blocks for novel nanostructures" Soft Matter *(2013), 9, 11188. The corresponding supporting information can be found in Appendix B.*

Introduction.

The need to address biological challenges across multiple hierarchical levels ranging from molecules to cells to tissue has increased the demand for synthetic strategies leading to well-defined structures on a nanometer to micron scale. Achieving such size ranges with classic synthetic strategies remains challenging. Tomalia proposed the utilization of dendrimers as quantized building blocks, termed "soft super atoms", combined with controlled assembly to substantially expand the range of size scales available for soft synthetic materials with controlled morphology and other physical properties.[1-4] Glotzer and Solomon have discussed an analogous proposal for the use of nanocrystals and colloidal particles as "hard super atoms".[5] To function as super atoms, it is necessary to have control over size, shape, and surface chemistry (i.e. reactivity) to create materials with nano-periodic trends independent of variations in the monomeric material. The assembly of synthetic nanomaterials or super atoms generates larger nano to microscale structures that fall into the following classes: I) Extended Nanostructures, which extend infinitely in one, two or three dimensions, a class that includes fibers, sheets, and lattices II) Stochastic Nanoclusters and III) Precise Nanoclusters (Figure 3.1). Extended Nanostructures have precise control of local architecture in one, two, or three dimensions and stochastic sizes. Stochastic Nanoclusters have control of particle size with heterogeneity in terms of numbers of super atoms per particle. Precise Nanoclusters have monodisperse assemblies of super atoms, allowing for a digital control of nanocluster size and properties. Substantial

progress has been made in the assembly of hard super atoms for all three classes employing rigid polymers,[6, 7] gold,[8-13] and other particles.[14] Substantial efforts have also been made in the area of soft super atoms, despite the challenges associated with polydispersity of polymeric building blocks. It is the use of polymers as soft super atoms, which offer tunable surface qualities such as charge and conjugation chemistry that can enhance solubility, biological compatibility, and allow for modification with drugs, dyes, and targeting agents of interest,[15] that are the focus of this report.

The dendritic polymer architecture has the potential to provide a well-defined and highly functionalizable structure for utilization as a soft super atom, building block. Assemblies utilizing dendrimers as the monomer units result in larger polymer-like structures or megamers.[16, 17] Work in this field has been pioneered by Tomalia[18-21] with the "tecto-dendrimer" strategy of self-assembling shell dendrimers around a core dendrimer followed by covalent cross-linking. This class of nanostructures utilizes steric hindrance to saturate the core dendrimer with various sized (i.e. generation) shell dendrimers to create megamers resulting in precise

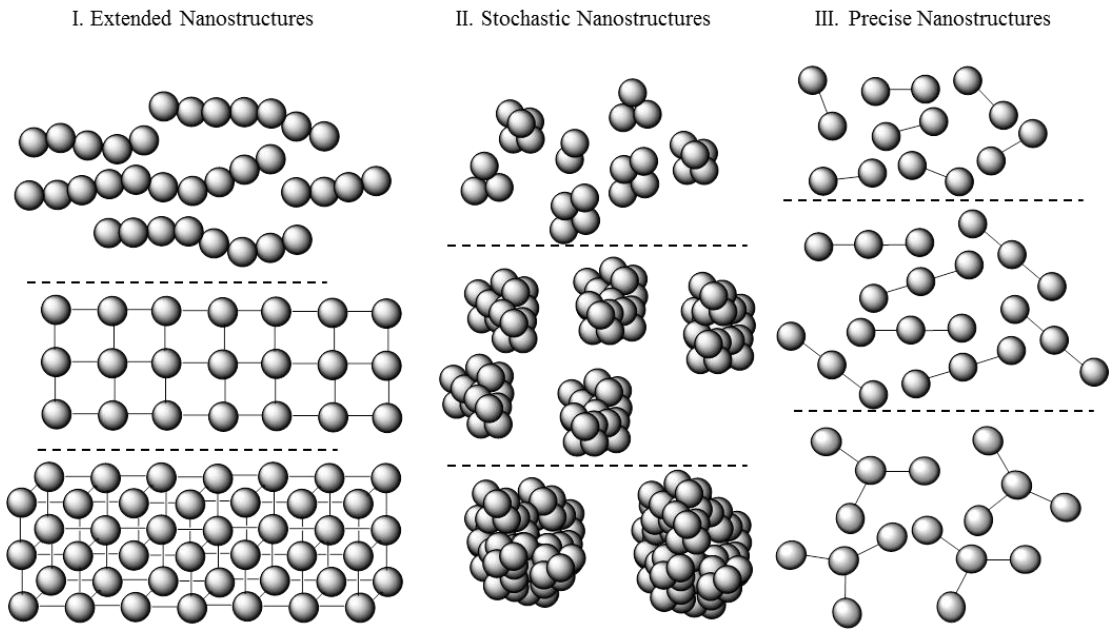

Figure 3.1. Controlled super atom-based nanostructures can be classified as: I) Extended Nanostructures including in one to three dimensions (for example: fibers, sheets, and lattices) II) Stochastic Nanoclusters and III) Precise Nanoclusters.

nanostructures. Surface modification, with reactions such as acetylation, allows for fewer shell dendrimers to saturate the surface to give modular control of the resulting structures, but relying on stochastic reactions leads to a loss of precisely controlled structures.[22] Tecto-dendrimer assembly allows for building large megamers without encountering limiting generation effects[23] such as loss of flexibility, low solubility, and increased polydispersity of monomeric dendrimers of similar size ranges.[18] The self-assembly approach has been shown to yield structures of Class II with a fairly narrow mass and size range but does not allow systematic, modular variation of the number of components.

An alternative approach has been to use cross-linkers to assemble groups of small dendrimers or dendrons into hierarchical structures. Such techniques have been successfully employed to synthesize extended supramolecular structures such as Class I porous networks[17, 24, 25], one dimensional structures[26], and two and three dimension structures (exemplified by Percec et al.).[27, 28] There are also examples of the assembly of dendrimers into Class II supramolecular nanoparticles with modular size control via crosslinking with linear polymers.[29]

Class III precise, three-dimensional architectures have been synthesized using chemistries to specifically link controlled numbers of dendrons together through the focal point[30] or through single ligands on two dendrimers.[31, 32] The former approach, while resulting in precise nanoclusters, is limited by control over functionality of both the linking system and the dendron. To date, only small (4,000 to 30,000 Da) precise dendron-based dumbbell nanostructures have been assembled.[30, 33] A particularly interesting example by Liu et al. assembled dendrons around a

Table 3.1. Summary of soft superatom synthetic approaches and characterization.

streptavidin to form tetramer-like clusters, an approach limited by the number of binding sites on the protein linker system.[34] Table 3.1 gives a summary of the synthesis strategy and characterization of previous soft super atom Class II and III materials.

Reference	System	Class	Mass Range	Chromatography	Mass Spec	LS	NMR	Microscopy
Present work	Dendrimer/click ligand clusters	III	30-150 kDa	GPC, rp-HPLC	MALDI	No	Proton	No
[24]	Dendrimer/click ligand dumbells	II	~60 kDa	GPC	No	No	Proton	No
[21, 25, 26]	Tecto-dendrimers	III	300 kDa	PAGE	MALDI	No	No	AFM
[27]	Dendrimer/PEI clusters	II	na	No	No	Yes	No	TEM
[28]	PEG/dendron dumbbells	III	5 kDa	GPC	MALDI	No	Proton, Carbon	No
[29]	DNA/Dendron/Strept avidin	III	~100 kDa	PAGE	No	Yes	Proton	No
[30]	DNA/Dendron Dumbbells	III	10-30 kDa	PAGE	MALDI	No	No	No

Table 3.1. Summary of soft superatom synthetic approaches and characterization.

Poly(amidoamine) (PAMAM) dendrimers are of particular interest for implementation as soft super atoms due to their advantageous properties such as aqueous solubility, biocompatibility, and functionalizable surface groups. The dendrimers implemented in this work are fifth generation synthesized divergently from an ethylenediamine core.[35] In this work, the positively charged primary amine surface has been neutralized via acetylation, which decreases the cytotoxicity of the material and increases resolution of the species in the reverse-phase high performance liquid chromatography (rp-HPLC) methods employed. Although previous studies indicated the potential of dendrimers to serve as soft super atoms, synthetic by-products in PAMAM dendrimer lead to trailing generation and oligomeric impurities ranging from 1.4 to 115 kDa (Figure 3.2). The presence of these impurity species represent an important

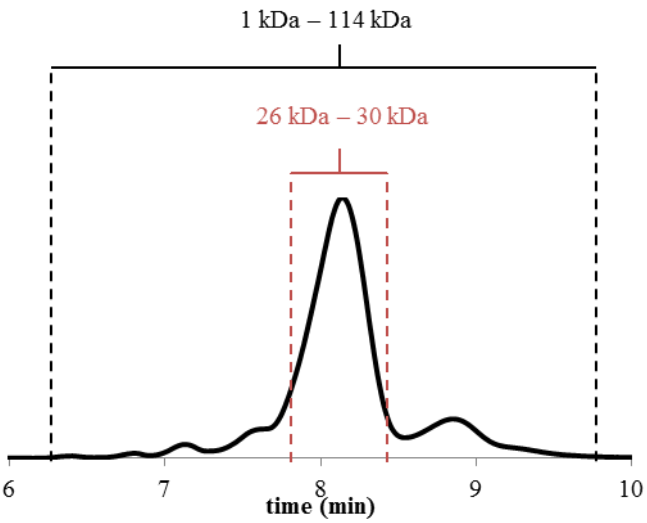

Figure 3.2. The monomer G5 PAMAM material used for this study is indicated by the 26 – 30 kDa fraction within the dashed red lines. Isolation of monomer G5 reduces size range of PAMAM building blocks by over an order of magnitude.

limitation on the degree of homogeneity one can hope to achieve for the self-assembled or linked megamer products and represent an important difference between this class of super atoms and the actual atoms they are meant to mimic.

Recent work by van Dongen, Banaszak Holl et. al has enabled the isolation of monomeric PAMAM dendrimer for use as a soft super atom.[36] Here, we implement a method to synthesize assemblies of monomeric dendrimers via click chemistry. Our approach differs from previous strategies in the following ways: 1) our soft super atom, G5 PAMAM, does not contain the trailing generations, dimer, and trimer that typically remain in G5 and higher generation PAMAM preparations[36, 37] 2) we assemble dendrimers containing defined numbers of ligands per dendrimer particle, 3) a digital set of precise, flexible structures has been generated ranging from 30 to 150 kDa using ~30 kDa units. This strategy differs from previous approaches that relied on self-assembly determined by dendrimer size or employed dendrimers containing a stochastic distribution of ligands per dendrimer or polymer particle.

Materials. All chemicals and materials were purchased from Sigma Aldrich or Fischer Scientific and used as received unless otherwise specified. Monomer G5 PAMAM dendrimer was purchased from Dendritech and purified as previously reported to remove trailing and oligomer impurities.[36] Click-Easy™ MFCO-N-hydroxysuccinimide was purchased from Berry & Associates Synthetic Medicinal Chemistry. 3-(4-(2-azidoethoxy)phenyl)propanoic acid (azide ligand) was prepared as described previously.[38]

Preparation of G5-Ac-MFCO$_{4.0(avg)}$ and G5-Ac-Azide$_{4.0(avg)}$ conjugates. Conjugates were prepared using monomer G5, and azide ligand or Click-Easy™ MFCO-N-hydroxysuccinimide. Amine-terminated G5 (319.6 mg for azide conjugate, 299.5 mg for MFCO conjugate) was dissolved to give a 0.16 uM solution in deionized water (DI). The azide ligand (10 mg) was pre-activated in a solution at 22 mM in acetonitrile (2.5 mL) with 58 mM 1-ethyl-3-(3-dimethylaminopropyl)carbodiimide (24.1 mg) and 60 mM N-hydroxysuccinimide (14.4 mg). Click-Easy™ MFCO-N-

hydroxysuccinimide (9.3 mg) was not pre-activated and was prepared by dissolving to 10.5 uM in acetonitrile (2.3 mL). Four molar equivalents of the ligand solution was added dropwise via syringe pump to the dendrimer solutions. The solutions were stirred overnight. The products were purified using Amicon Ultra Centrifugal units, 10kDa cutoff membranes, 2 PBS washes and 4 DI washes. A white solid was isolated via lyophillization for each conjugate (204.7 mg for azide conjugate, 231.1 mg for MFCO conjugate). The materials were then fully acetylated by re-dissolving in anhydrous methanol (0.19 uM, 30 mL) and adding 450 equiv of triethylamine and 360 equiv of acetic anhydride, stirring for 4 hours, the methanol was then removed and the sample redissolved in water, purified by the same centrifugation protocols previously described, and isolated by lyophillization. G5-Ac-$MFCO_{4.0(avg)}$ and G5-Ac-$Azide_{4.0(avg)}$ were characterized by rp-UPLC and ^{1}H-NMR (see supporting information).

Isolation of conjugates containing precisely defined ratios of G5-Ac-$MFCO_n$ (n = 1 – 4) and G5-Ac-$Azide_n$ (n = 1 – 4). Dendrimers containing precise ratios of MFCO or azide ligands per particle were isolated via rp-HPLC. Multiple injections of G5-Ac-$MFCO_{4.0(avg)}$ or G5-Ac-$Azide_{4.0(avg)}$ were performed on a C18 column using a water/acetonitrile gradient with 0.1% TFA. Fractions were collected as the material eluted and combined to obtain samples with ratios of n = 0, 1, 2, 3, and 4 MFCO or azide ligands, and a final sample that contained dendrimer with 4 or more click ligands. Products were purified using PD-10 desalting protocols as specified in the instruction manual, with DI used as the equilibration buffer and samples initially dissolved in 10xPBS, then lyophilized to dry. Samples were characterized by rp-UPLC and ^{1}H-NMR. Curve fitting of UPLCs using Igor Pro was performed to provide yield, purity, and rp-HPLC number of MFCO averages (see supporting information).

Synthesis of megamer samples. n (n = 1 - 4) equivalents of G5-Ac-$Azide_1$was dissolved to give a 300 µM solution in dimethylsulfoxide. To this, 1 equivalent of G5-Ac-$MFCO_n$ (n = 1 - 4) was added. For example, to prepare the tetramer sample (n = 3), 2.7 mg of G5-Ac-$Azide_1$ was dissolved in 273 µL of DMSO, then 0.9 mg of G5-

Ac-$MFCO_3$ was added. Solutions were protected from light and agitated for 48 hours. The samples were lyophilized to give white solids.

Methods.

High Performance Liquid Chromatography. Isolation of G5-Ac-$MFCO_n$ (n = 1 – 4) and G5-Ac-$Azide_n$ (n = 1 – 4) fractions was achieved using a Phenomenex Jupiter 300Å C18 Prep Column (21.2 x 150 mm, 5 µm particles) equipped with a Waters 600 Controller, Waters 2707 Autosampler, and Waters 2998 Photodiode Array running Empower 2 Software, additionally equipped with a Waters Fraction Collector III. The weak solvent (Solvent A) was HPLC Grade Water with 0.1% TFA, and the strong solvent (Solvent B) was HPLC Grade Acetonitrile with 0.1% TFA. The gradient employed was as follows: 2.1 min load step at 95%A/5%B, 3.9 min gradient to 80%A/20%B, 15 min gradient to 65%A/35%B, 5 min gradient to 55%A/45%B, followed by 3 min was at 20%A/80%B, then equilibrating at starting conditions for 5 min before next injection. G5-Ac-$MFCO_{4.0(avg)}$ or G5-Ac-$Azide_{4.0(avg)}$ was dissolved to 20 mg/mL concentration and 910 uL injections were used. Five second fractions were collected starting at 9 min 30 sec into each run for a total of 120 fractions. rp-UPLCs were performed with a scaled method using an Agilent 2.1 x 100 mm column.

LC Peak Fitting. rp-UPLC chromatograms were fit with Gaussian peaks using Igor Pro Version 6.0.3.1 software. Peak widths within a chromatogram were kept constant.

Nuclear Magnetic Resonance Spectroscopy. NMR experiments were performed on Varian VNMRS 500. ^{1}H-NMR spectra were obtained used 10 second pre-acquisition delays and a total of 64 scans. All sample solutions were set to an approximate dendrimer concentration of 5 mg/mL in deuterium oxide.

Gel Permeation Chromatography. Gel permeation chromatography experiments were performed on an Alliance Waters 2695 separation module equipped with a 2487 dual wavelength UV absorbance detector (Waters Corporation), a Wyatt HELEOS Multi Angle Laser Light Scattering (MALLS) detector, and an Optilab rEX differential

refractometer. Columns employed were TosoHaas TSK-Gel Guard PHW 06762 (75 mm × 7.5 mm, 12 mm), G 2000 PW 05761 (300 mm × 7.5 mm, 10 mm), G 3000 PW 05762 (300 mm × 7.5 mm, 10 mm), and G 4000 PW (300 mm × 7.5 mm, 1 mm). Column temperature was maintained at 25 ± 0.1 °C with a Waters temperature control module. The isocratic mobile phase was 0.1 M citric acid and 0.025 wt % sodium azide, pH 2.74, at a flow rate of 1 mL/min. The sample concentration was 10 mg/5 mL with an injection volume of 100 μL. This was used to calculate the weight average molecular weight, Mw, and the number average molecular weight, Mn, with Astra 5.3.2 software. Values for dn/dc were kept at a constant of 0.215.

Mass Spectrometry. Matrix-assisted Laser-Desorption Time-of-Flight Mass Spectrometry (MALDI-TOF-MS) was performed using a MALDI Micro MX running MassLynx Version 4.0 software. Dendrimer samples were prepared by dissolving in DI water at concentration 10 mg/mL, then serial diluting with methanol 1:1, then 1:4. The samples were then mixed 1:1 with the matrix dihydroxybenzoic acid (concentration of 10 mg/mL in 1:1 water/acetonitrile) and spotted on to a MALDI plate. Samples were calibrated using bovine serum albumin with a matrix of sinapic acid. At least 150 laser shots were compiled for each spectrum. The spectra were smoothed using the MassLynx Software settings of Smooth window (channels) equals 12, and Number of smooths equals 12. No baseline subtraction or peak centering was performed.

Results and Discussion.

PAMAM dendrimers have been extensively studied as nanoscale biomedical devices due to their low polydispersity, multiple sites for chemical modification, flexibility, water solubility at high generations, and biocompatibility.[15, 39, 40] Recent work has employed rp-HPLC to remove both generational and oligomer (primarily dimer and trimer) impurities from generation 5 (G5) PAMAM to obtain samples of G5 monomer with a PDI under 1.02 (Figure 2).[36] The mass dispersity of the building block materials has been reduced from greater than 100 kDa to less than 3 kDa. In

order to assemble these monomeric units into controlled megamer units, we have employed our methods for attaching precise numbers of click conjugation functional groups per dendrimer particle.[38, 41, 42] This synthetic strategy generates materials with precise ligand/particle ratios in a manner that is independent of the mass dispersity of the soft super atom scaffold, thus decoupling mass dispersity and particle assembly. Although work in the tecto-dendrimer field has been successful in generating highly homogenous assemblies of dendrimers, the size of these clusters is pre-determined by the size of the core and shell dendrimers and cannot be modularly controlled. For example, assembly of G5 PAMAM around a core G7 PAMAM yielded primarily $G7(G5)_{12}$, with incompletely packed shells containing 9 to 11 G5 per G7 also observed.[20] The self-assembly process does not allow for the generation of a controlled set of samples to stoichiometry $G7(G5)_n$ were n is digitally varied. In addition, dispersity in numbers of G5 packing around G7 may arise from the molecular weight distribution present in both the G5 and G7 samples including trailing generations and oligomers.

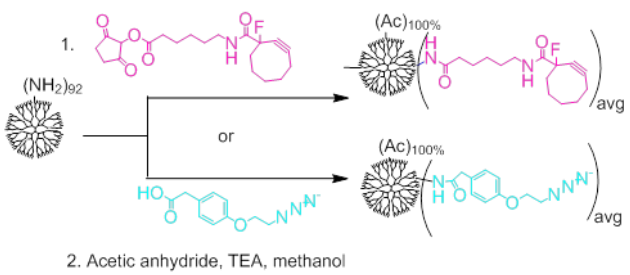

Scheme 3.1. Synthesis of acetylated stochastic ligand-dendrimer conjugates.

The synthetic strategy for the click conjugates and megamers is outlined in Scheme 3.1. First, a stochastic conjugation via a peptide bond to an azide or ring-strained cyclooctyne click ligand is followed by acetylation of all remaining primary amine groups (Scheme 3.1). These materials are designated G5-Ac-$MFCO_{n(avg)}$ and G5-Ac-$Azide_{n(avg)}$. In order to optimize the amount of material for isolation of dendrimer containing 1-4 click linkers, an initial stochastic average of 3-4 ligands/particle was typically employed. Isolation of dendrimer samples containing precise click-ligand/dendrimer ratios, as opposed to an average ratio made of up a Poisson distribution, was achieved using semi-preparative scale rp-HPLC (Figure 3.3 a) following previously published protocols.[38, 41] The dendrimers are retained on the

hydrophobic C18 column as a function of the number (n) of hydrophobic ligands conjugated to the dendrimer surface. This model is supported by the increased resolution of the MFCO conjugate, which contains the hydrophobic cyclooctyne entity and a 5 carbon linker, as compared to the azide conjugate. The successful application of this isolation process to the commercially available MFCO ligand demonstrates a broader versatility for this separation process. rp-UPLC was employed to confirm that successful separation was achieved (Figures 3.3 b, B1). The initial stochastic distribution of click ligand on the dendrimer can be visualized[43] and subsequently separated via rp-HPLC due to increased retention time with the increasing numbers of hydrophobic ligands available for interaction with the hydrophobic C18 stationary phase.[38, 41, 42] These materials are designated G5-Ac-$MFCO_n$ (n = 1 – 4) and G5-Ac-$Azide_n$ (n = 1 – 4). ^{1}H NMR also confirmed that the desired click-ligand/dendrimer ratios had been achieved (Figures B2, B3; Tables B1, B2). In assessing the purity of each isolated fraction containing the precisely defined ligand/particle ratio (n ligands per dendrimer), rp-UPLC provides the most direct measure. The separation is based on the number of hydrophobic ligands per particle and excellent separation is achieved. The G5 PAMAM dendrimers are flexible enough to effectively display the ligands to the hydrophobic C18 support regardless of their relative conjugation point on the PAMAM scaffold. The assessment of the ligand/particle ratio by ^{1}H NMR requires a number of key assumptions and relies on average polymer properties at key points of the analysis. The NMR-based ratio is determined by comparing the integration of the ligand protons to the integration of the terminal –$NHC(O)CH_3$ groups on the

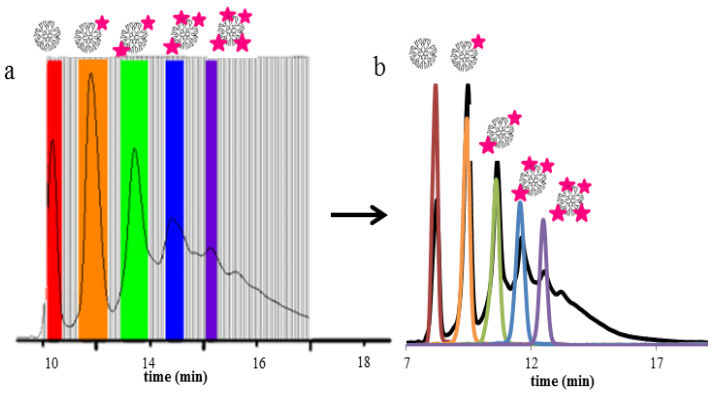

Figure 3.3. (a) Semi-prep rp-HPLC isolation of precisely defined G5-$MFCO_n$ species, colored bars represent combined fractions. (b) UPLC of combined fractions demonstrates that each sample now contains a single particular ligand/dendrimer ratio.

dendrimer. This analysis suffers from comparing a small value (the ligand) to a large value (acetamide group) and from having to employ an average number of these groups for G5 PAMAM of 93, although this number varies from ~70 to 116 for each particle. For these reasons, we believe the rp-UPLC measurement provides the better quantitative analysis of ligand/particle ratio.

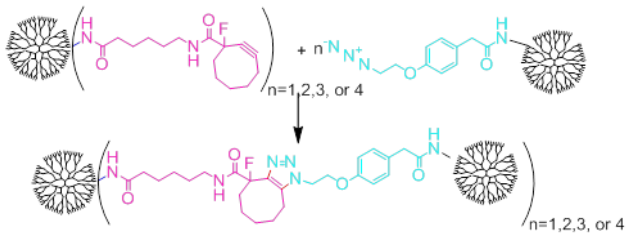

Scheme 3.2. Click reaction for synthesis of megamers from precisely defined dendrimer conjugates.

Peak fitting of rp-UPLC also allows for an estimation of the relative amount of each ligand/particle ratio in the initial averaged sample and in turn for an estimation of percent recovery of the precise product from the stochastic mixture (supporting information). The recovery of the components utilized in this work (G5-Ac-$MFCO_n$ n =1 – 4 and G5-Ac-$Azide_1$) range from 43% to 77%. These represent the yield of the final clicked megamer products as well since complete recovery of samples is possible without further purification.

Through combination of precise ratio ligand-to-dendrimer G5 monomers containing n = 1 azide ligand and n = 1 - 4 cyclooctyne ligands, we have synthesized a digital set of modular and precise megamer nanostructures (Scheme 3.2, Figures 3.4 and 3.5).

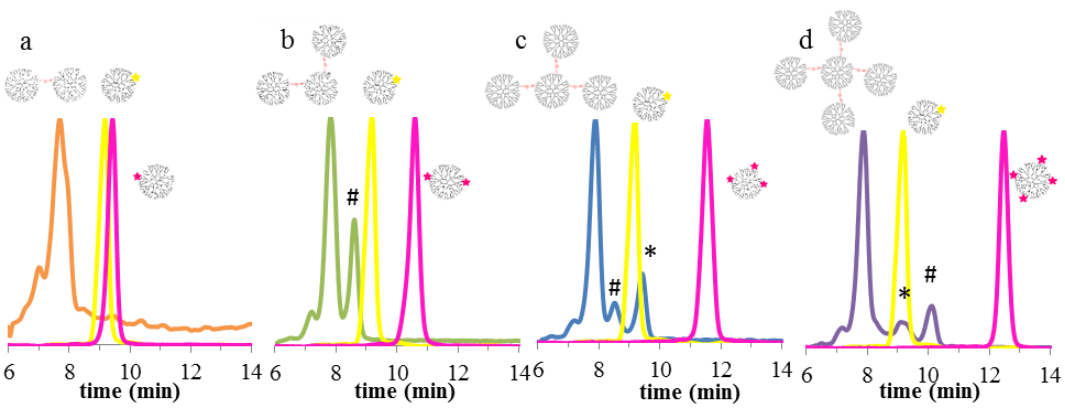

Figure 3.4. (a-d) UPLC chromatograms at 210 nm of dimer (a, orange), trimer (b, green), tetramer (c, blue), and pentamer (d, purple) products with the starting materials, G5-Ac-$Azide_1$ (cyan) and corresponding G5-Ac-$MFCO_n$ (n= 1 - 4) (pink). The symbol "#" indicates peaks that have been assigned as incompletely clicked products and "*" indicates unreacted G5-Ac-$Azide_1$ in the product.

G5 dimers, trimers, tetramers (one core with three shell dendrimers), and pentamers (one core with four shell dendrimers) have been synthesized from a click reaction between G5 with 1 azide ligand to G5 conjugated to 1, 2, 3, and 4 monofluorinated cyclooctyne (MFCO) ligands, respectively. Briefly, G5-Ac-$Azide_1$ was added in equimolar, two-fold, three-fold, or four-fold equivalents to 1-2 mg G5-Ac-$MFCO_n$ (n = 1 - 4), respectively and mixed for 48 hours. The product peaks illustrated in Figure 3.4 (orange for dimer, green for trimer, blue for tetramer, purple for pentamer, color designations that will be kept for the remainder of this article) are shifted to the left with respect to the G5-Ac-$Azide_1$ starting material (yellow) and G5-Ac-$MFCO_n$ (n = 1 - 4) starting material (pink), indicating less interaction with the hydrophobic column after formation of the click linkage. Solid samples were isolated for G5-$(G5)_n$ (n = 1 - 4) megamers by lyophillization. For n = 1 and 2, each reactant peak was entirely consumed. For n = 3 and 4, smaller peaks (*) are present in addition to the desired product peak that are most likely unreacted G5-$Azide_1$ although partially reacted G5-Ac-$MFCO_{4-n}$-(G5-Ac-$Azide_n$) cannot be ruled out. Small peaks for partially reacted G5-$G5_m$-$MFCO_{n-m}$ species also appear for the trimer, tetramer, and pentamer samples (#), which may result from cyclooctyne ligands becoming sterically blocked by previously clicked dendrimers on the particle or by small errors in the stoichiometry

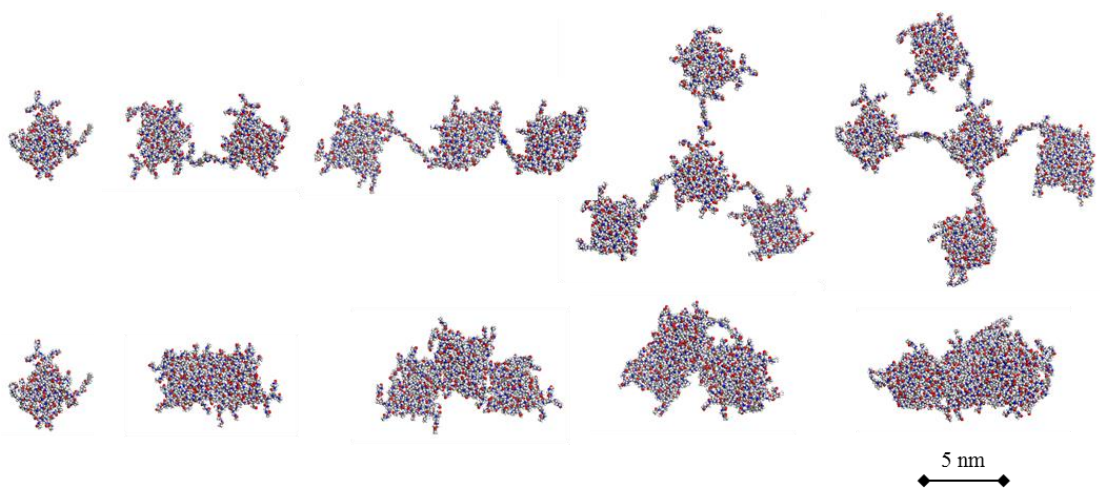

Figure 3.5. Scale cartoons of monomer and megamer structures generated using the COMPASS force-field in Materials Studio. The top row illustrates megamers separated by the largest distance allowed by the linker system (~4 nm). The bottom row depicts structures in which the dendrimers units are at a van der Waals separation distance.

of addition. Other possible assignments for the * and # peaks include regioisomers of the location of the clicked dendrimers on the central dendrimer surface as well as structural isomers resulting from the two possible click isomers. We do not favor these last two hypotheses since we do not anticipate this large of a shift (click regioisomers) and believe a broad distribution of products (resulting from surface regioisomers) is unlikely to result in the discrete peaks observed. Possible side products resulting from incomplete reaction and the regiochemistry of the click reaction are schematically depicted in Figure B4. The purity of the isolated materials as illustrated in Figure 3.4 can be compared to anticipated distribution of products if stochastic averages of G5-Ac-Azide$_1$ and G5-Ac-MFCO$_n$ (n = 1 - 4) had been employed. Combining the stochastically prepared materials for cycloalkyne n_{avg} 1 – 4 and azide n_{avg} = 1 would yield mixtures containing roughly 16, 24, 28, and 36 primary products.[41, 42]

In order to help visualize the structures, scale models are illustrated in Figure 3.5. The top row, with dendrimer units spaced apart, emphasizes the connectivity, although it is important to note that for all megamer samples the dendrimers on the periphery are bound to a distribution of the flexible surface arm locations. The bottom row, with dendrimer units in van der Waals contact, is likely the more realistic view of megamer structure in aqueous solvent based on previous computational work.[44]

MALDI-TOF-MS (Figure 3.6) was consistent with the rp-UPLC structure assignments. A mass increase of approximately 30 kDa, corresponding to expected molecular weight change from the monomer (red), to the dimer (orange), trimer (green), tetramer (blue), and pentamer (purple) is observed. In the pentamer, the $[M_5]^+$ peak can be readily seen at approximately 150 kDa, which is not present in the monomer sample. Additionally, a distinct 75 kDa peak corresponds to $[M_5]^{2+}$. Similarly, the $[M_3]^+$ peak is present for the trimer at 90 kDa with a $[M_3]^{2+}$ peak evident at 45 kDa. A peak for the parent ion of $[M_4]^+$ appears at 120 kDa along with a peak at the expected mass of 60 kDa for $[M_4]^{2+}$; however, in this case an interfering peak precludes an unambiguous assignment for the doubly ionized species. Similarly,

a peak is apparent at 60 kDa for dimer $[M_2]^+$ although the monomer also gives some signal at this position, albeit at a substantially reduced intensity. These data are consistent with the formation of the controlled ratio materials; however, similar to the NMR analysis it is complicated by the dispersity of the monomer G5 scaffold, which has mass distribution ranging from roughly 22,000 to 27,000 kDa.[36]

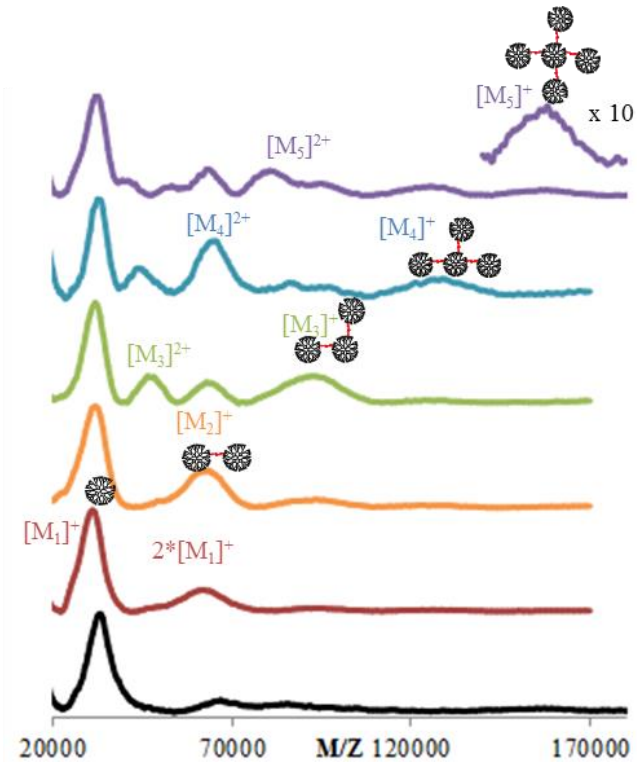

Figure 3.6. Normalized MALDI-TOF-MS spectra of commercial G5 PAMAM (black), G5 monomer (red), dimer (orange), trimer (green), tetramer (blue), and pentamer (purple). The $[M_5]^+$ peak has been magnified by 10 for ease of visualization.

The samples were further

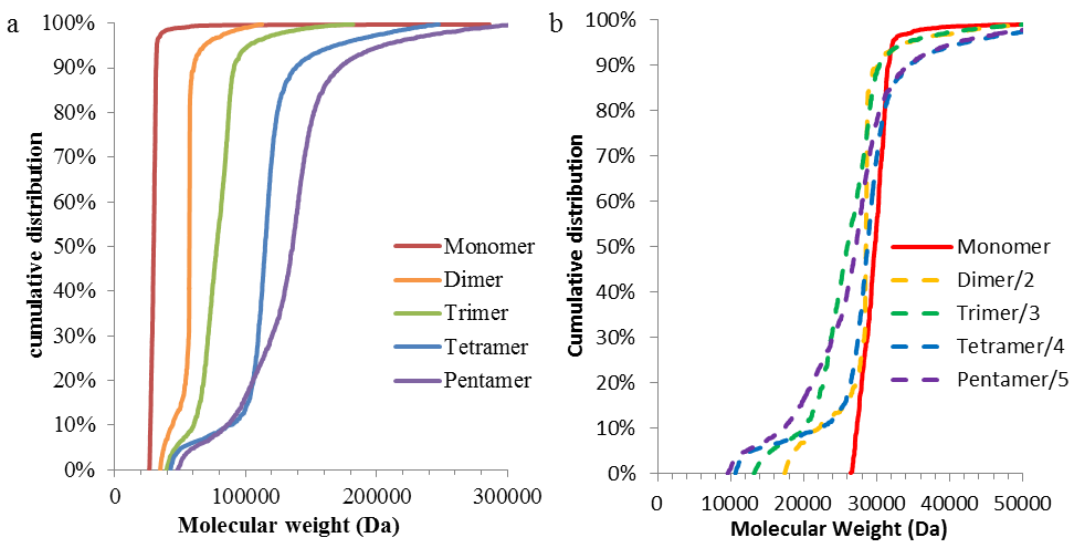

Figure 3.7. (a) Cumulative data function of M_n from GPC results. (b) Cumulative data function of each n-mer divided by n.

characterized by gel permeation chromatography (GPC). The cumulative data function shows steps of approximately 30 kDa, corresponding molecular weight of the acetylated G5 monomer (Figure 3.7a). Increased heterogeneity, as demonstrated by deviation of the megamer slopes from vertical, arising from additive branching-type structural defects that are still present in the G5 monomer starting material, is both expected and observed as number of monomer units increases from 1 (red, monomer) to 5 (purple, pentamer).

Species	Mn	Mw	PDI	Mn (megamer)/Mn (monomer)
Monomer	29,790	31,333	1.052	1.0
Dimer	57,340	59,340	1.017	1.9
Trimer	79,230	81,560	1.029	2.7
Tetramer	116,700	120,700	1.035	3.9
Pentamer	131,500	139,800	1.063	4.4

Table 3.2. Quantitative summary of GPC results.

This can be further demonstrated by dividing each megamer structure by the number of monomer units it contains (e.g. dimer by 2, trimer by 3, see Figure 7b) where the resulting plots have similar slopes. In this instance, the presence of the mass dispersity actually provides additional support for the assigned structures. Steps in the larger megamers are also seen, corresponding to small amounts of incompletely reacted materials still present in the sample. Table 3.2 summarizes the GPC molecular weight results. The average molecular weight changes in multiples of the monomer mass. The less-than-ideal ratio for the pentamer is consistent the presence of unreacted partial click reaction as observed by UPLC.

The removal of oligomeric defects that constituted over 20% by mass of commercial PAMAM material has enabled the synthesis of these megamer structures with low polydispersity. As demonstrated in previous work from this group[36], the rp-HPLC methods employed here to isolate dendrimers as a function of number of hydrophobic ligands also separate oligomer defects within the G5 PAMAM. As a result, oligomers conjugated to n-1 ligands co-elute with monomers conjugated to n ligands (for example, Dimeric G5-$MFCO_1$ co-elutes with Monomeric-$MFCO_2$). Such impurities in

the starting material would create side products in megamer assembly with molecular weights double the theoretical value and greatly increase the polydispersity. The successful removal of the oligomeric side products reduces the high molecular weight impurities as measured by GPC in Figure 3.7 a.

Conclusions.

This work, demonstrating the use of PAMAM dendrimers containing precisely defined ligand/particle ratios as building blocks for generating controlled nanostructures in the 30 to 150 kDa size range, advances the use of dendrimers as quantized building blocks for homogenous megamers the size of large proteins and multi protein constructs. The HPLC isolation platform has proven to be efficient and versatile,[38, 41] with similar preparation and isolation procedures for at least 4 complimentary click ligands to date allowing for diverse chemistries to be utilized with high (30%-80%) recovery of precise ligand/particle materials from the stochastic mixture. The one-pot self-assembly creates stable, covalently bound megamers that are soluble in water and organic solvents methanol and dimethylsulfoxide, making them promising candidates for both biological environments and functionalization.

References:

1. Tomalia, D.A., *Dendrons/dendrimers: quantized, nano-element like building blocks for soft-soft and soft-hard nano-compound synthesis.* Soft Matter, 2010. **6**: p. 456-474.
2. Tomalia, D.A., *In quest of a systematic framework for unifying and defining nanoscience*. J. Nanopart. Res., 2009. **11**(6): p. 1251-1310.
3. Tomalia, D.A., J.B. Christensen, and U. Boas, *A Quantized BUilding Block Concept Leading to a New Nano-periodic System*, in *Dendrimers, Dendrons and Dendritic Polymers: Discovery, Applications, the Future*. 2012, Cambridge University Press: NY. p. 293-377.
4. Christensen, J.B. and D.A. Tomalia, *Designing Dendrimers*, in *Dendrimers as Quantized Nano-modules in the Nanotechnology Field*, S. Campagna, P. Ceroni, and F. Puntoriero, Editors. 2012, J. Wiley & Sons: Hoboken. p. 1-33.
5. Glotzer, S.C. and M.J. Solomon, *Anisotropy of building blocks and their assembly into complex structures.* Nature Materials, 2007. **6**(8): p. 557-562.

6. Chen, Q., et al., *Supracolloidal Reaction Kinetics of Janus Spheres.* Science, 2011. **331**(6014): p. 199-202.
7. Wang, Y.F., et al., *Colloids with valence and specific directional bonding.* Nature, 2012. **491**(7422): p. 51-U61.
8. Mirkin, C.A., et al., *A DNA-based method for rationally assembling nanoparticles into macroscopic materials.* Nature, 1996. **382**(6592): p. 607-609.
9. Alivisatos, A.P., et al., *Organization of 'nanocrystal molecules' using DNA.* Nature, 1996. **382**(6592): p. 609-611.
10. Feng, L., et al., *DNA Patchy Particles.* Advanced Materials, 2013. **25**(20): p. 2779-2783.
11. Ofir, Y., B. Samanta, and V.M. Rotello, *Polymer and biopolymer mediated self-assembly of gold nanoparticles.* Chemical Society Reviews, 2008. **37**(9): p. 1814-1823.
12. Zhang, C., et al., *A general approach to DNA-programmable atom equivalents.* Nature Materials, 2013. **12**: p. 741-746.
13. Larson-Smith, K. and D.C. Pozzo, *Scalable synthesis of self-assembling nanoparticle clusters based on controlled steric interactions.* Soft Matter, 2011. **7**(11): p. 5339-5347.
14. Tang, Z.Y., et al., *Self-assembly of CdTe nanocrystals into free-floating sheets.* Science, 2006. **314**(5797): p. 274-278.
15. Svenson, S., *Dendrimers as versatile platform in drug delivery applications.* Eur. J. Pharm. Biopharm., 2009. **71**(3): p. 445-462.
16. Khopade, A.J. and H. Mohwald, *Statistical Megamer Morphologies and Materials from PAMAM Dendrimers.* Macromol. Rapid Comm., 2005. **26**: p. 445-449.
17. Kiran, B.M. and N. Jayaraman, *Thiol-Disulfide Interchagne Mediated Reversible Dendritic Megamer Formation and Dissociation.* Macromolecules, 2009. **42**: p. 7353-7359.
18. Tomalia, D.A., *Birth of a new macromolecular architecture: dendrimers as quantized building blocks for nanoscale synthetic polymer chemistry.* Progress in Polymer Science, 2005. **30**: p. 294-324.
19. Uppuluri, S., et al., *Rheology of Dendrimers. I. Newtonian Flow Behavior of Medium and Highly Concentrated Solutions of Polyamidoamine (PAMAM) Dendrimers in Ethylenediamine (EDA) Solvent.* Macromolecules, 1998. **31**(14): p. 4498-4510.
20. Betley, T.A., et al., *Tapping Mode Atomic Force Microscopy Investigation of Poly(amidoamine) Core-Shell Tecto(dendrimers) Using Carbon Nanoprobes.* Langmuir, 2002. **18**: p. 3127-3133.
21. Li, J., et al., *Characterizations of Core-Shell Tecto-(Dendrimer) Molecules by Tapping Mode Atomic Force Microscopy.* Langmuir, 1999. **15**(7347): p. 7347-7350.
22. Tomalia, D.A., et al., *Partial shell-filled core-shell tecto(dendrimers): A strategy to surface differentiated nano-clefts and cusps.* Proc. Natl. Acad. Sci. USA, 2002. **99**: p. 5081-5087.
23. de Gennes, P.G. and H. Hervet, *Statistics of Starburst Polymers.* J. Physique Lett., 1983. **44**: p. 351-360.
24. Brahmi, Y., et al., *Hieracrchially porous nanostructures through phosphonate-metal alkoxide condensation and growth using functionalized dendrimeric building blocks.* Chem. Comm., 2011. **47**: p. 8626-8628.

25. Kozaki, M., et al., *Stepwise construction of a cross-shaped covalent assembly of dendrimers.* Tetrahedron Lett., 2008. **49**: p. 2931-2934.
26. Garzoni, M., et al., *Ion-Selective Controlled Assembly of Dendrimer-Based Functional Nanofibers and Their Ionic-Competitive Disassembly.* J. Am. Chem. Soc., 2012. **134**: p. 3349-3357.
27. Percec, V., et al., *Controlling polymer shape through the self-assembly of dendritic side-groups.* Nature, 1998. **39**: p. 161-164.
28. Percec, V., et al., *Structural Analysis of Cylindrical and Spherical Supramolecular Dendrimers Quantifies the Concept of Monodendron Shape Control by Generation Number.* J. Am. Chem. Soc., 1998. **120**: p. 11061-11070.
29. Wang, H., et al., *A Supramolecular Approach for Preparation of Size-Controlled Nanoparticles.* Angew. Chem. Int. Ed. Engl., 2009. **48**: p. 4344-4348.
30. Sung, S.R., et al., *Convergent Synthesis and Charcterization of Dumbbell Type Dendritic Materials by Click Chemistry.* B. Kor. Chem. Soc., 2011. **32**: p. 3933-3940.
31. Mullen, D.G., et al., *Design, Synthesis, and Biological Functionality of a Dendrimer-Based Modular Drug Delivery Platform.* Bioconjugate Chem., 2011. **22**: p. 679-689.
32. DeMattei, C.R., B. Huang, and D.A. Tomalia, *Designed Dendrimer Syntheses by Self-Assembly of Single-Site, ssDNA Functionalized Dendrons.* Nano Letters, 2004. **4**(5): p. 771-777.
33. Rudzevich, Y., et al., *Self-assembled dendrimers with uniform structure.* Org. Biomol. Chem., 2008. **6**: p. 2270-2275.
34. Chen, P., et al., *A pH responsive dendron-DNA-protein hybrid supramolecular system.* Soft Matter, 2010. **6**(10): p. 2143-2145.
35. Tomalia, D.A., J.B. Christensen, and U. Boas, *The Dendritic State*, in *Dendrimers, Dendrons and Dendritic Polymers: Discovery, Applications, the Future*

2012, Cambridge University Press

NY. p. 30.
36. van Dongen, M.A., et al., *Quantitative analysis of generation and branch defects in G5 poly(amidoamine) dendrimer.* Polymer, 2013. **54**: p. 4126-4133.
37. Mullen, D.G., et al., *Best Practices for Purification and Characterization of PAMAM Dendrimer.* Macromolecules, 2012. **45**: p. 5316-5320.
38. Mullen, D.M., et al., *Isolation and Characterization of Dendrimers with Precise Numbers of Functional Groups.* Chemistry: A European Journal, 2010. **10**: p. 10675-10678.
39. Pettit, M.W., et al., *Poly(amidoamine) polymers: soluble linear amphiphilic drug-delivery systems for genes, proteins and oligonucleotides.* Therapeutic Delivery, 2011. **2**(7): p. 907-917.
40. Tomalia, D.A., L.A. Reyna, and S. Svenson, *Dendrimers as multi-purpose nanodevices for oncology drug delivery and diagnostic.* Biochemical Society Transactions, 2007. **35**(1): p. 62-67.
41. Mullen, D.M. and M.M. Banaszak Holl, *Heterogeneous ligand-nanoparticle distributions: a major obstacle to scientific understanding and commercial translation.* Accounts of Chemical Research, 2011. **44**: p. 1135-1252.

42. Mullen, D.G., et al., *A Quantitative Assessment of Nanoparticle-Ligand Distributions: Implications for Targeted Drug and Imaging Delivery in Dendrimer Conjugates.* ACS Nano, 2010. **4**: p. 657-670.
43. Fréchet, J.M.J., et al., *Reversed-phase high-performance liquid chromatography of functionalized dendritic macromolecules.* Journal of Chromatogr. A, 1994. **667**: p. 284-289.
44. Kelly, C.V., et al., *Poly(amidoamine) dendrimers on lipid bilayers I: Free energy and conformation of binding.* Journal of Phys. Chem. B, 2008. **112**: p. 9339-9345.

Chapter 4

Avidity of Dendrimer-Folic Acid Conjugates with Controlled Valency

Introduction.

Folic acid (FA) targeting has been extensively studied for improving the therapeutic index of drugs.[1-5] Although the structure of this interaction has only recently been fully elucidated,[6] substantial progress has still been made over the last 20 years in FA targeting with four drug conjugates advancing to clinical trials. Targeting of a drug or drug conjugate exploits the interaction of this vitamin with a high affinity (K_d ~ 0.1 nM)[2] folate receptor, which is overexpressed in many cancer cells. This receptor is also found in healthy epithelial cells; however, these are generally inaccessible to FA bearing conjugates in the blood,[2] making it an ideal target to exploit cytotoxic effects of drugs while minimizing the concern of collateral damage in healthy tissues. In addition to cell surface targeting, FA conjugation provides a selective uptake pathway for the conjugated drug via folate receptor mediated endocytosis and release of the FA/conjugate from the receptor and endosome.[7, 8] Many drug delivery designs have been employed to take advantage of this highly specific interaction to target small molecule chemotherapeutics such as doxorubicin,[9] methotrexate,[10] protein toxins,[11] imaging agents,[12, 13] and immunotherapeutics[14] both *in vitro* and *in vivo* by exploiting carrier mechanisms including liposomes,[15] inorganic nanoparticles,[12] and organic polymers.[16-18]

Multivalent conjugates of ligands to nanomaterials are often employed, purposefully to increase the avidity and/or specificity of an interaction, or accidently as a result of stochastic synthetic approaches. The enthalpic and entropic mechanisms through which multivalency increases the interaction of a ligand and its target have been extensively studied from a theoretical viewpoint.[19-23] Briefly, there are two main multivalent effects that may contribute to the system studied here; those dependent on the increased effective or local concentration, and those due to multiple binding events occurring for a

single conjugate.[24] The term effective concentration describes the localization of many ligands in a nanoscale volume by a carrier (scaffold or vector), resulting in a local concentration of ligands much higher than a solution containing an equivalent amount of free ligands. Higher local concentrations can result in higher affinities, and an increased chance of re-binding upon dissociation of the initial interaction ("statistical re-binding"). The binding of one ligand to a target brings the other ligands on that vector into closer proximity to the target (and the surface if the target is immobilized), increasing the chances of additional binding events.[25, 26] These binding events can be of three types; (1) Interaction with a nonequivalent site on the same receptor, (2) Interaction with an equivalent site on a oligomeric receptor , or (3) Interaction with a site on a second receptor (also known as receptor clustering). These multivalent classifications have been discussed and reviewed elsewhere by Kiessling, [27, 28] Whitesides,[24] and Cloninger.[25]

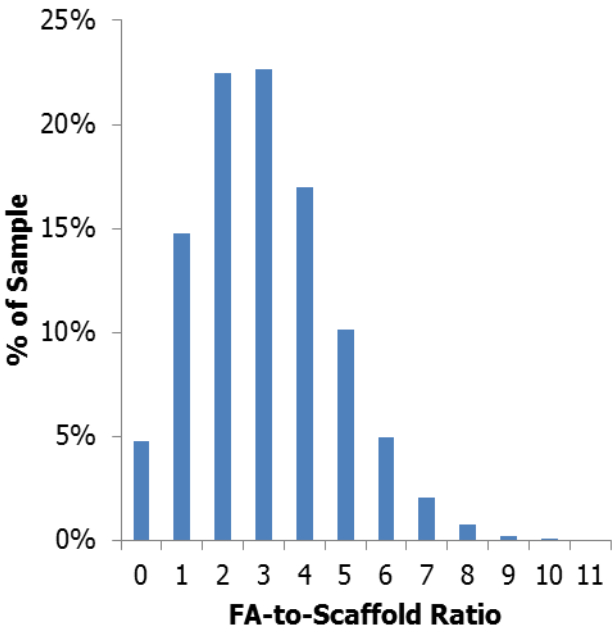

Figure 4.1. Distribution of conjugates resulting from a stochastic conjugation of 3 equivalents of FA to 1 equivalent of scaffold.

Although multivalent conjugates of many dyes, drugs, and targeting ligands (including FA) have been developed, the actual impact of the specific number of ligands on improvements in avidity and/or biological activity has been difficult to analyze due to the heterogeneous mixtures generated by statistically random conjugation chemistries employed in their synthesis.[29] For example, a stochastic conjugation of 3 equivalents of FA to a scaffold with multiple functionalizable sites (≥30) results in a sample with a mean of ~3 FA per scaffold, but also a distribution of unique conjugates with FA-to-scaffold ratios ranging from 0 to ~11 FA molecules per scaffold (Figure 4.1). Previous efforts to quantify multivalent binding constants have employed surface plasmon

resonance (SPR) to measure increases in binding between materials containing different average numbers of ligands (folic acid[30] and methotrexate[31-33]) and folate binding protein (FBP) modified surfaces. Although these studies have reported a general trend of greater avidity with increased valency, the utilization of averaged materials did not allow for precise understanding of the mechanisms involved in multivalent binding, or elucidation of the relative activity of the various components in the sample. For example, does the entire population illustrated in Figure 4.1 with 2 or more conjugated FA (80% of the population) enable equivalent receptor clustering in a cell? Or does a higher valency, and consequently higher effective concentration, such as 5-11 FA-per-scaffold (18% of the population) contribute all of the observed activity?

Poly(amidoamine) (PAMAM) dendrimer is an extensively studied vector for the multivalent, targeted delivery of drugs, genes, and imaging agents.[34, 35] The dendritic architecture has many advantages for biomedical applications, including very low polydispersity, internal core space available for the entrapment of drugs, and multiple branches providing terminal groups for functionalization.[36] PAMAM dendrimer is particularly suited for such applications due to its protein-like architecture, low immunogenicity, ability to solubilize hydrophobic small molecules, and easily functionalized primary amine terminal surface groups.[37-39] The size of generation 5 (G5) PAMAM (5 nm) is also ideal for vascular delivery and excretion due to kidney filtration.[40] Recent advancements[41] have enabled the isolation of monomeric G5 PAMAM dendrimers from oligomeric (dimer, trimer, etc.) and trailing generation defects (G1 – G4), narrowing the experimentally realized size distribution of this vector from 1 kDa-115 kDa to 25 kDa to 29 kDa. Possible convolution of results by large mass differences and vector-accessible surface area is eliminated by removing both trailing generations and oligomers from the G5 PAMAM monomer material.

In 2007, Banaszak Holl et. al. employed SPR to examine the increased avidity to FBP and cellular uptake of G5 PAMAM-FA conjugates as a function of average number of attached FAs (Figure 4.2).[30] The dissociation constant (k_d) was observed to exponentially decrease as the average valency of FA increased; however, this calculation assumed that given a long enough experiment all bound materials would dissociate from

the surface and that the experimental sensogram would return to the level of signal present prior to G5-$FA_{n(avg)}$ exposure. The nonlinear behavior in k_d was attributed to a saturation of FA-FBP binding events limited by the immobilized protein density on the SPR flow cell surface and not to the valency of FA (Figure 4.2a). Interestingly, the same trend in signal saturation as a function of FA valency was observed for mean fluorescence as measured by flow cytometry when equivalent conjugates labeled with a dye were evaluated for binding to folic acid receptor upregulated KB cells. This observation was interpreted as an indication that the dendrimer conjugates do not trigger receptor clustering on the cell surface, which would allow for higher affinities as more proteins became available.

Subsequent analyses of this data set have employed different assumptions in the analysis of the data. These interpretations have resulted in two alternate mechanisms for explaining the changes in binding as a function of average valency. In 2010, Sander et al.

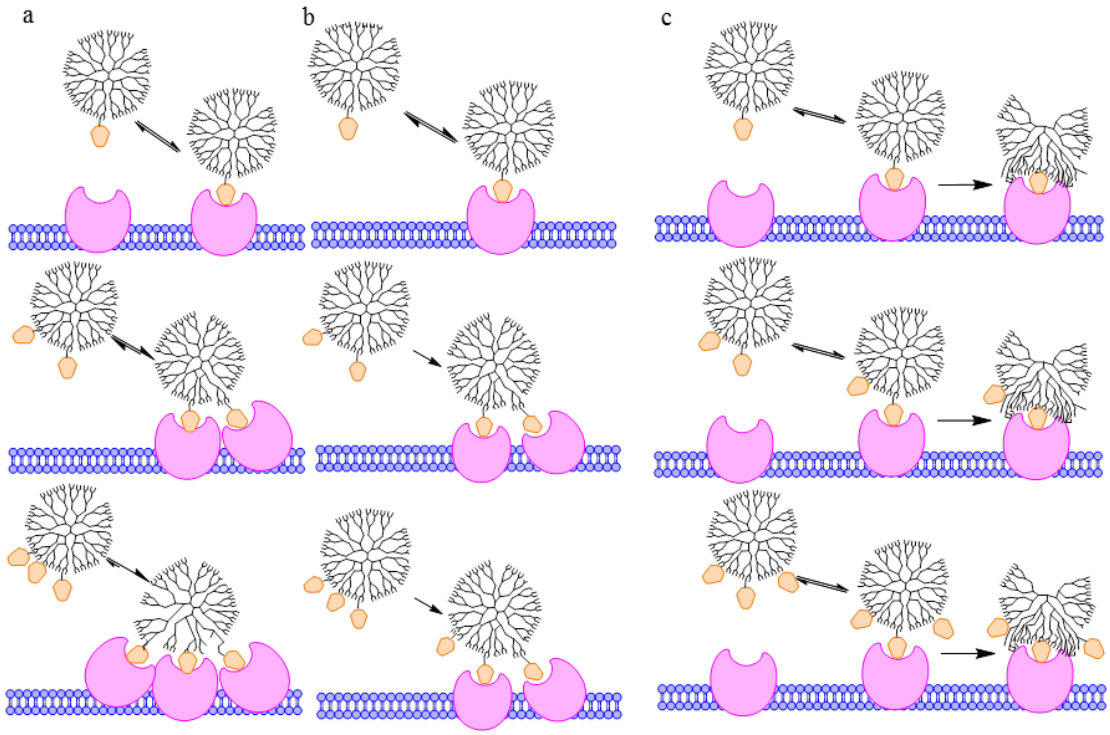

Figure 4.2. Proposed models for enhanced G5-FA binding to FBP. (a) Multivalent binding increases avidity with increasing valency. (b) Any multivalent binding (2 or more interactions) is irreversible and monovalent binding is reversible. (c) FA "keys" the initial interaction between conjugate and FBP, which is followed by strong nonspecific interaction between the dendrimer and protein.

proposed that the binding of the conjugates occurs via two distinct interactions.[42] This

mechanism acknowledges the broad distribution of ligand-to-dendrimer ratios present in stochastically synthesized materials, including dendrimers that have zero FA, one FA, or two or more FA. It was proposed that (1) monovalent interaction between G5-FA_1 and on FBP attributes to the binding that is reversible on the time scale of the experiment and (2) multivalent binding between G5-$FA_{\geq 2}$ to two or more FBPs is permanent on the SPR experimental timescale (Figure 4.2 b). The authors argue that the increased avidity attributed to valency increase by Banaszak Holl et al.[30] is actually a result of decreased amounts of zero-functional and mono-functional conjugates in the stochastic average material. This mechanism still proposes that FA-based multivalent binding is important. Indeed, it ascribes the binding constant for G5-$FA_{\geq 2}$ as large enough to prevent any measurable dissociation over the timescale of the experiment. The original flow cytometry data can be similarly interpreted; receptor clustering is achieved by bivalent conjugates and further increasing of valency has no measureable effect on the cell. A very different mechanism based on kinetic limitations of cooperativity to explain the plateau of high avidity of the conjugate species was proposed by Licata and Tkachenko in 2008.[43] This study concludes that the increased avidity proposed for the G5-$FA_{n(avg)}$ conjugates[30] is higher than can be attributed to cumulative effects of multivalent binding and that kinetic limitations actually prevent the type of multivalent interactions proposed in Figures 2a and 2b. They propose that the enhanced interaction observed by SPR is a result of non-specific surface (van der Waals) interactions between the polymer vector and protein/surface that are enabled by the initial key-lock binding between FA and FBP (Figure 4.2c).

The broad distribution of folic acid-to-dendrimer ratios present in each sample, including both monovalent and multivalent conjugates in the low averaged materials, prevented a clear experimental elucidation between the three mechanisms. In particular, a conjugate with precise ratio of 1 FA-per-dendrimer (G5-FA_1) was lacking to determine if the observed increase in avidity was a product of multivalent binding between the conjugate and SPR surface (Banaszak Holl and Sander mechanisms)[30, 42] or a single FA-FBP lock-and-key combined with non-specific polymer/surface interaction (Licata and Tkachenko mechanism).[43]

In order to address these materials-based challenges to understanding multivalency, we have developed click chemistry and reverse-phase High Performance Liquid Chromatography (rp-HPLC) methods to isolate dendrimers conjugated to precise numbers of ligands (ie G5-L_n n = 1-5 where n is not a mean value).[29, 44, 45] These methodologies, which have been previously demonstrated to be successful for azide[29, 44, 46] and fluorinated, ring-strain-promoted click ligands,[46] are now extended to a second ring strain promoted ligand (cyclooct-1-yn-3-glycolic acid (COG)), which has been used in previous G5-$FA_{n(avg)}$ SPR studies.[32] In principle, isolating the precise ratio samples G5-FA_n, n = 1, 2, 3, etc., would allow SPR experiments where the multivalent binding effect are decoupled from the heterogeneity of stochastic samples (G5-$FA_{n(avg)}$). In order to generate non-stochastic FA-dendrimer ratios, dendrimer samples conjugated to 1, 2, 3, or 4 ring-strain promoted click ligands were isolated by semi-preparative scale rp-HPLC. This isolation was followed by a click reaction with a γ-azide-Lys-Asp-FA derivative (γ-azide-FA). The resulting samples include a G5-PAMAM dendrimer with a FA-to-dendrimer ratio of 0.96 that contains no multivalent G5-$FA_{\geq 2}$ species. This conjugation provides the key G5-FA_1 sample needed to differentiate the three mechanistic hypotheses proposed to date. The remainder of the click reactions did not proceed with 100% efficiency, but still yielded samples that contained a well defined high-n cutoff and had a narrower-than-stochastic distribution of FA-to-dendrimer ratios. The binding kinetics of these conjugates were analyzed by SPR on both high and low protein density surfaces. The results indicate that at either surface FBP density, the total folic acid concentration present is the dominant factor leading to increased amount of bound material with increased valency. A small deviation from the overall binding trend was observed for the monovalent G5-FA_1 sample. In this case, the lower amount of binding as compared to the G5-$FA_{\geq 2}$ species was attributed the difference in local effective concentration. In other words, a small multivalent effect is observed for G5-$FA_{\geq 2}$ material because of increased statistical rebinding as compared to G5-FA_1. Most importantly, the G5-FA_1 sample exhibited the same irreversible binding to the FBP surface, on the SPR timescale, as the G5-$FA_{\geq 2}$ samples. This observation conclusively rules out the earlier mechanistic hypotheses by Banaszak Holl et al.[30] and by Sander et

al.[42] and provides strong experimental support for the key-lock/non-specific binding mechanism proposed by Licata and Tkachenko.[43]

Experimental Section

Materials. All chemicals and materials were purchased from Sigma Aldrich or Fischer Scientific and used as received unless otherwise specified. G5 PAMAM dendrimer was purchased from Dendritech and purified as previously reported to remove trailing generation and G5 oligomer impurities.[41] Cyclooct-1-yn-3-glycolic acid (COG) was synthesized from a modified literature preparation (see Supporting Information).[47]

Preparation of G5-Ac-COG$_{4.0(avg)}$ conjugates. Conjugates were prepared from G5 dendrimer and COG via amide coupling. In brief, amine-terminated G5 was dissolved to 0.16 uM in DI. COG was activated by dissolving to 10.5 uM in acetonitrile with 2.65 equiv of 1-ethyl-3-(3-dimethylaminopropyl)carbodiimide) (EDC) and 2.78 equiv of N-hydroxysuccinimide (NHS) and stirring for 2 hours. The activated COG was added drop-wise via syringe pump to the dendrimer solution and allowed to stir overnight. The product was purified using Amicon Ultra Centrifugal units, 10kDa cutoff membranes, with 2 phosphate buffered saline (PBS) washes and 4 deionized water (DI) washes. Product was isolated via lyophillization. The material was then fully acetylated (converting 100% of the remaining primary amines to acetyl groups, henceforth designated "Ac") by re-dissolving in anhydrous methanol (0.19 µM) and adding 450 equiv of triethylamine and 360 equiv of acetic anhydride, stirring for 4 hours, purified by centrifugation and isolated by lyophillization. G5-Ac-COG$_{4.0(avg)}$ was characterized by rp-UPLC.

Isolation of precisely defined G5-Ac-COG$_x$ conjugates. Dendrimers with precise ratios of COG ligands per dendrimer were isolated via rp-HPLC according to literature procedures.[46] Briefly, multiple injections of the averaged material were performed with a C18 column on a water/acetonitrile gradient with 0.1% TFA. Fractions were collected as the material eluted and combined to obtain samples with precisely x = 0 - 4 COG ligands per dendrimer. Products were purified using PD-10 desalting protocols, with DI

as the equilibration buffer and samples dissolved in 10xPBS, then lyophilized to dry. Samples were characterized by rp-UPLC and ^{1}H-NMR spectroscopy. Curve fitting of chromatograms by Igor Pro was performed to assess purity of precise ratio materials and to determine the average number of COG ligands of stochastic materials (Table S1).

Synthesis of γ-azide-Lys-Asp-Folic Acid (γ-azide-FA). FA-Azide derivative was obtained from collaborators at Purdue University.

Synthesis of G5-Ac-FA$_n$ conjugates. Dendrimers with well-characterized numbers of covalently bound folic acids were synthesized via click reaction of G5-Ac-COG$_x$ conjugates and γ-azide-FA. Briefly, dendrimer conjugates were dissolved in methanol to 40 mM with respect to COG, and a 10 fold excess of γ-azide-FA (40 mM in DMSO) was added. Solutions were agitated for 24 hours, then an additional 5 volume equivalents of DMSO was added to fully dissolve the dendrimer. Solutions were agitated for an additional 24 hours, then diluted to 2.5 mL with DI and purified using PD-10 desalting columns, gravity protocols, followed by 16 rounds of dialysis against DI. The samples were then further purified by repeating the PD-10 desalting column using 10X PBS to dilute the sample, followed by 2 rounds of dialysis against 1X PBS and 4 rounds against DI. Recovered samples were characterized by ^{1}H-NMR spectroscopy and rp-UPLC. Curve fitting of chromatograms provided yield, purity, and FA average and distribution species for G5-FA$_n$ materials.

Methods.

High Performance Liquid Chromatography. Isolation of G5-Ac-COG$_x$ was achieved using a Waters 600 Controller, Waters 2707 Autosampler, and Waters 2998 Photodiode Array running Empower 2 Software, additionally equipped with a Waters Fraction Collector III on a Phenomenex Jupiter 300Å C18 Prep Column (21.2 x 150 mm, 5 µm particles). The weak solvent (Solvent A) was HPLC Grade Water with 0.1% TFA, and the strong solvent (Solvent B) was HPLC Grade Acetonitrile with 0.1% TFA. The gradient employed at 16 mL/min was as follows: 2.1 min load step at 95%A/5%B, 3.9 min gradient to 80%A/20%B, 15 min gradient to 65%A/35%B, 5 min gradient to

55%A/45%B, followed by 3 min was at 20%A/80%B, then equilibrating at starting conditions for 5 min before next injection. Averaged conjugate was dissolved to 20 mg/mL concentration and 910uL injections were used. Five second fractions were collected starting at 9 min 30 sec into each run for a total of 120 fractions. Analytical chromatograms were collected on a Waters Acquity UPLC equipped with a scaled method using an Phenomenex Jupiter 4.6 x 100 mm column.

LC Peak Fitting. Chromatograms were fit with Gaussian peaks using Igor Pro Version 6.0.3.1 software. Peak widths from chromatogram to chromatogram were kept constant.

Nuclear Magnetic Resonance Spectroscopy. NMR spectroscopy experiments were performed on a Varian MR400 instrument. ^{1}H NMR spectra were obtained used 10 second pre-acquisition delays and a total of 64 scans. All sample solutions were set to a dendrimer concentration of 1-5 mg/mL in deuterium oxide.

Surface Plasmon Resonance Spectroscopy. SPR experiments were conducted in a Biacore® X instrument (Pharmacia Biosensor AB). Two immobilized folate binding protein (FBP) chips were prepared following the instrument prompted protocols, using a solution of 0.2 M EDC and 0.05 M NHS as an activating solution, an immobilization solution of FBP at 1mg/mL for the "low density" chip and 1.5 mg/mL for the "high density" chip, with ethanolamine as the deactivation solution. Flow cell two was employed as a control cell by activating and deactivating the surface without the addition of protein. The chips were characterized using free FA solutions and checked for non-specific binding with a control of G5-Ac containing no COG or FA. Immobilization and free FA chromatograms can be found in the Supporting Information. The "high density" chip contains roughly double the amount of immobilized FBP according to total change in response units. Conjugate samples were dissolved in fresh HBS-EP buffer at 100 µM and serially diluted to 20, 10, 5, 2.5, and 1.25 µM in HBS-EP buffer from Fischer Scientific. Runs were multichannel, FC1-FC2, at 10 µL/min. The system was allowed to equilibrate at the beginning of each run for no less than 300 seconds, followed by a 2 minute, 30 µL (50-5-5-5 bubble method) injection. The system was monitored for no less than 500 seconds post-injection. Between each run, the chip was washed with a 5 µL

injection of pH 1.5 buffer to remove bound materials followed by an instrument prime step.

Results.

Preparation of G5-Ac-COG$_{4.0(avg)}$ conjugates (Figure 4.3a). 41.2 mg of G5-Ac-COG conjugate was prepared with an average of 4.0 COGs per dendrimer as calculated by rp-UPLC peak fitting (overall yield 39%). All samples were characterized by ^{1}H-NMR spectroscopy and rp-UPLC.

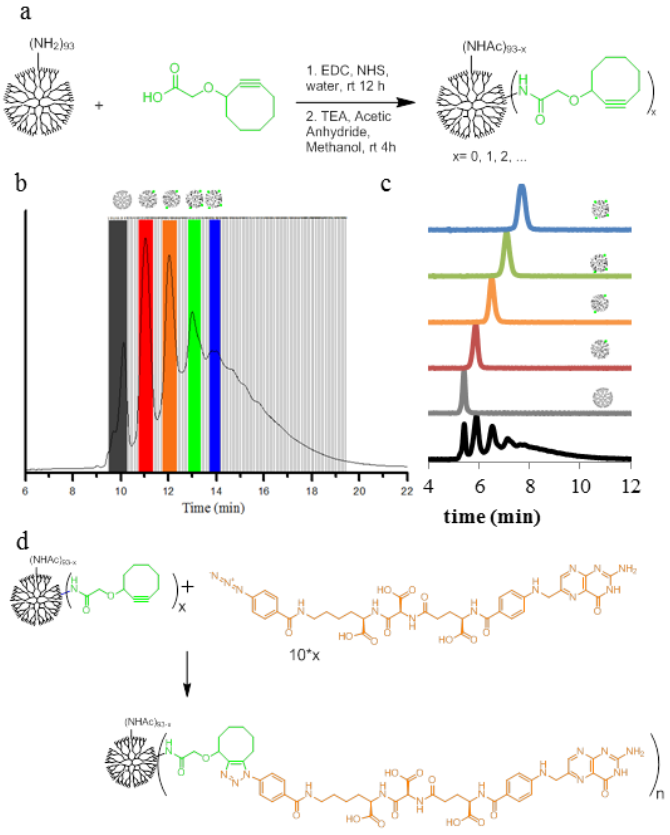

Figure 4.3. (a) Synthesis of PAMAM-COG conjugate. (b) Semi-prep rp-HPLC isolation of PAMAM with 1, 2, 3, 4, or 5 COGs. (c) Isolated samples elute from rp-UPLC as a function of ligand-to-dendrimer ratio. (d) Scheme of G5-COG click reaction of γ-azide-FA.

Isolation of G5-Ac-COG$_x$ conjugates with precise COG-to-dendrimer ratios (Figure 4.3b-c). Dendrimer samples with x = 0-4 were isolated in quantities ranging from 1 to 8 mg. All samples were characterized by ^{1}H-NMR spectroscopy (Figure C1) and rp-UPLC (Table C1).

Synthesis of G5-Ac-FA$_n$ conjugates (Figure 4.3d). One equivalent of G5-Ac-COG$_x$ and 10*x (x = 1 - 4) equivalents of γ-azide-FA were dissolved to give a dendrimer concentration of 10 mg/mL in DMSO. Reactions were shaken for 48 hours with occasional vortexing. Samples were then desalted according to the manufacturer's gravity protocol with PD-10 desalting columns (equilibration buffer as DI, sample dissolved in 10xPBS), and then dialyzed against DI using 10,000 Da cutoff membranes (16 media changes). Large amounts of unreacted γ-azide-FA remained after initial purification as detected by rp-UPLC. Two additional rounds of dialysis against 1xPBS buffer followed

	n of FA			% of n (FA)=				
x (COG)	n (HPLC avg)	n (NMR avg)	Click Efficiency	0	1	2	3	4
1	1.0	1.3	96%	4	96	0	0	0
2	1.2	1.5	60%	9	60	33	0	0
3	1.9	2.3	63%	4	24	49	23	0
4	2.7	3.5	60%	4	14	15	33	18

Table 4.1. Quantitative analysis of click products.

by 4 rounds against DI removed all visible traces of unreacted γ-azide-FA as assessed by rp-UPLC. Samples were characterized by rp-UPLC (Figure C2) and ^{1}H-NMR spectroscopy (Figure C3). The n=1 click reaction had an efficiency of 96%, while all other efficiencies ranged from 54-64% with mass recoveries over 95%. A detailed analysis of each sample's fractional composition is summarized in Table 4.1.

Surface Plasmon Resonance Spectroscopy. Sensograms for G5-Ac-FA$_n$ (n = 0, 1.0, 1.2, 1.0, 2.7) were collected for both the low (Figure 4.4) and high (Figure 4.5) density chips. The unfunctionalized, neutral conjugate (n = 0) showed no specific binding at either chip density across all concentrations tested. All G5-FA conjugates showed specific binding to the FBP immobilized flow cell 1, which increased in an FA concentration dependent manner. After injection completion, all FA conjugated samples had a release profile. The association and

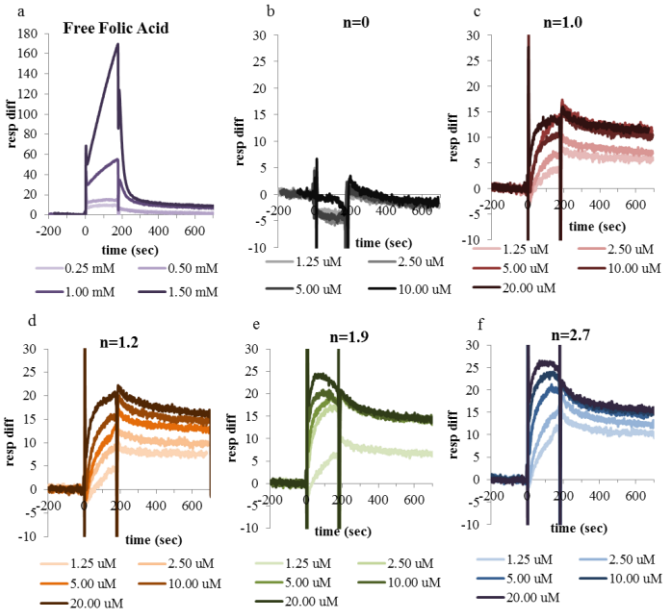

Figure 4.4. SPR sensograms of conjugates a) (n=1.0, red; n=1.2, orange; n=1.9, green; n=2.7, blue) and controls (n=0, grey; free FA, purple) on lower density chip. The color gradient represents concentration from low (light) to high (dark). Free FA samples were run at milimolar as opposed to micromolar concentrations to obtain adequate signal.

dissociation phases were fit with various models for evaluation of k_a, k_d, and K_d.

Discussion.

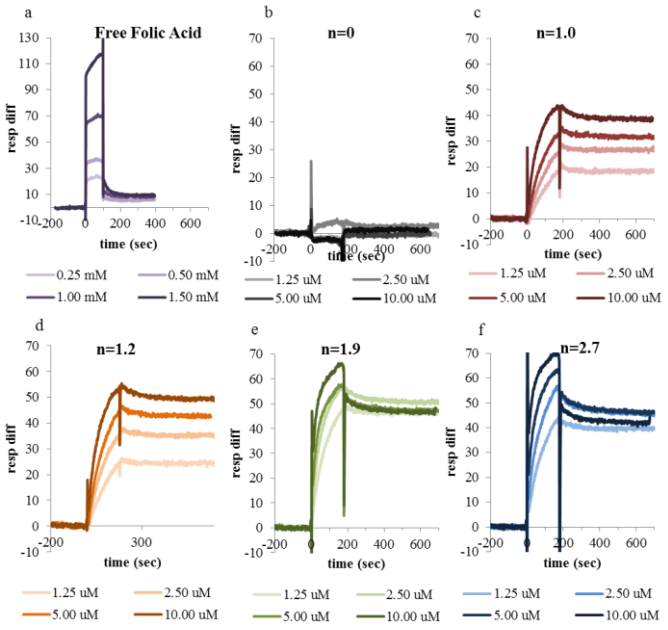

Figure 4.5. SPR sensograms of conjugates (n=1.0, red; n=1.2, orange; n=1.9, green; n=2.7, blue) and controls (n=0, grey; free FA, purple) on higher density chip. The color gradient represents concentration from low (light) to high (dark).

rp-HPLC has shown to be an effective tool for isolating dendrimers with precise numbers of clickable ligands.[44, 45] To date, four unique click ligands have been employed using the same gradient, with functional groups of azide,[46] alkyne, a fluorinated ring strain promoted ligand,[46] and the cyclooctyne ligand presented here for the first time. The robust methodology developed has proven effective for isolating various species containing single ligand/dendrimer ratios from heterogeneous, averaged samples containing 10 or more species. Due to the flexible nature of the PAMAM dendrimer and transient interaction of the ligand with the hydrophobic column, this technique has proven to be non-specific to the relative location of the multiple ligands conjugated to the same sample, i.e. all dendrimer conjugated to three ligands co-elutes, simplifying the separation process. Isolation of the G5-Ac-COG_x conjugates utilized in this paper reflect the success of prior studies with other click ligands. All isolated samples of G5-Ac-COG_x had single species purities over 95%. In the averaged sample, the most common species was dendrimer conjugated to 2 COG ligands, and this precise ratio comprised only 16% of the sample. However, the isolated sample labeled G5.Ac-COG_2 contained only G5 conjugated to 2 ligands as measured by rp-UPLC, with no detectable presence of dendrimer conjugated to 0, 1, 3, or other numbers of ligands.

Here, we present the first application of the G5 PAMAM precise ligand-to-dendrimer ratio materials to a multivalent targeting system. Folate binding protein, employed as a model for the folic acid receptor overexpressed in various cancer cell lines, and the interaction of this target with folic acid has been a highly studied system for both cancer cell targeting of chemotherapeutics and for the more basic understanding of multivalent nanoparticle interactions. To understand how multivalency affects nanoparticle-ligand conjugates behavior in biological systems, it is vital to compare monovalent particles to those with 2 or more targeting ligands. However, stochastically synthesized conjugates contain a distribution of ligands per particle, making it difficult to distinguish the behaviors of the individual populations. The controlled ligand/dendrimer ratio conjugates allowed for the synthesis of functional G5-FA_n materials with well-defined sub-populations, including a conjugate with a FA-to-dendrimer ratio of 1, with no higher valencies present. These materials, when studied by SPR, allowed comparison of the binding strength and potential for multivalent interaction of conjugates containing no more than 1, 2, 3, or 4 FA ligands (Table 4.1).

Reaction of the conjugates with precise ligand-to-dendrimer ratios with complimentary click functionalized FA allows for the generation of dendrimers with well-defined numbers of covalently conjugated FAs via orthogonal click chemistry between the ring-strained cyclooctyne on the dendrimer and an azido group on the modified FA. The reaction between G5-Ac-COG_1 and γ-azide-FA yielded a product that has 96% conjugate with a FA-to-dendrimer ratio of precisely 1 and 4% of a conjugate with no FA. Because the original sample had no dendrimer conjugated to 2 or more COG ligands, the resulting product has no material with the ability to undergo multivalent binding. The lack of multivalent products allows us to test both the Licata and Tkachenko key-lock/non-specific binding interaction mechanism (Figure 4.2c),[43] which attributes the irreversible binding to dendrimer-protein van der Waals interactions and not multivalent FA binding, and the Sander mechanism[42] that assumes monovalent behavior will significantly differ from bivalent and higher behavior. This critical piece of data would also have prevented the (incorrect) assessment by Banaszak Holl et al. that avidity increase is an exclusive function of conjugate valency.[30]

The remaining click reactions with the higher COG valent material went to about 60% completion despite a ten-fold excess of the γ-azide-FA. This result has been duplicated for G5-COG_x conjugates with this γ-azide-FA and other small molecules (unpublished data) within the lab, where reaction times greater than 48 hours were tested. Similar reaction conditions employed in the literature between a G5-Ac-$COG_{\sim 20(avg)}$ conjugate and a γ-azide-modified methotrexate yielded 100% reaction efficiency, however in this case the limiting reagent was the small molecule.[47] This observation suggests that limiting the number of COG ligands on the dendrimer may limit accessibility for click reaction, perhaps via folding of hydrophobic ligands into the dendrimer core. The interior cavity of G5 PAMAM is limited, therefore with a high number (i.e. 20) of conjugated COG ligands, the dendrimer cannot internalize all the ligands at once, so at any given time COG ligands are available conjugation. However, at lower numbers of COG ligands (i.e. 1 – 4 as described here) there is likely enough void volume in the dendrimer to hold all COG ligands at once, therefore preventing click reaction with solution species. Additionally, utilization of click chemistry with γ-azide-FA eliminates the less active α-FA that is bound through the α-carboxylic acid. Both structural isomers of the click reaction are likely present, although this fact would not be expected to have great effect on binding to the FBP. The presence of both isomers may contribute to peak broadening of the products in rp-UPLC (See Figure C2). rp-UPLC also provides a useful tool for monitoring the click reaction, as the reaction of the hydrophobic ligand leads to a decrease in retention of the dendrimer conjugate on the C18 column. This technique provides a more accurate measurement of FA-to-dendrimer ratio of the product than techniques such as NMR, which only provides an average number and provides no detail about the individual ligand-to-dendrimer ratios that are present within a sample. For this measurement the NMR spectroscopy based averages suffer from low signal for the conjugated species as compared to the polymer scaffold, and from the polydispersity of the scaffold employed (see Supporting Information).

Figure 4.6a compares the monovalent sample, G5-Ac-$FA_{1.0}$, to the Poisson distribution expected for a stochastically synthesized G5-FA conjugate with an average ratio of 1. By way of comparison, G5-Ac-$FA_{1.0}$ has only 4% unfunctionalized material compared to

37% in the stochastic material. More importantly, 26% of the stochastic material has two or more FA covalently attached, meaning this material is not truly representative of monovalent behavior. The G5-Ac-$FA_{1.0}$ material may only undergo a single, monovalent specific interaction with a single FBP. Although the higher FA conjugates are not monodisperse, their heterogeneity has been significantly reduced as compared to an equivalent average stochastic conjugation. rp-UPLC has also revealed the relative amount of each ratio present in the samples (Figure 4.6 b–d), allowing for a much better

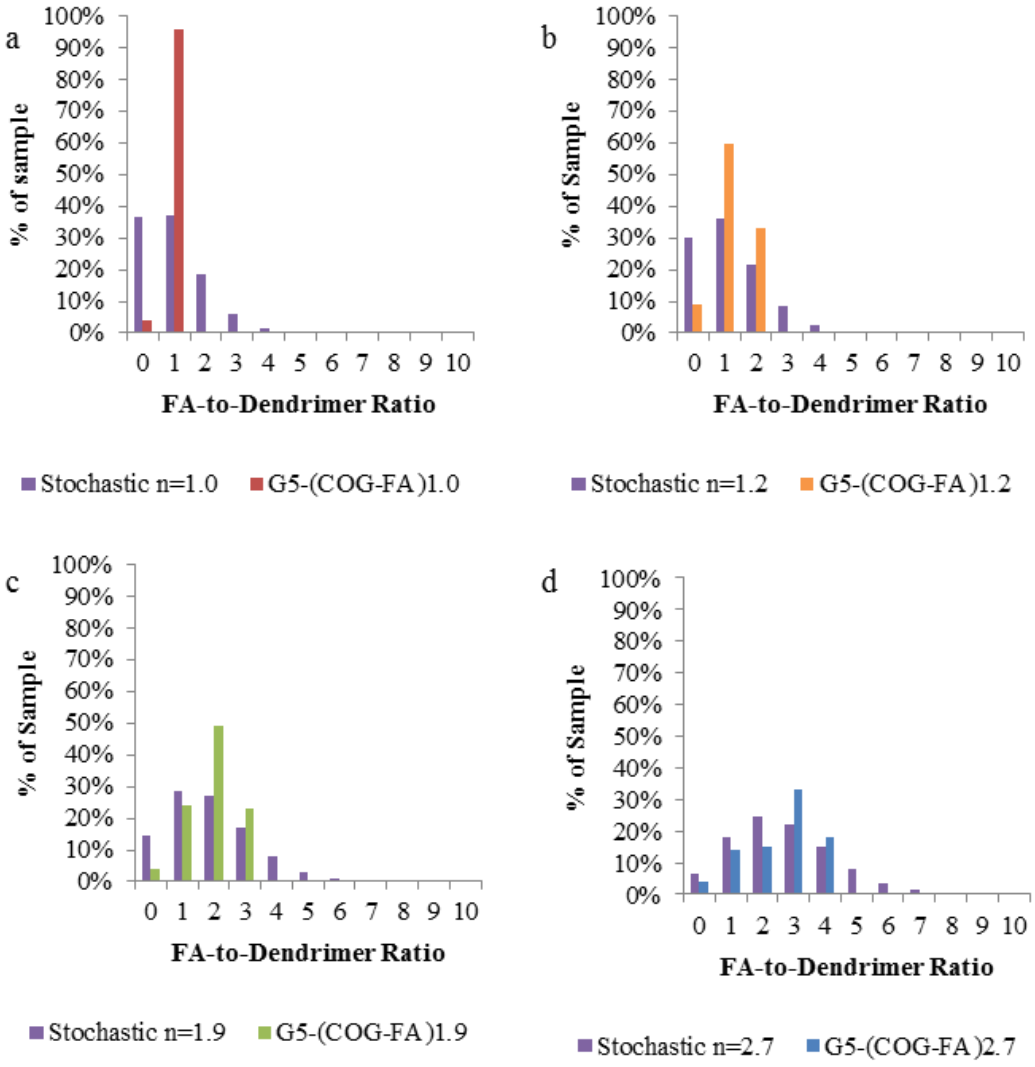

Figure 4.6. Comparison of distributions in click reaction products vs. theoretical stochastically conjugated products (purple bars) of the same average for ratios of (a) 1.0 (red bars) (b) 1.2 (orange bars) (c) 1.9 (green bars) and (d) 2.7 (blue bars).

understanding of the contribution of each "n" valency species in the sample to the binding as a whole. For example, the product of the G5-Ac-COG_3 click reaction (G5-Ac-$FA_{1.9}$) has an average of ~2 FAs per dendrimer, but UPLC reveals that 23% of the material has three FAs attached, while 49% has two FAs, 24% is monovalent, and only 4% of the material has zero FA. The presence of dendrimer conjugated to more than 3 FA is not possible as the starting material contained no dendrimer conjugated to 4 or more COG. The equivalent stochastic average of n = 1.9 has significant concentrations of 10 unique FA-to-dendrimer ratios (ranging from 0 to ~9), and ~15% of the sample has zero FA. The decreased sample complexity and improved characterization for the samples summarized in Table 4.1 allow for more accurate interpretation of subsequent SPR results.

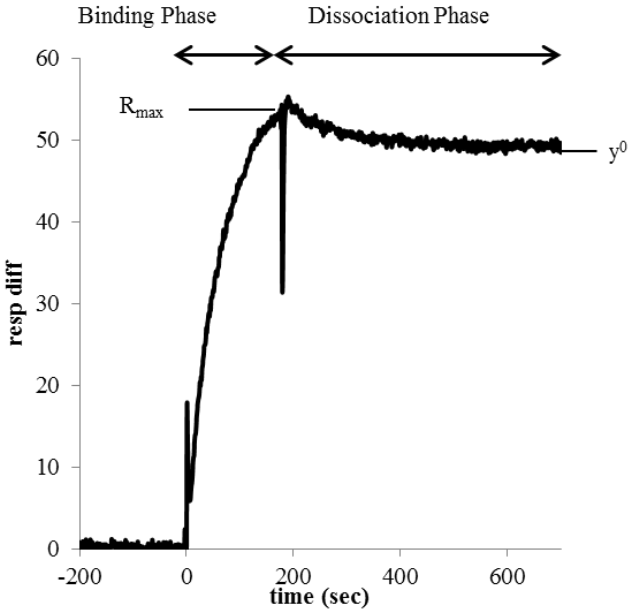

Figure 4.7. Definition of fitting parameters.

As illustrated in Figures 4.4 and 4.5, G5-Ac-FA_0 shows no binding to either of the FBP immobilized chips at the concentrations tested. However, G5-$FA_{n=1.0-2.7}$ have a binding curve that saturates at higher concentration. The total signal during binding phase (0 – 200 sec) (Figure 4.7) increases as a function of polymer concentration, FA valency (n), and density of protein immobilization.

At 200 sec, injection is complete and the dissociation phase begins (Figures 4.4 and 4.5). Several noteworthy observations can be made. First, at free FA concentrations ~100 fold higher than the equivalent conjugated FA conditions, free FA returns to baseline in the low density chip and nearly to baseline in the high density chip. This observation is consistent with the expected, reversible binding of FA to FBP. G5-Ac-FA_0 also returns to baseline, indicating no permanent interaction with the surface on the timescale of the

experiment. Most significantly, monovalent G5-Ac-$FA_{1.0}$ has a significantly reduced dissociation rate as compared to FA (Figures 4.4 c and 4.5 c). In addition, G5-Ac-$FA_{1.0}$ does not return to baseline during the time scale of the experiment (500 sec) at any concentration for either FBP surface density. The dissociation level off substantially above the initial baseline, indicating a portion of the material remains bound to the surface. This observation is true even though the highest relative FA concentration tested for G5-Ac-$FA_{1.0}$ (10 µM) is 25 times lower than the lowest FA concentration (0.25 mM). The permanent binding on the time scale of the SPR experiment has previously been attributed to multivalent binding between the conjugate and receptor,[30, 42] *however that cannot be the case for this purely monovalent conjugate*. This data strongly supports the key-lock/non-specific binding mechanism proposed by Licata and Tkachenko[43] in which only one FA to FBP interaction is necessary to initiate the stronger interaction between the dendrimer and FBP, which itself is a result of the summation of many weak van der Waals interactions. This result contradicts the mechanism proposed by Sander et al.[42] that attributed all observed reversible binding to the G5-Ac-FA_1 species.

More generalized observations can be made for the higher average conjugates. All G5Ac-$FA_{n=1.0\text{-}2.7}$ have dissociation sensorgrams similar to those previously reported results on both the high and low density chips.[30] All samples appear to have a portion of material that is permanently bound to the FBP surface on the timescale of this experiment (Figures 4.4 and 4.5). The saturation value (y^o in Figure 4.7) changes as function of FBP surface density (Figure 4.8). On the low-density chip, the maximum signal from

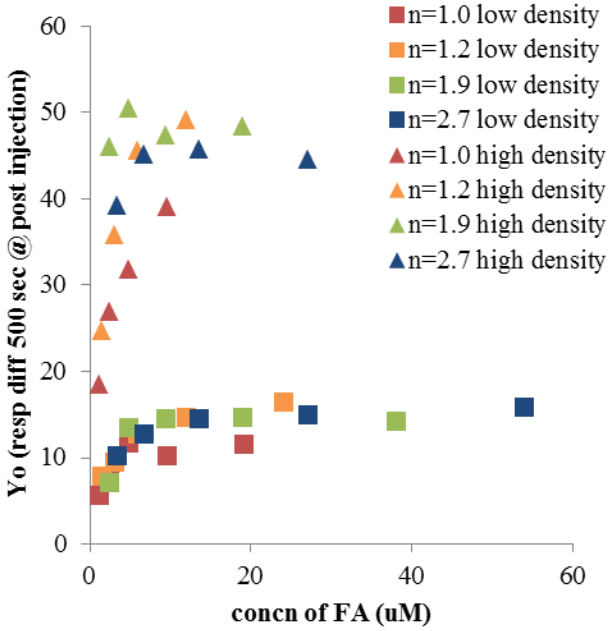

Figure 4.8. Saturation of permanent bound material (y^o) as a function of FA concentration.

permanently bound material is 14 ± 2 response units, which is achieved at a total FA solution concentration of ~10 μM. On the high-density surface, the response unit values saturate at 46 ± 4 at ~10 μM. The only exception is G5-Ac-$FA_{1.0}$ for which 10 μM is the highest concentration tested. For both low and high FBP density, this conjugate did not reach the saturation value by 10 μM.

This surface density-dependent saturation of signal is indicative of a limiting number of FBP binding sites available for binding to the conjugates. Figure 8 also suggests that the total amount of permanently bound material is determined primarily by (i) total FA concentration in solution and (ii) surface FBP density. All differences in the permanently bound fraction for the multivalent (n = 1.2 – 2.7; orange, green, and blue) samples can be attributed to the difference in FA concentration of these samples, which completely saturates when total FA concentration is ~10 μM. The monovalent material (G5-Ac-$FA_{1.0}$, red) appears to have slightly lower binding compared to the multivalent samples based on total FA concentration. This occurrence may result from the enhanced effective concentration in the multivalent samples due to dendritic architecture forcing the multiple FAs into a ~5 diameter spherical area. This effect is small, and there appears to be no additional effect when valency is increased above n = 2.

Qualitative observations (i.e. permanent binding fraction in the G5-Ac-$FA_{1.0}$ sample and nonzero y^o) indicate that this data will not adhere to the simple single phase Langmuir isotherm. To demonstrate this observation quantitatively, the data was fit with several models. In a single event binding between conjugate species A (here, G5-$FA_{n=1.0-2.7}$) and species B (here, FBP immobilized on the SPR chip):

$$A + B \rightarrow AB \qquad \textit{Equation 1}$$

The response difference (R) from SPR in the association phase at a given time (t) can be written as:

$$R(t) = \frac{k_a C R_{max}}{k_a C + k_d}(1 - e)^{-(k_a C + k_d)t} \qquad \textit{Equation 2}$$

where k_a is the association rate constant, k_d the dissociation rate constant, and C is the conjugate concentration (in μM).[48] Assuming a single association event leads to a

single dissociation event, and acknowledging that the monovalent interaction between FA and FBP is reversible, the dissociation can be modeled by an exponential decay:

$$R(t) = Ae^{-k_d t} + y' \qquad \textit{Equation 3}$$

where A relates to the initial condition and y' is equal to zero, because the species is expected to completely dissociate. Initially the dissociation phase was fit with equation 3 to obtain k_d. This value for k_d is then employed when fitting the association phase with equation 2 to obtain k_a.

Alternatively, two event association models allow for both permanently bound and transiently bound fractions. A two phase association in SPR can be modeled as:

$$R(t) = \frac{k_{a1}CR_{max}}{k_{a1}C+k_{d1}}(1-e)^{-(k_a1C+k_{d1})t} + \frac{k_{a2}CR_{max}}{k_{a2}C+k_{d2}}(1-e)^{-(k_{a2}C+k_{d2})t} \qquad \textit{Equation 4}$$

Equation 4 can be simplified according to several models. If the assumption is made that there are two binding events; a "permanent" binding (the fraction of response is equal y^o and $k_{d1} = 0$) and a transient binding (the fraction responsible for the remainder of R(t)); and all observed dissociation is from transient bound material, then the dissociation phase can be fit with:

$$R(t) = Ae^{-k_{d2}t} + y^0 \qquad \textit{Equation 5}$$

and Equation 4 becomes:

$$R(t) = y^0(1-e)^{-(k_{a1}C)t} + \frac{k_{a2}C(R_{max}-y^o)}{k_{a2}C+k_{d2}}(1-e)^{-(k_{a2}C+k_{d2})t} \qquad \textit{Equation 6}$$

If one assumes that all transient binding is attributed to nonspecific interactions between remaining unfunctionalized (n = 0) dendrimer and the protein, the binding phase can be modeled with:

$$R(t) = y^0(1-e)^{-(k_{a1}(C-n_0C)t} + \frac{k_{a2}n_0C(R_{max}-y^o)}{k_{a2}C+k_{d2}}(1-e)^{-(k_{a2}n_0C+k_{d2})t} \qquad \textit{Equation 7}$$

where n_0 is the percentage of the sample that corresponds to G5-Ac-FA_0. Conversely, if one assumes that both unfunctionalized and monovalent interactions are transient, than n_0

is the equal to the sum of the percentages of G5-Ac-FA_0 and G5-Ac-$FA_{1.0}$. Binding phases were fit with Equation 7 with both assumptions. The fit for the G5-Ac-$FA_{1.0}$ samples was poor with the second assumption, as expected, since this model would assume no permanent bound material, even though these samples clearly do not completely dissociate. A quantitative summary of the four fitting models is found in Tables 4.2 and 4.3, where K_d is defined as:

$$K_d = \frac{k_d}{k_a} \; or \; \frac{k_{d2}}{k_{a1}+k_{a2}} \qquad \textit{Equation 8}$$

			K_d (nM)	k_a (nM^{-1} s^{-1})	k_d (s^{-1})
Single assoc. (Equations 2 & 3)	Com-bined	Avg	**60**	**5.2**	**0.31**
		St Dev		3.0	0.20
	High Density	Avg	20	6.0	0.12
		St Dev		3.2	0.53
	Low density	Avg	100	4.6	0.47
		St Dev		2.7	0.12

Table 4.2. Quantitative summary of single phase assoc. fit.

			observed K_d (nM)	k_{a1} (nM^{-1} s^{-1})	k_{a2} (nM^{-1} s^{-1})	k_{d2} (s^{-1})
Two assoc. (Equations 5 & 6)	Combined	Avg	**480**	**5.4**	**14**	**9.1**
		St Dev		3.7	17	6.5
	High Density	Avg	570	5.9	17	1.3
		St Dev		3.4	17	8.1
	Low Density	Avg	380	5.0	11	6.1
		St Dev		3.9	17	0.9
Two assoc., n0 = 0 (Equations 5 & 7)	Combined	Avg	**190**	**6.8**	**42**	**9.1**
		St Dev		3.4	50	6.5
	High Density	Avg	210	6.5	2.2	6.1
		St Dev		3.2	3.0	0.9
	Low Density	Avg	180	7.1	66	13.0
		St Dev		3.6	61	8.4
Two assoc., n0 = 0 ,1 (Equations 5 & 7)	Combined	Avg	**300**	**7.5**	**23**	**9.1**
		St Dev		6.4	36	6.5
	High Density	Avg	570	5.9	17	13.0
		St Dev		3.4	17	8.1
	Low Density	Avg	230	6.4	20	6.1
		St Dev		5.2	45	0.9

Table 4.3. Quantitative summary of two phase assoc. fits.

As indicated in Tables 4.2 and 4.3, the measured k_a and k_d values vary from sample to sample, but values are on the same order of magnitude for each run and fit value. Although the absolute values vary from injection to injection, the individual fits of the data are much more consistent. Figure 4.9 gives some exemplar data (solid lines) and corresponding fits (dotted lines). The full set of data can be found in the supporting information (Figures C6 and C7).

Several qualitative observations can be made. Firstly, as expected, a single phase model that assumes complete dissociation of the complex is a poor fit for the dissociation phase of all samples (dotted green lines). The single phase association appears to have a good fit with the experimental data, however as this equation is dependent on the single phase

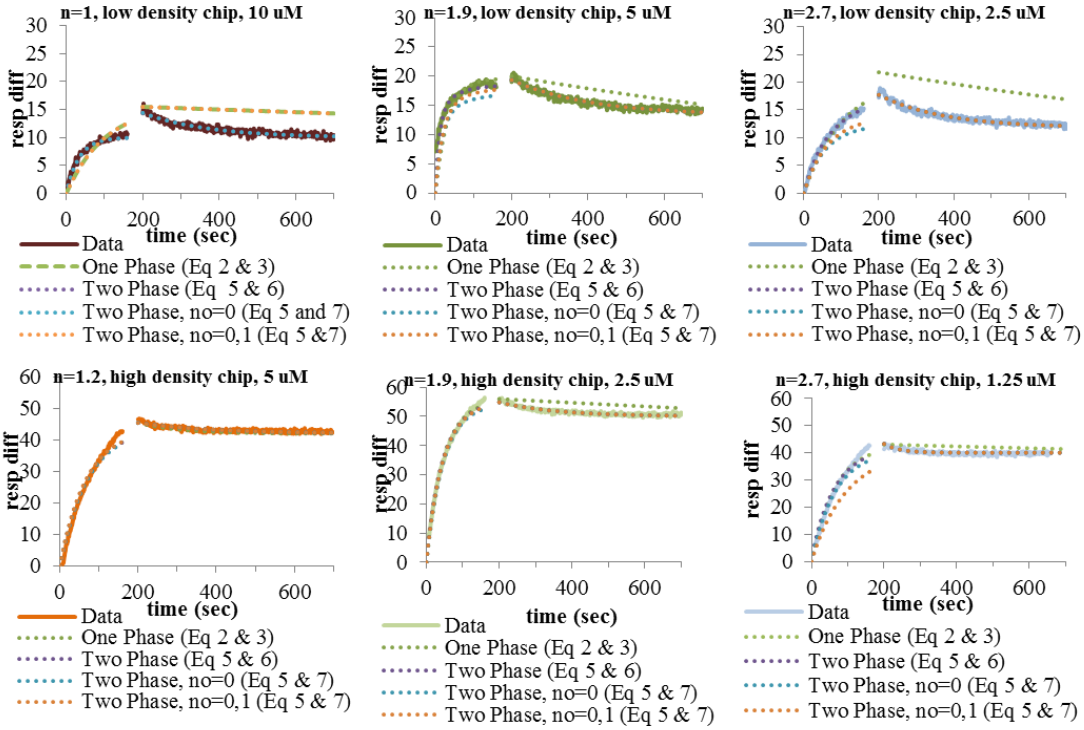

Figure 4.9. Examples of modeled data (dotted lines) compared to experimental data (solid lines).

dissociation constant, the overall mechanism is still invalid. Secondly, because the two event model where n_o = 0, 1 (dotted orange lines) is equivalent to a single event model for the monovalent case, this model results in a poor fit for all the G5-Ac-$FA_{1.0}$ data. For some data (Figure 4.9d,e) all models fit the data approximately the same, while in other cases particular models clearly fit the data better (Figure 4.9c, purple dotted line) or worse (Figure 9f, orange dotted line) than others. To assess which mathematical model provide the best global fit to the data, the average residual (difference between calculated and actual data) was taken for both the association phase and dissociation phase for each model at each valency and concentration tested (Table C2). The two phase dissociation model (Equation 5) had a ten-fold better fit for all samples when compared to the single (total) dissociation model (Equation 2). For the low density chip, the basic two phase association model (Equation 6) had the lowest average residual for all valencies tested with an average residual across all valencies of 0.44 response units. By comparison, the next best model (single phase, equation 3) had an average residual across all valencies of 0.95 units. However, the poor fit of the corresponding dissociation phase data for Equation 3 renders this model invalid. The high density chip had slightly higher residuals

for the association phase, with the lowest average across all valencies being the single phase (Equation 3) at 1.84 response units. As this mechanism is still ruled out due to poor agreement with the dissociation phase, it is important to note that the simple two phase model (Equation 6) had the next best fit with an average residual of 2.39 response units. The alternative two phase model (Equation 7) had the poorest agreement with experimental data for $n_0 = 0$ for both chip densities, and the second poorest agreement when $n_0 = 0, 1$. From this analysis, two main conclusions can be drawn: (1) There are at least two types (or steps) of association for G5-FA_n to the immobilized FBP, which leads to (2) the presence of both a transiently and permanently bound material for all G5-FA_n, including monovalent material.

The initial model proposed by Banaszak Holl et al.[30] (Figure 4.2a) is mathematically equivalent to Equations 2 and 3, where K_d is expected to change with average number of FAs per conjugate sample. Clearly, in the original analysis of SPR data by Banaszak Holl et al., (Figure 2a) the assumption that all bound material would eventually dissociate (i.e. $y' = 0$) from the surface was erroneous. The model proposed by Sander et al.[42] (Figure 4.2b) correctly noted that a fraction of the material remained bound to the surface for the length of the experiment (essentially permanently); however, the additional assumption that G5-FA_1 was entirely responsible for the observed dissociation in stochastic mixtures of G5-FA_n was incorrect. This model is clearly contradicted by the G5-Ac-$FA_{1.0}$ results, which are poorly fit by Equation 2, and which clearly show enhanced binding to the FBP over free FA. When the other samples were fit with Equations 7, allowing for $n = 0$ or $n = 0$ and 1 to reversibly bind and $n \geq 3$ to irreversibly bind, poor association phase fits were observed (especially at lower FBP densities). The third theory, put forth by Licata and Tkachenko,[43] proposed that an initial binding event between conjugate and FBP is keyed by FA, then the binding strength becomes dominated by van der Waals forces between the ~30 kDa polymer and ~40 kDa protein (Figure 4.2c). These summed weak interactions are responsible for the increased avidity for the conjugates, which the authors hypothesized are too great to be attributed to the comparatively weak (K_d ~ 0.1 nM) FA/FBP interaction. Mathematically, this model would not show a dependence of K_d on degree of FA valency and is best represented by Equation 6, which allows all conjugates to undergo both transient and permanent binding events. The increased avidity for the

G5-Ac-$FA_{1.0}$ conjugate as compared to free FA on both the low and high surface density chips, which is not further improved even with the G5-Ac-$FA_{2.7}$ conjugate, best agrees with this model qualitatively and quantitatively.

Therefore, we propose that the binding between G5-Ac-FA_n conjugates and immobilized FBP can be explained by a two-fold mechanism. First, G5-Ac-FA_n binds to a FBP immobilized on the chip surface. This interaction has an association constant (k_{a2}) of ~14 nM^{-1} s^{-1}. Because the initial binding is dependent on the concentration of FA, there is an apparent enhancement of avidity due to an increased total concentration of FA when multiple copies of the ligand are attached to the same dendrimer. This effective concentration may also lead to an increased chance of rebinding, as the FA/FBP dissociation constant (k_{d2}) of ~9 s^{-1} allows for dissociation of the conjugate from the surface on the SPR experimental timescale. Therefore, although strong binding is observed for all samples, the G5-Ac-$FA_{1.0}$ binds slightly less total material at the same relative FA concentration as compared to higher valency samples. In the second step, the acetylated dendrimer arms, which are brought close to the protein surface by the initial FA-FBP key-lock interaction, interact via van der Waals forces with the protein and/or dextran surface of the SPR chip. The interaction may be further energetically driven by desolvation of both the protein and dendrimer surfaces. Because these interactions are short ranged, it is only observed when are there are both conjugated FA and immobilized FBP available (i.e. it is not observed for G5-Ac-FA_0 control or on the unfunctionalized Flow Cell 2. Although van der Waals interactions are weak, the sum of many interactions available between the two ~5 nm entities, and the associated desolvation, creates a force that is irreversible over timescale of these SPR experiments.

Conclusions

In summary, we have synthesized a monovalent G5-Ac-$FA_{1.0}$ conjugate that allows for the distinction between three previously proposed mechanisms for the high avidity interaction with FBP. We have also synthesized multivalent G5-FA conjugates with narrow FA-to-dendrimer ratio distributions to examine the kinetics of interaction between dendrimer-conjugated FA and FBP. The removal of trailing generation and oligomers in

the PAMAM dendrimer starting material enabled the decoupling of mass and polymer surface area effects from FA valency. rp-HPLC enabled the isolation of dendrimers containing precise ratios (1, 2, 3, and 4) of a copper-free, ring strain promoted click ligands to a dendrimer scaffold. A γ-azide-FA was clicked to these precise ratio conjugates to synthesize FA functionalized dendrimers with narrow, well defined distributions of FA with average ratios of up to 2.7 FAs-per-dendrimer. Importantly, the monovalent conjugate G5-Ac-$FA_{1.0}$ was synthesized with no portion of the sample having more than 1 conjugated FA, allowing for the distinction of polymer contributions (i.e. solubility and van der Waals interactions with the surface) from multivalent contributions (i.e. effective concentration and chelate binding) to the increased binding of dendrimer conjugates to FBP surfaces.. SPR studies revealed that G5-Ac-FA_1 experiences the enhanced avidity over free FA that has previously been attributed to multivalent FA binding. Through examination of four quantitative models, it was concluded that the mechanism of interaction between G5-Ac-FA_n and surface immobilized FBP is two-fold: an initial, reversible, FA concentration dependent key-lock interaction between the conjugate and protein, followed by irreversible interaction between the dendrimer and protein surfaces. The confirmation that these samples exhibit permanent binding on the time scale of the FA experiment disproves, *even for a monovalent sample*, the original Banaszak Holl et al.[30] These findings also provide evidence against the model proposed by Sander et al.,[42] which attributed the increase in avidity to dendrimer species with 2 or more conjugated FA and assigned all dissociated material as G5-Ac-FA_1. However, the model proposed by Licata et al.[43] explains the original data[30] and agrees well with these new findings.

The interaction of G5-Ac-FITC-FA_n with folic acid receptor upregulated KB cells, reported along with the original SPR experiments,[30] exhibited the same saturation behavior. Based on the data and mechanistic interpretation presented here and in the work of Licata and Tkachenko,[43] the observed enhancement of residence on the KB cell surface as a function of n could result from a combination of overall increase FA concentration and increased rebinding with increasing n. Alternatively, it is possible that conjugate-initiated receptor clustering occurs on the cell membrane. An event that is impossible for the FBP immobilized to a dextran model system. Experiments to

synthesize fluorescent materials containing precise ratios of FA targeting ligand for cell culture and *in vivo* experiments are in progress.

References

1. Leamon, C., *Folate-targeted chemotherapy.* Advanced Drug Delivery Reviews, 2004. **56**(8): p. 1127-1141.
2. Hilgenbrink, A.R. and P.S. Low, *Folate receptor-mediated drug targeting: From therapeutics to diagnostics.* Journal of Pharmaceutical Sciences, 2005. **94**(10): p. 2135-2146.
3. Paulos, C., *Folate receptor-mediated targeting of therapeutic and imaging agents to activated macrophages in rheumatoid arthritis.* Advanced Drug Delivery Reviews, 2004. **56**(8): p. 1205-1217.
4. York, A.W., et al., *Facile Synthesis of Multivalent Folate-Block Copolymer Conjugates via Aqueous RAFT Polymerization: Targeted Delivery of siRNA and Subsequent Gene Suppression†.* Biomacromolecules, 2009. **10**(4): p. 936-943.
5. Liu, H., et al., *Targeted Tumor Computed Tomography Imaging Using Low-Generation Dendrimer-Stabilized Gold Nanoparticles.* Chemistry - A European Journal, 2013. **19**(20): p. 6409-6416.
6. Chen, C., et al., *Structural basis for molecular recognition of folic acid by folate receptors.* Nature, 2013. **500**(7463): p. 486-489.
7. Leamon, C.P. and P.S. Low, *Delivery of macromolecules into living cells: a method that exploits folate receptor endocytosis.* Proceedings of the National Academy of Sciences, 1991. **88**(13): p. 5572-5576.
8. Kamen, B.A. and A. Capdevila, *Receptor-mediated folate accumulation is regulated by the cellular folate content.* Proceedings of the National Academy of Sciences, 1986. **83**(16): p. 5983-5987.
9. Wang, Y., et al., *Targeted delivery of doxorubicin into cancer cells using a folic acid–dendrimer conjugate.* Polymer Chemistry, 2011. **2**(8): p. 1754.
10. Zong, H., et al., *Bifunctional PAMAM Dendrimer Conjugates of Folic Acid and Methotrexate with Defined Ratio.* Biomacromolecules, 2012. **13**(4): p. 982-991.
11. Leamon, C.P., I. Pastan, and P.S. Low, *Cytotoxicity of folate-Pseudomonas exotoxin conjugates toward tumor cells. Contribution of translocation domain.* Journal of Biological Chemistry, 1993. **268**(33): p. 24847-54.
12. Liong, M., et al., *Multifunctional Inorganic Nanoparticles for Imaging, Targeting, and Drug Delivery.* ACS Nano, 2008. **2**(5): p. 889-896.
13. Shi, X., et al., *Dendrimer-Entrapped Gold Nanoparticles as a Platform for Cancer-Cell Targeting and Imaging.* Small, 2007. **3**(7): p. 1245-1252.
14. Lu, Y., et al., *Folate receptor-targeted immunotherapy of cancer: mechanism and therapeutic potential.* Advanced Drug Delivery Reviews, 2004. **56**(8): p. 1161-1176.
15. Gabizon, A., et al., *Targeting Folate Receptor with Folate Linked to Extremities of Poly(ethylene glycol)-Grafted Liposomes: In Vitro Studies.* Bioconjugate Chemistry, 1999. **10**(2): p. 289-298.

16. Kukowska-Latallo, J.F., et al., *Nanoparticle Targeting of Anticancer Drug Improves Therapeutic Response in Animal Model of Human Epithelial Cancer.* Cancer Research, 2005. **65**(12): p. 5317-5324.
17. Majoros, I.J., et al., *PAMAM Dendrimer-Based Multifunctional Conjugate for Cancer Therapy: Synthesis, Characterization, and Functionality.* Biomacromolecules, 2006. **7**(2): p. 572-579.
18. Quintana, A., et al., *Design and Function of a Dendrimer-Based Therapeutic Nanodevice Targeted to Tumor Cells Through the Folate Receptor.* Pharmaceutical Research, 2002. **19**(9): p. 1310-1316.
19. Djohari, H. and E.E. Dormidontova, *Kinetics of Nanoparticle Targeting by Dissipative Particle Dynamics Simulations.* Biomacromolecules, 2009. **10**(11): p. 3089-3097.
20. Wang, S. and E.E. Dormidontova, *Nanoparticle Design Optimization for Enhanced Targeting: Monte Carlo Simulations.* Biomacromolecules, 2010. **11**(7): p. 1785-1795.
21. Wang, S. and E.E. Dormidontova, *Nanoparticle targeting using multivalent ligands: computer modeling.* Soft Matter, 2011. **7**(9): p. 4435-4445.
22. Martinez-Veracoechea, F.J. and D. Frenkel, *Designing super selectivity in multivalent nano-particle binding.* Proceedings of the National Academy of Sciences, 2011. **108**(27): p. 10963-10968.
23. Kitov, P.I. and D.R. Bundle, *On the Nature of the Multivalency Effect: A Thermodynamic Model.* Journal of the American Chemical Society, 2003. **125**(52): p. 16271-16284.
24. Krishnamurthy, V.M., L.A. Estroff, and G.M. Whitesides, *Multivalency in Ligand Design*, in *Fragment-based Approaches in Drug Discovery*. 2006, Wiley-VCH Verlag GmbH & Co. KGaA. p. 11-53.
25. Wolfenden, M.L. and M.J. Cloninger, *Multivalency in Carbohydrate Binding*, in *Carbohydrate Recognition*. 2011, John Wiley & Sons, Inc. p. 349-370.
26. Chittasupho, C., *Multivalent ligand: design principle for targeted therapeutic delivery approach.* Therapeutic Delivery, 2012. **3**(10): p. 1171-1187.
27. Kiessling, L.L., J.E. Gestwicki, and L.E. Strong, *Synthetic multivalent ligands in the exploration of cell-surface interactions.* Current Opinion in Chemical Biology, 2000. **4**(6): p. 696-703.
28. Kiessling, L.L., L.E. Strong, and J.E. Gestwicki, *Chapter 29. Principles for multivalent ligand design*, in *Annual Reports in Medicinal Chemistry*. 2000, Academic Press. p. 321-330.
29. Mullen, D.G. and M.M. Banaszak Holl, *Heterogeneous Ligand–Nanoparticle Distributions: A Major Obstacle to Scientific Understanding and Commercial Translation.* Accounts of Chemical Research, 2011. **44**(11): p. 1135-1145.
30. Hong, S., et al., *The Binding Avidity of a Nanoparticle-Based Multivalent Targeted Drug Delivery Platform.* Chemistry & Biology, 2007. **14**(1): p. 107-115.
31. Kuroiwa, Y., et al., *Identification and Characterization of the Direct Interaction between Methotrexate (MTX) and High-Mobility Group Box 1 (HMGB1) Protein.* PLoS ONE, 2013. **8**(5): p. e63073.
32. Silpe, J.E., et al., *Avidity Modulation of Folate-Targeted Multivalent Dendrimers for Evaluating Biophysical Models of Cancer Targeting Nanoparticles.* ACS Chemical Biology, 2013. **8**: p. 2063-2071.
33. Zhang, Y., et al., *Polyvalent saccharide-functionalized generation 3 poly(amidoamine) dendrimer–methotrexate conjugate as a potential anticancer agent.* Bioorganic & Medicinal Chemistry, 2011. **19**(8): p. 2557-2564.

34. Wiener, E.C., et al., *Targeting Dendrimer-Chelates to Tumors and Tumor Cells Expressing the High-Affinity Folate Receptor.* Investigative Radiology, 1997. **32**(12): p. 748-754.
35. Patri, A., J. Kukowskalatallo, and J. Bakerjr, *Targeted drug delivery with dendrimers: Comparison of the release kinetics of covalently conjugated drug and non-covalent drug inclusion complex.* Advanced Drug Delivery Reviews, 2005. **57**(15): p. 2203-2214.
36. Mintzer, M.A. and M.W. Grinstaff, *Biomedical applications of dendrimers: a tutorial.* Chemical Society Reviews, 2011. **40**(1): p. 173-190.
37. Christensen, J.B. and D.A. Tomalia, *Designing Dendrimers*, in *Dendrimers as Quantized Nano-modules in the Nanotechnology Field*, S. Campagna, P. Ceroni, and F. Puntoriero, Editors. 2012, J. Wiley & Sons: Hoboken. p. 1-33.
38. Tomalia, D.A., J.B. Christensen, and U. Boas, *The Dendritic State*, in *Dendrimers, Dendrons and Dendritic Polymers: Discovery, Applications, the Future*
2012, Cambridge University Press
NY. p. 30.
39. Tomalia, D.A., et al., *Structure control within poly(amidoamine) dendrimers: size, shape and regio-chemical mimicry of globular proteins.* Tetrahedron 2003. **59**: p. 379-3813.
40. Chauhan, A.S., N.K. Jain, and P.V. Diwan, *Pre-clinical and behavioural toxicity profile of PAMAM dendrimers in mice.* Proceedings of the Royal Society A: Mathematical, Physical and Engineering Science, 2010. **466**(2117): p. 1535-1550.
41. van Dongen, M.A., et al., *Quantitative analysis of generation and branch defects in G5 poly(amidoamine) dendrimer.* Polymer, 2013. **54**: p. 4126-4133.
42. Waddell, J.N., et al., *Origin of broad polydispersion in functionalized dendrimers and its effects on cancer-cell binding affinity.* Physical Review E, 2010. **82**: p. 036108.
43. Licata, N.A. and A.V. Tkachenko, *Kinetic Limitations of Cooperativity-Based Drug Delivery Systems.* Physical Review Letters, 2008. **100**: p. 158102.
44. Mullen, D.G., et al., *A Quantitative Assessment of Nanoparticle-Ligand Distributions: Implications for Targeted Drug and Imaging Delivery in Dendrimer Conjugates.* ACS Nano, 2010. **4**: p. 657-670.
45. Mullen, D.G., et al., *Isolation and Characterization of Dendrimers with Precise Numbers of Functional Groups.* Chemistry – A European Journal, 2010. **16**(35): p. 10675-10678.
46. van Dongen, M., S.m.u.e. Vaidyanathan, and M.M. Banaszak Holl, *PAMAM Dendrimers as Quantized Building Blocks for Novel Nanostructures.* Soft Matter, 2013.
47. Huang, B., et al., *Copper-free click conjugation of methotrexate to a PAMAM dendrimer platfrom.* Tetrahedron Letters, 2011. **52**: p. 1411-1414.
48. Fägerstam, L.G., et al., *Biospecific interaction analysis using surface plasmon resonance detection applied to kinetic, binding site and concentration analysis.* Journal of Chromatography A, 1992. **597**(1–2): p. 397-410.

Chapter 5

Methotrexate/PAMAM Conjugates: A Comparison of Key, Scaffold, and Linkers

Introduction

Multivalent drug-polymer conjugates, in which multiple copies of a drug are covalently attached to a polymeric scaffold either directly or through linker chemistry, are a highly studied pathway to improve therapeutic index. Particularly, conjugation of the chemotherapeutic methotrexate (MTX) to a poly(amidoamine) (PAMAM) dendrimer has been extensively studied, with over 100 related publications since their first introduction in 2002.[1] The clinical potential of dendrimer conjugated MTX has been shown in many biological studies, which indicate favorable activity compared to free MTX.[2-4] However, to date, the ability to produce large-scale quantities of such materials while retaining desirable activities has been elusive.[5] Several variations to the system have been attempted to examine the impact on activity, including conjugation of targeting agents,[6] employment of various linker systems,[6, 7] and perturbation of valency.[8] In a recent study by Silpe, Choi et al., dendrimers conjugated to an average of 10 MTX exhibited stronger binding to surface immobilized folate binding protein (FBP) and more cytotoxicity to folic acid receptors (FAR) on KB cells than those with an average of 5 MTX.[8] However, there are often disadvantages to employing high valent systems, such as loss of solubility of the conjugate or loss of targeting specificity.[9] Systems containing an average number of ligands also contain a wide range of ligand-to-vector ratios present within a sample,[10-12] complicating identification or in-depth mechanistic study of the active components. Although work to date has made progress in improving sample reproducibility and activity, full mechanistic understanding is not yet achieved.

MTX is a structural derivative and competitive inhibitor of folic acid (FA), therefore multivalent MTX conjugates may have a similar mechanism of increased binding and uptake as the related multivalent FA system. A study from 2007 by Hong, Banaszak Holl

et al.[13] reported increasing avidity for stochastic average conjugates of FA to PAMAM dendrimer as a function of increasing valency. The authors attributed this effect to the multivalent effect of increasing clusters of folic acid-folate binding interactions (for example, 3 interactions having a stronger affinity than 2 interactions, which is stronger than a single interaction). For thorough descriptions of this type of ligand-based multivalent binding mechanism see reviews by Whitesides[14], Cloninger,[15] and Kiessling[16]). Since the original report of the FA-PAMAM conjugate multivalency in 2007, two alternate mechanisms to explain the data have been proposed. Waddell, Sander et al.[12] proposed that two types of interactions dominate the system: weak monovalent interactions and strong bivalent interactions. The apparent difference in observed avidity was attributed to different amounts of unfunctionalized and monovalent material in the stochastic distributions. Licata and Tkachenko,[17] proposed that the increased avidity reported was too large to be the sum of the relatively low affinity folic acid-protein interactions, and instead was due to van der Waals type interactions between the polymer vector and protein surface. In this mechanism, folic acid keys the initial binding between the conjugate and protein, bringing the polymer close enough to the protein surface for the van der Waals interactions to occur.

The original data, obtained using material containing consisting stochastic averages of FA per dendrimer, cannot distinguish between these three mechanisms. However, recent work by van Dongen, Banaszak Holl et al.[18] has enabled a closer examination of the PAMAM-FA multivalent system. In this work, a conjugate with exactly one FA per generation 5 (G5) PAMAM dendrimer was prepared. This sample was unique in that it provided a means to distinguish between avidity increases due to the polymer itself interacting with the protein (possible in a monovalent conjugate) and avidity increases due to multivalent FA binding (not possible in a monovalent system). The monovalent folic acid-dendrimer conjugate had similar avidity increases as the multivalent conjugates, strongly supporting the "lock and key" theory by Licata and Tkachenko, wherein FA serves is a strong key to unlock the nonspecific (van der Waals) polymer/protein interactions.[17] However, there are still many aspects of this system that should be more thoroughly studied. For example, MTX is a "weak key" as compared to FA. Can the weaker MTX key still initiate the van der Waals interactions? How does

vector size influence binding avidity in this lock-and-key system? And finally, as proposed by Licata and Tkachenko, what is the impact of tuning key strength by varying the linker used in conjugating the key to the polymer?

PAMAM dendrimers are often employed as multivalent vectors due to their low immunogenicity, ability to solubilize hydrophobic molecules, and the presence of multiple primary amines available for multivalent modifications.[19-21] They are also highly flexible vectors,[22] which allow them to deform and possibly reach multiple surface-immobilized receptors at time.[23] The size and number of functional groups of dendrimers increases with increasing generation, and consequently the amount of surface area that they can reach goes up as well.[24] Therefore, generation number gives a mechanism to control vector size. Unlike many polymer architectures, dendrimers have a narrow mass range which also makes them more ideal as vectors. However, recent work by van Dongen, Banaszak Holl et al. indicates that the presence of oligomers in G5 PAMAM dendrimer creates subpopulations within a sample that are two, three, or four times larger than the expected weight of the monomer.[25] These larger vectors may impact the chemical and biological behavior of resulting conjugates as they can potentially cover twice as much surface area. Recent results quantifying the amount of dimer (D), trimers and even tetramer present in G5 PAMAM dendrimer are particularly interesting in light of the Licata and Tkachenko models as the presence of the oligomers substantially changes the total magnitude of non-specific van der Waals interactions that are possible per particle. In the process of developing the rp-HPLC-based characterization of oligomers, the methods to separate and isolate the monomer G5 from the other oligomers were also elucidated. This accomplishment allowed a direct test of the role that varying the ratio of non-specific interactions to key-locks would play in surface adsorption.

In this work, we examine the individual and combined impacts of vector size variation, linker chemistry, and dendrimer valency by synthesizing monomeric (~30,000 MW) and dimeric (~60,000 MW) G5 conjugates with well-defined numbers of MTX attached to the dendrimer through two linker systems. Recent protocols developed to isolate precise

ratio ligand-to-dendrimer conjugates from stochastic distributions[26, 27] were employed to create conjugates with narrow, well-defined populations. We employ both chemical and biological assays to measure the impact of these parameters on sample activity. Several new conclusions can thus be drawn. (1) We have found that dimeric material present in commercial PAMAM dendrimer, and consequently conjugates synthesized from this material, contributes significantly to observed chemical and biological activities. Conjugates to MTX of dimer isolated from commercial PAMAM exhibit binding via surface plasmon resonance, in particular binding that is irreversible on the timescale of the experiment, similar to that observed in previous studies[8] employing commercial PAMAM. Additionally, multivalent conjugates of monomeric dendrimer to methotrexate did not exhibit a change avidity derived from multiple MTX binding events, presumably because the MTX is a "weak key" and cannot initiate the polymer/protein interactions at the same valencies as the "strong key", folic acid. (2) A longer and more flexible linker system is also shown to negatively impact the conjugate's ability to bind to FBP when compared to a shorter, less hydrophobic linker. This observation is attributed to increased hydrophobicity which could have several effects including reducing the overall enthalpy of the interaction and increasing the time that the linker, and consequently the attached MTX, spends in the interior regions of dendrimer. (3) We observe increased avidity over free MTX only at minimum valencies of n = 3 in dimer systems. This sample has an average composition, so it may still require more than three MTX-per-conjugate to trigger this behavior. Monomer systems were only tested to a valency of 3, which was not able to trigger higher avidity.

Experimental Section

Materials. All chemicals and materials were purchased from Sigma Aldrich or Fischer Scientific and used as received unless otherwise specified. G5 PAMAM dendrimer was purchased from Dendritech and purified into monomer (G5) and dimer (D) samples as previously described.[25] Click-Easy™ MFCO-N-hydroxysuccinimide was purchased from Berry & Associates Synthetic Medicinal Chemistry. γ-azido-MTX was synthesized as described previously.[7] Cyclooct-1-yn-3-glycolic acid (COG) was synthesized as previously reported (see Appendix C).

Preparation of G5-Ac-COG$_{4.7(avg)}$ conjugate. Conjugates were prepared using G5 via EDC-NHS coupling. In brief, 240.4 mg of amine-terminated monomer G5 was dissolved to 0.16 μM in DI. 12.0 mg of COG ligand was activated by dissolving to 10.5 μM in acetonitrile with 2.65 equiv of EDC and 2.78 equiv of N-hydroxysuccinimide and stirring for 2 hours. The activated COG solution was added dropwise via syringe pump to the dendrimer solution and allowed to stir overnight. The product was purified using Amicon Ultra Centrifugal units, 10kDa cutoff membranes, 2 PBS washes and 4 DI washes. 170.6 mg of white solid was isolated via lyophillization. The material was then fully acetylated (100% of remaining primary amines converted to acetyl groups, henceforth termed "Ac") by re-dissolving in anhydrous methanol (0.19 μM) and adding 450 equiv of triethylamine and 360 equiv of acetic anhydride, stirring for 4 hours, purified by centrifugation and isolated by lyophillization. G5-Ac-COG$_{4.7(avg)}$ was characterized by rp-UPLC.

Preparation of G5-Ac-MFCO$_{2.0(avg)}$ conjugate. Conjugates were prepared using G5 and Click-Easy™ MFCO-N-hydroxysuccinimide. In brief, amine-terminated G5 was dissolved to 0.16 μM in DI. Click-Easy™ MFCO-N-hydroxysuccinimide was activated by dissolving to 10.5 μM in acetonitrile and added dropwise via syringe pump to the dendrimer solution. The solution was stirred overnight. The product was purified using Amicon Ultra Centrifugal units, 10kDa cutoff membranes, 2 PBS washes and 4 DI washes. Product was isolated via lyophillization. The material was then fully acetylated by re-dissolving in anhydrous methanol (0.19 μM) and adding 450 equiv of triethylamine and 360 equiv of acetic anhydride, stirring for 4 hours, purified by centrifugation and isolated by lyophillization. G5-Ac-MFCO$_{2.0(avg)}$ was characterized by rp-UPLC.

Preparation of D-Ac-COG$_{4.8(avg)}$ conjugate. Conjugates were prepared using EDC/NHS coupling to isolated G5 dimer according to the same procedures outlined for the monomer utilizing 100.8 mg of dimer and 5 equiv of CO ligand. D-Ac-COG$_{4.8(avg)}$ was characterized by rp-UPLC.

Preparation of D_Ac-MFCO$_{6.2(avg)}$ conjugate. Conjugates were prepared using Click-Easy™ MFCO-N-hydroxysuccinimide to isolated G5 dimer according to the same procedures outlined for the monomer utilizing 115.5 mg of dimer and 6.4 equiv of MFCO ligand. D_Ac-MFCO$_{6.2(avg)}$ was characterized by rp-UPLC.

Isolation of precisely defined G5-Ac-COG$_x$, G5-Ac-MFCO$_x$, D-Ac-COG$_x$ and D-Ac-MFCO$_x$ conjugates (x = 0-3, 3+, or 4+) (Figure 1). Dendrimers with precise ratio COG or MFCO ligands per dendrimer were isolated via reverse-phase HPLC according to modified literature procedures.[11] Briefly, multiple injections of the averaged material were performed with a C18 column on a water/acetonitrile gradient with 0.1% TFA. Fractions were collected as the material eluted and combined to obtain monomer samples with precisely x = 0-5 COG ligands, or x = 0-4, 5+ MFCOs, and dimer samples with x = 0-2, 3+ COGs. Products were purified using PD-10 desalting protocols, with DI as the equilibration buffer and samples dissolved in 10xPBS, and then lyophilized to dry. Samples were characterized by UPLC. Curve fitting of UPLCs by Igor Pro was performed to provide yield, purity, and HPLC number of MFCO averages.

Synthesis of G5-Ac-(COG-MTX)$_n$ G5-Ac-(MFCO-MTX)$_n$, D-Ac-(COG-MTX)$_n$, D-Ac-(COG-MYX)$_{4.0(avg)}$ and G5-Ac-(MFCO-MTX)$_{4.0(avg)}$ conjugates. Dendrimers with defined numbers of covalently bound methotrexates were synthesized via click reaction of precise ratio G5-Ac-COG/MFCO$_n$ or D-Ac-COG/MFCO$_n$ conjugates and γ-azido-MTX. Briefly, dendrimer conjugates were dissolved in DMSO to 40 mM with respect to the click ligand, and a 10 fold excess of γ-azido-MTX (40 mM in DMSO) was added. Solutions were agitated for 48 hours, then diluted to 2.5 mL with 10xPBS and purified using PD-10 desalting columns, gravity protocols. Further purification was performed via 10kDa cut-off dialysis against DI with 16 media changes. Dried samples were characterized by ^{1}H-NMR spectroscopy and UPLC (see Supporting Information). Curve fitting of UPLCs provided yield, purity, and HPLC MTX averages.

Methods.

High Performance Liquid Chromatography. Isolation of precise conjugates was achieved using a Waters 600 Controller, Waters 2707 Autosampler, and Waters 2998 Photodiode Array running Empower 2 Software, additionally equipped with a Waters Fraction Collector III on a Phenomenex Jupiter 300Å C18 Prep Column (21.2 x 150 mm, 5 µm particles). The weak solvent (Solvent A) was HPLC Grade Water with 0.1% TFA, and the strong solvent (Solvent B) was HPLC Grade Acetonitrile with 0.1% TFA. The

gradient employed at 16 mL/min was as follows: 2.1 min load step at 95%A/5%B, 3.9 min gradient to 80%A/20%B, 15 min gradient to 65%A/35%B, 5 min gradient to 55%A/45%B, followed by 3 min was at 20%A/80%B, then equilibrating at starting conditions for 5 min before next injection. Averaged conjugate was dissolved to 20 mg/mL concentration and 910uL injections were used. Five second fractions were collected starting at 9 min 30 sec into each run for a total of 120 fractions. Analytical chromatograms were collected on a Waters Acquity UPLC equipped with a scaled method using a Phenomenex Jupiter 4.6 x 100 mm column.

.LC Peak Fitting. UPLC chromatograms were fit with Gaussian peaks using Igor Pro Version 6.0.3.1 software. Peak widths within a chromatogram were kept constant.

Nuclear Magnetic Resonance Spectroscopy. NMR experiments were performed on Varian VNMRS 500 and Varian MR400 instruments. ^{1}H-NMR spectra were obtained used 10 second pre-acquisition delays and a total of 64 scans. All sample solutions were set to a dendrimer concentration of 5 mg/mL in deuterium oxide.

Dihydrofolate Reductase Assay. Dihydrofolate Reductase Activity Assay was purchased from Sigma Aldrich and employed according to the manufacturer's directives.

Isothermal Titration Calorimetry. G5-Ac-(MFCO-MTX)$_{4.0(avg)}$ (70, 200, 400 µM with respect to MTX), G5-Ac-(MFCO-MTX)$_{4+}$ (313.3 µM with respect to MTX), free MTX (200 µM) and FBP (4 µM) solutions were prepared in PBS buffer and then degassed for 25 minutes. Before loading, the syringe and cell were each rinsed with degassed PBS buffer 3 times. The reference cell of the ITC was refilled with degassed, nano-pure water every two days. After flushing the sample cell with buffer, the project syringe with buffer the syringe was filled with the MTX solution and the sample cell was filled with the FBP solution. Using ITCRun software the parameters of the ITC were set (Stir Rate: 250 rpm, Injection Interval: 1000 s, Injection Volume: 12 µL, Injections: 20, Temperature: 25°C) and the instrument to allowed auto equilibrate before starting the titrations. Controls were performed by injecting PBS buffer into the same concentration of FBP solution as used in the experiments with MTX. These control runs were then be subtracted from the experimental runs to account for heat from mixing or dilution. After the control was subtracted from the experimental run, the data was analyzed using NanoAnalyze software. The new points were then graphed and fit to a binding curve

(independent model) which then gave the thermodynamic parameters of the binding interaction.

Surface Plasmon Resonance. SPR experiments were conducted in a Biacore® X instrument (Pharmacia Biosensor AB). An immobilized folate binding protein (FBP) chip was prepared following the instrument prompted protocols, using a solution of 0.2M EDC and 0.05M NHS as an activating solution, 1mg/mL FBP solution as the immobilization solution, and ethanolamine as the deactivation solution. The chip was characterized using free FA and methotrexate solutions ranging from 0.1 to 2mM. Conjugate samples were dissolved in fresh HBS-EP buffer (Fischer Scientific) at 60uM and serially diluted to 10, 5, 2.5, and 1.25 µM in buffer. Runs were multichannel, (FC1-FC2) at 10 mL/min. The system was allowed to equilibrate at the beginning of each run for no less than 300 seconds, followed by a 2 minute, 30 µL (50-5-5-5 via bubble method) injection. The system was monitored for no less than 500 seconds per injection. Between each run, the chip was washed with a 5 µL injection of pH 1.5 buffer to remove bound materials followed by a prime step prior to the next injection.

KB FAR+ Cytotoxicity. KB cells overexpressing folic acid receptors were plated at 10,000 cells/well in 96-well plates for incubation overnight at 37°C. Treatment (free MTX and monomer conjugates) was done in triplicate for 48 hours in complete media without folic acid (dialyzed serum used), after which XTT assays were performed.

Results.

Preparation of average dendrimer/ligand conjugates (Scheme 5.1). All conjugates prepared were white solids. Overall reaction yields ranged from 37-43%. Peak fitting of the UPLC chromatograms was employed to determine the average ligand-to-

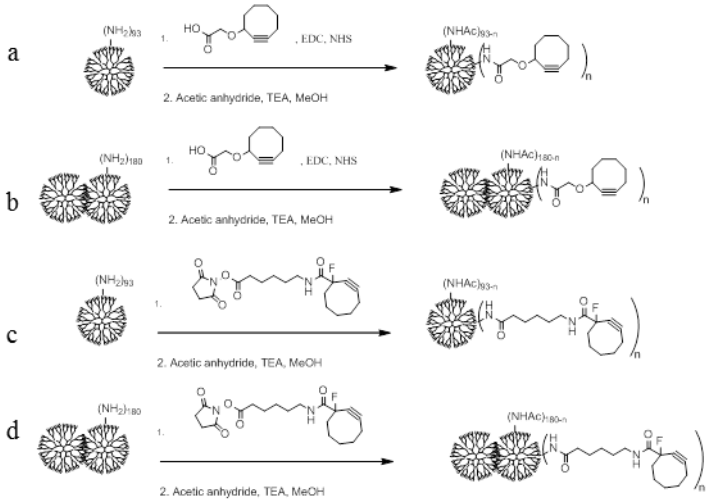

Scheme 5.1. Conjugation of (a) monomer to COG and (b) dimer to COG via EDC/NHS coupling, and (c) monomer to MFCO, and (d) dimer to MFCO by direct. Conjugations followed by full neutralizing of the dendrimer surface with acetic anhydride.

dendrimer ratio.

Isolation of dendrimer conjugates contain precise ratios of COG and MFCO click ligands (Figure 5.1). The quantitative results of the three isolations are summarized in Table 1. The purities of the target valency of the isolated, precise ratio ligand-to-particle conjugates range from 90-100%. Samples containing a high average number of MFCO ligands, G5-Ac-MFCO$_x$, D-Ac-MFCO$_x$, and D-Ac-COG$_x$, conjugates were obtained with averages of 6.6, 5.3, and 6.2 ligands-per-particle respectively. Importantly, these samples contain no unfunctionalized (x = 0) or monofunctional (x = 1) materials, making them good controls for the observation of multivalent (e.g. chelation) effects. A summary of the isolations can be found in Table 5.1.

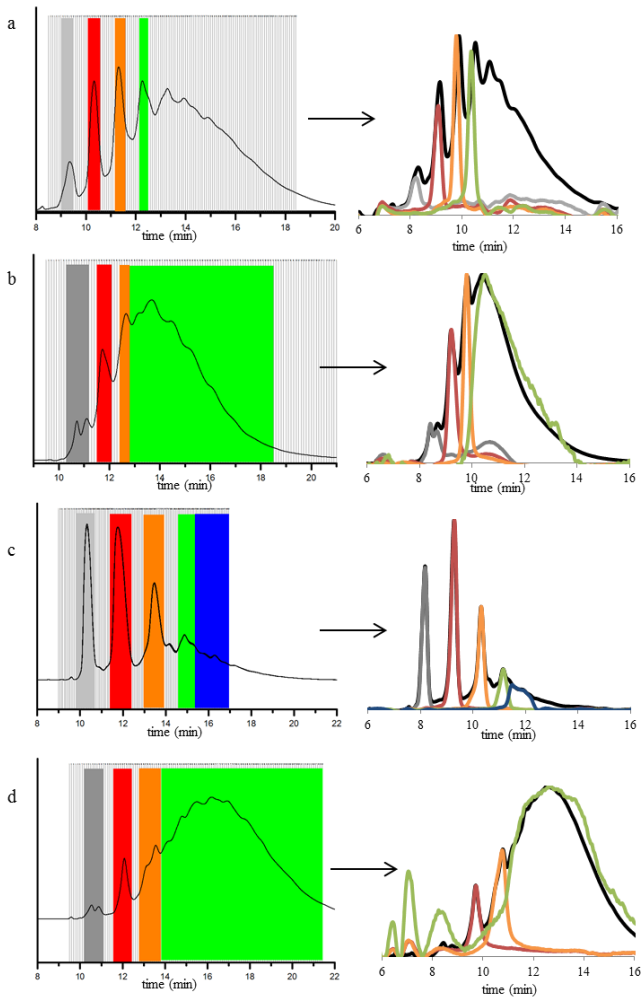

Figure 5.1. (left) rp-HPLC traces and fractions collected from average conjugations of (a) G5-Ac-COG$_x$ (b) D-Ac-COG$_x$ (c) G5-Ac-MFCO$_x$ and (d) D-Ac-MFCO$_x$ (right) rp-UPLC traces of average conjugation (black) and each collected fraction.

Synthesis of dendrimer/MTX conjugates (Scheme 5.2). Click reactions efficiencies ranged from 46-100% with mass recoveries over 95%. A detailed analysis of each sample's fractional composition is summarized in Table 5.2.

Dihydrofolate Reductase Assay (Figure 5.2). Results are summarized in Figure 2. The negative control (FA with no inhibitor) showed a change in absorbance at 235 nm of 0.04-0.05 units. G5-Ac (isolated from G5-Ac-COG$_{n(avg)}$ sample) served as additional negative control and had similar results to the uninhibited sample. The positive control

(FA inhibited by free MTX) showed complete inhibition of enzyme activity at all three concentrations of MTX (1nM, 10 nM, 100 nM) tested. G5-Ac-$(COG\text{-}MTX)_n$ samples did not effectively inhibit at a dendrimer concentration of 1 nM, only partially inhibited the protein activity at 10nM, and fully inhibited the activity at 100 nM. D-Ac-$(COG\text{-}MTX)_1$ partially inhibited the protein activity (20-40%) at all three concentrations, while D-Ac-$(COG\text{-}MTX)_{3+}$ partially inhibited (~60%) the activity at 1 nM and 10 nM, and had complete inhibition of the protein at 100 nM.

Vector	Ligand	Target Valency	UPLC Avg	UPLC Purity
Monomer	COG	0	0.0	100%
Monomer	COG	1	1.1	100%
Monomer	COG	2	1.9	90%
Monomer	COG	3	2.8	93%
Dimer	COG	0	0.0	100%
Dimer	COG	1	1.1	91%
Dimer	COG	2	2.0	100%
Dimer	COG	3+	6.2	n/a
Monomer	MFCO	0	0.0	100%
Monomer	MFCO	1	1.0	100%
Monomer	MFCO	2	1.9	91%
Monomer	MFCO	3	3.0	99%
Monomer	MFCO	4+	6.6	n/a
Dimer	MFCO	0	0.0	100%
Dimer	MFCO	1	1.1	100%
Dimer	MFCO	2	2.1	100%
Dimer	MFCO	3+	5.3	n/a

Table 5.1. Summary of isolated, precisely defined conjugates.

Isothermal Titration Calorimetry (Figure D1). The free MTX control showed the

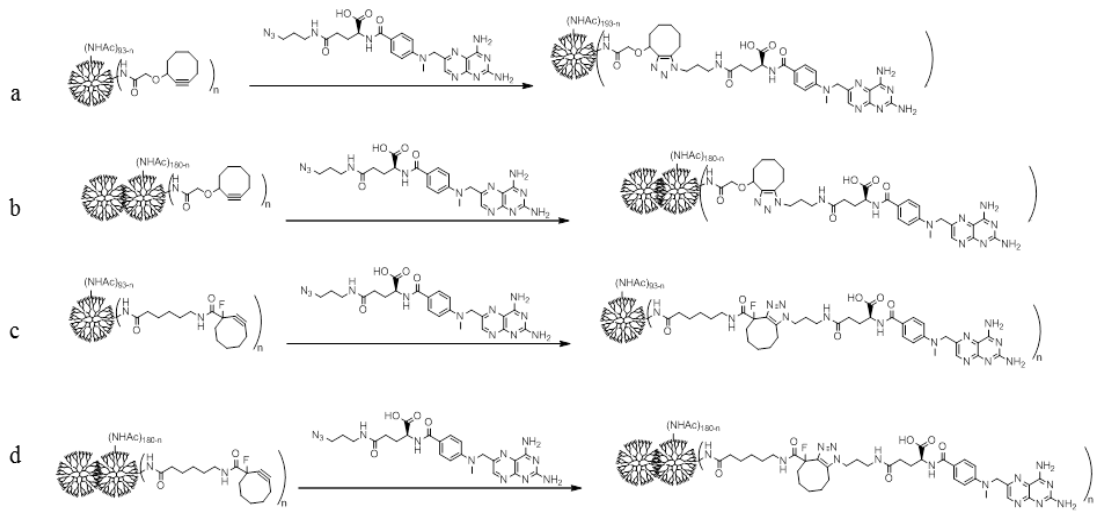

Scheme 5.2. Click of precisely defined G5-Ac-COGx, G5-Ac-MFCOx, D-Ac-COGx, and D-Ac-$MFCO_x$ conjugates to γ-azido-MTX.

expected exothermic binding behavior to FBP. The stochastically conjugated monomer G5-(MFCO-MTX) sample (Figure D1a) displayed endothermic binding, demonstrating a thermodynamic cost for binding to the substrate. The high average G5-Ac-(MFCO-MTX)$_{4.4}$ sample showed no interaction (neither endothermic nor exothermic) with the FBP substrate via this technique.

					% of "n" MTX				
Vector	Ligand	Target Valency	HPLC Avg Click Yield of MTX	(%)	n=0	n=1	n=2	n=3 (+)	n=4+
Monomer	COG	0	0.0	n/a	100	0	0	0	0
Monomer	COG	1	0.9	90	10	90	0	0	0
Monomer	COG	2	1.9	46	14	78	7	0	0
Monomer	COG	3	2.9	63	3	18	66	13	0
Dimer	COG	0	0.0	n/a	100	0	0	0	n/a
Dimer	COG	1	1.1	100	0	89	11	0	0
Dimer	COG	2	2.0	100	0	0	100	0	0
Dimer	COG	3+	6.0	n/a	0	0	3	97	n/a
Monomer	MFCO	0	0.0	n/a	100	0	0	0	0
Monomer	MFCO	1	1.0	100	0	100	0	0	0
Monomer	MFCO	2	1.7	87	6	15	79	0	0
Monomer	MFCO	3	2.7	89	0	0	35	62	3.1
Monomer	MFCO	4+	4.4	n/a	0	0	0	21	79
Dimer	MFCO	0	0.0	n/a	100	0	0	0	n/a
Dimer	MFCO	1	1.1	100	0	95	5	0	0
Dimer	MFCO	2	2.1	100	0	0	91	9	0
Dimer	MFCO	3+	4.4	n/a	0	0	0	100	n/a

Table 5.2. Quantitative summary of click products.

Surface Plasmon Resonance (Figure 5.3). G5-Ac-(COG-MTX)$_n$ (n = 0.9, 1.9, 2.9) samples all indicated only weak, reversible binding at all concentrations tested. D-Ac-(COG-MTX)$_n$ (n = 1.1, 2.0) samples were also dominated by reversible binding, however D-Ac-(COG-MTX)$_{6.0}$ had a fraction that did not completely dissociate on the timescale of this study. There was a corresponding, but smaller, amount of slow dissociating material in flow cell 2 for this material (See Figure D2). G5-Ac-(MFCO-MTX)$_n$ samples all had an undesired interaction with the surface in the control flow cell 2, rendering these samples unusable by this technique (Figure D3).

KB FAR+ Cytotoxicity. G5-Ac-(CO-MTX)$_n$ samples were not cytotoxic. All observed cytotoxicity in initial studies was attributed to 3-8% free MTX in the samples as determined by rp-UPLC (see Figure D4). G5-Ac-(MFCO-MTX)$_n$ samples had no cytotoxicity (Figure D5).

Discussion

PAMAM dendrimer is an extensively studied vector for the multivalent delivery of hydrophobic drugs.[2, 4, 28-30] Specifically, the conjugation of methotrexate to G5 PAMAM has been examined thoroughly for many years.[1, 30-32] Although early studies showed that this system has great promise for *in vivo* applications,[30] challenges in scalability and reproducibility of the results have prevented clinical advancements. In

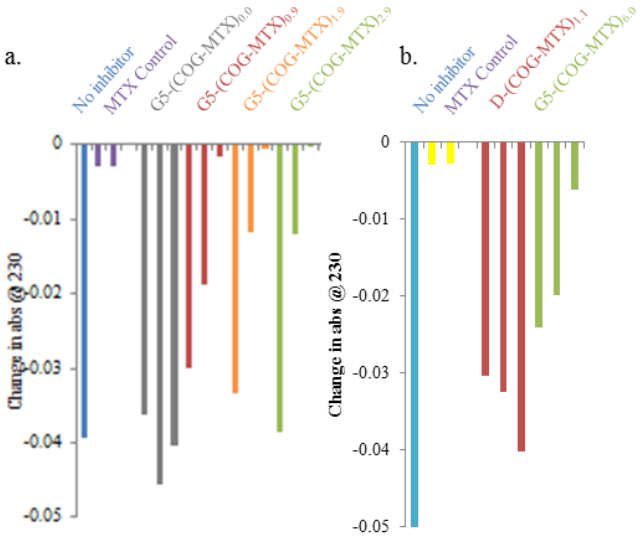

Figure 5.2. DHFR inhibition assay results for (a) G5-COG-MTX conjugates and (b) D-COG-MTX conjugates. Colors are consistent with Figure 1. All assays were performed at 3 concentrations for free MTX or conjugate (1 nM, 10 nM, and 100 nM) which are displayed from left to right respectively.

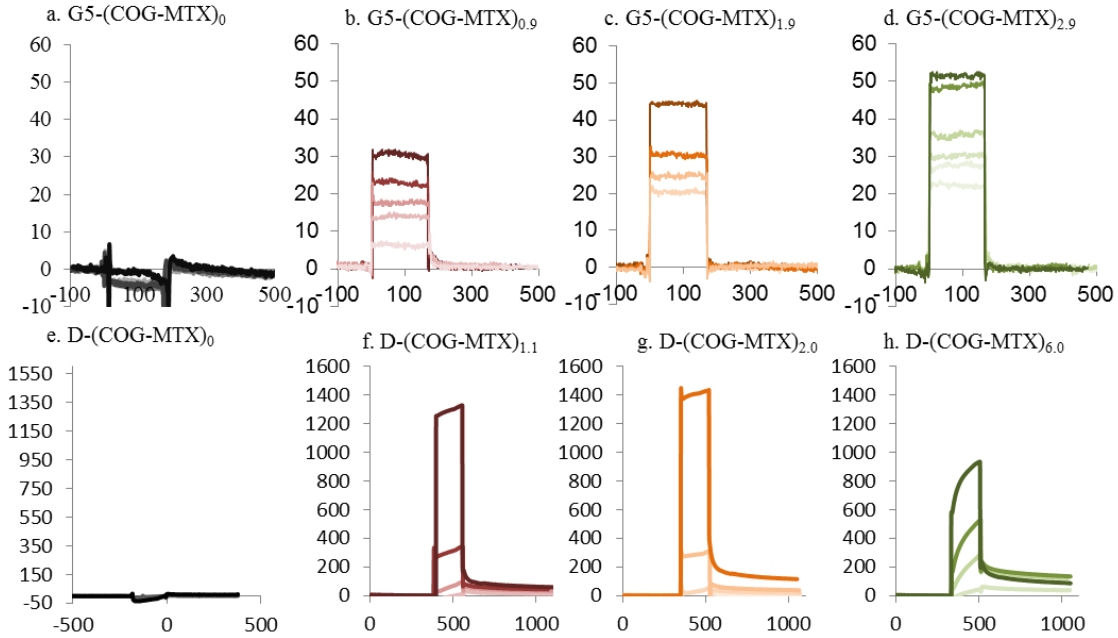

Figure 5.3. SPR results of all click products. Color gradients represent least concentrated (light) to most concentrated (dark) injections. (a) G5-Ac (b) G5-Ac-$(COG-MTX)_{0.9}$ (c) G5-Ac-$(COG-MTX)_{1.9}$ (d) G5-Ac-$(COG-MTX)_{2.9}$ (e) D-Ac (f) D-Ac-$(COG-MTX)_{1.1}$ (g) D-Ac-$(COG-MTX)_{2.0}$ (h) D-Ac-$(COG-MTX)_{6.0}$

addition, detailed scientific understanding of these systems has been hampered by the presence of trailing generations (G1-G4) and oligomers in the dendrimer employed for synthetic and biological studies. Recently developed methods of isolating PAMAM materials as a function of dendrimer size[25] and conjugate valency[10, 11, 27] have created a unique opportunity to analyze biological activity of multivalent conjugates and substantially improve valency control and characterization of multivalent conjugates. Here, we present the first comparison of PAMAM monomer and dimer conjugate by measuring binding characteristics (SPR and ITC) and biological activities (DHFR assay and cytotoxicity). These experiments probe the effect of vector size both as a design principle for its own sake and to attribute chemical/biological behaviors to both species, which are present in previous materials. In addition to valency, the influence of linker length/flexibility/hydrophobicity for the system has also been explored.

Previous studies have indicated that commercially available G5 PAMAM conjugated to the CO ligand then clicked to either 5 or 10 γ-azido-MTX demonstrated multivalency by SPR, cellular uptake, and cytotoxicity.[8] This material contained both monomer and dimer materials, convoluting the analyses of the SPR (a mass-sensitive technique). The samples studied were also stochastically conjugated, with the #MTX = 5 and #MTX = 10 containing approximately 15 and 22 ligand-to-particle combinations respectively. While this study showed an increase in binding avidity, uptake, and cytotoxicity when #MTX increased, the complicated mixture of vector size and ligand-to-particle ratios makes an exact mechanistic assignment difficult. The methods employed here allow for the de-convolution of both factors from vector size (i.e. increased molecular weight, increased reachable surface area do to a larger radius, and decreased solubility) and valency.

Briefly, G5 PAMAM dendrimer monomer (G5) and dimer (D) were isolated from commercially available material as outlined previously.[25] Stochastic conjugations to fluorinated (MFCO) and non-fluorinated (COG) ring strain promoted click chemistry ligands were performed via amide coupling for both vectors. The resulting materials contained averaged numbers of conjugated ligands, with ~14 different ligand-to-dendrimer ratios in each sample (ranging from 0 to 13 covalently attached ligands). These stochastic mixtures were then isolated by rp-HPLC following previously reported protocols.[27] The HPLC methods described here have proven versatile, being

successfully employed to isolate monomer and dimer PAMAM conjugates to 3 published ligands to date. The presumed mechanism allowing this isolation protocol is a favorable interaction between the conjugated, hydrophobic ligand and the reverse phase column. The MFCO ligand, which contains a longer carbon chain in addition to the fluorine on the cyclooctyne, has significantly higher resolution than the shorter COG ligand. This fact is visualized by comparing Figure 5.1a and c, where G5-Ac-$MFCO_{2.0(avg)}$ has baseline resolution between n = 0 and 1, and n = 1 and 2 samples (Figure 5.1 c) whereas G5-Ac-$COG_{4.7(avg)}$ has peak overlap for all peaks, even n = 0 and n = 1 (Figure 5.1 a). The difference between the x = 1 and x = 2 peak centers is 0.64 min for the G5-Ac-COG conjugates compared to 1.02 for the MFCO conjugates. The improved resolution likely results from the greater hydrophobicity of the longer chain resulting in greater interaction with the C18 stationary phase, leading to increased retention as a function of number of ligands. The increased resolution is repeated in the dimer conjugates; however the resolution of both dimer species is less than their corresponding monomer. As the time difference in peak centers for x = 1, 2 is nearly identical between the monomer and dimer for both ligands (0.59 and 1.04 for dimer conjugated to COG and MFCO, respectively), the reduced resolution is the result of the increased peak width of the dimer species (this broadening is the result of a broader distribution of branching defects[25]). Better HPLC resolution allows for the isolation of higher precise numbers, increased yield of all conjugates, and increased purity of resulting samples.

The conjugate samples, containing G5 monomer or dimer conjugated to precise numbers (x = 0 – 3) or high average (3+ or 4+) numbers of either ligand, were then "clicked" to γ-azido-MTX. Click efficiencies were approximately equal for monomer and dimer conjugates. As expected, the fluorinated MFCO ligand had higher click efficiencies under similar conditions to the non-fluorinated COG. While not all reactions went to 100% completion, the MFCO conjugates resulted in fewer conjugate species than the corresponding COG conjugates (Table 5.2). For example, the click reaction of monomer with 3 MFCO ligands went to 89% completion with 62% of the product containing 3 clicked MTX by UPLC. By way of contrast, the reaction employing 3 COG ligands had 63% click efficiency with only 13% of the product containing 3 conjugated MTX.

To test if the clicked dendrimer-MTX products retained the anti-folate activity of free

MTX, DHFR inhibition assays were performed. Both the monomer and dimer COG-MTX conjugates showed activity (Figure 5.2). As such, it can be concluded that conjugation of MTX to the dendrimer through the COG linker does not completely extinguish its inhibition activity against DHFR. A few additional important observations can be made. Firstly, both vector types required approximately 100 times the equivalent solution MTX concentration to reach similar inhibition levels as free MTX. Therefore, the inhibition activity of MTX is substantially reduced by conjugation through this linker. Secondly, for the monomer samples, there is no apparent relationship between the conjugate valency (n = 1 – 3) and inhibition ability within the detection limits of the experiment (Figure 5.4a). Figure 5.4b illustrates that total solution MTX concentration the inhibition capabilities of the conjugates, with full inhibition starting around 100 nM effective MTX concentration (compared to free MTX, which fully inhibited the assay at 1 nM). Inhibition assays for the MFCO conjugates are still ongoing (shortage of assay kit).

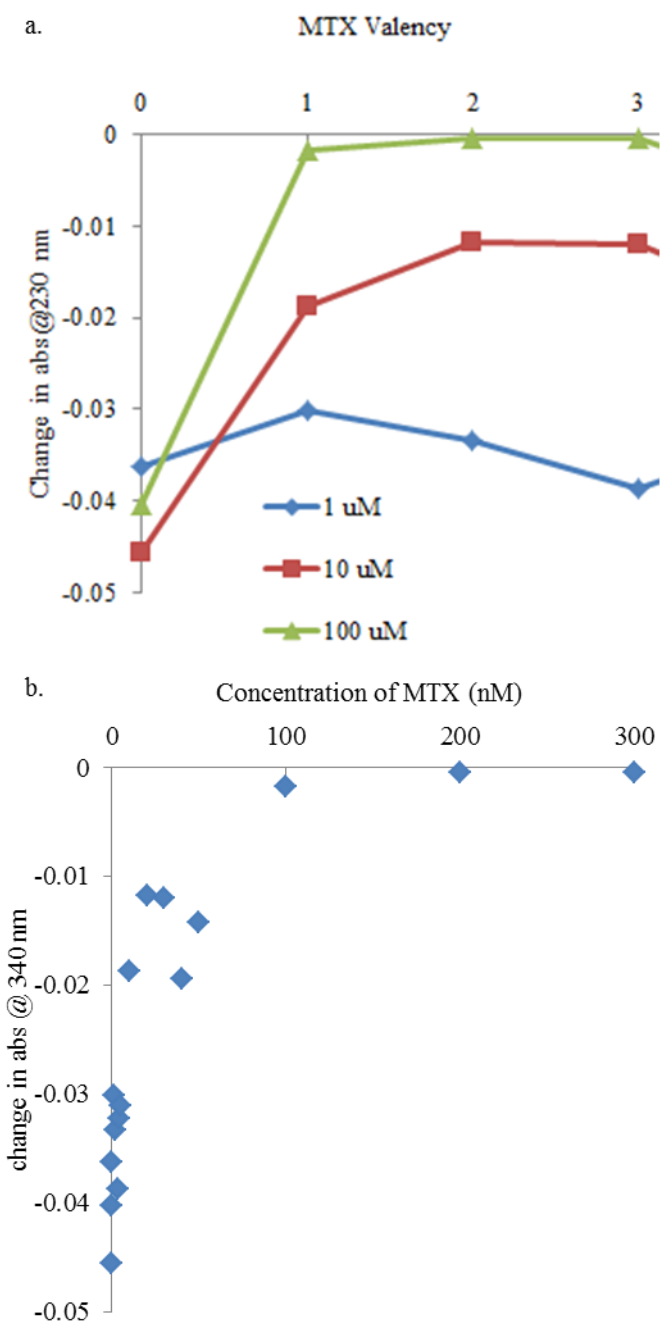

Figure 5.4. Inhibition assay results of G5-Ac-(COG-MTX)$_n$ compared by (a) valency and (b) relative MTX concentration.

The ability of the G5-MFCO-MTX conjugates to bind to FBP was measured using ITC. ITC measures the thermodynamics of binding between a ligand (i.e. free or conjugated MTX) and receptor (i.e. FBP) in solution. In a simplistic experiment, a favorable interaction between a ligand and receptor will give a net increase in heat, indication that the reaction is exothermic. This observation is the case for free MTX binding to FBP. For the case of the stochastically conjugated G5-Ac-$(MFCO\text{-}MTX)_{4.0(avg)}$, which has an average of 4.0 MTX but contains dendrimers clicked to 0 to ~13 MTX, the heat of binding was endothermic. This observation indicates that binding between the conjugate and protein can occur, but there is an energetic cost. By contrast, there was no observable binding between the isolated high average G5-Ac-$(MFCO\text{-}MTX)_{4.4}$ sample, which contains only dendrimer clicked to 3 or more MTX. On interpretation of these results would be that the flexibility and hydrophobicity of the MFCO linker cause it to fold into the interior regions of the G5 dendrimer, and consequently the enthalpic penalty to hydrate the ligand and allow for MTX/protein interaction is significantly higher which negatively impacts the enthalpy of binding. Because the lower average sample shows some interaction with the protein, it is possible that there is cooperativity within the MFCO linkers that further block the MTX from interacting with the protein in the higher average sample. An alternative explanation of this data would be that the rp-HPLC isolation protocols cause a fundamental change to the dendrimer (i.e. protonation of internal amines by trifluoroacetic acid in the HPLC eluent causing a conformational change in the three dimensional dendrimer structure) which blocks the protein interaction and/or decreases the time the clicked MTX is outside of the dendrimer interior. This theory would explain the difference between the "high averaged" conjugate (which displayed no binding) and the stochastic average G5-Ac-$(COG\text{-}MTX)_{avg\sim4}$ conjugate (which displayed endothermic binding).

SPR experiments allow for the extraction of kinetic information about the binding between a ligand (i.e. free or conjugated MTX) in solution flowing over a surface of immobilized receptors (i.e. FBP on a dextran surface). A second chip surface is employed as a control, which does not contain the protein, allowing for the subtraction of non-specific interactions of the conjugate and the surface. Both vectors and linker systems were evaluated by SPR. As indicated by Figure D3, both monomer and dimer samples

conjugated to MTX through the MFCO linker have a negative overall subtracted signal in injection/association phase which would indicate "negative" binding, an impossibility. Closer examination of the individual flow cell data reveals that while both flow cells have positive signal in the injection phase, the signal in the unmodified cell is higher than that in the FBP immobilized cell (FC1). This obsevation indicates that the conjugates have more interaction with the dextran surface that does not contain any FBP (FC2). Theoretically, this non-specific interaction should be equivalent in both flow cells. However, because the chip employed had a very high percentage of surface coverage with FBP, there is less dextran available in FC1 for nonspecific interaction. While this non-specific interaction prevents analysis of the MFCO linker data, it can be qualitatively observed that the dimer high average sample, D-Ac-$(MFCO\text{-}MTX)_{4.4}$ (Figure D3h), appears to have enough specific interaction with FBP on FC1 to overcome the contribution of the non-specific interaction and be observed in the association phase. The dissociation phase of this data also has a standard shape; however without a solid understanding of the non-specific interactions, quantitative fits of this data are not sound.

Both the monomer and dimer sample sets clicked to the MTX through the COG linker bound to the FBP with minimal nonspecific interaction with FC2. The control samples (fully acetylated monomer and dimer with no MTX) have similar binding to both chips, which when subtracted give relatively flat chromatograms (Figure 5.3a and e). In contrast, all three tested valencies for the monomer show both a dendrimer and total solution MTX concentration dependent binding with the FBP surface. Figure 5.5 reveals two interesting conclusions. Firstly, the monomer data shows enhanced binding during the association phase as valency increases (Figure 5.5a). However, this trend is readily explained by the increased total concentration of MTX as valency increases (Figure 5.5b). There is no multivalency effect for increasing the MTX valency on the G5 monomer. The dimer data shows a slightly different trend. Solution concentration of MTX does not explain the trend of binding in the association phase (Figure 5.5d) and dimer more a greater average number of MTX ligands actually show less surface binding for a given total concentration of MTX. However, there does appear to be a dependence on signal during association strictly on dendrimer concentration (Figure 5.5c). This observation suggests that what is primarily being observed during association is a

nonspecific mass effect. The interaction still must be "keyed" by conjugated MTX, as

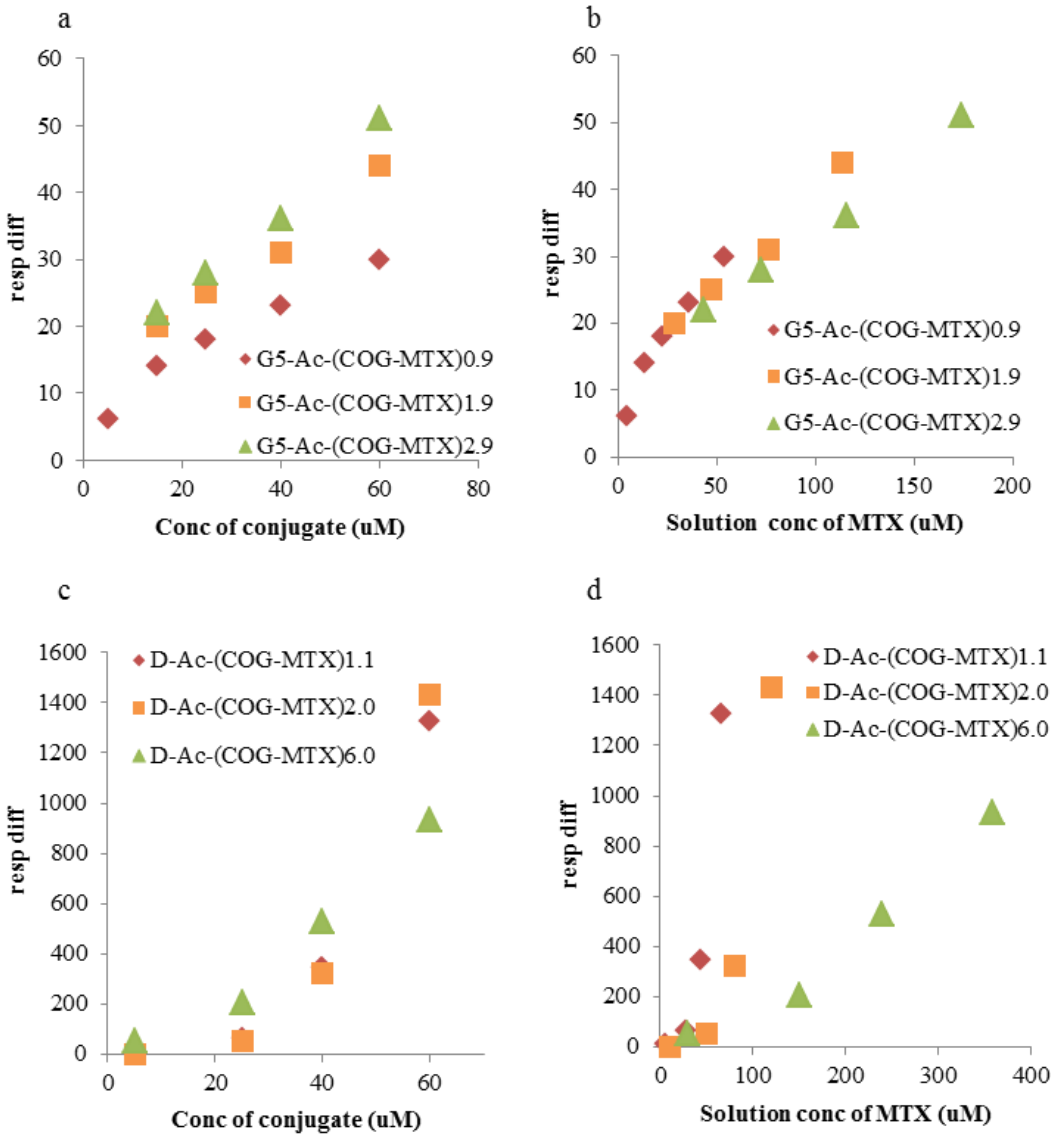

Figure 5.5. Saturation of SPR signal during the binding phase as a function of (a) conjugate concentration for monomer samples, (b) solution MTX concentration for monomer samples (c) conjugate concentration for dimer samples, and (d) solution MTX concentration for dimer samples.

there is negligible accumulation observed in the D-Ac sample (Figure 5.3e), however the non-specific van der Waals binding quickly dominates any MTX effects.

For all injections, the signal initially rises sharply at the beginning of the injection and quickly reaches equilibrium between association and dissociation. This behavior is indicative of a fast-on, fast-off relationship. At the end of the injection, all chromatograms quickly return to baseline, confirming the fast dissociation of all bound

species. This observation suggests that even the divalent (66%) and trivalent species (13%) in the G5-Ac-(COG-MTX)$_{2.9}$ experience only monovalent binding to the FBP surface.

By comparison, a recent similar study by van Dongen, Banaszak Holl et al.[18] observed greatly increased avidity via SPR for monomeric G5-Ac-(COG-FA)$_n$ (n = 0, 1, 1.2, 1.9, 2.7) conjugates, with a significant portion of bound material not dissociating over the timescale of the experiment. Because this observation held true for even a purely monovalent (folic acid-to-dendrimer ratio of 1) sample, it was concluded that the observation of increased avidity was due to the sum of weak van der Waals interactions between the dendrimer and protein surface. It was also determined that this interaction must be initiated by an interaction between a single conjugated FA and the FBP on the SPR chip surface. MTX, as a structurally modified competitive inhibitor of FA, may undergo a similar interaction with the FBP. However, although the experiments here were performed on surfaces with both higher protein densities and higher conjugate concentrations, a similar avidity increase was not observed at even the highest valency tested for the monomer(3). For the MTX case, there are indications of multivalency for the high averaged sample, however, when comparing the overall shape of the G5-FA and D-MTX sensograms (Figure 5.6) it becomes clear that there are some fundamental differences. For the G5-FA samples, nearly all materials that bound (to a chip density dependent saturation point) remained permanently attached to the surface. By contrast, a large percentage of the D-MTX material quickly dissociates after the conjugate flow has stopped.

The D-Ac-(COG-MTX)$_n$ conjugates show a dendrimer concentration, not MTX concentration, dependent association to the protein surface (Figure 5.5c). The absolute signal, when compared to that of the monomer/MTX conjugates, is approximately 10x higher in the dimer species at equivalent molar concentrations.

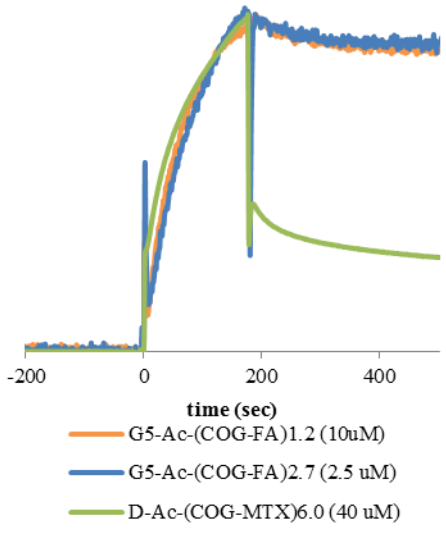

Figure 5.6. Comparison of the SPR sensograms of a D-Ac-(COG-MTX) sample to two different G5-Ac-(COG-FA) samples, with total signal normalized.

A 2 fold increase may be expected by this technique due to doubling in mass. This increase leads to a qualitative assumption that more binding occurs for equivalent total solution MTX concentrations in dimer samples than monomer samples. This five-fold increase over the "expected" signal in the association signal is likely the larger mass and radius of the dimer and its lower solubility[25] increasing the nonspecific interaction between the dendrimer/FBP. A chelate-type binding can be ruled out as the primary cause of exceptionally high signal in the association phase as it is seen in the monovalent D-Ac-$MTX_{1.1}$ sample. When examining the dissociation phase, the primarily monovalent (n = 1.1) and divalent (n = 2.0) dimer-MTX conjugates completely and quickly dissociate at the lowest three concentrations (5 µM, 25 µM, 40 µM), indicating a dominance of weak, monovalent binding for these species. However, the high average sample at all concentrations and divalent sample, at the highest concentrations of the mono and bivalent samples, are distinguished by dissociation phases that do not return to the original baseline over the time course of the SPR experiment. This behavior indicates a much stronger interaction between the conjugate and protein surface, indicating a separate mechanism of binding. There are several possible explanations for this observation. (1) As there is some nonselective binding at all concentrations for the high average sample in FC2, the permanently bound fraction may be due to reduced solubility due to the relatively high amount of conjugated MTX. However, this explanation does not adequately explain why there is significantly more permanent binding in the FC1, or why the total amount of permanent bound material is constant and not concentration dependent. Also, the 60 µM injections for mono and bivalent dimer do not have any permanent nonselective binding in FC2 but do not completely return to baseline in FC1. This observation suggests that while there is some nonselective interaction occurring in the high averaged sample, there is still significantly more interaction with the FBP immobilized surface. (2) Because the dimer vector is twice as large as the monomer vector, it can access roughly 4 times the surface area on the SPR chip. This additional surface accessibility may enable chelate-type binding (or multiple weak key interactions in the terms of Licata and Tkachenko)[17] of a single conjugate and multiple FBP receptors. This type of binding should be achievable for bivalent and higher conjugates but not the monovalent conjugate. Instead, the monovalent conjugate behaves identically

to the bivalent conjugate, with a small fraction of permanently bound material achieved at the highest concentration. (3) The solution MTX concentration in the high average sample and highest concentrations in the mono and bivalent samples is finally high enough to trigger a lock-and-key mechanism as observed in the folic acid system. The relative weakness of the MTX binding is overcome only when the vector is much larger (which decreases the solubility/entropy of the vector and increases the total van der Waals interactions) and the relative MTX concentration higher (which is achieved by the high averaged sample by high local concentrations at lower relative concentrations). In the related FA study, any material bound by the lock-and-key mechanism was permanently bound. In this case, a significant amount of the bound material still dissociates. Thus, the mechanism cannot be identical for MTX and FA. At this point, no single proposed mechanism is sufficient to explain all the MTX/dimer data. It is possible that the binding seen at the highest concentrations (60 μM) of all dimer valencies is the beginning of a MTX-keyed nonspecific interaction, and that the binding at lower concentrations of the high valency system is due to multiple MTX/FBP interactions for a single conjugate. Further work would need to be done to test this theory, including testing higher concentrations of the mono and bivalent systems, and lowering the FBP density to eliminate the possibility of multiple interactions in the high valent system.

Previous SPR studies on dendrimer-COG-MTX conjugates containing mixtures of dimer and monomer indicated both monovalent and multivalent binding occurred for stochastic valencies of n = 5 and n = 10.[8] The present work indicates that the mechanism for the multivalent portion of this binding is the presence of dimers conjugated to 3 or more MTX. Considering that the original dendrimer material contained ~14% dimer[25] and assuming a Poisson distribution, the "multivalent" portion of the n = 5 and 10 samples would be 13% and 14%, respectively. It is possible, therefore, that observed permanent binding portion in the previous work is contributed exclusively by high valency dimer materials. This work does not examine monomers conjugated to 4 or more MTX, so the potential activity of those conjugates cannot be commented on.

Free MTX is cytotoxic to KB FAR+ cells (Figure D5). Previous work[8] has indicated that MTX bound to a commercial G5 dendrimer (containing monomer and dimer impurities) through the CO linker discussed here is also cytotoxic. However, the present

work indicates that both vector-MTX conjugates are non-toxic to KB FAR+ when bound through the longer, MFCO linker. This observation further confirms, in addition to the ITC and SPR results, that this linker is not ideal for this specific system, although it gives higher yields in both HPLC isolation and click reaction protocols. Monomer-CO-MTX conjugates initially showed similar cytotoxicity profiles as previous results (data not shown), however this toxicity was later attributed to a small amount (<5%) of unbound MTX remaining in the sample (See Figure D2). Studies to determine if the dimer sample is cytotoxic are still ongoing.

Conclusions

New chromatographic methods have enabled the examination of vector molecular weight effects (monomer vs. dimer), linker system effects (COG vs. MFCO), and valency effects on the highly studied drug delivery system of PAMAM dendrimer conjugated to methotrexate. The combined experimental data from DHFR inhibition, ITC, SPR, and *in vitro* experiments allow for several major conclusions to be drawn. Firstly, the presence of G5 PAMAM dimers, which contribute to 14% or more of a commercial dendrimer sample, contribute significantly to observed activities. They are often overlooked in data interpretation, but in mass sensitive techniques such as SPR they actually contribute larger signal per particle. They also can reach a larger surface area due to their larger size, which can potentially create new activity mechanisms. In this system, dimer appears to be responsible for signal previously attributed to pure valency effects via SPR. When comparing this data to the mechanism of increased avidity for similar PAMAM-folic acid conjugate, it was determined that the MTX/FBP interaction is not strong enough to "key" the nonspecific interaction between the polymer and protein until the solution MTX concentration is significantly higher, or the dendrimer scaffold is much larger. Further, the observed binding is not nearly as strong for MTX as for FA, further distancing the two mechanisms. Alternatively, the possibility of a multiple MTX-FBP bridges for the high valency dimer cannot be eliminated as it was for the FA system. This idea was first described by Licata and Tkachenko,[17] who proposed that weakening the FA bond may slow the formation of the nonspecific interactions between dendrimer and protein to allow the formation of bridges, and MTX is essentially a weaker-binding derivative of

FA.

Secondly; some specific observations for the influence of linkers can be made. Linkers can affect both chemical and biological activity. Here, a more hydrophobic linker with fluorine modification (MFCO) had more favorable chemical behavior leading to higher product yields compared to the original linker (COG). However, this system proved to be inactive biologically by three separate techniques. The flexibility of the PAMAM vector may limit the importance of the decreased rigidity of this linker and contribute to unfavorable thermodynamic costs for binding (i.e. interaction of the hydrophobic linker with the aqueous environment). Careful examination of linker effects must be undertaken specific to the desired application. Finally, conjugate valency has been examined. Here, solution based techniques (inhibition assay) showed little dependence on valency outside of effective concentration. However, in a surface based application (SPR), higher valency created a new binding mechanism through the chelate effect. Careful consideration of vector size and purity, linker chemistry, and conjugate valency are critical for creating biologically successful polymeric drug delivery systems.

References

1. Quintana, A., et al., *Design and Function of a Dendrimer-Based Therapeutic Nanodevice Targeted to Tumor Cells Through the Folate Receptor.* Pharmaceutical Research, 2002. **19**(9): p. 1310-1316.
2. Goonewardena, S.N., et al., *Design considerations for PAMAM dendrimer therapeutics.* Bioorganic & Medicinal Chemistry Letters, 2013. **23**(10): p. 2872-2875.
3. Thomas, T.P., et al., *Folate-targeted nanoparticles show efficacy in the treatment of inflammatory arthritis.* Arthritis & Rheumatism, 2011. **63**(9): p. 2671-2680.
4. Ward, B.B., et al., *Targeted Dendrimer Chemotherapy in an Animal Model for Head and Neck Squamous Cell Carcinoma.* Journal of Oral and Maxillofacial Surgery, 2011. **69**(9): p. 2452-2459.
5. Mullen, D.G., et al., *Best Practices for Purification and Characterization of PAMAM Dendrimer.* Macromolecules, 2012. **45**(12): p. 5316-5320.
6. Zong, H., et al., *Bifunctional PAMAM Dendrimer Conjugates of Folic Acid and Methotrexate with Defined Ratio.* Biomacromolecules, 2012. **13**(4): p. 982-991.
7. Huang, B., et al., *Copper-free click conjugation of methotrexate to a PAMAM dendrimer platfrom.* Tetrahedron Letters, 2011. **52**: p. 1411-1414.
8. Silpe, J.E., et al., *Avidity Modulation of Folate-Targeted Multivalent Dendrimers for Evaluating Biophysical Models of Cancer Targeting Nanoparticles.* ACS Chemical Biology, 2013. **8**: p. 2063-2071.

9. Martinez-Veracoechea, F.J. and D. Frenkel, *Designing super selectivity in multivalent nano-particle binding.* Proceedings of the National Academy of Sciences, 2011. **108**(27): p. 10963-10968.
10. Mullen, D.G. and M.M. Banaszak Holl, *Heterogeneous Ligand–Nanoparticle Distributions: A Major Obstacle to Scientific Understanding and Commercial Translation.* Accounts of Chemical Research, 2011. **44**(11): p. 1135-1145.
11. Mullen, D.G., et al., *A Quantitative Assessment of Nanoparticle-Ligand Distributions: Implications for Targeted Drug and Imaging Delivery in Dendrimer Conjugates.* ACS Nano, 2010. **4**: p. 657-670.
12. Waddell, J.N., et al., *Origin of broad polydispersion in functionalized dendrimers and its effects on cancer-cell binding affinity.* Physical Review E, 2010. **82**: p. 036108.
13. Hong, S., et al., *The Binding Avidity of a Nanoparticle-Based Multivalent Targeted Drug Delivery Platform.* Chemistry & Biology, 2007. **14**(1): p. 107-115.
14. Krishnamurthy, V.M., L.A. Estroff, and G.M. Whitesides, *Multivalency in Ligand Design*, in *Fragment-based Approaches in Drug Discovery*. 2006, Wiley-VCH Verlag GmbH & Co. KGaA. p. 11-53.
15. Wolfenden, M.L. and M.J. Cloninger, *Multivalency in Carbohydrate Binding*, in *Carbohydrate Recognition*. 2011, John Wiley & Sons, Inc. p. 349-370.
16. Kiessling, L.L., L.E. Strong, and J.E. Gestwicki, *Chapter 29. Principles for multivalent ligand design*, in *Annual Reports in Medicinal Chemistry*. 2000, Academic Press. p. 321-330.
17. Licata, N.A. and A.V. Tkachenko, *Kinetic Limitations of Cooperativity-Based Drug Delivery Systems.* Physical Review Letters, 2008. **100**: p. 158102.
18. van Dongen, M.A., et al., *Evaluation of Avidity of Dendrimer-Folic Acid Conjugates with Controlled Valency via Surface Plasmon Resonance.* In preparation.
19. Christensen, J.B. and D.A. Tomalia, *Designing Dendrimers*, in *Dendrimers as Quantized Nano-modules in the Nanotechnology Field*, S. Campagna, P. Ceroni, and F. Puntoriero, Editors. 2012, J. Wiley & Sons: Hoboken. p. 1-33.
20. Tomalia, D.A., J.B. Christensen, and U. Boas, *The Dendritic State*, in *Dendrimers, Dendrons and Dendritic Polymers: Discovery, Applications, the Future*

2012, Cambridge University Press

NY. p. 30.
21. Tomalia, D.A., et al., *Structure control within poly(amidoamine) dendrimers: size, shape and regio-chemical mimicry of globular proteins.* Tetrahedron 2003. **59**: p. 379-3813.
22. Betley, T.A., et al., *Tapping Mode Atomic Force Microscopy Investigation of Poly(amidoamine) Dendrimers: Effects of Substrate and pH on Dendrimer Deformation.* Langmuir, 2001. **17**: p. 2768-2773.
23. Mecke, A., et al., *Deformability of poly(amidoamine) dendrimers.* The European Physical Journal E, 2004. **14**(1): p. 7-16.
24. Mecke, A., et al., *Direct observation of lipid bilayer disruption of poly(amidoamine) dendrimers.* Chemistry and Physics of Lipids, 2004. **132**: p. 3-14.
25. van Dongen, M.A., et al., *Quantitative analysis of generation and branch defects in G5 poly(amidoamine) dendrimer.* Polymer, 2013. **54**: p. 4126-4133.
26. Mullen, D.G., et al., *Isolation and Characterization of Dendrimers with Precise Numbers of Functional Groups.* Chemistry – A European Journal, 2010. **16**(35): p. 10675-10678.

27. van Dongen, M., S.m.u.e. Vaidyanathan, and M.M. Banaszak Holl, *PAMAM Dendrimers as Quantized Building Blocks for Novel Nanostructures.* Soft Matter, 2013.
28. Esfand, R. and D.A. Tomalia, *Poly(amidoamine) (PAMAM) dendrimers: from biomimicry to drug delivery and biomedical applications.* Drug Discovery Today, 2001. **6**(8): p. 427-436.
29. Shukla, R., et al., *Tumor angiogenic vasculature targeting with PAMAM dendrimer–RGD conjugates.* Chemical Communications, 2005(46): p. 5739.
30. Kukowska-Latallo, J.F., et al., *Nanoparticle Targeting of Anticancer Drug Improves Therapeutic Response in Animal Model of Human Epithelial Cancer.* Cancer Research, 2005. **65**(12): p. 5317-5324.
31. Majoros, I.J., et al., *PAMAM Dendrimer-Based Multifunctional Conjugate for Cancer Therapy: Synthesis, Characterization, and Functionality.* Biomacromolecules, 2006. **7**(2): p. 572-579.
32. Li, M.-H., et al., *Dendrimer-based multivalent methotrexates as dual acting nanoconjugates for cancer cell targeting.* European Journal of Medicinal Chemistry, 2012. **47**(0): p. 560-572.

Chapter 6

Conclusions and Future Directions

This dissertation examines the impacts of polymer scaffold and conjugation chemistry heterogeneity on the design, synthesis, characterization, and application of multivalent polymer conjugates for drug delivery. Several platform design factors were systematically studied, including vector size and homogeneity, valency, and linker chemistry. Methods to isolate precise ligand-to-vector ratios were expanded to include new linker ligand, to generate novel nanostructures, and synthesize well defined dendrimer-drug conjugates for mechanistic study. The ability to produce polymer conjugates of low mass dispersity and high ligand-to-scaffold ratio purities makes this system an ideal candidate for both mechanistic studies and as a future clinical candidate.

One of the first design principles that must be considered in developing a multivalent drug delivery platform with any hope for FDA approval and clinical application is the ability to reproduce the material at large scales without loss of activity. To accomplish this goal, the scaffold to which drugs, targeting entities, or imaging agents are conjugated must be carefully selected. The dendrimer architecture has potential due to its low polydispersity/narrow mass range compared to branched or linear polymers. However, the work in Chapter 2 shows that the polydispersity of PAMAM dendrimer is often overlooked. Importantly, the conclusions of Chapter 5 suggest that oligomer defects, which compose ~30% of the commercial material, can have an impact on both characterization and observed activity of conjugates containing the oligomeric mixtures. Chapter 2 introduces methodology to isolate the monomeric scaffold of interest, reducing the mass range by several orders of magnitude. This advancement allows for subsequent synthesis of multivalent conjugates that employ dendrimer scaffolds with very narrow size ranges, allowing the decoupling of mass effects (i.e. solubility, biodistribution, surface area, etc.) from multivalent effects. Consequently, the studies in Chapter 5 comparing the activities of multivalent monomer-MTX and dimer-MTX conjugates conclude that the increased mass and surface area of dimer present in commercial

dendrimer significantly impacts the observed binding of the subsequent conjugate. Further *in vitro* and eventually *in vivo* work is necessary to provide insight to larger impacts of high weight materials in present and future dendrimer conjugates. Alternatively, the megamers introduced in Chapter 3 may provide a synthetic strategy to achieve vectors of the desired size (i.e. synthetic dimers instead of isolated dimer fractions) whilst retaining the properties, such as solubility and ease of synthesis, of the lower generation. Continued investigation of these synthetic megamers may provide a route to modular, bifunctional nanostructures with precise valency. Such advancements would require synthesis and isolation of precise ratio ligand-to-dendrimer conjugates with primary amine surfaces remaining for functionality. This work is currently ongoing in the Banaszak Holl group.

As highlighted in Chapter 1, the presence of a distribution of ligand-to-vector ratios can also impede the advancement of a drug delivery platform. These distributions are difficult to characterize by commonly employed techniques, therefore they can go unnoticed. However, different distributions in ligand-to-vector ratios lead to the presence of significantly different populations in samples that appear identical by many characterization techniques. Problems with sample reproducibility is likely to become more prevalent as a platform is scaled from the research laboratory to the clinic, as mass transport and controlling reaction conditions becomes more challenging. The isolation of conjugates with precise click ligand-to-dendrimer ratios, first introduced by Mullen, Banaszak Holl et al. and further developed in the work featured in Chapters 3-5 of this dissertation, provides one synthetic strategy to overcome such challenges. While the synthesis of precise ratios of biologically active entities, such as folic acid or methotrexate, has not yet been successful, the narrow and well-defined distributions resulting from the reaction of precise conjugates to modified drugs is a major step forward. One of the most significant advances in the work presented here, however, is the synthesis of dendrimer-drug conjugates with valencies of precisely one drug per dendrimer. This accomplishment has allowed us to distinguish between mechanisms of binding due to polymer interactions and multivalent drug interactions. For both cases examined here, it has been determined that increased avidity (as measured by SPR) of multivalent dendrimer conjugates, which has been previously attributed to a multivalent

FA or MTX binding effect, are due to a keyed summation of weak van der Waals forces between the dendrimer scaffold and protein surface. While the interaction between the polymer and protein itself is nonspecific, the relatively stronger and specific initial interaction between the conjugated FA or MTX and surface-immobilized protein is necessary to initiate the observed binding. This fact is further emphasized because dendrimers with no folic acid do not have significant binding to the FBP. FA is a "strong key" for this system, and is able to initiate high avidity binding for a monovalent dendrimer conjugate at the lowest concentrations studied in Chapter 4. It is clear that the mechanism of free folic acid binding to the FBP is different, as this interaction quickly and completely dissociates even at much higher solution concentrations. These results have allowed for direct experimental evidence favoring a FA-keyed mechanism that was one of three proposed mechanisms in the literature to explain the observation of high avidity in folic acid-dendrimer systems. Thirty-six experimental measurements at various valencies and concentrations have also allowed for the development of a kinetic model for this system which involves two binding populations; a dissociating population and a permanently bound population. The SPR studies with methotrexate provide a "weak key" analogue to this study. The much weaker interaction between methotrexate and the FBP was shown to not be able to initiate this strong binding mechanism until much higher relative concentrations. The lock-and-key mechanism, which has not received much attention in the literature, has proven to be consistent with the results of these two cases. It therefore should be considered for possibly playing a role in other polymer conjugates. Further exploration of monovalent dendrimer conjugates must therefore be done. For example, multivalent dendrimer-vancomycin conjugates have shown significantly enhanced binding to surfaces that mimic both vancomycin susceptible cell surfaces ("strong key") and vancomycin resistant cell surfaces ("weak key"). A monovalent conjugate is necessary to determine whether this binding is due to multivalent binding of the conjugate to the surfaces or a vancomycin keyed interaction of the dendrimer with the surface. The work presented in Chapters 4 and 5 demonstrate the importance of obtaining non-stochastic average conjugates for the determination of active populations in multivalent systems. Methodology of obtaining and applying such samples has been successfully demonstrated. Further studies of current and future multivalent systems will

add to the greater understanding, development, and improvement of polymer-based drug delivery systems.

Linker chemistry between a vector and drug can have a beneficial impact on the activity of the system, providing flexibility and longer range to allow for multivalent interaction with a surface immobilized target. However, there can also be thermodynamic penalties associated with longer linkers. These tradeoffs have been the subject of many theoretical and experimental studies to date with no encompassing conclusions. Hence, it is important to consider the needs of the specific scaffold and target in question when designing a multivalent conjugate. For example, a rigid scaffold (such as a "hard" nanoparticle) may need a more flexible linker to provide the conjugated drug the necessary sampling space for binding to a target. An inherently flexible scaffold (like a PAMAM dendrimer) may not need this additional added flexibility to achieve binding. In the system examined in this dissertation, the linker chemistry has another important role: providing the mechanism by which precise ligand-to-dendrimer conjugates can be isolated. Hydrophobic interactions between the linker and stationary phase via HPLC causes an increased retention time as a function of valency. One of the strengths of this system is it's robustness, with eight ligands successfully employed in separations to date (the two ring-strain promoted click ligands and azide ligand described in Chapters 3-5, plus the alkyne ligand in previous literature work, two hydrophobic dyes, and two additional click ligands (alkene and thiol) which have not yet been published in peer-reviewed literature). This versatility provides a good platform for further modification bioactive molecules. Further functionalities should continue to be tested, such as primary amine terminated ligands for peptide coupling, and charged ligands for studies of controlled numbers of charges on a nanoparticle surface for cell membrane interaction. More hydrophobic linkers have a greater interaction with the reverse-phase column employed here, therefore longer carbon chains and ring structures provide better peak separation. This property provides a handle by which the yields and purities of isolations may be manipulated. For example, the mono-fluorinated cyclooctyne structure used in Chapters 3 and 6 provides the best peak resolution of any system studied to date, possibly due to the 5 methylene chain compared to 1 methylene of the shorter cyclooctyne ligand. Another benefit of this particular ligand is that fluorine modification significantly

improves the subsequent click reaction efficiencies. As such, this ligand seemed the most promising for drug delivery applications. However, subsequent testing revealed that the conjugates utilizing this linker are inactive. It may be that the very property that improves the conjugate's HPLC resolution (hydrophobicity) causes its inactivity. Hydration of the longer carbon chain may be so thermodynamically unfavorable that the ligand, and consequently clicked drug, spends most of the time folded into the interior space of the dendrimer, which in return means the clicked entity (MTX) is less available for interaction with solution and surface targets (FBP on a SPR chip surface). Therefore, future studies should target ring-strain ligands that contain the fluorine modification but with a shorter methylene chain. This work as a whole demonstrates the necessity of carefully selecting the proper linking chemistry for the particular system in question.

This dissertation has highlighted some of the remaining challenges in creating successful multivalent conjugates for biomedical applications. In particular, PAMAM dendrimers were discussed as a potential scaffold due to their favorable chemical and biological properties, and methodology to produces gram-scale quantities of low mass range G5 dendrimers has been introduced. The low mass range and hydrophilic nature of dendrimers has also allowed for the development of dendrimer conjugates with precise ligand-to-dendrimer ratios, allowing for the generation of drug-functionalized conjugates with well-defined valency. This accomplishment allows for the determination of active populations (i.e. stronger binding) within a stochastic mixture. Future directions for this system should focus on developing linker chemistries with optimized properties for isolation and click reaction. Further mechanistic and biological testing of drug conjugates should also occur, including the FA and MTX systems studied here additionally conjugated to precise numbers of dye and other systems such as the vancomycin conjugates previously mentioned. Additionally, future studies employing lower generations of dendrimer (for example, G3 with a molecular mass approximately one quarter of the G5 monomer) with the "strong key" folic acid would allow for a quantitative assessment of the contributions of polymer mass to the nonspecific interactions allowing for increased avidity in the FA/FBP system.

Appendix A

Supplementary Information for Chapter 2

Size Exclusion Chromatography. Size exclusion experiments were performed by gel permeation chromatography on an Alliance Waters 2695 separation module equipped with a 2487 dual wavelength UV absorbance detector (Waters Corporation), a Wyatt HELEOS Multi Angle Laser Light Scattering (MALLS) detector, and an Optilab rEX differential refractometer. Columns employed were TosoHaas TSK-Gel Guard PHW 06762 (75 mm × 7.5 mm, 12 mm), G 2000 PW 05761 (300 mm × 7.5 mm, 10 mm), G 3000 PW 05762 (300 mm × 7.5 mm, 10 mm), and G 4000 PW (300 mm × 7.5 mm, 17 mm). Column temperature was maintained at 25 ± 0.1 °C with a Waters temperature control module. The isocratic mobile phase was 0.1 M citric acid and 0.025 wt % sodium azide, pH 2.74, at a flow rate of 1 mL/min. The sample concentration was 10 mg/5 mL with an injection volume of 100 µL. This was used to calculate the weight average molecular weight, M_w, and the number average molecular weight, M_n, with Astra 5.3.2 software.

Potentiometric Titration. Potentiometric titration was carried out using a Mettler Toledo DL55 Titrator equipped with a Mettler Toledo DG-111-SC pH probe and custom software. A known mass of sample was dissolved in 20 mL of 0.1 M NaCl solution and the pH was adjusted to 2-2.5 with 0.1 M HCl. The solution was then autotitrated with volumetric standardized 0.1 M NaOH with 0.02 mL injections until pH 12 was reached. The results were analyzed using GPC M_n to give the average number of primary amines per dendrimer in a sample.

Determination of Extinction Coefficients. Solutions were diluted in DI water to 0.1-0.25 mg/mL. Measurements were taken on a Shimazdzu UV-1601. Each measurement

was done in triplicate representing a separate isolation batch to determine standard deviation.

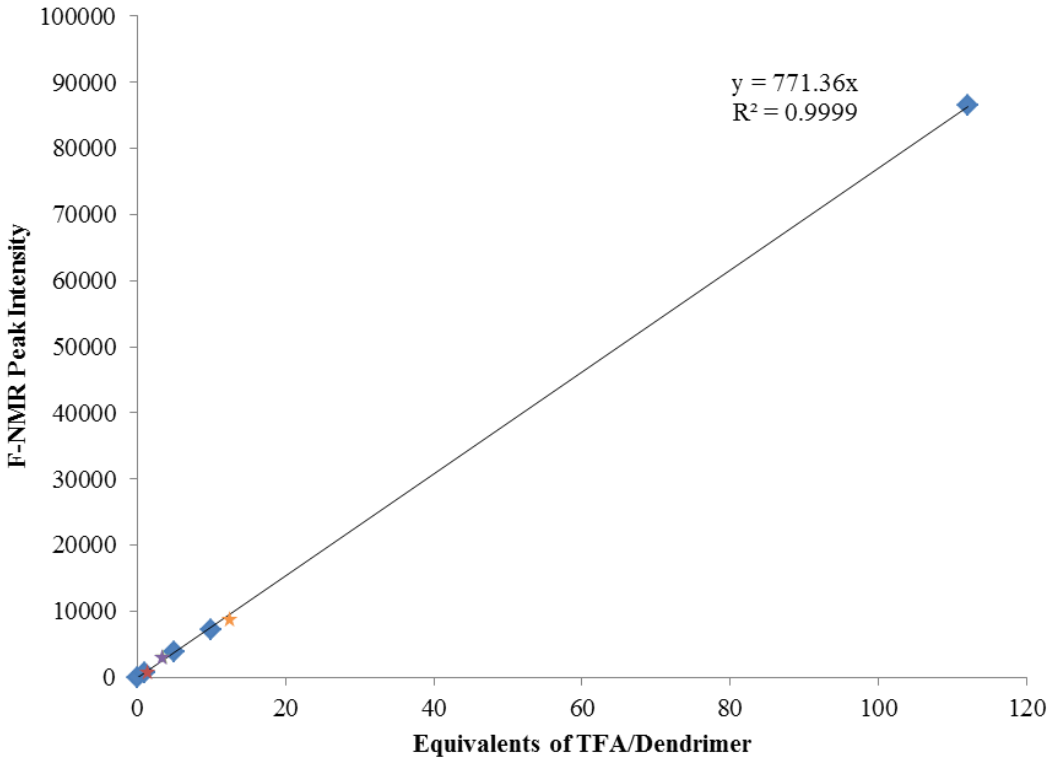

Figure A1. Known amounts of TFA spiked into dendrimer samples (blue diamonds) have a linear relationship with ^{19}F NMR peak intensity. Effective TFA removal depends on the G5 mass. loading of the PD-10 columns, as seen by colored stars: 5 mg (red), 10 mg (green), 40 mg (purple), and 100 mg (orange).

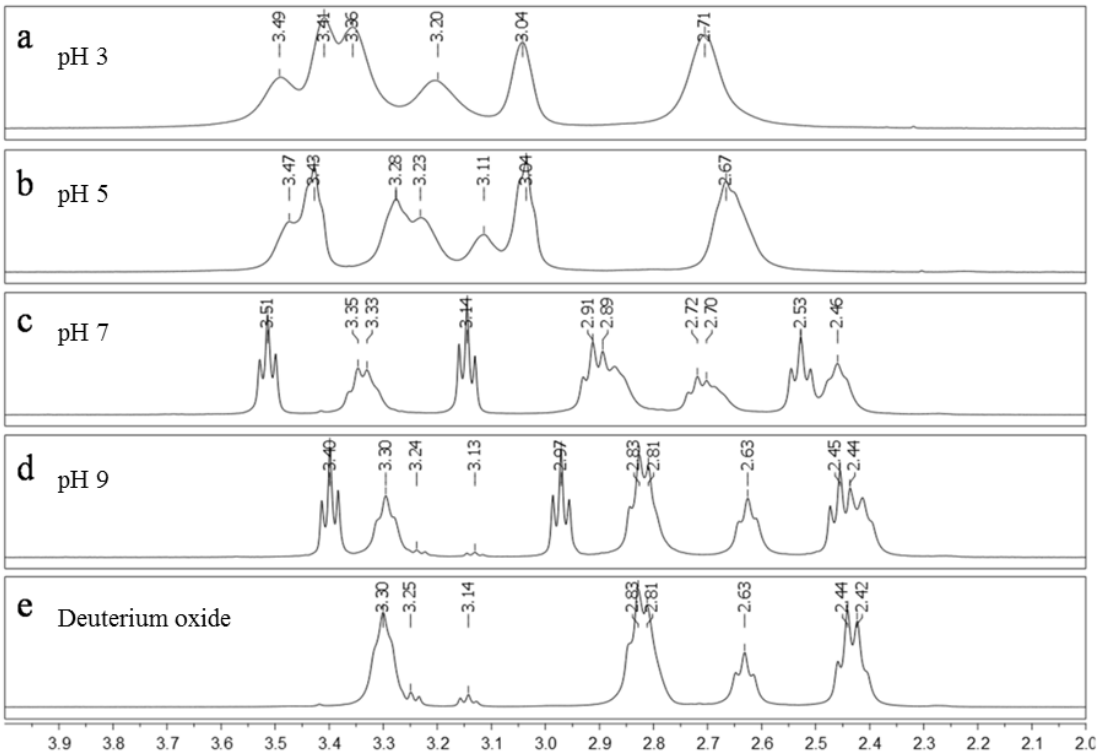

Figure A2. Change in NMR spectra of as-received G5 PAMAM as a function pH.

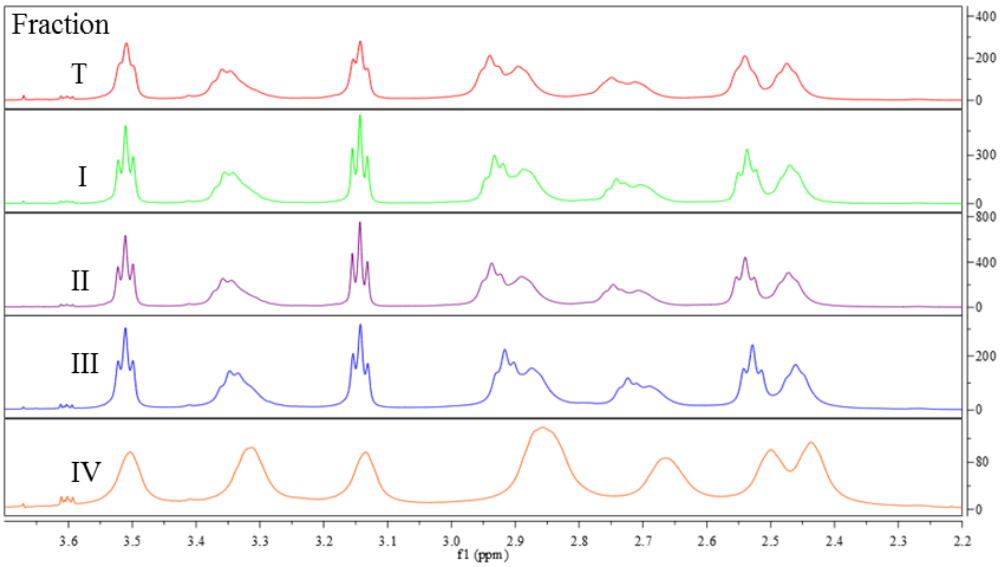

Figure A3. ^{1}H NMR spectra of fractions T and I-IV.

Sample	MALDI-TOF-MS peaks	GPC M_n	GPC M_w	GPC PDI
As received G5	13,700	28,270	30,820	1.090
	26,400			
	52,400			
	79,100			
T (Trailing Generations) Fractions 23-30	7,100	19,980	21680	1.085
	14,500			
	27,400			
I (Monomer) Fractions 38-52	14,000	27,100	27,160	1.019
	28,500			
	58,100			
II (Dimer) Fractions 59-63	27,600	51,740	53,380	1.032
	53,800			
III (Trimer) Fractions 69-71	29,000			
	42,000	72,160	75,860	1.051
	58,500			
	84,200			
IV (Tetramer) Fractions 75-78	28,800	88,710	101,100	1.151
	43,700			
	56,700			
	84,500			
	110,100			

Table A1. Summary of mass analyses on fractions T and I-IV.

ppm	T	I	II	III	IV**
3.5	88	153	278	317	264
3.3	108	177	331	405	404
3.1	93	152	218	321	293
2.9	182	312	578	711	691
2.7	101	171	316	331	369
2.5	185	314	570	694	638

Table A2. Integration values for ^{1}H NMR of fractions T and I-IV relative to an internal dioxane spike. *Fraction IV had low solubility in experimental conditions.

Fraction	MALDI-TOF-MS Peak Max (Da)	GPC Mn	Mw	PDI
As-received G5	26,400	28,270	30,820	1.090
i (F38)	21,000	21,060	21,200	1.007
ii (F42)	27,200	25,940	26,210	1.024
iii (F47)	29,600	28,560	28,860	1.010
iv (F52)	29,800	31,160	31,500	1.045

Table A3. Summary of mass analysis of fractions i-iv.

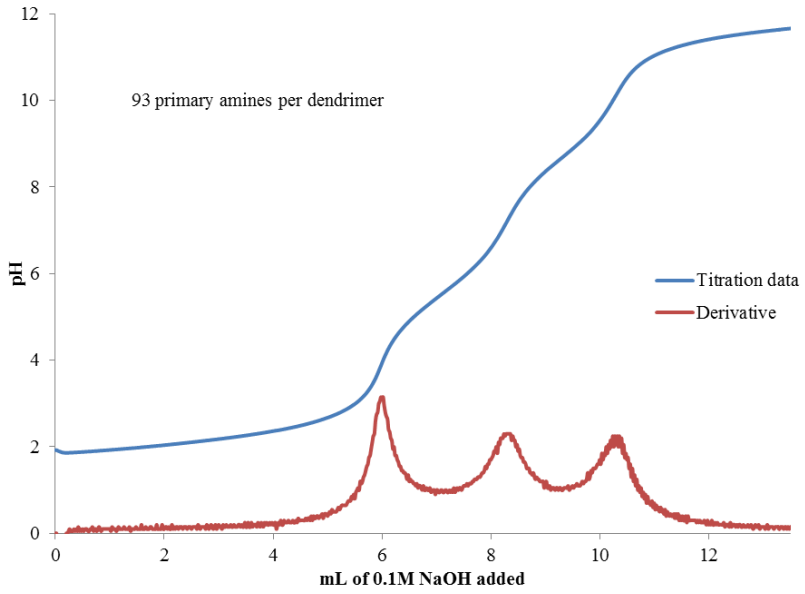

Figure A4. Titration of 57.8 mg of fraction I.

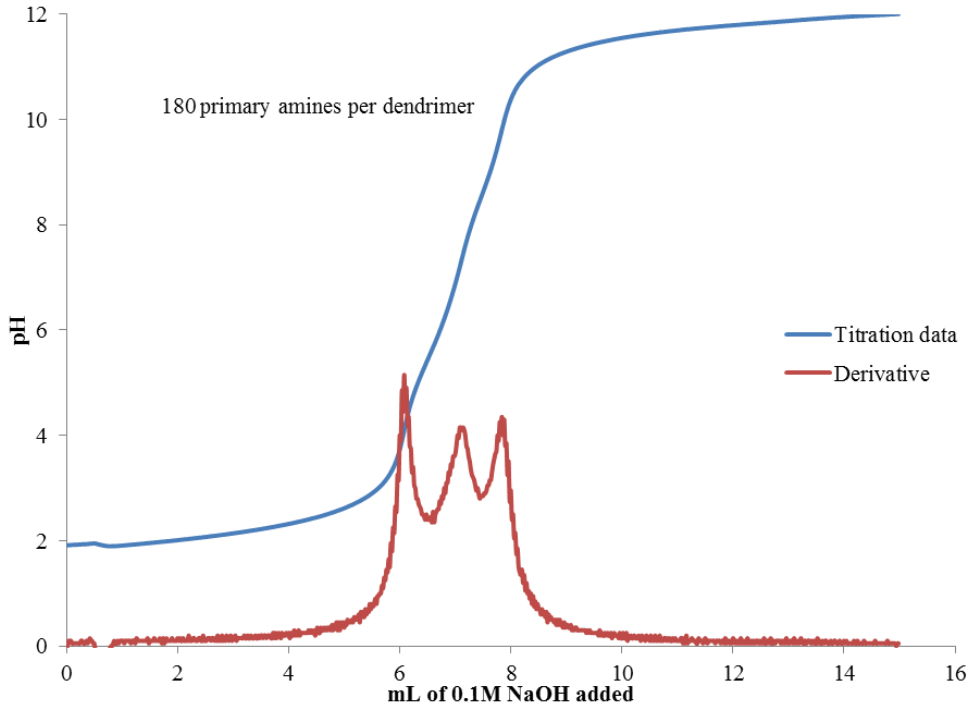

Figure A5. Titration of 21.7mg of fraction II.

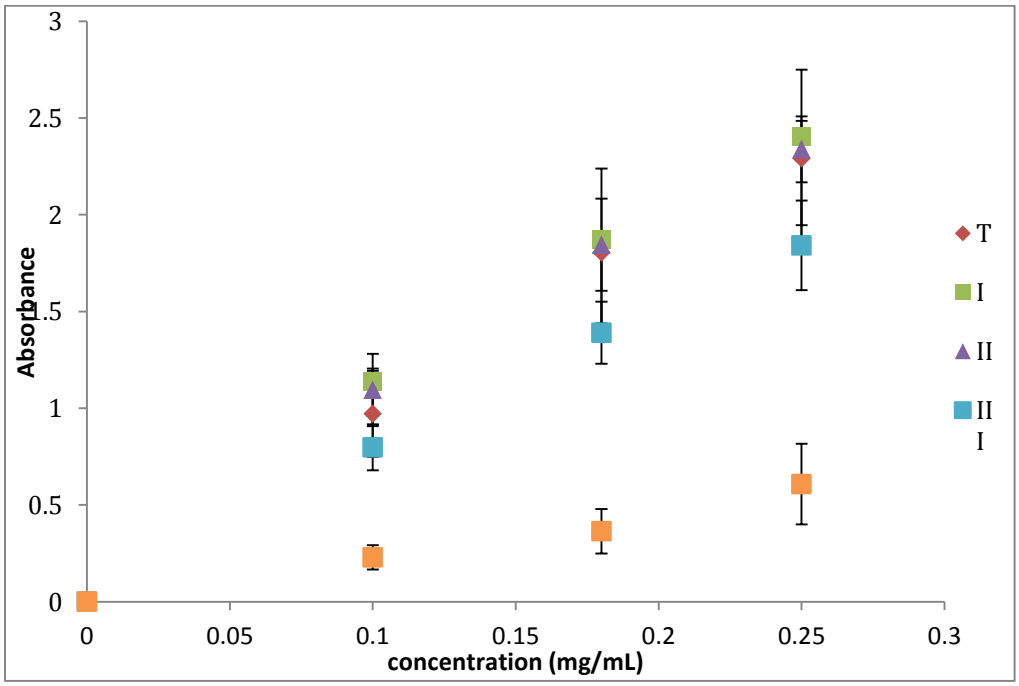

Figure A6. Calibration curves used to determine extinction coefficients of fractions T and I-IV at 210 nm.

Sample	Extinction Coefficient [(mg/mL)$^{-1}$]	Extinction Coefficient [M^{-1}]
T	9.5(+/-2.0)	1.7(+/-0.6)E+05
I	10.0(+/-0.3)	2.7(+/-0.1)E+05
II	9.8(+/-0.9)	4.9(+/-0.4)E+05
III	7.5(+/-1.0)	5.3(+/-0.6)E+05
IV	2.3(+/-0.7)	2.1(+/-0.7)E+05

Table A4. Extinction coefficients of samples at 210 nm. M_n from GPC was used in the molarity calculation.

Appendix B

Supplementary Information for Chapter 3

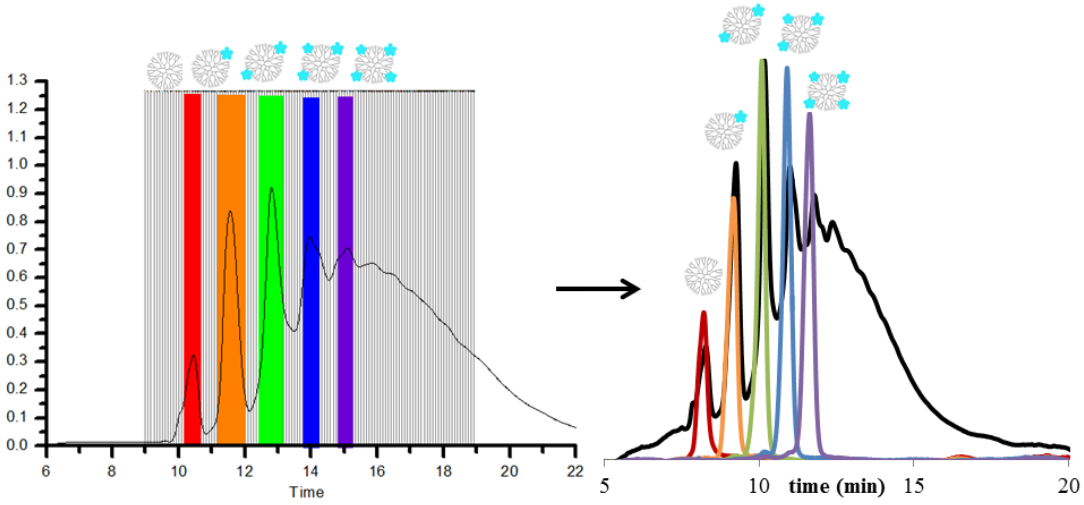

Figure B1. (left) Semi-prep HPLC isolation of precisely defined G5-Azide$_n$ species, colored bars represent combined fractions (right) Subsequent reinjection into a UPLC shows peaks do not recenter, analogous to the MFCO conjugate separation, indicating that each sample now contains a single, particular ligand/particle ratio.

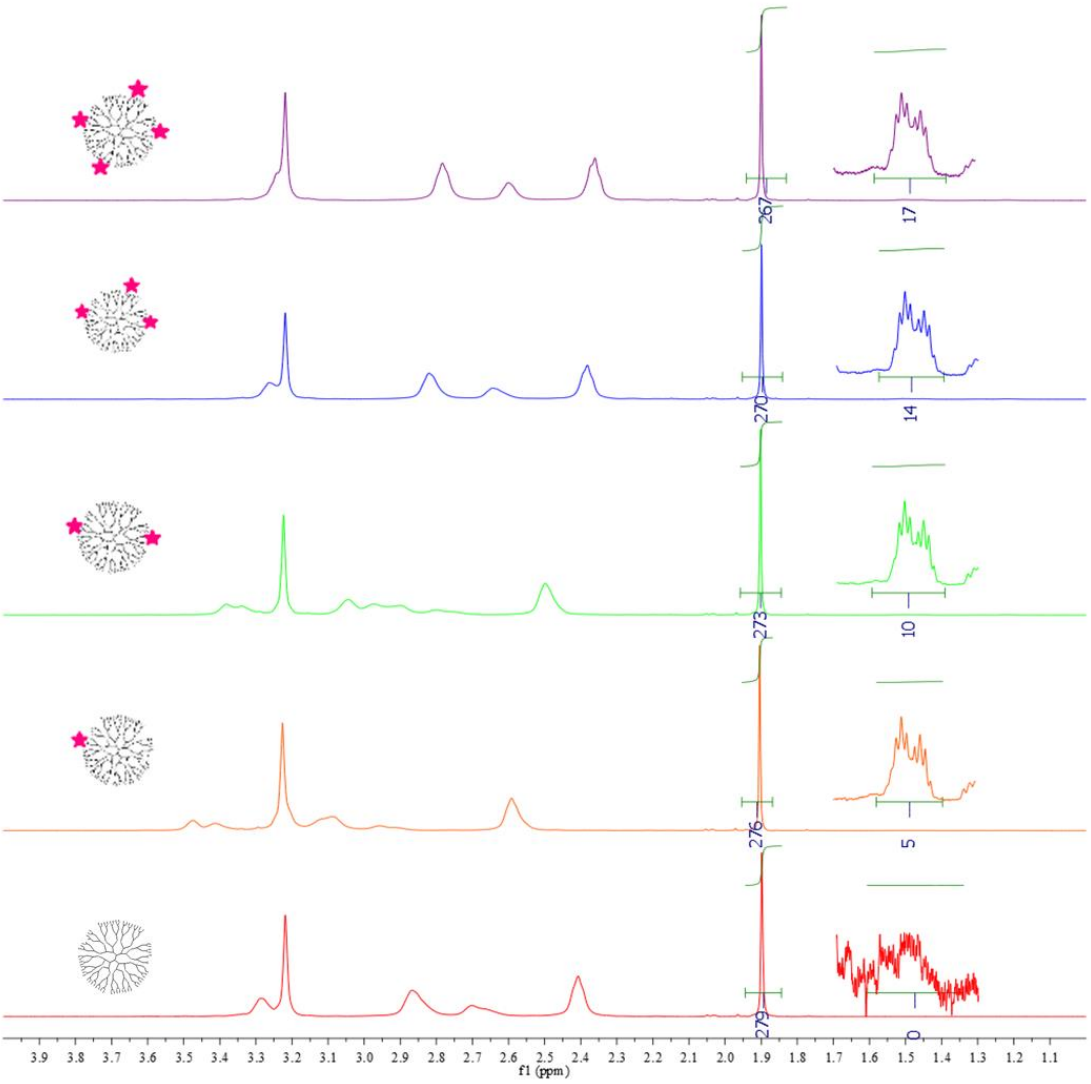

Figure B2. NMRs of G5-MFCO$_n$. Ratio between acetylated peak at 1.9 (3 protons per each of 93 primary amines as determined by potentiometric titration) compared to 5 protons between 1.5 and 1.3 on MFCO ligand.

n	avg (by NMR)	avg (by UPLC)	% Purity (UPLC)	% Recovered
0	0.0	0.0	>95%	47%
1	1.0	1.0	>95%	58%
2	2.0	2.0	>95%	77%
3	2.8	3.0	>95%	46%
4	3.4	4.0	>95%	43%

Table B1. Quantitative summary of G5-MFCO$_n$ HPLC separation.

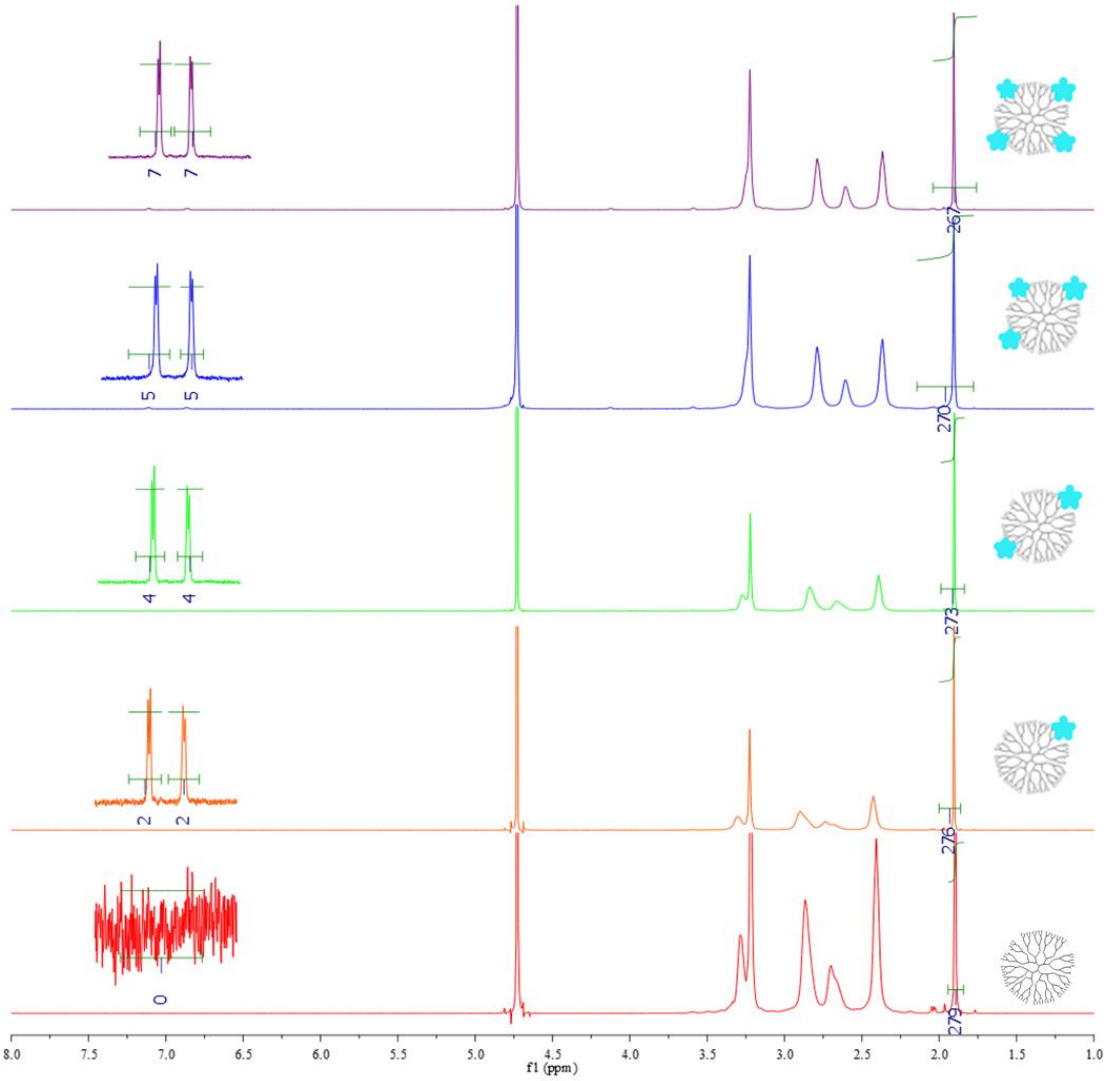

Figure B3. NMRs of G5-Azide$_n$. Ratio between acetylaed peak at 1.9 and the aromatic peaks of the azide ligand.

n	avg (by NMR)	avg (by UPLC)	% Purity (UPLC)	% Recovered
0	0.0	0.0	>95%	59%
1	1.0	1.0	>95%	70%
2	2.0	2.0	>95%	41%
3	2.5	3.0	>95%	38%
4	3.5	4.0	>95%	33%

Table B2. Quantitative summary of G5-Azide$_n$ HPLC separation.

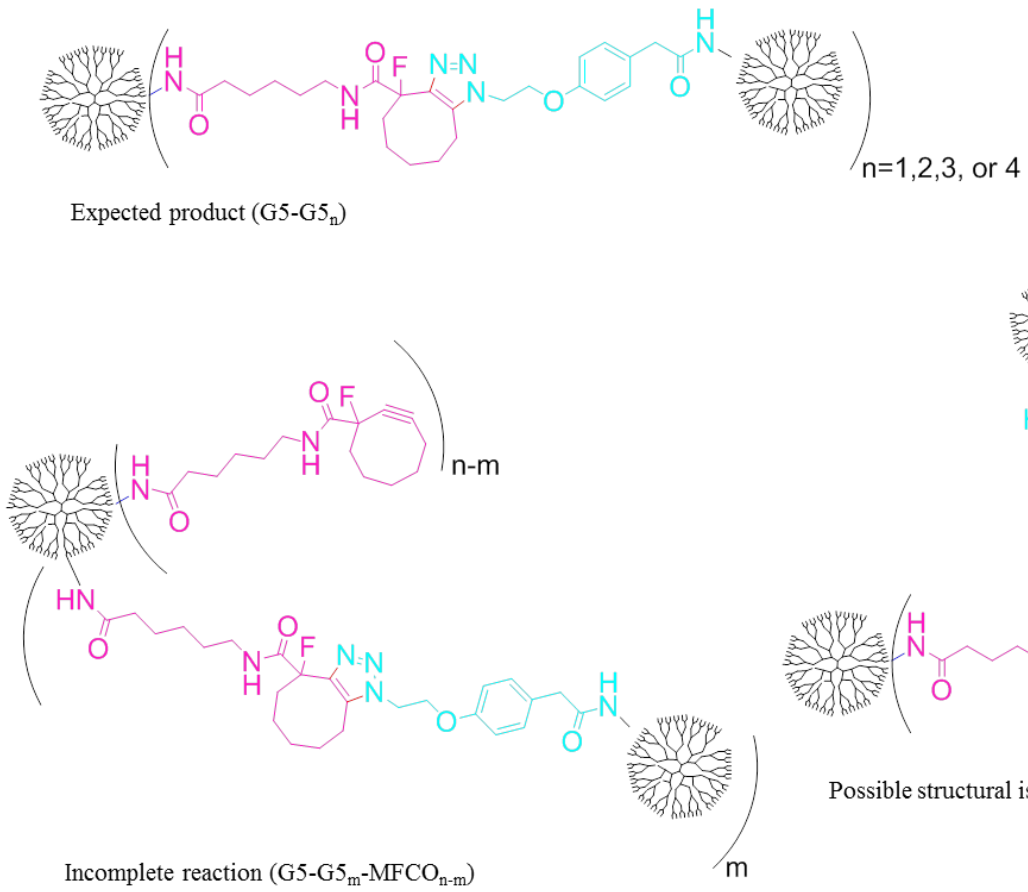

Figure B4. Possible side products of click reaction.

Appendix C

Supporting Information for Chapter 4

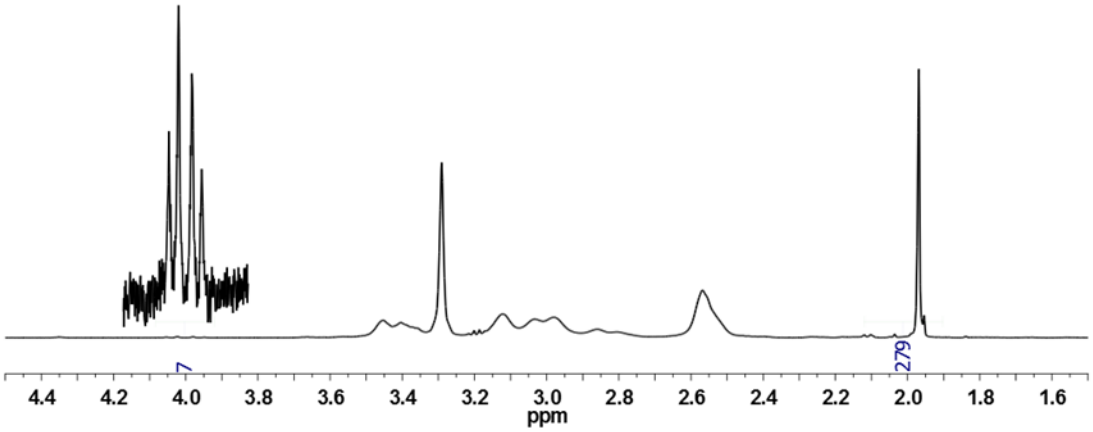

Figure C1. ^{1}H-NMR of G5-Ac-COG$_{4.0(avg)}$ in D_2O. The peak at 1.97 ppm is the acetyl peak for the dendrimer arm, equal to 93*3-x (93 is the number of arms on G5 monomer, 3 protons per acetyl group, and x being number of arms functionalized with COG). The multiplet at 4 ppm should integrate to 5 protons per COG on a dendrimer, giving an NMR average for this conjugate of 1.4.

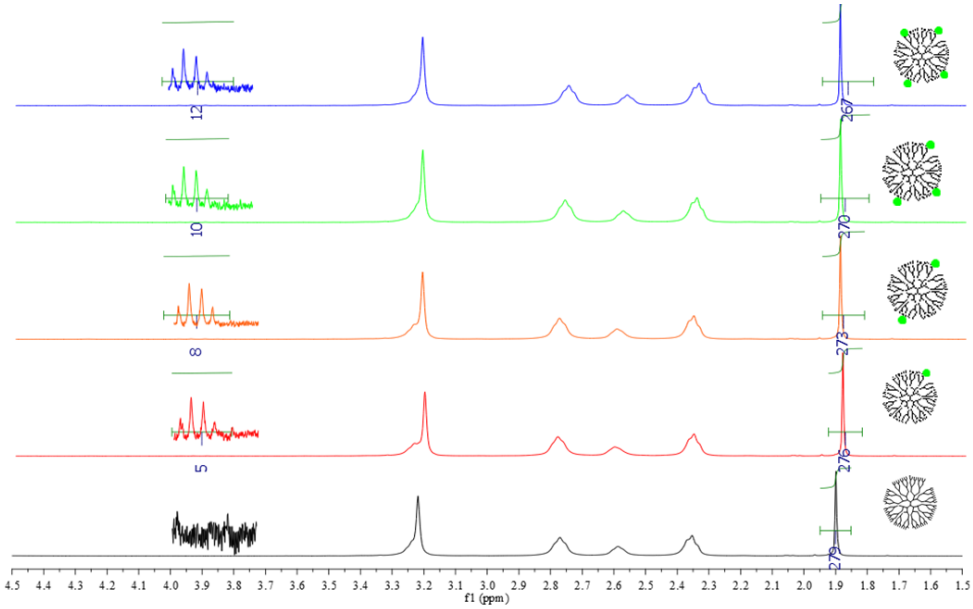

Figure C2. ^{1}H- NMR of isolated G5-COG$_x$ (x=0, black; x =1, red; x = 2, orange; x = 3, green; x = 4, blue) in D_2O.

x (COG)	Avg (UPLC)	Avg (NMR)	Purity of "x"
0	0.0	0.0	>95%
1	1.0	1.0	>95%
2	2.1	1.6	93%
3	3.0	2.0	>95%
4	4.0	2.4	>95%

Table C1. G5-Ac-COG_x Isolation Results

^{1}H-NMR values are skewed, especially at higher valencies, because they assume that each dendrimer in the population has the same number of primary amines. However, branching defects have been shown to contribute to the peak width observed in rp-HPLC. Additionally, all work to date shows that the “more perfect” dendrimer (i.e. with more arms and less defects) is better retained on the column. Therefore, at higher valencies, when a more narrow set of fractions is collected to maintain high sample purity, the number of end groups per dendrimer is decreased by an undetermined amount.

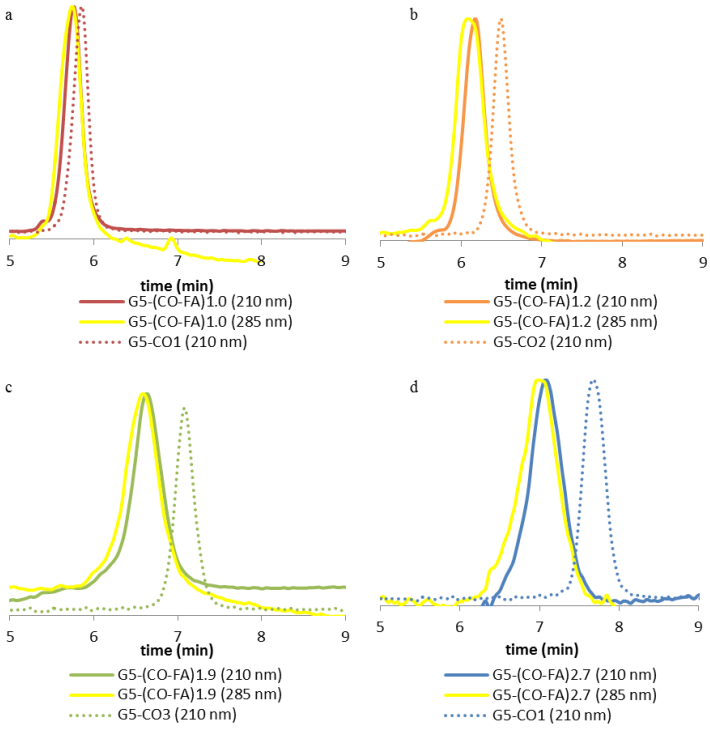

Figure C3. UPLC of starting materials (dotted lines), and click products at 285 nm (yellow lines) and 210 nm for (a) n=1, red (b) b) n=2, orange (c) n=3, green (d) n=4, blue.

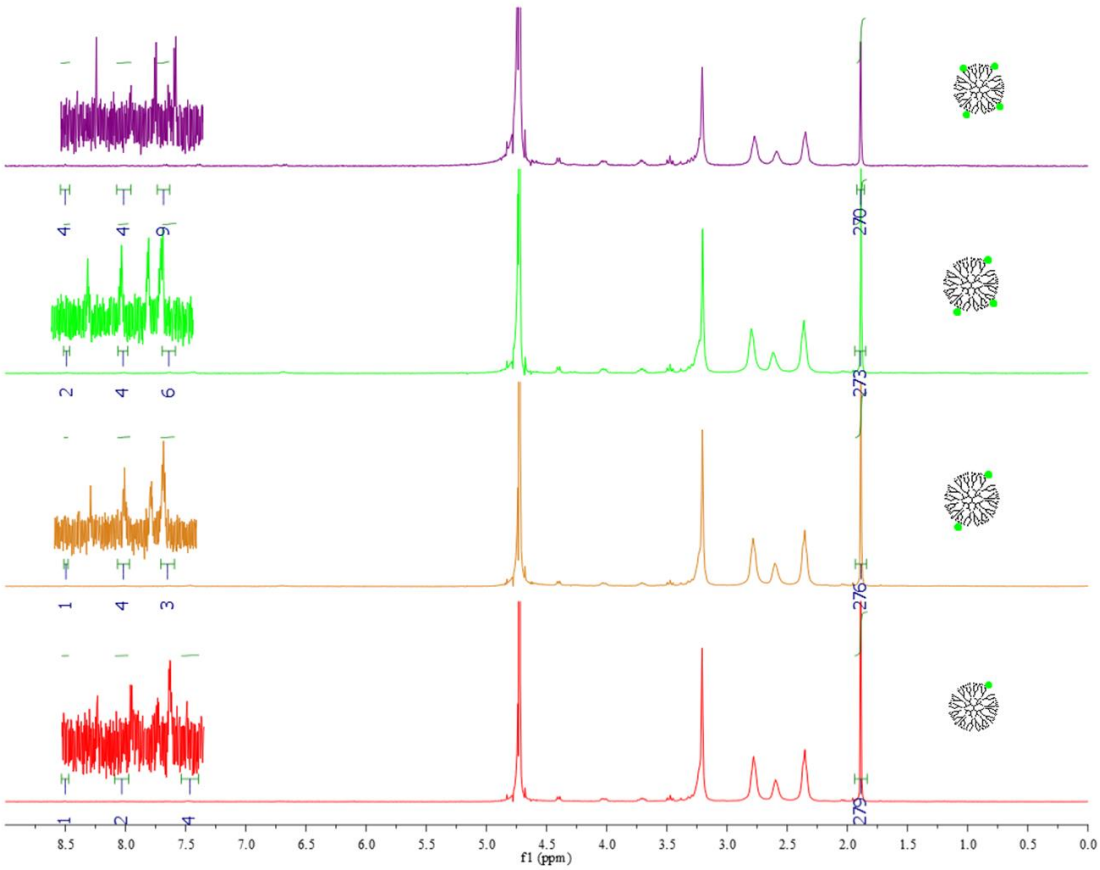

Figure C4. NMR of click products in D_2O for n=1.0 (red), 1.2 (orange), 1.9 (green), 2.7 (blue) from bottom to top. The peak at 8.6 ppm should integrate to 1 proton per MTX on the dendrimer, and the peaks at 7.7 and 6.8 ppm as 2 protons per MTX.

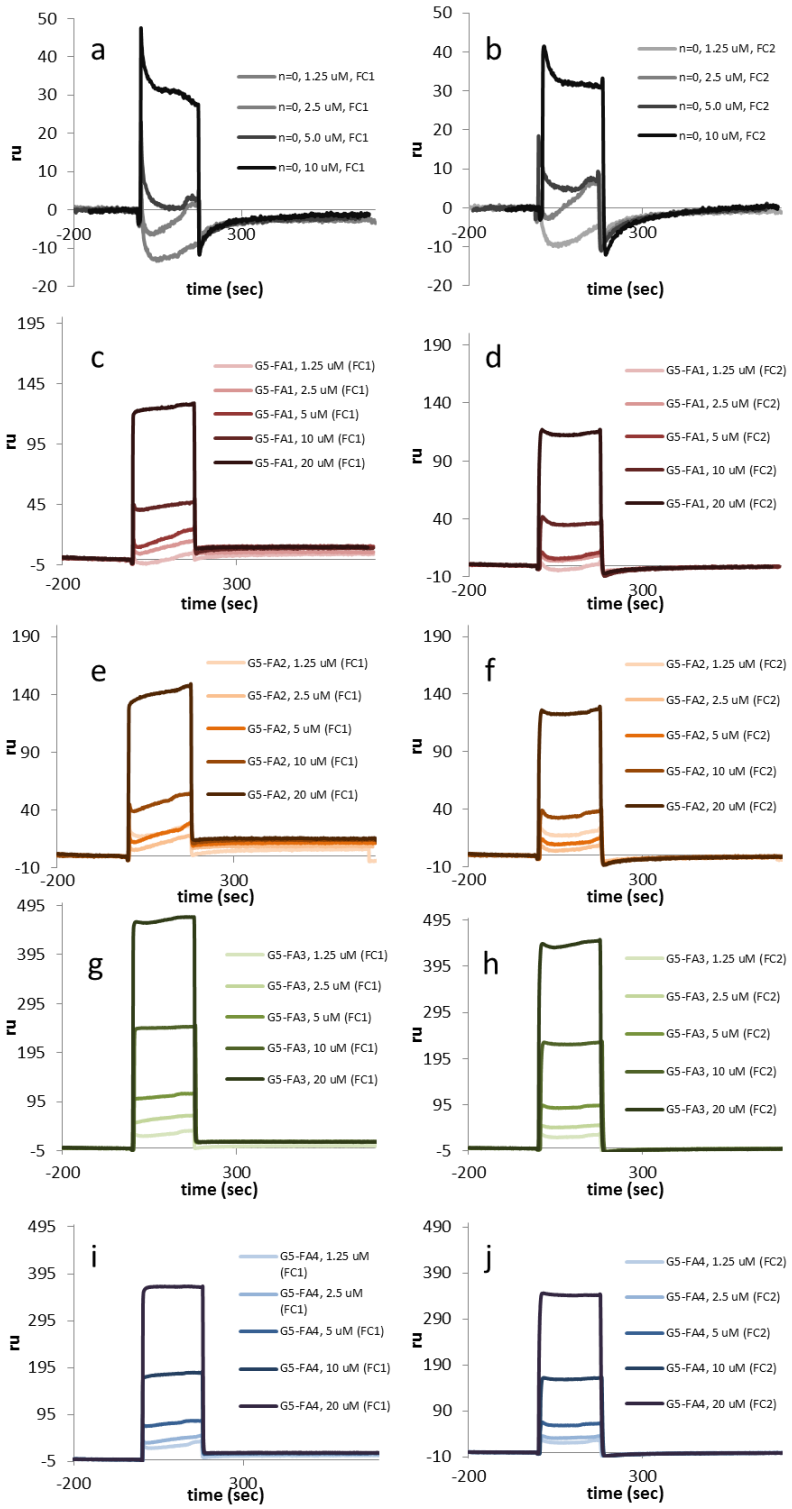

Figure C5. Individual flow cell chromatograms for low density chip. (a) n = 0, FC1 (b) n = 0, FC2 (c) n = 1.0, FC1 (d) n = 1.0, FC2 (e) n = 1.2, FC1 (f) n = 1.2, FC2 (g) n = 1.9, FC1 (h) n = 1.9, FC2 (i) n = 2.7, FC1 and (j) n = 2.7, FC2.

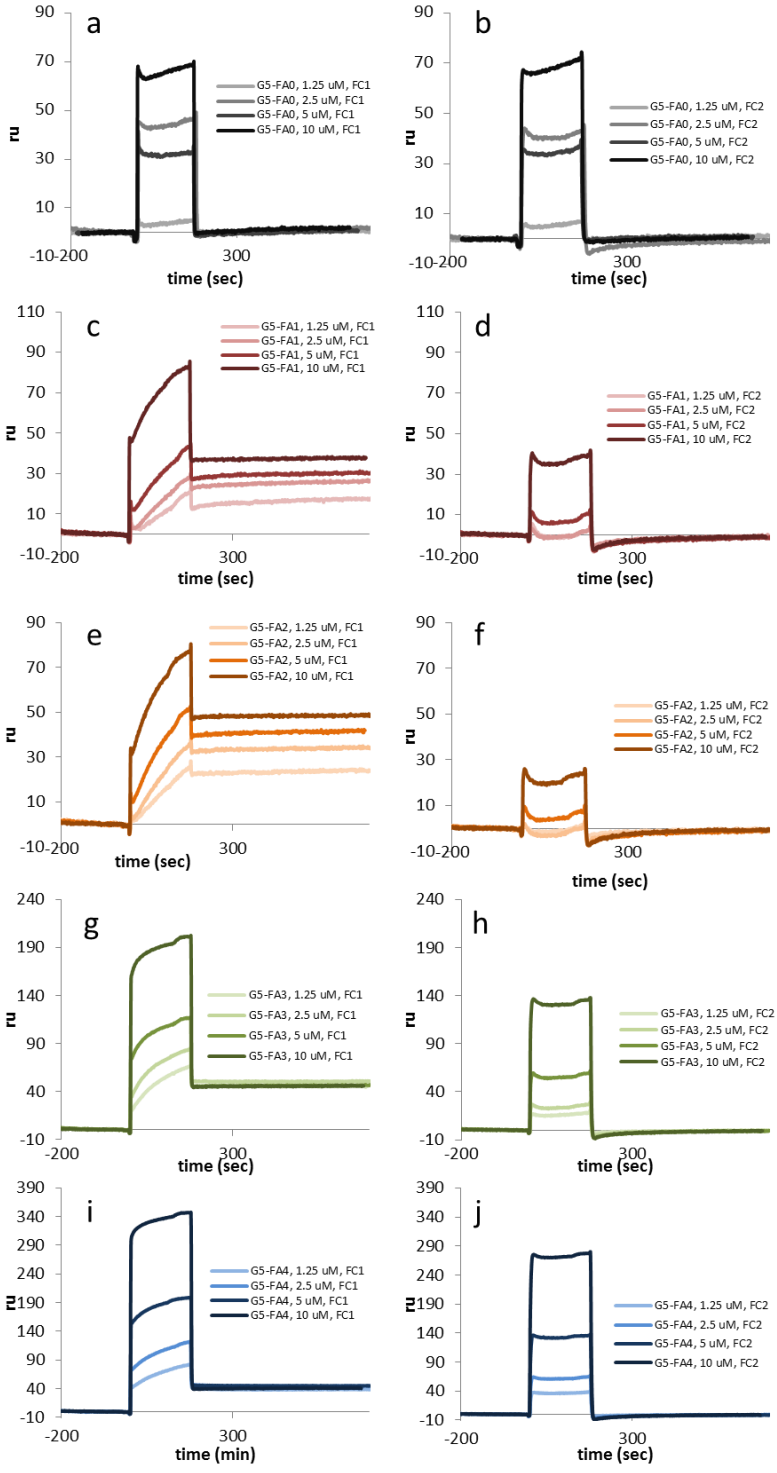

Figure C6. Individual flow cell chromatograms for high density chip. (a) n = 0, FC1 (b) n = 0, FC2 (c) n = 1.0, FC1 (d) n = 1.0, FC2 (e) n = 1.2, FC1 (f) n = 1.2, FC2 (g) n = 1.9, FC1 (h) n = 1.9, FC2 (i) n = 2.7, FC1 and (j) n = 2.7, FC2.

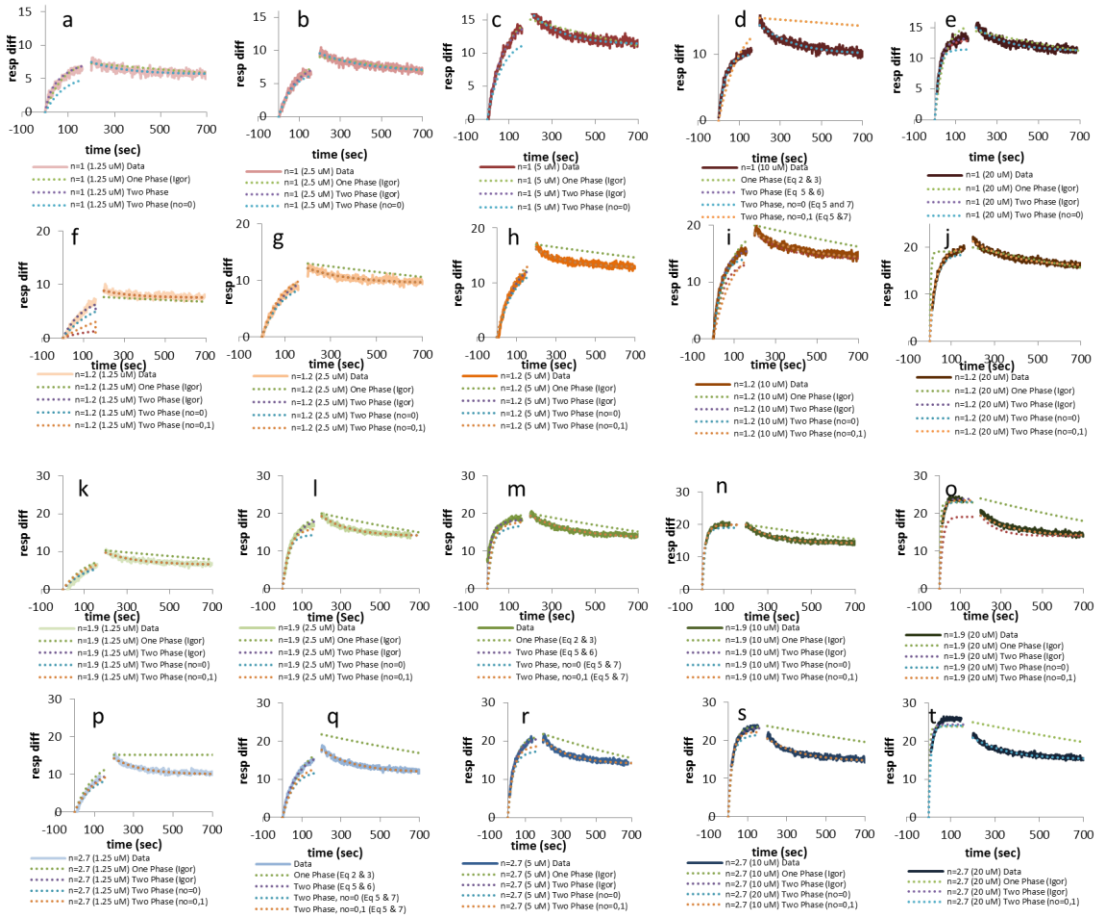

Figure C7. SPR chromatograms (solid lines) on the low density chip overlaid with the four proposed fits (dotted lines). (a) n = 1.0, 1.25 µM (b) n = 1.0, 2.5µM (c) n = 1.0, 5 µM (d) n = 1.0, 10 µM (e) n = 1.0, 20 µM (f) n = 1.2, 1.25 µM (g) n = 1.2, 2.5µM (h) n = 1.2, 5 µM (i) n = 1.2, 10 µM (j) n = 1.2, 20 µM (k) n = 1.9, 1.25 µM (l) n = 1.9, 2.5µM (m) n = 1.9, 5 µM (n) n = 1.9, 10 µM (o) n = 1.9, 20 µM (p) n = 2.7, 1.25 µM (q) n = 2.7, 2.5µM (r) n = 2.7, 5 µM (s) n = 2.7, 10 µM (t) n = 2.7, 20 µM

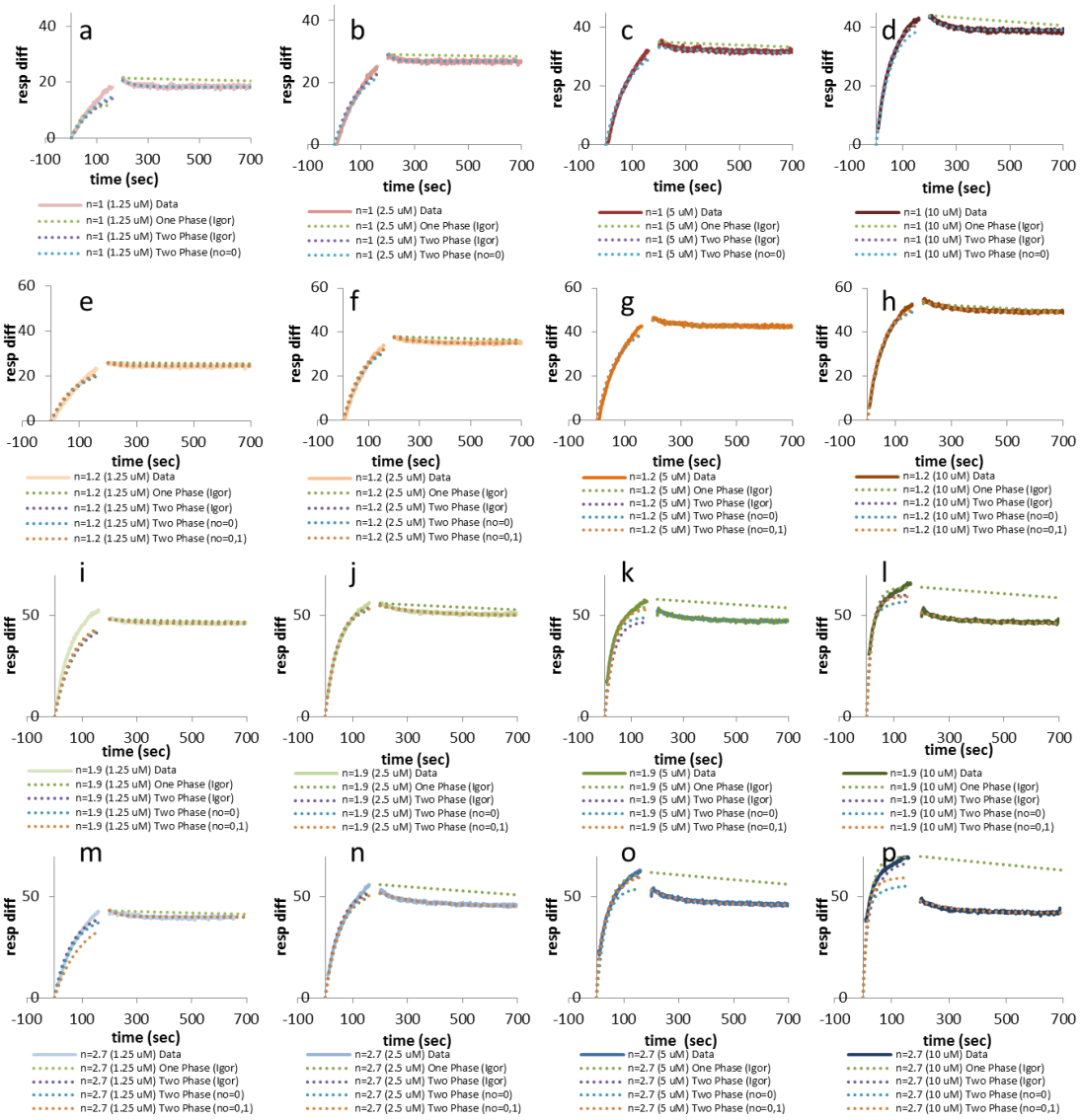

Figure C8. SPR chromatograms (solid lines) on the high density chip overlaid with the four proposed fits (dotted lines). (a) n = 1.0, 1.25 µM (b) n = 1.0, 2.5µM (c) n = 1.0, 5 µM (d) n = 1.0, 10 µM (e) n = 1.2, 1.25 µM (f) n = 1.2, 2.5µM (g) n = 1.2, 5 µM (h) n = 1.2, 10 µM (i) n = 1.9, 1.25 µM (j) n = 1.9, 2.5µM (k) n = 1.9, 5 µM (l) n = 1.9, 10 µM (m) n = 2.7, 1.25 µM (n) n = 2.7, 2.5µM (o) n = 2.7, 5 µM (p) n = 2.7, 10 µM.

Chip	n	Conc (uM)	One Phase	Two Phase	Two Phase (no=0)	Two Phase (no=0,1)	k_d (1)	k_d (2)
Low protein density chip	**1**	1.25	0.37	0.38	1.56	na	0.42	0.28
		2.5	0.37	0.32	0.46	na	0.30	0.27
		5	0.34	0.35	1.76	na	0.59	0.32
		10	1.26	0.32	0.32	na	3.44	0.30
		20	1.23	0.28	1.32	na	0.59	0.32
		Avg (n=1.0):	*0.71*	*0.33*	*1.08*	*na*	*1.07*	*0.30*
	1.2	1.25	0.47	0.48	1.05	2.26	0.78	0.35
		2.5	0.32	0.31	0.61	0.50	1.32	0.28
		5	0.51	0.46	0.83	0.83	1.98	0.28
		10	0.99	0.36	0.82	2.83	2.18	0.32
		20	2.32	0.28	0.77	0.32	0.41	0.29
		Avg (n=1.2):	*0.92*	*0.38*	*0.82*	*1.35*	*1.34*	*0.31*
	1.9	1.25	1.33	0.79	0.88	1.03	1.58	0.29
		2.5	0.82	0.46	1.73	0.87	1.94	0.28
		5	1.49	0.67	2.47	1.74	1.86	0.32
		10	0.31	0.28	0.92	0.28	2.07	0.31
		20	1.20	0.34	0.79	0.50	4.92	0.36
		Avg (n=1.9):	*1.03*	*0.51*	*1.36*	*0.88*	*2.47*	*0.31*
	2.7	1.25	1.24	0.51	0.84	0.59	3.97	0.32
		2.5	0.69	0.26	2.17	1.65	5.47	0.31
		5	0.57	0.31	2.13	1.20	2.60	0.35
		10	0.42	0.34	1.71	0.82	5.12	0.35
		20	1.83	1.23	1.37	na	5.28	0.31
		Avg (n=2.7):	*0.95*	*0.53*	*1.64*	*1.07*	*4.49*	*0.33*
		Avg (low density):	***0.90***	***0.44***	***1.23***	***1.10***	***2.34***	***0.31***
High protein density chip	**1**	1.25	2.33	2.03	1.49	na	2.38	0.32
		2.5	1.15	1.37	1.43	na	1.79	0.31
		5	1.15	1.27	1.36	na	1.88	0.42
		10	0.60	1.03	2.36	na	2.86	0.36
		Avg (n=1.0):	*1.31*	*1.42*	*1.66*	*na*	*2.23*	*0.35*
	1.2	1.25	1.25	1.39	1.30	1.44	1.19	0.32
		2.5	1.52	1.39	1.39	1.70	1.68	0.34
		5	1.76	1.80	1.76	1.89	0.59	0.40
		10	0.89	1.09	1.19	1.29	1.10	0.33
		Avg (n=1.2):	*1.35*	*1.42*	*1.41*	*1.58*	*1.14*	*0.35*
	1.9	1.25	6.46	8.18	7.19	6.77	0.90	0.32
		2.5	0.77	0.85	1.25	0.83	2.80	0.36
		5	2.29	7.36	4.29	2.83	7.61	0.34
		10	2.30	2.30	4.49	2.62	13.73	0.40
		Avg (n=1.9):	*2.96*	*4.67*	*4.31*	*3.26*	*6.26*	*0.35*
	2.7	1.25	1.38	1.73	1.77	6.24	2.09	0.38
		2.5	1.09	1.40	2.42	1.70	6.24	0.42
		5	1.65	1.24	5.00	1.21	11.28	0.37
		10	2.85	3.75	10.00	6.19	23.41	0.40
		Avg (n=2.7):	*1.74*	*2.03*	*4.80*	*3.83*	*10.76*	*0.40*
		Avg (high density):	***1.84***	***2.39***	***3.04***	***2.89***	***5.10***	***0.36***
		Avg (all):	**1.32**	**1.30**	**2.03**	**1.93**	**3.57**	**0.33**

Table C2. Average residuals for each fit parameter for both chip densities.

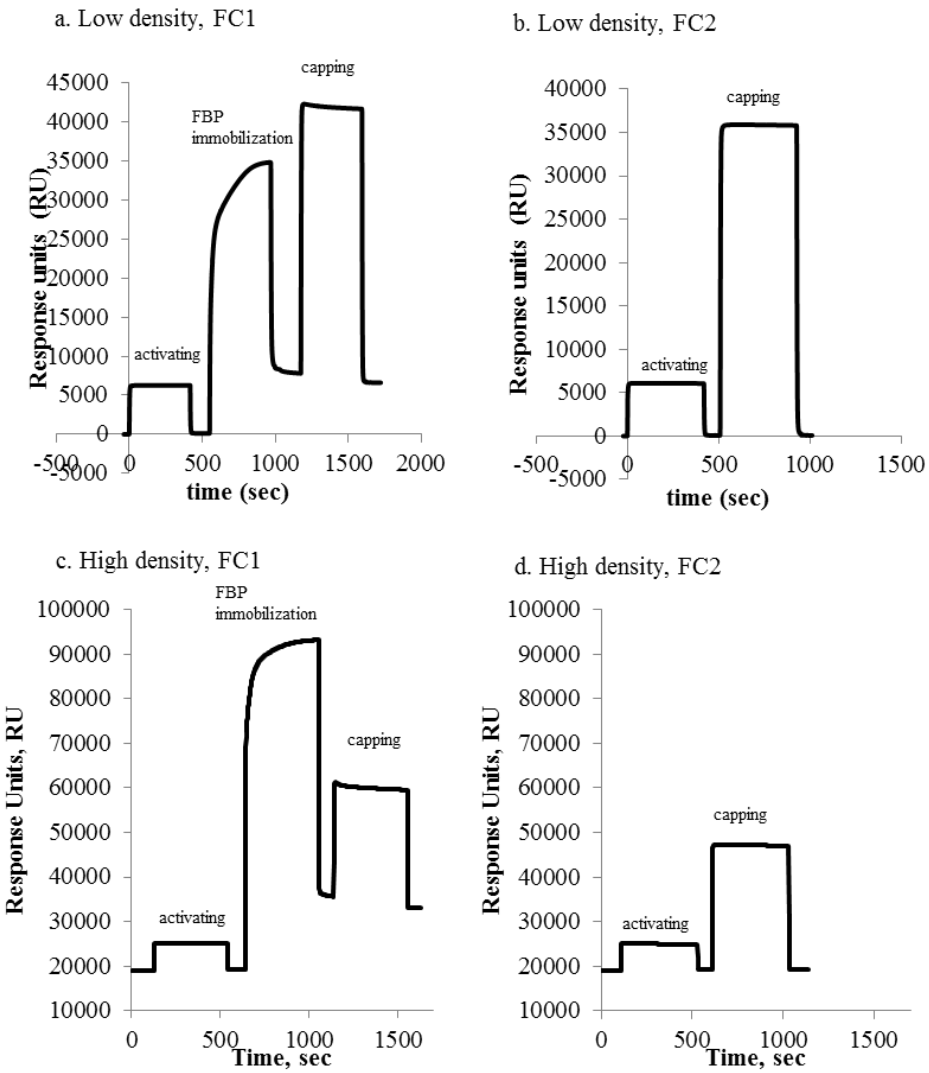

Figure C9. Sensograms generated during chip immobilizations. (a) Low density chip, FC1 (protein RUs: 10,000) (b) Low density, FC2 (c) High density, FC1 (protein RUs: 20,000) (d) High density, FC2

Synthesis of COG Ligand

Synthesis of 8,8-dibromobicyclo[5.0.1]octane (S1). In an oven dried flask under nitrogen, cycloheptene (4.43mL, 38mmol, 1.0equiv.), potassium tert-butoxide (8.52g, 76mmol, 2.0equiv.), and anhydrous hexanes (9mL) was added together. Mixture was stirred and cooled to -10°C in an ice/acetone bath. Once to temperature, bromoform (4.9mL, 57mmol, 1.5 equiv.)was added dropwise. Once the mixture appears as a milky brown color, it was brought to room temperature (25°C) and stir overnight. Water (50mL) was added and the mixture was acidified with concentrated hydrochloric acid. Extract with ethyl acetate (3x20mL) and wash with water (3x20mL). Mixture was dried with $MgSO_4$, filter, and solvent was removed under reduced pressure. No further purification necessary to produce a brown oil in 94% yield.

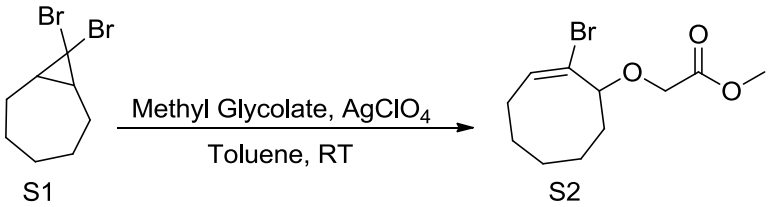

Scheme C1. Synthesis of Methyl-2-bromocyclooct-1-en-3-glycolate.

Synthesis of Methyl-2-bromocyclooct-1-en-3-glycolate (S2): In an oven dried flask under nitrogen, anhydrous toluene (5.0mL), **S1** (2.50g, 9mmol, 1.0equiv.), and methyl glycolate (6.35mL, 84mmol, 9equiv.) were added. Mixture was stirred at room temperature (25°C) and flask was covered with aluminum foil. Silver perchlorate (3.85g, 19mmol, 2 equiv.) was added to reaction flask and stirred for 90minutes. Silver salts filtered out and washed with ethyl acetate. Remove solvent under reduced pressure and immediately chromatograph using 2-15% ethyl acetate:cyclohexanes to produce a yellow oil in 62% yield.

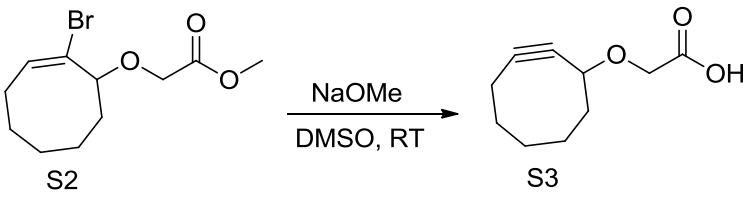

Scheme C2. Synthesis of cyclooct-1-yn-3-glycolic acid

Synthesis of cyclooct-1-yn-3-glycolic acid (S3): In an oven dried round bottom flask under nitrogen, Suspension of sodium methoxide (0.0278g, 0.5mmol, 0.5 equiv.) in DMSO (5mL) was made and S2 (0.2866g, 1mmol, 1.0equiv.) and DMSO (1mL) was addded. Stir at room temperature for 15 minutes. Additional sodium methoxide (0.0835g, 1.5mmol, 1.5 equiv.) and DMSO (0.5mL) was added and mixture stirred until reaction was completed (determined by TLC). Water was added (0.3mL) and solution stirred for one hour. Reaction was acidified with 1.0M HCl solution. Extract with ethyl acetate (2x25mL). Organic Layer was dried over $MgSO_4$, filtered, and removed solvent in vacuo. Chromatograph using 0-8% MeOH:Dichloromethane to obtain product as a yellow oil in 38% yield.

Appendix D

Supplementary Information for Chapter 5

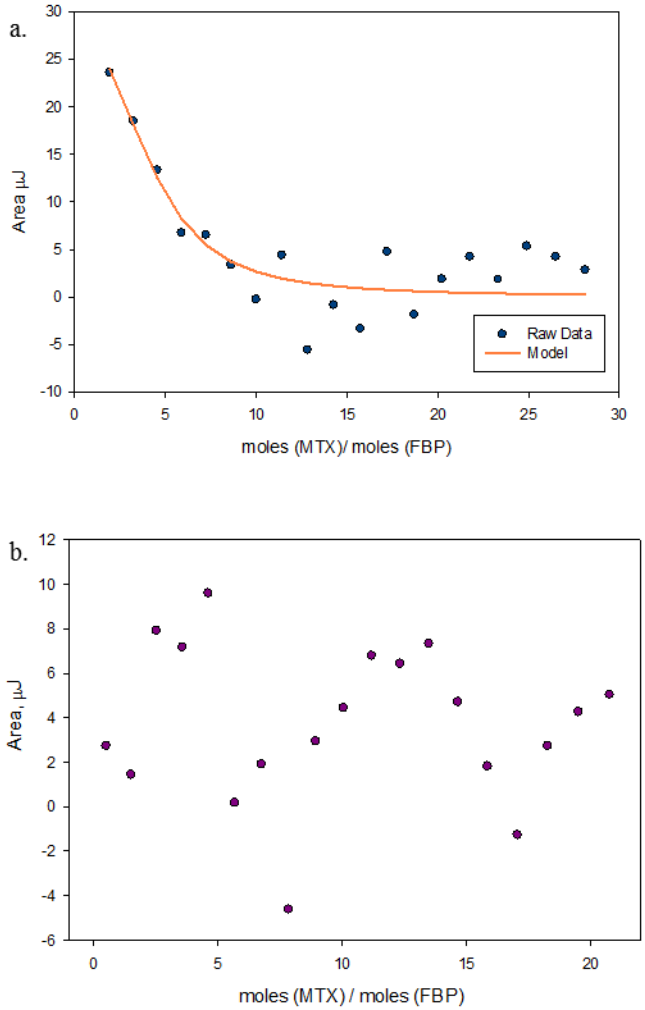

Figure D1. ITC results for (a) stochastic average G5-Ac-(MFCO-MTX) and (b) high average G5-Ac-(MFCO-MTX) showing endothermic and nonbinding behavior, respectively.

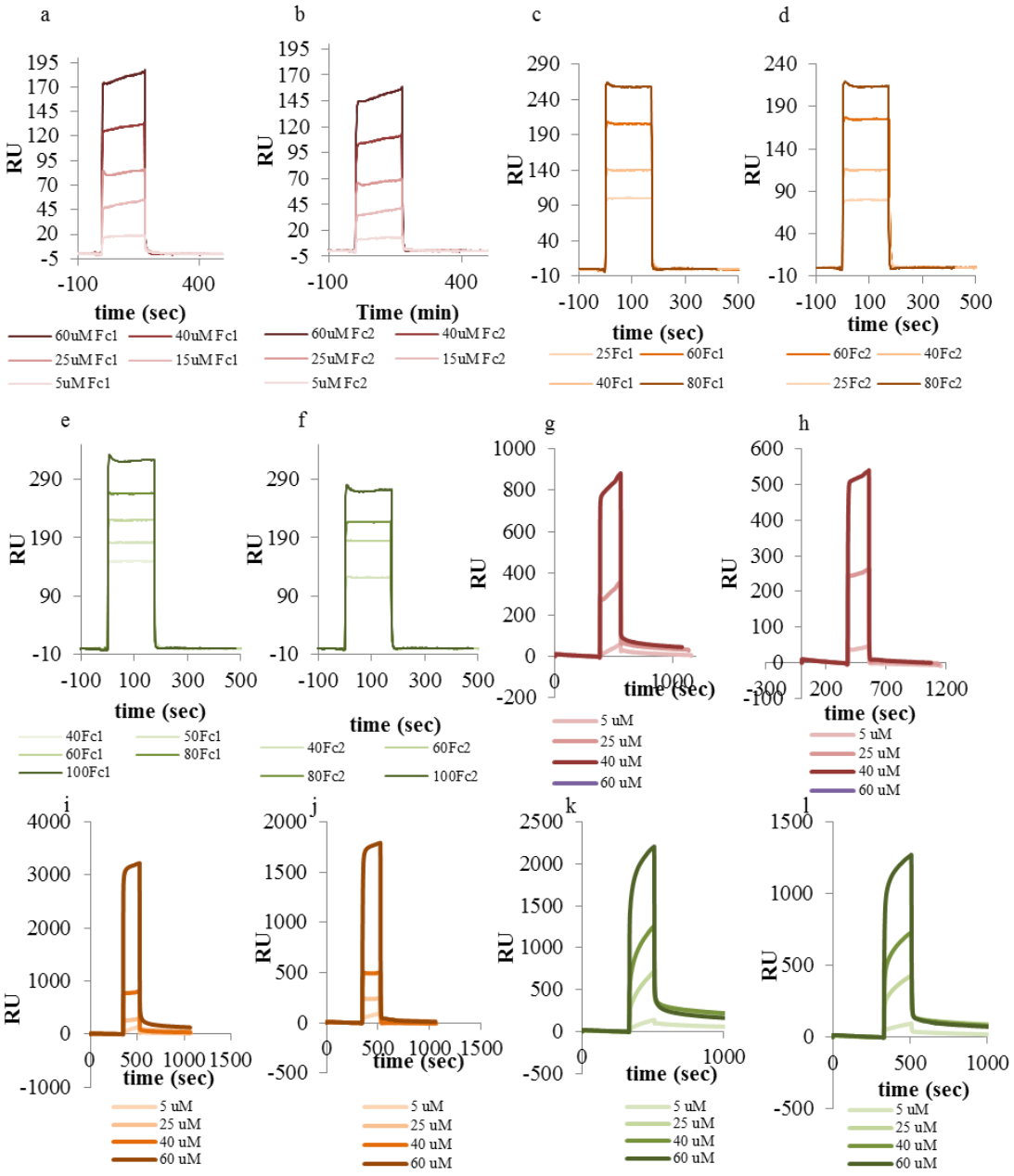

Figure D2. Individual flow cell data for dendrimer CO-MTX conjugates. (a) G5-Ac-$(COG\text{-}MTX)_{0.9}$ FC1 (b) G5-Ac-$(COG\text{-}MTX)_{0.9}$ FC2 (c) G5-Ac-$(COG\text{-}MTX)_{1.9}$ FC1 (d) G5-Ac-$(COG\text{-}MTX)_{1.9}$ FC2 (e) G5-Ac-$(COG\text{-}MTX)_{2.9}$ FC1 (f) G5-Ac-$(COG\text{-}MTX)_{2.9}$ FC2 (g) D-Ac-$(COG\text{-}MTX)_{1.1}$ FC1 (h) D-Ac-$(COG\text{-}MTX)_{1.1}$ FC2 (i) D-Ac-$(COG\text{-}MTX)_{2.0}$ FC1 (j) D-Ac-$(COG\text{-}MTX)_{2.0}$ FC2 (k) D-Ac-$(COG\text{-}MTX)_{6.0}$ FC1 (l) D-Ac-$(COG\text{-}MTX)_{6.0}$ FC2

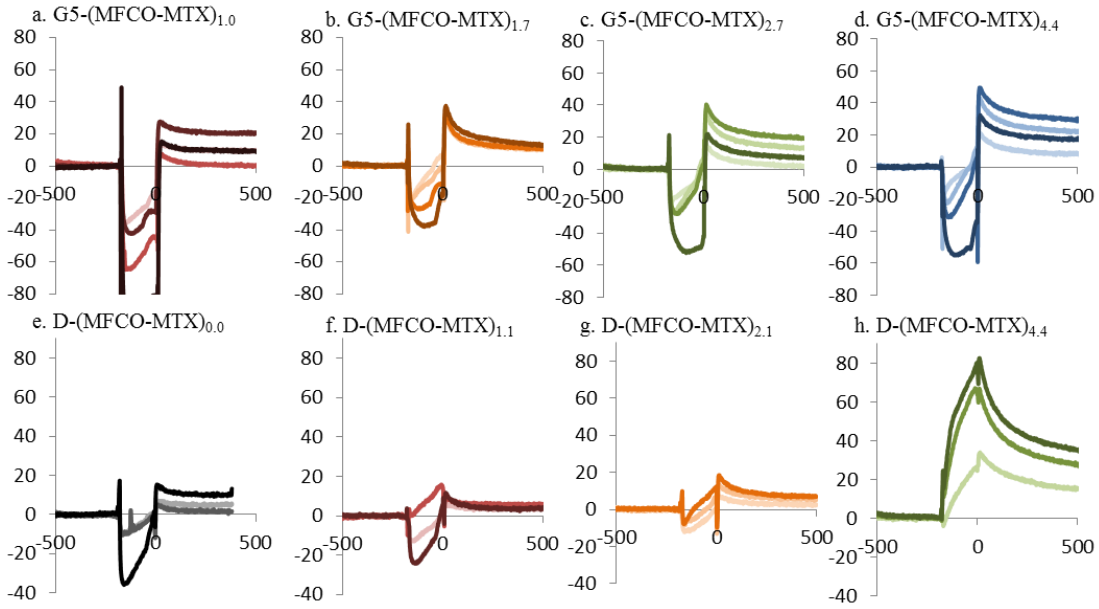

Figure D3. SPR sensograms for dendrimer-MFCO-MTX conjugates show negative binding phases, corresponding to high nonselective binding in FC2.

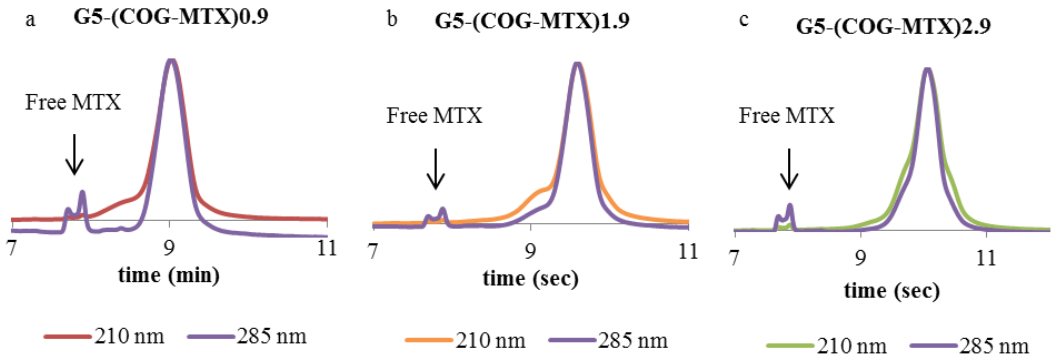

Figure D4. Free MTX is detected by absorbance at 285 nm (orange lines) but less so at 210 nm (purple lines) in G5-Ac-(COG-MTX)$_n$ samples. (a) G5-Ac-(COG-MTX)$_{0.9}$ (b) G5-Ac-(COG-MTX)$_{0.9}$ (c) G5-Ac-(COG-MTX)$_{2.9}$

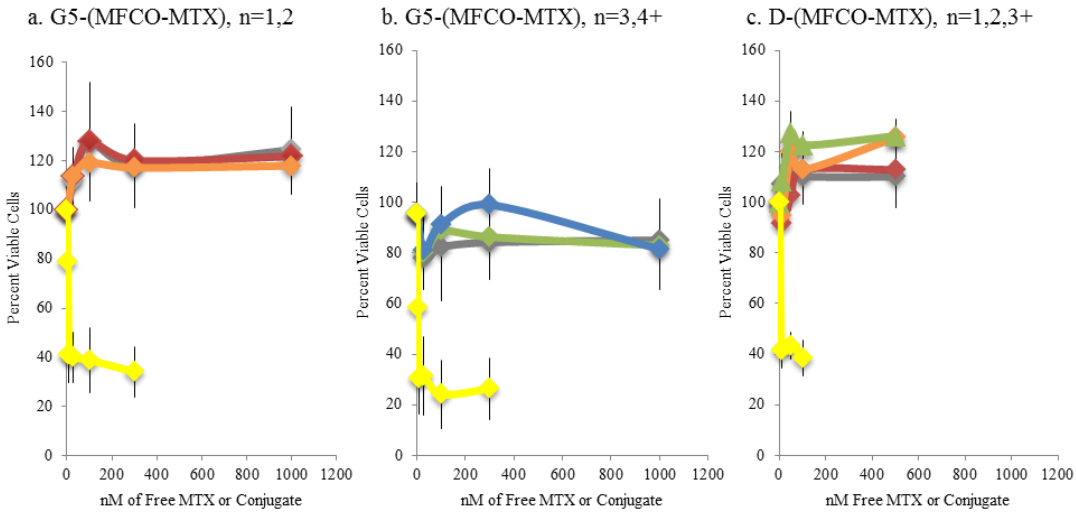

Figure D5. Cytotoxicity of (a and b) monomer (n = 1.0, red; n = 1.7, orange; n = 2.7, green; n = 4.4, blue) and (c) dimer (n = 1.1, red; n = 2.1, orange; n = 4.4, green) MFCO-MTX conjugates.

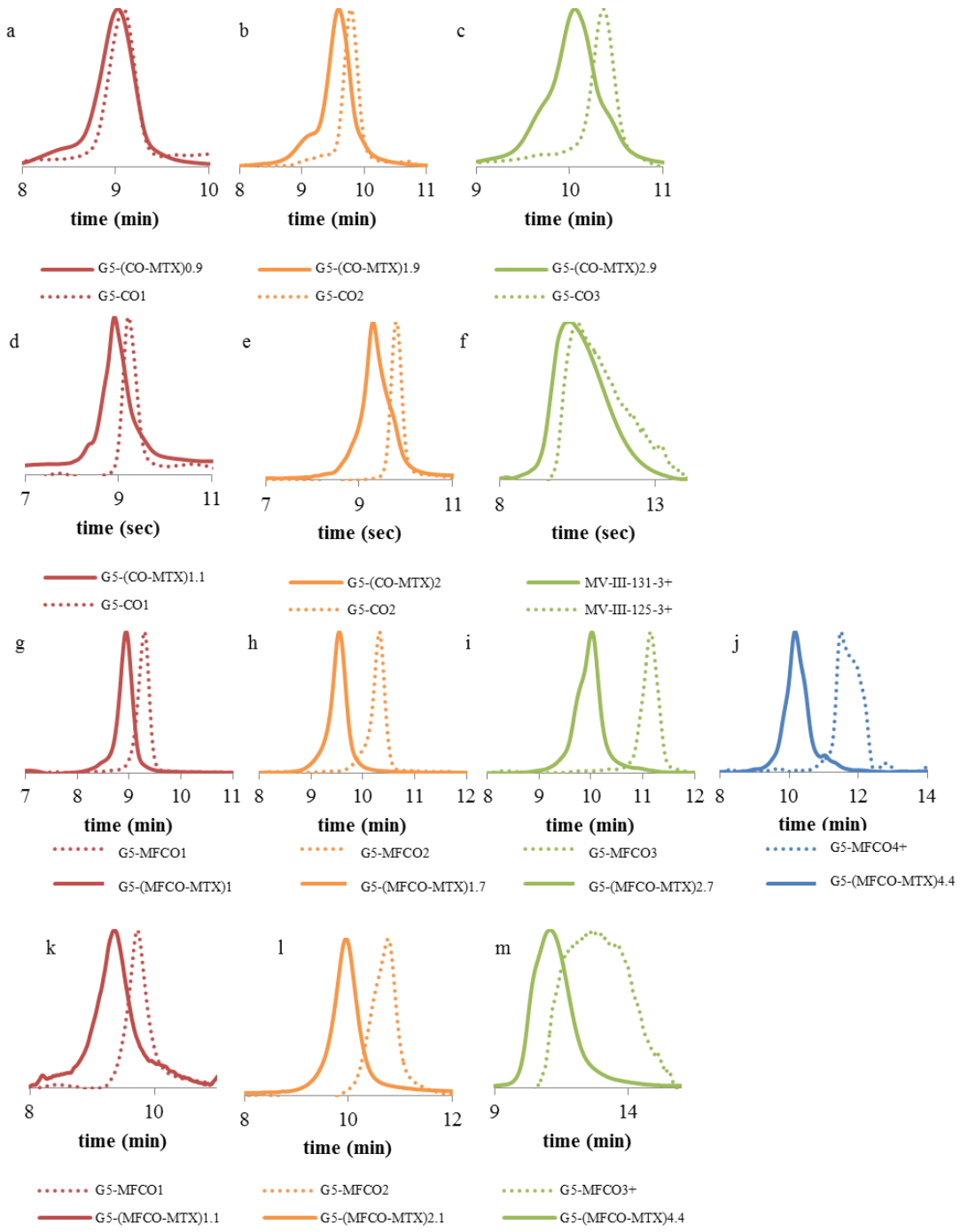

Figure D6. Comparison of UPLC chromatograms (210 nm) of click reaction starting materials (dotted lines) and click products (solid lines).

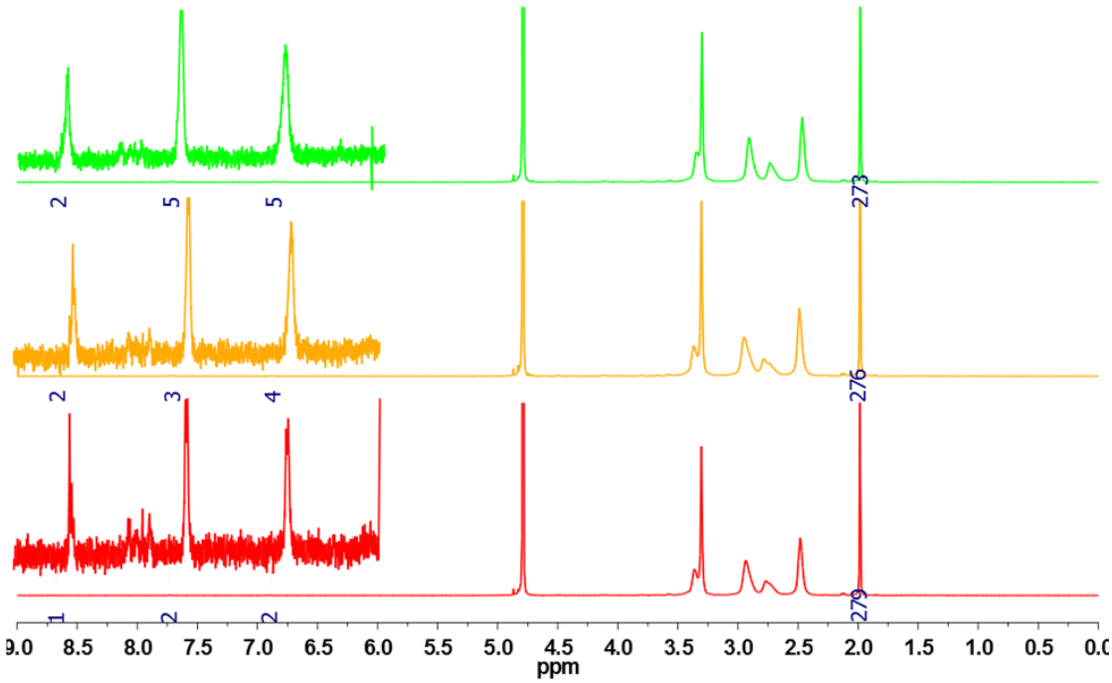

Figure D7. ^{1}H-NMR of G5-(COG-MTX)n, for n=0.9 (red), 1.9 (orange), and 2.9 (green).

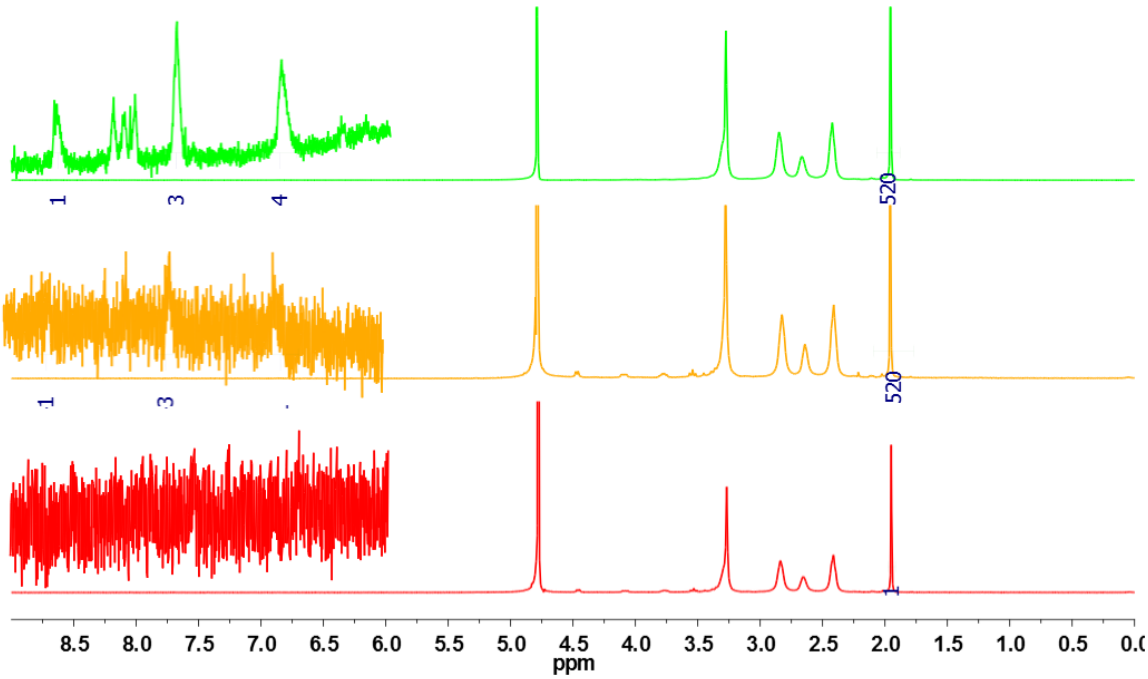

Figure D8. ^{1}H-NMR of D-(COG-MTX)n, n=1.1 (red), 2.0 (orange), and 6.0 (green).

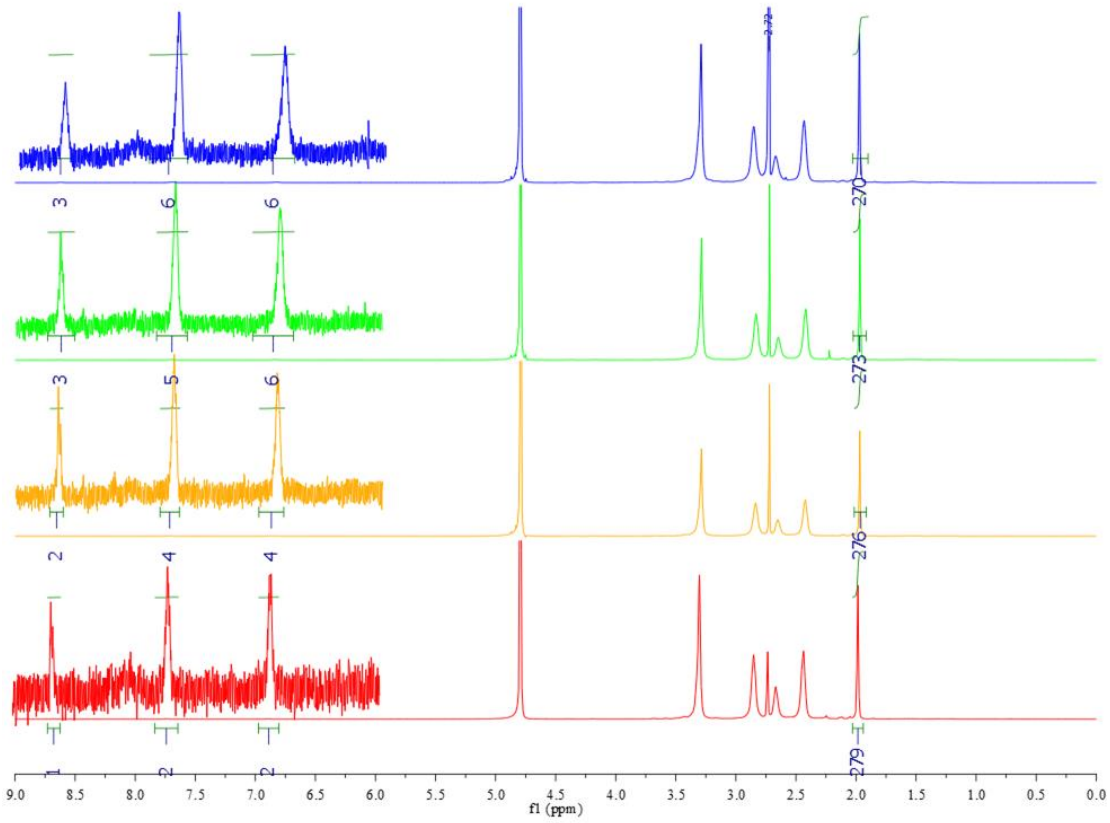

Figure D9. ^{1}H-NMR of G5-(MFCO-MTX)n, n=1.0 (red), 1.7 (orange), 2.7 (green) and 4.4 (blue).

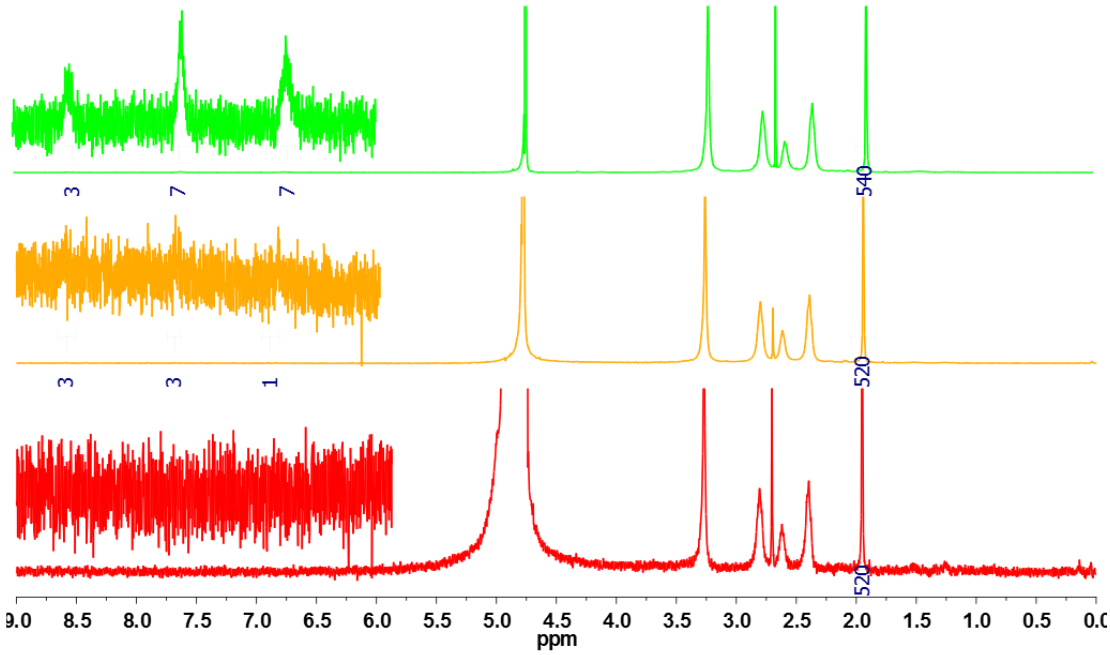

Figure D10. ^{1}H-NMR of D-(MFCO-MTX)n, n=1.1 (red), 2.1 (orange), and 4.4 (green).